Aalborg Universitet

Towards offshore wind digital twins

Application to jacket substructures

Augustyn, Dawid Jakub

[Link to publication from Aalborg University](#)

TOWARDS OFFSHORE WIND DIGITAL TWINS

APPLICATION TO JACKET SUBSTRUCTURES

BY
DAWID AUGUSTYN

DISSERTATION SUBMITTED 2021

AALBORG UNIVERSITY
DENMARK

Towards offshore wind digital twins

Application to jacket substructures

Dawid Augustyn

Faculty of Engineering and Science
Aalborg University

List of papers

The main body of the present thesis is composed of the following four papers, which are enclosed in Appendix A to D:

A **Augustyn, D.**, Smolka, U., Tygesen, U. T., Ulriksen, M. D. and Sørensen, J. D. (2020). Data-driven Model Updating of an Offshore Wind Jacket Substructure. *Applied Ocean Research*, 104, 102366,
doi: `https://doi.org/10.1016/j.apor.2020.102366`.

B **Augustyn, D.**, Pedersen, R., Ulriksen, M. D. and Sørensen, J. D. (2021). Feasibility of modal expansion for virtual sensing in offshore wind jacket substructures. *Marine Structures*, 79, 103019,
doi: `https://doi.org/10.1016/j.marstruc.2021.103019`.

C **Augustyn, D.**, Cosack, N. and Ulriksen, M. D. (2021). On the influence of environmental and operational variability on modal parameters of offshore wind support structures. *Marine Structures*, Manuscript submitted for publication.

D **Augustyn, D.**, Ulriksen, M. D. and Sørensen, J. D. (2021). Reliability Updating of Offshore Wind Substructures by Use of Digital Twin Information. *Energies*, 14(18), 5859,
doi: `https://doi.org/10.3390/en14185859`.

In addition to the main papers, the following relevant publications have been made during the Ph.D. study:

- **Augustyn, D.**, Tygesen, U. T., Ulriksen, M. D. and Sørensen, J. D. (2019). Data-Driven Design and Operation of Offshore Wind Structures. In *Proceedings of The Twenty-ninth (2019) International Offshore and Polar Engineering Conference, ISOPE2019*, Honolulu, USA, June 16th – June 21st, 2019.

- **Augustyn, D.**, Ulriksen, M. D. and Sørensen, J. D. (2021). Digital Twin for improved decision models of offshore wind structures. In *Proceedings of The Wind Energy Science Conference, WESC2021*, Hannover, Germany, May 25th – May 28th, 2021.

- Schwarz-wolf, B. M., Ulriksen, M. D., **Augustyn, D.**, Jensen, M. S. and Pedersen, R. R. (2021). Closed-loop updating of wind turbine models using blade pitch excitation. In *Proceedings of The Tenth (2021) International Conference on Structural Health Monitoring of Intelligent Infrastructure, SHMII10*, Porto, Portugal, June 30th – July 2nd, 2021.

The present thesis has been submitted for assessment in partial fulfilment of the Ph.D. degree. The thesis is based on the previously listed four submitted or published main scientific papers. Parts of the papers are used directly or indirectly in the extended summary of the thesis. As part of the assessment, co-author statements have been made available to the assessment committee and are also available at the Faculty. The thesis is not in its present form acceptable for open publication but only in limited and closed circulation as copyright may not be ensured.

Preface

The present industrial Ph.D. thesis, *Towards offshore wind digital twins: Application to jacket substructures*, has been completed during my Ph.D. study from October 2018 to November 2021. The project was carried out jointly at the Department of the Built Environment, Aalborg University, Denmark and at the Energy Department, Ramboll, Denmark. The thesis is presented as a collection of papers written while there.

Acknowledgments

First and foremost, I would like to thank my two academic Ph.D. supervisors: Prof. John Dalsgaard Sørensen and Asst. Prof. Martin Dalgaard Ulriksen. Prof. Sørensen inspired me to investigate this project in a probabilistic manner. His experience and dedication allowed me to confidently explore the field of structural reliability and execute the Ph.D. project in a highly efficient manner. Asst. Prof. Ulriksen provided great help and support throughout the execution phase of this project, especially in the field of structural dynamics. We had a lot of discussions which, hopefully, allowed me to think and act more consistently and rigorously. Looking back at the three years period of the Ph.D. project, I am grateful to have had Prof. Sørensen and Asst. Prof. Ulriksen as my academic supervisors.

The acknowledgment is extended to Ronnie Refstrup Pedersen from Ramboll, the main industrial Ph.D. supervisor. Ronnie was the first person I talked to about the idea of pursuing a Ph.D. degree. He not only supported me but also initiated and successfully executed the funding phase. My history with Ronnie started five years ago where we met at Aalborg University. Ronnie helped me get an internship at Ramboll, later supervised my M.Sc. project, and now is part of my Ph.D. journey. I would like to thank Ronnie for all the support he consistently provides.

Special gratitude is directed to Ursula Smolka and Ulf Tyge Tygesen who hosted me in their departments in Ramboll. Thanks to Ursula and her asset management team I had the opportunity to investigate the industrial need for

a digital twin in the offshore wind context. Ursula's insight into the business perspective allowed me to define and address some of the industrial needs in the Ph.D. project. Ulf Tyge Tygesen was very kind to share his experience and knowledge in developing and applying the True Digital Twin concept as Ramboll's state-of-the-art solution for oil and gas structures. His practical and conceptual insight helped me to understand the digital twin concept deeply.

Finally, I want to thank my family for their moral support, which helps me to strive in the challenging times and allows me to share and enjoy the highlights.

Dawid Augustyn
Aalborg University, November 11, 2021

Abstract

Offshore wind industry is constantly developing and is economically competitive with other renewable energy sources (nuclear, hydro, and solar) and even with conventional energy sources (coal, oil and gas). In order to maintain such a development pace, the costs of offshore wind structures must be driven even lower with a high focus on sustainability. We can achieve this by developing new structures more optimally (cost-wise) and by operating the existing ones longer. The design and operation methods are constantly being improved to generate more sustainable structures, mostly by understanding from where the conservatism inherent in design procedures comes and optimizing design procedures accordingly. One way to obtain such insight is by utilizing data from existing structures in a digital twin framework.

A digital twin is a virtual (digital) copy of a physical asset. A digital twin is realized by combining numerical models and measurement data. Such combination allows for establishing models that in an optimal way reflect in-situ responses of a structure. Digital twins have been successfully applied in a number of industries, resulting in improvements in the designs and operation of various mechanical and civil structures. Digital twins can, for example, be used to optimize the performance of an asset, to monitor its structural integrity, to plan repairs, and to manage risks. All these activities consequently drive costs down and thereby provide more sustainable structures. A similar potential can, in principle, be utilized for offshore wind structures. In fact, digital twins, at least to some degree, are being applied for the mechanical parts of wind turbines. However, applications of digital twins to structural parts, especially for substructures, are limited.

This thesis investigates the application of a digital twin concept to offshore wind jacket substructures. An existing state-of-the-art conceptual framework, initially developed for the oil and gas application, is extended to the offshore wind application. The theoretical and practical feasibility of the digital twin framework is investigated, accounting for offshore wind-specific challenges and limitations. Moreover, the thesis presents practical case studies exemplifying the benefit of digital twins for both existing and new substructures. The contributions of this thesis consist of 1) defining procedures for establishing

a digital twin of offshore wind jacket substructures and, subsequently, 2) applying the established digital twins to improve decision models of existing and new substructures.

The thesis presents numerical and experimental feasibility studies on how a digital twin can be established for an operating offshore wind jacket substructure. Specifically, practical feasibility studies covering the first two steps of in the proposed digital twin framework, namely, system identification and model updating, are provided. Subsequently, virtual sensing methods are investigated to obtain full-field measurements based on a few measurements in easy-access locations.

In the context of application of the digital twin concept, which is the second main contribution of this thesis, a probabilistic framework for optimizing decision models is proposed. In the framework, the established digital twins can be applied in order to improve decision models for existing structures (optimizing operation and maintenance) and for new structures (optimizing design of new structures). The framework applies state-of-the-art probabilistic methods, where the standard, generic-based uncertainties are substituted with the uncertainties quantified for specific structures based on information from digital twins. Subsequently, the structural reliability can be updated to reflect accurate and precise information on the structural integrity, which finally can be used to optimize decision models. The decision models can be updated based on the Bayesian decision theory, applying posterior and pre-posterior analyses for existing structures and pre-posterior analysis for new structures.

Resumé

Havvindenergi udvikler sig konstant og kan økonomisk konkurrere med andre vedvarende energikilder (atomkraft, vandkraft og sol) og endda med konventionelle energikilder (kul, olie og gas). For at opretholde et sådant udviklingstempo skal omkostningerne for havvindkonstruktioner reduceres endnu mere med et dedikeret fokus på bæredygtighed. Dette kan opnås ved at udvikle kost-effektive innovative nye konstruktioner og benytte de eksisterende i længere tid. Design- og driftsmetoderne bør forbedres konstant for at opnå mere bæredygtige og kost-effektive konstruktioner; primært ved at forstå, hvor konservatismer kommer fra, og optimere designprocedurer i overensstemmelse hermed. En måde, hvorpå en sådan indsigt kan opnås, er ved at bruge data fra eksisterende konstruktioner i en digital tvilling-formulering.

En digital tvilling er en virtuel (digital) kopi af et fysisk system. En digital tvilling realiseres ved at kombinere numeriske modeller og måledata. En sådan kombination gør det muligt at etablere modeller, der på en optimal måde afspejler opførslen af en konstruktion. Digitale tvillinger er blevet anvendt med succes i en række industrier, hvilket har resulteret i forbedringer i design og drift af forskellige mekaniske og civile konstruktioner. Digitale tvillinger kan eksempelvis bruges til at optimere et systems ydeevne, overvåge strukturel integritet, planlægge reparationer og styre risici. Alle disse aktiviteter driver omkostningerne ned og giver derved mere bæredygtige konstruktioner. Et lignende potentiale kan i princippet udnyttes for havvindkonstruktioner. Faktisk er digitale tvillinger, i det mindste til en vis grad, allerede blevet anvendt for de mekaniske dele af vindmøller. Imidlertid er anvendelsen af digitale tvillinger for konstruktionsdele, især for jacket- og monopile-fundamenter, dog begrænset.

Denne afhandling undersøger anvendelsen af et digitalt tvillingekoncept for havkonstruktioner til havvind. En eksisterende konceptuel ramme, der oprindeligt blev udviklet til olie- og gasapplikationer, udvides til at omfatte offshore-vindapplikationen. Den teoretiske og praktiske gennemførlighed af den digitale tvilling-formulering undersøges, idet der tages højde for offshore-vindspecifikke udfordringer og begrænsninger. Desuden præsenteres prak-

tiske casestudier, der eksemplificerer fordelene ved digitale tvillinger til både
eksisterende og nye konstruktioner. Bidragene i denne afhandling består
af 1) at definere procedurer for etablering af en digital tvilling og efter-
følgende 2) anvendelse af de etablerede digitale tvillinger til forbedring af
beslutningsmodeller for eksisterende og nye konstruktioner.

I afhandlingen præsenteres numeriske og eksperimentelle undersøgelser,
der dokumenterer, hvordan en digital tvilling kan etableres for en opererende
offshore-jacket-understruktur. Konkret leveres praktiske undersøgelser, der
dækker de to første trin i etableringen af en digital tvilling, nemlig sys-
temidentifikation og modelopdatering. Efterfølgende undersøges virtuelle
målemetoder for at opnå fuldstændige feltmålinger baseret på nogle få måle-
positioner, der er placeret på lettilgængelige steder.

I forbindelse med digital tvilling-applikationer, som er det andet hoved-
bidrag i denne afhandling, foreslås en probabilistisk procedure for etablering
af optimale beslutningsmodeller. De etablerede digitale tvillinger kan an-
vendes til at forbedre beslutningsmodeller for eksisterende konstruktioner
(optimering af drift og vedligeholdelse) og nye konstruktioner (optimering
af design af nye konstruktioner). Den foreslåede procedure anvender state-
of-the-art probabilistiske metoder, hvormed generiske usikkerheder erstat-
tes med usikkerhederne kvantificeret for specifikke konstruktioner baseret
på information fra digitale tvillinger. Efterfølgende kan den strukturelle
pålidelighed opdateres til at afspejle nøjagtige og præcise oplysninger om
den strukturelle integritet, som endelig kan bruges til at optimere beslut-
ningsmodeller. Beslutningsmodellerne kan opdateres baseret på Bayesiansk
beslutningsteori i forbindelse med posterior og pre-posterior analyser for ek-
sisterende konstruktioner og pre-posterior analyse for nye konstruktioner.

Contents

Contents

Part I

Thesis

Chapter 1

Introduction

The offshore wind industry plays a vital role in the energy transformation that we are experiencing at the moment (U.S. Department of Energy, 2018). The offshore wind leading role was made possible due to major cost reductions observed for the last years (Wind Europe, 2020). A large portion of this cost reduction is attributed to maturing the technology, standardizing productions, and gaining experience in developing offshore wind farms. As a result, 5,402 offshore wind turbines were operating in 2020 in Europe alone (Wind Europe, 2020). These structures will approach their design lifetime in the next 10-15 years, see Fig. 1.1. For example, in 2030 approximately 1,000 structures will exceed 20 years in operation, which is a typical lifetime for an offshore wind turbine. The number of structures older than 20 years is growing rapidly and will reach 3,000 in 2035. Consequently, the wind farm operators will have to develop methodologies to decide what to do with their assets, thereby developing end-of-life strategies.

Assuming no additional actions are taken, a structure reaching its intended lifetime must be decommissioned as its structural integrity, assessed based on standard design practices, is compromised due to degradation phenomena, such as corrosion, scour, and fatigue damage accumulation. Operators realized that there might be more cost-effective and sustainable solutions. One potential avenue is to explore end-of-life strategies (Pakenham et al., 2021; Velenturf, 2021). Instead of decommissioning, depending on the asset condition, an operator can consider partial decommissioning, partial repowering (exchanging some parts of the structure), full repowering (exchanging a structure completely), or lifetime extension. The strategy not to decommission is based on the premise that despite design predictions, there is still some reserve in the structure that allows for operating it longer. This can be the case if the structure has experienced, for example, less harsh loads during its lifetime, less uncertainty than assumed at the design stage, or conserva-
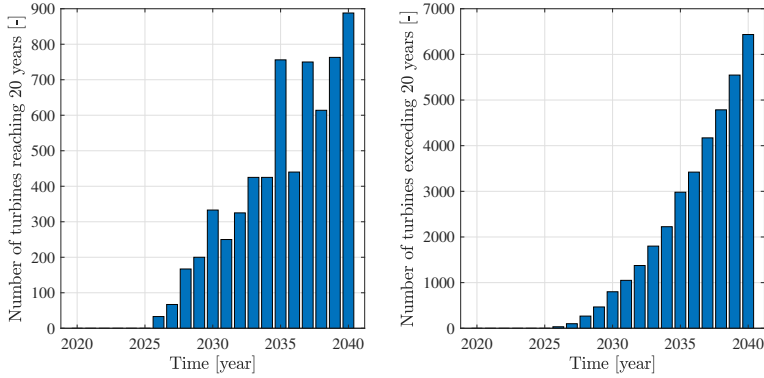
Fig. 1.1: Number of offshore wind turbines worldwide reaching (left) and exceeding (right) 20 years in operation. Data from (Global Wind Energy Council, 2020; Wind Europe, 2020).

tive design assumptions were made regarding, for example, a wind turbine class. In fact, such case is not uncommon, as many measurement campaigns indicate a large gap between the design predictions and the in-situ measured responses (Bom et al., 2020; Devriendt et al., 2013; Häckell and Rolfes, 2013). By understanding the origin of this gap, we can improve both the existing and new structures. The improvement of the former can be realized by optimizing operation and maintenance, thereby reducing costs related to the operation of structures (OPEX), or allowing for lifetime extension, and thereby increasing the revenue. New structures can be optimized by using knowledge gained from existing structures by indicating where the design standards are conservative and by removing this conservatism at the design stage, hence optimizing costs related to the commissioning of new structures (CAPEX). No matter which optimization strategy is sought, an accurate and precise estimation of the structural reliability (either relative or absolute) is key in making an end-of-life decision. One possible technology that can be utilized to gain such insight is a digital twin technology.

1.1 Motivation

The digital twin, in the context of structural dynamics, reliability assessment, and decision-making can be defined as *a virtual duplicate of a system built from a fusion of models and data* (Wagg et al., 2020). The key benefit in applying digital twin technology is its improved predictive capabilities compared with state-of-the-art numerical models developed based on the design standards. The improvement is attributed to new information attained from measurement data available in different format on different platforms that brings unique

knowledge about a specific structure. This allows for online updating of numerical models (physics-based or data-driven) to reflect in an optimal way conditions of an in-situ structure (physical twin). The improved prediction capacity is twofold; a digital twin is 1) more accurate (the mean value of predictions based on a digital twin is closer to the measurements) and 2) more precise (variance and thereby the uncertainty of digital twin predictions is reduced). The first aspect is obvious; the more precise estimation we have, the more optimal decisions we can make. However, the second one is not so well investigated, despite its potential to be equally as valuable if combined with appropriate methods, such as probabilistic, reliability-based methods. The reduced (or at least quantified) uncertainty in prediction can be utilized in a probabilistic context to update structural reliability, which is used to determine the fatigue lifetime and extreme load effects of existing structures and design parameters (structural dimensions) for new structures.

The paradigm of the digital twin as a tool to aid decision-making in asset management is well-known and has been successfully applied in multiple industries. The first application is attributed to the work of NASA in the context of the Apollo program in 1970. Subsequently, applications in the aerospace engineering, automotive, nuclear fusion, bridge engineering, and offshore structures followed. The potential of the digital twin technology is also being investigated for the offshore wind industry; although currently studies mostly focus on feasibility and conceptual level.

To further mature the digital twin technology in the context of offshore wind applications, some research projects have been proposed; for example, in the context of structural health monitoring (Ye et al., 2020), and more specifically in the wind turbine blades (Sayer et al., 2020) application. The decision to investigate health of wind turbine blades is driven by the high cost and probability of failure of this component. Hence, having a tool that can predict damage and can be coupled for predictive maintenance is highly valuable. However, especially for the remaining parts of the structure, research effort is rather limited. This component requires further attention due to its vital role in structural safety and the fact that it cannot be replaced without substantial cost involved. Consequently, support structures have been given large reliability requirements, which in many cases result in a conservative design, especially if varying reliability is assumed across the structural components. As a result, we might end up in a situation where the structural components like blades are designed to the limit, while the support structures are over-designed. To address this issue more interest in the support structure should be dedicated and in the first place to investigate and quantify the conservatism inherent in the current standards. Subsequently, a decision can be made if we want to keep having (hidden) conservatism in the standards, or if we decide to use it to optimize new structures. The outcome is not straightforward, and will not be addressed in this thesis (as there are

different business cases and cost optimization, especially CAPEX/OPEX is dependent on specific business cases and risk strategies taken by the operator). However, this thesis provides an investigation into establishing digital twins and subsequently generating value from digital twins.

Digital twin concept

Offshore wind structures are designed to sustain external environmental loads and operational loads induced by wind turbines. To make sure each structure is designed optimally, a number of design checks are performed, called limit states. Among others, an ultimate limit state and a fatigue limit state are considered. The ultimate limit state considers structural response to an extreme event (extreme loads with a low probability of occurrence), for example, a storm, hurricane, or earthquake but also unexpected events during operation, for example loss of electrical grid or failure of an electrical component. In this limit state, the structural stability is confirmed, including no buckling nor excessive yielding. The fatigue limit state is considered in the condition of normal operation, where loads of low to medium magnitude are present with a high probability of occurrence. In this instance, it is confirmed that a fatigue-induced crack does not exceed a critical value when uncontrolled cracking is initiated hence jeopardizing structural integrity. Other limit states, such as serviceability or accidental states, might also be required. Even though all components must fulfill all limit states, typically some limit states are critical for particular structural components. For example, the pile penetration length is typically determined based on the extreme limit state where an emergency shut down occurs, creating maximum compression loads in the piles. Joints (K/T joints in jackets or circumferential welds in monopiles) are typically driven by fatigue limit state due to excessive fatigue damage accumulation when a large number of cycles is accumulated due to wave and wind action.

Typically, joints are the most critical parts of a jacket structure and their fatigue design determines the lifetime of a structure. Hence, in this thesis, focus is given on developing a digital twin aiming at accurate and precise estimation of fatigue damage accumulation for joints and other fatigue-driven structural components. As a result we focus on normal production cases where most of the fatigue damage is generated; extreme cases are not considered. Among a number of developed digital twin frameworks, one that focuses specifically on the fatigue damage is the one initially proposed and applied on a conceptual level to oil and gas structures (Tygesen et al., 2018, 2019). The framework has an additional benefit in the context of the offshore wind application, as it was developed for oil and gas structures, which share some similarities with offshore wind structures; for example, the presence of wave loading. The framework has initially been investigated for offshore
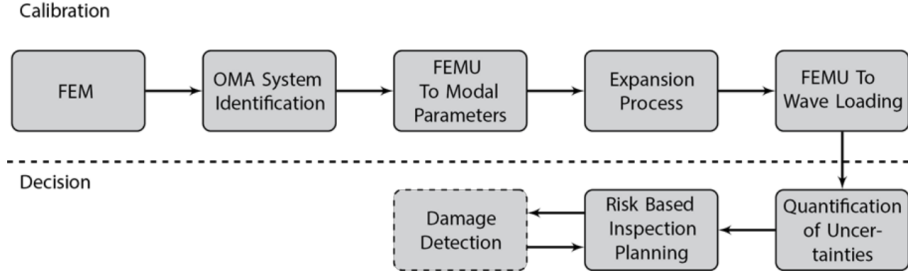
Fig. 1.2: Digital twin framework for improved decision models in an offshore oil and gas application (Tygesen et al., 2018, 2019).

wind application (Augustyn et al., 2019) and positive conclusions regarding its feasibility have been provided. Note that this framework, at least in the main steps, is consistent with the generic digital twin framework provided recently by (Wagg et al., 2020). Consequently, the (Tygesen et al., 2018, 2019) framework is considered as a state-of-the-art digital twin in the oil and gas context and will be further developed in this thesis for the offshore wind application.

The framework (Tygesen et al., 2018, 2019) is visualized in Fig 1.2 and briefly summarized in the following part of this section. The framework is divided into two main parts: calibration and decision.

Calibration

Calibration aims at updating structural and load models to increase the correlation between numerical predictions (digital twin) and in-situ measurements (physical twin). The process of establishing a digital twin consists of the following steps: 1) establishing a numerical model (FEM), 2) system identification based on operational modal analysis (OMA), 3) finite element (structural) model updating (FEMU) based on identified modal parameters, 4) expansion process to obtain structural responses in unmeasured locations, and 5) finite element (wave load) model updating based on measured wave input and expanded responses.

FEM A finite element model (FEM) consists of an initial numerical model which might be based on some measurement data. The initial numerical model reflects our best knowledge about the structural behavior of a physical twin represented by mass, stiffness, and damping parameters combined with a load model. Typically, the structural model and the load model are based on design assumptions and knowledge acquired at this stage of the structural life-cycle. After the structure is commissioned, new information becomes available, for example, as-built geometry and in-situ installation parameters

5

(exact pile penetration, secondary steel masses, and so forth). After some time of operation, measurement data reflecting the operational response of a structure can be collected, for example accelerations, strains, and inclinations. All this information can be used as data input for developing a digital twin, which is the subsequent step.

OMA System identification   The process of establishing a digital twin progresses with estimating features describing an in-situ system. Among a number of possible features, modal parameters are used extensively for dynamically sensitive structures. This choice is made due to the simplicity of extracting these parameters by means of system identification methods. Once the modal parameters are estimated they can be compared to the numerical predictions from the initial model.

FEMU To Modal Parameters   Given a large discrepancy is identified between in-situ and model-estimated features, the parameters of the numerical model are updated to minimize the discrepancy. In this step, only the parameters related to the structural model affecting the system's mass, damping, and stiffness are updated.

Expansion process   Due to practical reasons, responses are recorded in a few limited locations on the structure; typically in easy access locations above water level. In order to be able to calibrate the load model representative for all structural locations, we need to apply methods to estimate responses in all unmeasured locations. Expansion methods can be applied to obtain responses in unmeasured locations based on response measured in a few locations.

FEMU To Wave Loading   Load calibration aims at updating load models in order to reflect in an optimal way structural responses due to external load actions. For a typical oil and gas structure–for which the framework (Tygesen et al., 2018, 2019) is developed–wave loading is the major source of external loading, hence in this framework only the wave loading model is calibrated. Once the load models and structural model are updated, the updated models constitute the digital twin on level 3 according to (Wagg et al., 2020).

Decision

Based on the previous steps the decision model can be inferred. In the proposed framework, a decision model related to fatigue damage accumulation is considered.

Quantification of uncertainties The uncertainties associated with fatigue damage accumulation are modeled and quantified based on in-situ measurements and numerical model predictions.

Risk based Inspection Planning After the uncertainties (including mean value and variance) have been updated, a probabilistic model is used where these uncertainties are included and the structural reliability related to the fatigue limit state is updated. After the structural reliability is updated, it serves as input to decision models, which are used to derive economically optimal decisions for operation of existing structures. In the application to the oil and gas structures, this includes risk based inspection planning.

Damage Detection The framework allows for including information obtained from structural health algorithms to be incorporated in the risk based inspection planning. Such information can be used as an alternative to (expensive) physical inspection.

Limitation

The framework (Tygesen et al., 2018, 2019) has been developed with oil and gas structures in mind. This means that some parts of the framework should be adjusted to optimally address offshore wind structures. In the context of the offshore wind application, an obvious limitation of this framework is the presence of a wind turbine structure. The wind turbine attracts significantly more wind loading which must be taken into account. Additionally, the wind turbine behave in a non-linear and time-variant manner due to a wind turbine control system, which potentially leads to a need for extending the existing methods applied in the existing framework. Finally, the decision models proposed in the framework are adjusted to the oil and gas structures. In the offshore wind application, the decision model can be different due to, for example remote placing of the structures, increased cost of inspections, reduced risk of human loss, or a different CAPEX/OPEX costs split. Consequently, the mentioned limitations are considered in this thesis and offshore wind specific adjustments are proposed.

1.2   Aim and scope

The aim of this thesis is to develop and apply a digital twin framework for offshore wind substructures. The focus is on reviewing existing framework and investigating the feasibility of one particular framework, best suited for an offshore wind application. For that purpose, the conceptual digital twin
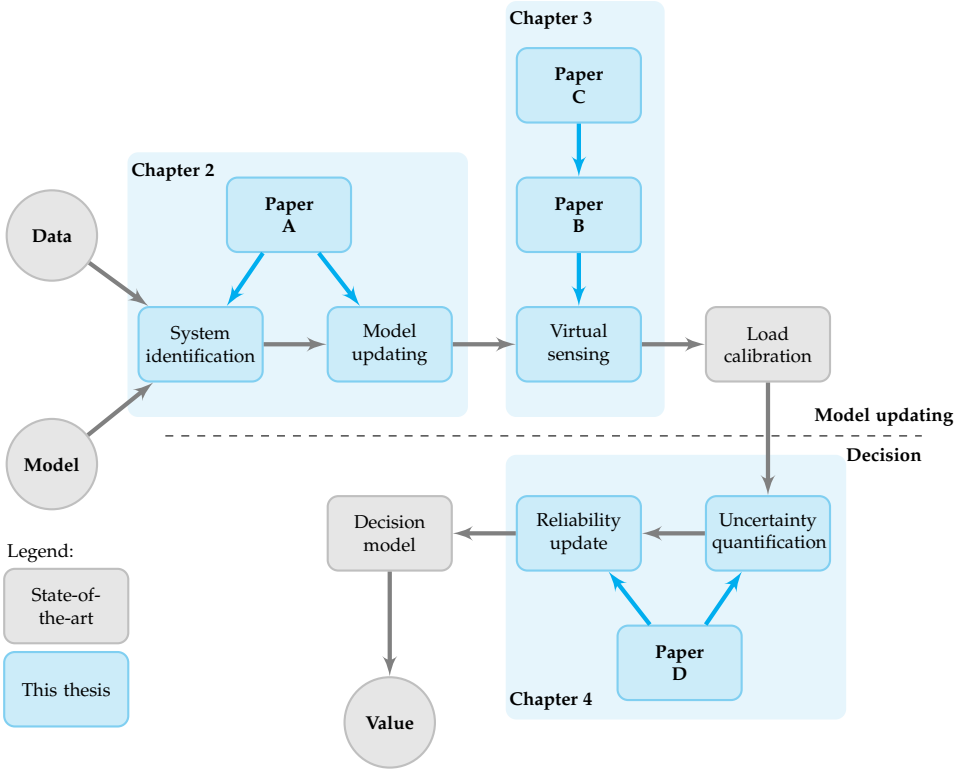
Fig. 1.3: Digital twin framework for improved decision models in the offshore wind application. The grey boxes indicate the state-of-the-art framework while the blue boxes indicate contributions developed in the course of this thesis. The new contributions are described in chapters 2-4 and papers A-D.

framework (Tygesen et al., 2018) initially developed for oil and gas structures is extended for the offshore wind substructures. The state-of-the-art framework and extensions addressed in this thesis are depicted in Fig. 1.3. The framework consists of a number of steps as initially indicated in (Tygesen et al., 2018). The state-of-the-art steps are indicated in grey. The required wind-related modifications, which are investigated in this thesis, are indicated in blue. Within each addressed step, a literature review is performed in order to choose a candidate method that would be best suited for an offshore wind application. Subsequently feasibility and limitations of the chosen methods are investigated based on the papers enclosed in this thesis. Depending on the maturity of the research field considered, an in-situ validation, numerical feasibility study, or theoretical development are considered. Wherever possible, the proposed digital twin framework applies well-established methods and procedures. It is important to notice that the

aim of this thesis is to investigate the feasibility of the digital twin technology in order to provide practical value. Hence, the focus is on practical applications rather than on the theoretical developments. The proposed framework is general for all types of substructures and other wind turbine components driven by fatigue limit state, for example tower and blades. However, the application studies are limited to jacket substructures. This type of substructure is chosen as it is widely applied in practice and can be expected to be used even more in the future when sites with larger water depths will be considered. Moreover, the jackets substructures provides some unique practical challenges, which have not yet been adequately addressed in the literature.

The following research questions and challenges are investigated in this thesis:

- How to establish a digital twin of an offshore wind jacket substructure?

  - Can existing system identification methods robustly and accurately estimate modal responses of in-situ offshore wind turbines?

  - How can structural model parameters be updated based on identified modal responses?

  - Can existing virtual sensing methods accurately and precisely predict vibrations of an offshore wind jacket substructure?

  - What is the impact of environmental and operational variability on modal parameters of an operating offshore wind turbine?

  - Can linear and time-invariant models approximate non-linear and time-variant systems?

- How can an established digital twin be utilized to improve decision models of existing wind turbine jacket substructures and optimize new substructures?

  - How to quantify uncertainty in fatigue damage accumulation from a digital twin?

  - How to update reliability estimates based on quantified uncertainty?

  - How to use information from a digital twin as a decision basis for assessment of existing and design of new wind turbine jacket substructures?

The research questions are investigated in the four papers summarized and discussed in chapters 2 to 4. The papers and their relation to specific boxes of the digital twin framework are indicated in Fig. 1.3. Specifically, papers A to C are related to establishing a digital twin and addressing challenges related to system identification, model updating, and virtual sensing.

Paper D introduces a framework on how the established digital twins can be used to improve decision models in an offshore wind context. Below, a brief summary of the four papers is provided with a focus on how these papers aim at answering the research questions.

Paper A presents an application study of system identification and subsequent model updating of an operational offshore wind jacket substructure. The effect of violating certain system identification assumptions (linear and time-invariant approximation of a non-linear and time-variant system) on the uncertainty of identified modal parameters is investigated. Subsequently, the numerical model parameters are updated to better reflect the identified modal parameters.

Paper B examines the theoretical feasibility of one particular virtual sensing method, namely modal expansion, for an offshore wind jacket substructure. The expansion of wave-induced vibrations is improved. The uncertainty related to model expansion—which forms an input to the study documented in paper D—is quantified.

Paper C investigates the environmental and operational variability of coupled wind turbines and substructures. The impact of such variability on modal parameters is investigated. The study further explores the reduction in expansion quality reported in paper B.

Paper D introduces a method to include established digital twins in a probabilistic framework for structural reliability reassessment. A method to quantify uncertainty based on digital twin information is proposed. The quantified uncertainty is subsequently used to update structural reliability which can be used as input to updating decision models.

1.3 Outline

The remainder of the thesis consists of four chapters and four appendices that contain the papers written during the course of this thesis. This section offers a brief outline of the content in Chapters 2 to 5 and Appendices A to D. The thesis is constructed in a way that aims at describing the whole process of establishing a digital twin according to the framework presented in Fig. 1.3.

Chapter 2 presents the basic theory and principles of system identification and model updating. The selected state-of-the-art method is applied. The

method is exemplified based on data from an operating offshore wind turbine. Paper A documents this work. Challenges and limitations associated with the applied method are indicated, and a discussion on a potential mitigation of limitations is provided.

Chapter 3 presents a review of virtual sensing methods and an application study. A particular method, namely modal expansion, is applied in the context of an offshore wind turbine jacket substructure with different sensor configurations considered. Particular limitations are addressed, namely wave expansion and wind turbine-substructure coupling based on the work described in papers B and C.

Chapter 4 introduces a framework where information from the established digital twins can be used to optimize decision models. A probabilistic model for reliability update of a fatigue-driven component is presented. A method is proposed to quantify the portion of total uncertainty related to the structural dynamics and load model. The chapter is based on the work presented in Paper D.

Chapter 5 concludes the main body of the thesis with a summary and discussion of the material presented. The main results achieved in the project are outlined, and suggestions for future work are provided.

Appendix A contains Paper A by Augustyn et al. (2020), titled: *Data-driven model updating of an offshore wind jacket substructure*.

Appendix B contains Paper B by Augustyn et al. (2021), titled: *Feasibility of modal expansion for virtual sensing in offshore wind jacket substructures*.

Appendix C contains Paper C by Augustyn et al. (2021), titled: *On the influence of environmental and operational variability on modal parameters of offshore wind support structures*.

Appendix D contains Paper D by Augustyn et al. (2021), titled: *Reliability Updating of Offshore Wind Substructures by Use of Digital Twin Information*.

Chapter 1. Introduction

Chapter 2

System identification and model updating
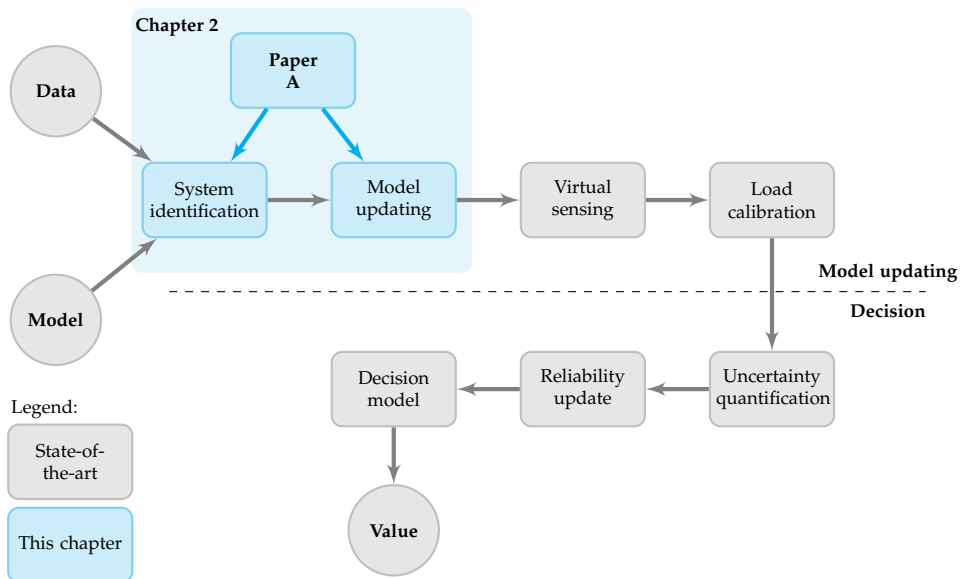
Fig. 2.1: Digital twin framework for improved decision models in the offshore wind application. The blue boxes indicate the parts of the framework discussed in chapter 2.

This chapter describes parts of the digital twin framework related to system identification and model updating as indicated in Fig. 2.1. In section 2.1, the state-of-the-art system identification and model updating methods are reviewed, and challenges associated with existing methods in the context of an

offshore wind application are provided. In section 2.2 an application study of system identification and model updating based on in-situ measurements of a particular jacket substructure is summarized based on the study described in paper A. The chapter closes with a summary provided in section 2.3.

2.1 State-of-the-art

In the present section, state-of-the-art methods for system identification and model updating are briefly described. The review merely aims at providing a general overview of the existing methods including limitations and merits for the particular offshore wind application. Based on that review, the method with the largest merit in the offshore wind application is considered for use in the digital twin framework. Limitations and challenges previously mentioned in the literature are highlighted and a few selected ones, which have not been addressed in the literature, are further investigated in section 2.2 based on the study described in paper A.

Regarding model updating, various methods have been validated for aerospace and automotive applications (Patelli et al., 2017; , Schedlinski et al.), for wind turbine blade structures (Luczak et al., 2014), and recently also for updating soil stiffness of a jacket substructure excluding a turbine superstructure (Bom et al., 2020). However, to the author's knowledge, no dedicated application study has been presented for model updating of a complete, operating offshore wind turbine jacket substructure.

The focus of this chapter is on investigating the feasibility of a selected system identification method for estimating modal parameters of an operating offshore wind turbine structure. Subsequently, the identified modal parameters are used as target features for model updating to improve the precision of an initial numerical model.

2.1.1 System identification

System identification methods aim at inferring a mathematical model of a dynamical system based on measured data. The modal parameters are inferred from the estimated parameters of the mathematical model. The system identification methods, for the purpose of this study, are categorized into three levels which are briefly discussed in this subsection. The levels are distinguished based on availability of input signals (level 1), domain of operation (level 2), and particular methods considered for offshore wind application (level 3). The categories are depicted in Fig. 2.2. The review is confined to identification of linear systems. For non-linear surveys, the reader is referred to the studies by (Kerschen et al., 2006) or (Noël and Kerschen, 2017).
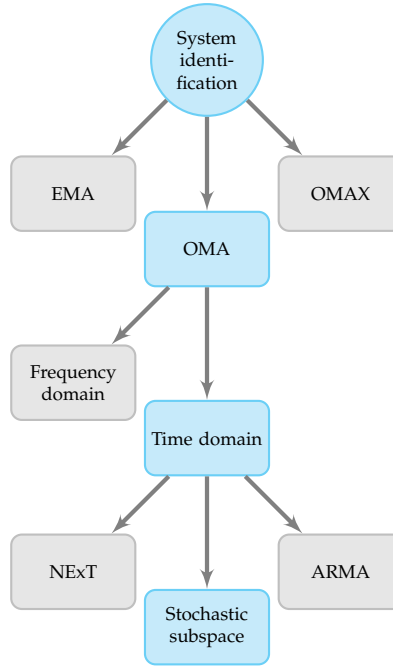
Fig. 2.2: Overview of linear system identification methods for engineering structures. The blue color indicates the approach/method applied in the digital twin framework.

Level 1: input signal

The system identification methods can be divided into three categories based on the type of data used in the procedure:

- Experimental modal analysis (EMA). In this approach, the input (excitation) and the output (response) of the system are measured. This approach is interchangeably called the deterministic or input-output.

- Operational modal analysis (OMA). In this approach, only the output is measured while for the input a statistical model with unknown parameters is assumed. This approach is called the stochastic (as unmeasured input is modeled in a stochastic manner) or output-only.

- Operational modal analysis with exogenous inputs (OMAX). In this approach, both the input and the output is used. OMAX combines EMA and OMA, where the excitation is measured and operational input is assumed stochastic.

The main distinguishing factor between the three approaches is the modeling of the input. An overview of input modeling for the three approaches is presented in Fig. 2.3.

Experimental modal analysis   Historically, the EMA approach has been developed first. This approach typically offers high accuracy of estimation in controlled, laboratory conditions. The EMA approach is, among others, used for modal testing of mechanical structures where the excitation is provided by, for example hammers or shakers with known input and where the response is measured in a number of output locations. The most widely used EMA approach is the frequency response function (FRF) method (Ewins, 2009), where the output in frequency domain is normalized by the input in frequency domain. The modal parameters are estimated by fitting a numerical model to results from the FRF. Other well-known EMA methods include the peak picking method (Bendat and Piersol, 1980), the circle fitting method (Kennedy and Pancu, 1947), the eigensystem realization algorithm (ERA) (Juang and Pappa, 1985), the extended Ibrahim method, and the polyreference complex exponential (PRCE) method. For a broad review of EMA methods, the interested reader is referred to (Heylen and Sas, 2005).

The main limitation of the EMA approach is related to a measured input; the input that must be known. The vast majority of civil structures are excited by uncontrolled ambient excitation, which is not straightforward to measure; for example, excited by traffic, wind, or waves. To address this challenge, the output-only approach has been developed.

Operational modal analysis   The OMA approach, otherwise known as the output-only approach, requires only the system's output in natural (operational) conditions. The methods adhering to the OMA approach are well-fitted for civil structures that cannot be excited by actuators and whene ambient loading cannot be neglected. The OMA approach assumes that the unmeasured, operational loading can be modeled by a stochastic process with unknown (yet to be estimated) properties, following some known behavior, for example, the white noise process. Among a number of output-only methods, the stochastic subspace identification (SSI) method is applied widely for civil engineering applications. Other well-known OMA methods include the natural excitation technique (NExT) and the auto-regression moving average (ARMA) method.

The main limitation of OMA approach lays in the assumption of the nature of the stochastic input. In many cases, the unmeasured, ambient excitation does not adhere to the properties of, for example, the white noise process. Consequently, not all of the modes can be excited, and the excited ones will be estimated with increased variance. Hence, in recent years there has been some research in combining the EMA and OMA approaches.

Operational modal analysis with exogenous input   The OMAX approach combines the unmeasured operational loading ever-present in civil struc-

Experimental Modal Analysis (EMA)   Operational Modal Analysis (OMA)   Operational Modal Analysis
with eXogenous inputs (OMAX)

$u^d(t)$ $\dot{u}^d(t)$ $u^d(t)$

| structure | | structure | | structure |

$\dot{u}^s(t)$ $y(t)$ $u^s(t)$ $y(t)$ $u^s(t)$ $y(t)$
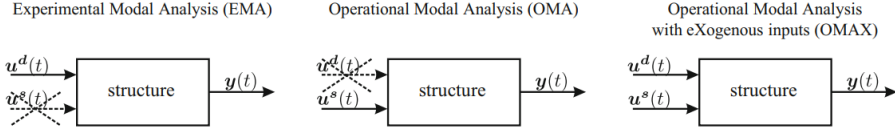
Fig. 2.3: Comparison of the EMA, OMA, and OMAX approaches to system identification (Reynders et al., 2010).

tures with artificial, measured excitation. One of the main advantages of this approach over EMA is that the unmeasured operational loading is included. The artificial excitation is included as known input, which is an extension compared to stochastic input in OMA methods. A few OMAX methods have been applied to civil structures, for example, the least-squares frequency domain (CLSF-IO) method (Cauberghe et al., 2003) and the combined deterministic-stochastic subspace identification (CSI) method (Reynders and Roeck, 2008; Reynders et al., 2010).

Despite the obvious advantages, the OMAX approach is still in the research phase. In the context of an offshore wind application, the main limitations at the moment lay in the application of external actuators. In an attempt to resolve this challenge, some researchers have recently started to explore the feasibility of using pitch excitation as deterministic input (Schwarz-Wolf et al., 2021; Ulriksen et al., 2021).

Discussion   The OMA approach is chosen for the digital twin application. Some discussion on the merit of the OMA method over the EMA and OMAX methods for the digital twin application of offshore wind substructures is presented below.

- It is impractical and expensive to measure external (ambient) loading or apply artificial excitation. The EMA approach is difficult to implement for large civil structures.

- OMA and OMAX estimate modal parameters for operational, in-situ conditions. If modal parameters are prone to operational and environmental variability the estimated modal parameters for a specific realization of the environmental and operational parameters may reflect such variability. This is, however, not the case for EMA, where the external (artificial) excitation is provided while the ambient excitation is assumed insignificant.

- In the context of offshore wind applications, variation in soil stiffness (load level dependent), damping (wind speed dependent), water level variation, and mode shapes (wind turbine-substructure variation) can be important.

Level 2: domain of operation

The OMA methods can be further classified based on the domain in which a particular method operates:

- frequency-domain

- time-domain

Frequency-domain   The frequency-domain (FD) OMA approach converts the measured temporal output into the frequency-domain, typically by using some variation of the fast Fourier transformation (FFT). Among a multitude of FD methods, the typical applications for civil structures are the complex model indication function (CMIF) method (Shih et al., 1988) and the polyreference least-squares complex frequency-domain (pLSCF) method—known under its commercial name polyMAX (Peeters et al., 2004). The former can be seen as an output-only version of the peak picking method. The latter has been initially developed for a fast, first estimation of the computationally demanding maximum-likelihood method. Some of the main limitations of the FD methods, summarized by (Shokravi et al., 2020), include poor quality of estimates of low-frequency content (Liu et al., 2011) and inaccurate damping estimates (Magalhães et al., 2007). The strive for improved accuracy compared to FD methods lead to the development of the time-domain OMA approach.

Time-domain   The time-domain (TD) OMA methods take advantage of the fact that measurements include time-series of vibration responses of the structure. The response time-series are analyzed by applying an observer gain matrix, a free decay function, or QR decomposition. The inputs to the system can be estimated by using auto- or cross-correlation functions. The modal parameters of a system are estimated by applying, for example, singular value decomposition, least-squares, QR decomposition, or eigenvector decomposition. The main advantage of the TD methods compared to the FD methods lies in the direct processing of time-series, which is suited for continuous monitoring.

Among the TD OMA methods, three major types of methods are typically distinguished:

- Natural excitation technique (NExT)

- Auto-regressive moving average (ARMA)

- Stochastic Subspace identification (SSI)

Discussion   The time domain approach is chosen for the digital twin application. A few points on choosing the time over the frequency domain approach in the context of offshore wind applications are provided below.

- Measurements consist of time-series of vibrations (accelerations, strains, inclinations).

- TD approaches use time-series directly.

- FD approaches require an additional pre-processing step to convert TD output into FD.

- No benefit of using specific FD methods, as most of the successfully applied FD methods have their TD equivalent.

- The time-domain approach extracts more complete sets of modal parameters, especially when a large number of modes exists in a wide frequency range (Shokravi et al., 2020).

- On the contrary, one merit associated with FD approaches is the interpretability.

Level 3: considered methods

Basd on the discussion provided above the following three methods are considered for application in the proposed digital twin framework.

Natural excitation technique   The NExT method was developed to address the issue of noisy signals in combination with EMA methods (Reynders, 2012). The method assumes that the output containing the response of the structure to random excitation can be computed using correlation functions and expressed as a summation of decaying sinusoids. The modal properties of each sinusoid correspond to the modal parameters of an eigenmode of the structural system. The NExt methods include the least-squares complex exponential method (Vold et al., 1982), the polyreference complex exponential (PRCE) method, the eigensystem realization algorithm observer Kalman filter identification (ERA-OKID) method (Juang, 1994), and the ouptut-only observer Kalman filter identification (O3KID) method (Vicario et al., 2015). Many of these methods are initially developed for the EMA approach, and then they have been adapted to the OMA setting (with stochastic input) by implementing correlation matrices. Successful applications of NExt methods have been demonstrated for civil structures, including wind turbines (James et al., 1993).

Auto-regressive moving average   The auto-regressive moving average (ARMA) method is an example of the prediction-error method (PEM) where the model parameters are estimated by minimizing the prediction error. The method applies a non-parametric approach, where varying polynomials are applied. The auto-regressive part of the model approximates the linear time-history of the output, while the moving average captures the varying part of the response. Depending on the level of sophistication of the used polynomials, the ARMA method can be rather simple (representing a mass-spring system) or complex (representing a multi-degree of freedom system). A number of application studies have been documented (Bertha and Golinval, 2017; Bodeux and Golinval, 2003; Huang, 2001). However, the method performs poorly when large systems are analyzed. Moreover, the method suffers from numerical instabilities due to non-linear optimization.

Stochastic subspace identification   The stochastic subspace identification (SSI) methods provides a framework for estimating modal parameters of a dynamic system. The method makes use of a parametric framework, estimating parameters of a state-space model. The SSI methods are particularly efficient in estimating parameters of multivariable systems (Gil et al., 2015). The two most used SSI methods include the covariance-driven (SSI-cov) method and the data-driven (SSI-data) method. The former is a two-step method where the output time-series are used to estimate correlation functions (covariance of the unknown input), while the data-driven method is directly from the measured outputs.

The main advantage of the SSI methods lay in its efficiency and accuracy, compared to the remaining TD OMA methods. On the other hand, SSI methods require experience from a human operator to assess the appropriate model order, which, if chosen improperly, can lead to imprecise results (Magalhães et al., 2007).

Discussion   The SSI TD method is considered for further implementation and a brief discussion in comparison to the ARMA and NExT is provided below.

- The SSI method is computationally robust and effective as it employs well-established methods from linear algebra (RQ- and singular value decomposition). The results are, under the method's assumptions, unbiased.

- Although no strict asymptotic optimum is guaranteed (as for maximum likelihood methods), subspace methods yield precise results in practice (Reynders, 2012).

- Moreover, compared to other methods, the SSI TD method is rather accurate and efficient. The methods, in specific conditions, provide a more accurate estimate on damping compared to the ARMA method (Ceravolo and Abbiati, 2013) and a more reliable estimate on mode shapes compared to the NExT method (Moaveni et al., 2011)

- Several successful applications of the SSI method for onshore (Tcherniak et al., 2011; Zhao et al., 2020) and offshore wind turbine structures (Devriendt et al., 2013; Dong et al., 2014; Häckell and Rolfes, 2013) are presented in the literature.

System identification implementation

A number of system identification methods have been reviewed in this section. The focus is put on their limitations and applicability towards offshore wind substructures. Based on this review, the SSI method is chosen for further investigation. The basic theory of the SSI-cov method is briefly described.

The basic problem of SSI methods can be summarized as (van Overschee and de Moor, 1996):

- Given m output measurements and stochastic relations of the input, estimate the state sequences and the order of the unknown model which minimize the variance of the error of the state-space model outputs and the measured output.

- From the estimated state sequence, estimate the state and output matrices of the state-space system.

- Estimate modal parameters from the estimated state-space matrices.

Consider the state-space formulation of a stochastic LTI system (Augustyn et al., 2020):

$$\begin{bmatrix} \mathbf{x}_{i+1} \\ \mathbf{y}_i \end{bmatrix} = \begin{bmatrix} \mathbf{A} \\ \mathbf{C} \end{bmatrix} \mathbf{x}_i + \begin{bmatrix} \mathbf{w}_i \\ \mathbf{v}_i \end{bmatrix}, \tag{2.1}$$

where $\mathbf{x}_i \in \mathbb{R}^n$ and $\mathbf{y}_i \in \mathbb{R}^m$ are the state and output vectors for time instance t_i. $\mathbf{A} \in \mathbb{R}^{n \times n}$ and $\mathbf{C} \in \mathbb{R}^{m \times n}$ are the state and output matrices, respectively. The unknown (stochastic) input $\mathbf{w}_i \in \mathbb{R}^n$ and measurement noise $\mathbf{v}_i \in \mathbb{R}^m$ are modeled as zero mean, white-Gausian discrete sequences; thus, $\mathbf{w}_i \sim \mathcal{N}(\mathbf{0}, \boldsymbol{\Sigma}_W)$ and $\mathbf{v}_i \sim \mathcal{N}(\mathbf{0}, \boldsymbol{\Sigma}_v)$. Then the covariance matrices can be expressed as:

$$\mathbb{E}\left[\begin{pmatrix} \mathbf{w}_p \\ \mathbf{v}_p \end{pmatrix} \begin{pmatrix} \mathbf{w}_q^T & \mathbf{v}_q^T \end{pmatrix} \right] = \begin{bmatrix} \boldsymbol{\Sigma}_{\mathbf{w}} & \boldsymbol{\Sigma}_{\mathbf{wv}} \\ \boldsymbol{\Sigma}_{\mathbf{wv}}{}^T & \boldsymbol{\Sigma}_{\mathbf{v}} \end{bmatrix} \delta_{pq} \succcurlyeq 0, \tag{2.2}$$

where δ_{pq} is the Kronecker delta, $\mathbf{\Sigma}_w \in \mathbb{R}^{n \times n}$, $\mathbf{\Sigma}_v \in \mathbb{R}^{m \times m}$, and $\mathbf{\Sigma}_{wv} \in \mathbb{R}^{n \times m}$. Both noise contributions are assumed uncorrelated (spatially and temporally). The assumption is one of the main challenges when applying the SSI method in practical applications, as the external, ambient loading is never white-Gaussian. This challenge is discussed in the other part of this paragraph.

The state matrices can be estimated based on a number of numerical algorithms, for example, numerical algorithms for subspace state-space system identification (N4SID) (Van Overschee and De Moor, 1994), multivariable output-error state space (MOESP) (Verhaegen, 1994), and canonical variate analysis (CVA) (Larimore, 1990). The algorithms differ in their weighting matrices and algebraic ways to estimate the system matrices. Below a widely-used N4SID algorithm is used to exemplify the SSI implementation procedure (van Overschee and de Moor, 1996).

1. Calculate the oblique projections of future outputs

2. Calculate the singular value decomposition of the weighted oblique projections. Here the algorithms differ by assuming varying formulations of weighting matrices

3. Determine the system order. This step depends on the user. Some heuristic way of choosing the system order can be implemented based on stabilization diagrams (Rainieri and Fabbrocino, 2014)

4. Compute the observability matrix

5. Estimate the state sequence

6. Estimate the system matrices

For the full implementation, the reader can consult (van Overschee and de Moor, 1996). Below, the selected steps are presented.

Let $\mathbf{Y}_{i|i} \in \mathbb{R}^{m \times j}$ be the output block-Hankel matrix and $\hat{\mathbf{X}}_i \in \mathbb{R}^{n \times j}$ a state sequence estimate. The state-space matrices can then be estimated as

$$\begin{bmatrix} \hat{\mathbf{A}} \\ \hat{\mathbf{C}} \end{bmatrix} = \begin{bmatrix} \hat{\mathbf{X}}_{i+1} \\ \mathbf{Y}_{i|i} \end{bmatrix} \hat{\mathbf{X}}_i^{\dagger}, \tag{2.3}$$

where superscript $\dagger$ denotes Moore-Penrose pseudo-inverse. From $\hat{\mathbf{A}} \in \mathbb{R}^{n_s \times n_s}$ and $\hat{\mathbf{C}} \in \mathbb{R}^{m \times n_s}$, the eigenfrequencies, mode shapes, and damping ratios can be extracted.

Challenges related to system identification   The challenges related to system identification for offshore wind applications are discussed in paper A Augustyn et al. (2020). In the present, the main assumptions related to the SSI-cov method are summarized along with the validity of the assumptions in the offshore wind application.

The SSI-cov method hinges on three main assumptions:

- The system is LTI.

- The input is ergodic, white-Gaussian, and spatially and temporally uncorrelated.

- Linear viscous damping model is used.

An LTI system is convenient from a numerical point of view. However, each system exhibits some non-linear and time-variant characteristics. In the context of the offshore wind application, the non-linear behavior is present due to the turbine controller and partially due to non-linear soil characteristics. Moreover, the turbine controller adjusts its properties (yaw and pitch) to optimize power production as wind conditions vary over time. Consequently, the system exhibits time-variant characteristics.

The SSI-cov method models the input as white-Gaussian, ergodic, and uncorrelated both in time and space. The wind and wave properties change from one sea state to another, hence the ergodic assumption is violated. In addition, the frequency spectrum of both the wind and wave excitation does not adhere to the white-noise Gaussian model due to the peak period in the wave spectrum, rotating machinery, and the turbulence in the wind spectrum.

Finally, major assumptions are taken when modeling damping. In the state-space formulation in Eq. 2.1, a linear viscous damping model is used. The model is established on the classical distribution (Caughey and O'Kelly, 1965). Such a model is not suited for capturing all sources of damping present in the offshore wind application, for example, aerodynamic damping, soil damping, and hydrodynamic damping.

Despite the noted assumptions being violated for all practical applications, useful results have been documented when using the SSI-cov method for wind turbine and oil and gas applications. For example, the method was used to estimate modal parameters of onshore turbines (Tcherniak et al., 2011), offshore wind monopile wind turbines (Devriendt et al., 2013), and oil and gas offshore jacket platforms (Tygesen et al., 2018). Based on these successful applications, this thesis explores the applicability of the SSI-cov method for estimating modal parameters of an offshore wind turbine supported by a jacket substructure.

2.1.2   Model updating

Numerical models are widely used in engineering. Accurate numerical models allow for designing robust and economically feasible structures. The success of numerical model applications in engineering is based on the assumption that the numerical model can accurately and precisely mimic the behavior of an in-situ structure. A number of studies indicate a considerable discrepancy between predictions from numerical models and measurements (Bom et al., 2020; Luczak et al., 2014). The discrepancy arises from a number of simplifications, idealizations, uncertainties, and decisions made in the modeling phases. The sources of errors can be assigned into one of the three classes (Mottershead et al., 2011):

1. Idealization errors introduced when idealizing a physical system with a mechanical model, for example mass distribution, erroneous modeling of boundary conditions (especially soil-structure interaction) joint modeling, and approximating non-linear system with a linear model.

2. Discretization errors inherent in finite-dimensional models, for example mesh size.

3. Natural variation in physical parameters included in the model (aleatory uncertainty), for example material properties (Young's modulus, density), cross-section properties, stiffness, and added masses.

   The first two classes of errors can lead to significant errors if poor assumptions regarding idealization and discretization are taken. Ewins and Imregun (1988) documented large discrepancy in numerical model predictions obtained independently by 12 engineers. Recently, a similar study has been performed in the context of offshore wind modeling (Mühle et al., 2018), and despite significant improvement in the fidelity of numerical models, some variation has also been reported in the referred study.

   Assuming the idealization and discretization errors are negligible, some discrepancy can still be noticed due to parameter variation. Here, the model updating approach can be used. Model updating methods aim at reducing the discrepancy between model predictions and in-situ estimates of a given feature (vibration time-series, modal parameters, etc.). Historically, a number of methods have been investigated for model updating, including least-squares parameter estimation (Åström and Eykhoff, 1971) and the maximum likelihood method (Åström, 1980). The model updating can be achieved either by direct or indirect parameter estimation approach. The former approach updates entries in a numerical model of a system directly, for example, direct update of specific entries in a mass, stiffness, and/or damping matrix in a finite element methods (Bernal et al., 2022). The latter approach aims at updating a numerical model indirectly, through updating

parameters of a numerical model, such as geometrical properties of elements, local or global stiffness parameters, density, and so forth (Mottershead et al., 2011). In the thesis, indirect model updating is considered due to a large number of successful applications in engineering. In the context of engineering applications, (Collins et al., 1974) presented work that leads to two main philosophies of model updating, which are briefly summarized below:

- Bayesian methods (Beck and Katafygiotis, 1998; Katafygiotis and Beck, 1998)

- sensitivity-based method (Mottershead et al., 2011)

Bayesian model updating

The Bayesian methods aim at deriving distributions of the updated parameters, which results in a stochastic approach. The methods are based on Bayes' rule (Yuen, 2010), where the updated (posterior) distributions are derived based on the prior distributions (assumed or known) and measurement data (likelihood). The posterior distribution is multi-dimensional in the parameter space, which is difficult to sample from, and in many cases, a closed-form solution is not available. Consequently, posterior distributions can be obtained by approximate, numerical methods such as the Markov Chain Monte Carlo (MCMC) method (Berg, 2004).

The Bayesian methods applied in the context of model updating gained attention mainly due to the work of (Beck and Katafygiotis, 1998; Katafygiotis and Beck, 1998). Later, their work was revised by (Beck and Au, 2002) who applied the methods to update a mass-spring-damper system by use of the Adaptive Metropolis-Hastings algorithm (one of the MCMC methods). Ching and Chen (2007) applied the transitional MCMC method to improve efficiency in the sampling algorithm. Soize (2003) extended the method to include estimation based on a non-parametric probabilistic approach. The Bayesian methods are at least 20 years younger in application compared to the sensitivity-based methods. The delay is most likely due to the large computational resources required in the Bayesian methods, which was limited in the early days of adaptation. To reduce the computational burden, surrogate models were investigated. Goller et al. (2011) applied artificial neural networks for aerospace structures, McFarland et al. McFarland et al. (2008) investigated Gaussian process emulators, and (Zhang et al., 2011) applied polynomial chaos expansion theory to quantify modeling errors.

Sensitivity-based model updating

The sensitivity-based method aims at estimating model parameters in a deterministic sense. The parameters are found by using a sensitivity matrix—

hence the name—which holds the relation between the parameters and the responses. The relation, in a general case, is non-linear, which is typically linearized. The parameters are found via an iterative procedure where the residuals in measured and model-predicted responses are minimized in the weighted least-squares sense.

The sensitivity-based method has been successfully applied in a wide range of case studies over the past 50 years. The initial application is attributed to Mares et al. (2006) who used a multivariate gradient regression to investigate natural variability in the dynamics of nominally identical specimens. Govers and Link (2010) extended the sensitivity-based method to include estimation of not only the mean but also the covariance matrix of the updated parameters.

Model updating implementation

The the discrepancies in responses, $\Delta\mathbf{\Lambda}$, defined as a difference between estimated responses, $\mathbf{\Lambda}_S$, and numerical predictions, $\mathbf{\Lambda}_{\mathcal{M}(\Theta)}$, are minimized by adjusting the model's parameters, Θ. Typically, undamped eigenfrequencies and eigenmodes are applied as responses. $\Delta\mathbf{\Lambda}$ can be estimated by the linear Taylor expansion (Mottershead et al., 2011)

$$\Delta\mathbf{\Lambda} \approx \mathbf{S}\Delta\mathbf{\Theta}, \tag{2.4}$$

where $\Delta\mathbf{\Theta}$ is the parameter update to be estimated and $\mathbf{S}$ is the sensitivity matrix. The sensitivity matrix contains derivatives of the selected responses, for example, eigenmodes and eigenfrequencies, with respect to the selected parameters, thus

$$S_{jk} = \left[\frac{\partial \Lambda_j}{\partial \Theta_k}\right], \tag{2.5}$$

where Λ_j is the j'th response and Θ_k is the k'th parameter. The sensitivity matrix can be obtained via perturbations directly from the numerical model. Alternatively, the terms in the sensitivity matrix can be computed using analytical methods by differentiation of the undamped eigenvalue equation (Fox and Kapoor, 1968)

$$S_{jk} = \mathbf{\Phi}_j^T \left(-\lambda_j \frac{\partial \mathbf{M}}{\partial \Theta_k} + \frac{\partial \mathbf{K}}{\partial \Theta_k}\right) \mathbf{\Phi}_j, \tag{2.6}$$

where λ_j and $\mathbf{\Phi}_j$ are the j'th undamped eigenvalue and eigenmode respectively, while $\mathbf{M}$ and $\mathbf{K}$ are mass and stiffness matrices, respectively, obtained from the numerical model. The analytical method has merits when large numerical models are considered. The derivatives of eigenmodes can be obtained analogically, as described by (Fox and Kapoor, 1968).

The optimal parameters are obtained by minimizing the discrepancy between the numerical predicted and in-situ estimated responses. The parameters are derived by minimizing (2.4) including response uncertainties, that is,

$$J = \Delta\mathbf{\Lambda}^T \mathbf{W}_\Lambda \Delta\mathbf{\Lambda}, \tag{2.7}$$

where $\mathbf{W}_\Lambda = \mathrm{diag}\left(\sigma_{\Lambda_j}^2\right)^{-1}$ is a diagonal weighting matrix with the variances of the responses, $\sigma_{\Lambda_j}^2$, along the diagonal. Note that the derived parameters do not reflect the true values of the physical system, but the system that is identified by the system identification procedures. The difference between the true and estimated system stems from inherent uncertainties in the system identification methods, which must be reflected in the estimation procedure.

In a general case, a large number of parameters can be updated in the model. These parameters are typically truncated to a subset of selected parameters. Depending on the number of parameters and responses, the optimization problem to solve (2.7) can either result in a well- or ill-posed problem. The unique solution can be expected only if a well-posed setting is obtained, meaning when the number of parameters is lower than the number of responses. In such case, the optimal parameter set is obtained iteratively by minimizing the objective function in Eq. 2.7,

$$\arg\min_{\Delta\Theta} J, \tag{2.8}$$

hence

$$\mathbf{\Theta}_{i+1} = \mathbf{\Theta}_i + \left[\mathbf{S}_i^T \mathbf{W}_\Lambda \mathbf{S}_i\right]^\dagger \mathbf{S}_i^T \mathbf{W}_\Lambda \Delta\mathbf{\Lambda}_i. \tag{2.9}$$

Challenges related to model updating The main challenge with sensitivity-based methods is the selection of responses and parameters to be updated, as it will determine the uniqueness of the solution and therefore the quality of the updated parameters' sets. The challenge is well known and has been addressed in the literature by use of, for example, a regularization procedure. The prior selection of the model parameters and responses has been addressed by (Friswell et al., 1998). These challenges are further investigated in the offshore wind application in this thesis. Specifically, the reasoning of how to choose a subset of parameters to be updated and how to establish weighting matrices used in the regularization approach is discussed.

2.2 System identification and model updating of an offshore wind jacket substructure

Paper A further explores the challenges and limitations in system identification mentioned in subsection 2.1.1 and model updating indicated in subsection 2.1.2. Specifically, the feasibly of the SSI-cov method for an offshore wind jacket case study is investigated. The violation of the main assumptions is considered. Moreover, the ill-posed optimization problem in the sensitivity-based model updating context is discussed and addressed.

In paper A, see appendix A, the application of system identification and model updating is presented for offshore wind jacket substructure exposed to wide range of environmental and operational parameters. Therein, sensitivity-based model updating is applied, employing a subset of experimentally estimated modal parameters as responses, to update physical parameters of a model to more accurately reflect in-situ conditions. In the considered case study the initial discrepancy in eigenfrequency (model-predicted vs. experimentally estimated) is reduced from 30% to 1% after the update. The majority of discrepancy is attributed to highly uncertain soil stiffness parameters.

System identification

In paper A, modal parameters of an operating offshore wind turbine structure have been estimated based on the SSI-cov method. The modal parameters are extracted based on approximately one month of monitoring data. During that period of time, a wide range of wind speeds, yaw angles, and operational turbine states were observed. In the range of interest (0-2.5 Hz in this study), a large number of frequencies is identified. The identified modes include structural eigenmodes, spurious modes related to loading conditions (P-frequencies stemming from revolving rotor), and erroneous modes.

To distill the structural modes and minimize uncertainties stemming from the violation of the SSI-cov assumptions, a multi-step selection algorithm is developed as presented in Tab. 2.1. The idling cases are recommended to be used for further model updating to minimize the white noise excitation assumption and pitching/yawing of a turbine to comply with the LTI system assumption. The assumptions regarding identified modes are related to the particular sensor setup and are case study-specific, hence not relevant in the general context. After the application of the proposed selection criteria, a reduced subset of modal parameters is derived which is subsequently used in the model updating procedure.

Table 2.1: Selection criteria for model updating input (Augustyn et al., 2020).

Assumptions	Criteria
LTI system	no yawing or pitching
white-noise excitation	idling/parked condition
1st and 2nd modes	four eigenmodes identified
FA/SS symmetry planes	perpendicular modes

Model updating

In a typical model updating application, the number of parameters to be updated is greater than the number of identified responses from the physical structure. In such a setting the model updating solution yield a non-unique solution. To address this problem, a regularization scheme, originating from Tikonov (Willoughby, 1979), is applied in paper A to penalize the objective function. The formulation is extended with a regularization coefficient, α, which minimizes the parameter change. The value of α provides a balance between the measurements residual, $\Delta\boldsymbol{\Lambda}^T\mathbf{W}_\Lambda\Delta\boldsymbol{\Lambda}$, and the parameter change, $\Delta\boldsymbol{\Theta}^T\mathbf{W}_\Theta\Delta\boldsymbol{\Theta}$ (Mottershead et al., 2011). Link (1993) provides some guidance on the choice of the regularization parameter, where he suggests that α^2 should range between 0 and 0.3. High values are recommended for highly ill-posed cases with a large number of insensitive parameters. On the other hand, a value close to 0 results in no regularization.

The objective function, extending (2.7) to account for the regularization, is defined as

$$J = \Delta\boldsymbol{\Lambda}^T\mathbf{W}_\Lambda\Delta\boldsymbol{\Lambda} + \alpha\Delta\boldsymbol{\Theta}^T\mathbf{W}_\Theta\Delta\boldsymbol{\Theta}, \tag{2.10}$$

where $\mathbf{W}_\Theta = \text{diag}\left(\sigma^2_{\Theta_k}\right)^{-1}$ is a diagonal weighting matrix expressing uncertainties in the model parameters. The optimal parameter set is obtained iteratively by minimizing the objective function in Eq. 2.10, $\arg\min_{\Delta\Theta} J$, hence

$$\boldsymbol{\Theta}_{i+1} = \boldsymbol{\Theta}_i + \left[\mathbf{S}_i^T\mathbf{W}_\Lambda\mathbf{S}_i + \alpha\mathbf{W}_\Theta\right]^\dagger \mathbf{S}_i^T\mathbf{W}_\Lambda\Delta\boldsymbol{\Lambda}_i. \tag{2.11}$$

The main contribution of paper A in the context of sensitivity-based model updating is an application study including a regularization term to alleviate the ill-posed setting and provide more reasonable solutions based on the parameters' uncertainties. The paper proposes candidate parameters for model updating of a generic jacket substructure. The parameters are chosen based on high sensitivity and uncertainty criterion. The sensitivity of the parameters is estimated based on perturbations in the numerical model of the substructure. The uncertainties are estimated based on a literature review supplemented with engineering judgment in lieu of literature references.

2.3 Summary

This chapter investigates system identification and model updating. It is outlined how state-of-the-art methods can be applied in the context of the offshore wind digital twin framework.

Paper A discusses the following thesis research question:

- Paper A directly addresses the first research question defined in section 1.2, namely: *How to establish a digital twin of an offshore wind substructure?* Paper A provides an application study, in which the first two steps in establishing a digital twin are presented. The study investigates the practical feasibility of system identification and model updating of an operating offshore wind turbine substructure.

Furthermore, the first two research sub-questions, addressing challenges in the current state-of-the-art, are investigated:

- *Can existing system identification methods robustly and accurately estimate modal responses of in-situ offshore wind turbines?* The chosen system identification method can robustly estimate modal parameters of an offshore wind turbine structure under some specific conditions. The idling conditions are sufficiently close to the method's assumptions and provide stable, high-quality results. The operational conditions violate the method's assumptions regarding the system being linear and time-invariant. Hence, the system identification results for operational conditions are disregarded.

- *How can structural model parameters be updated based on identified modal responses?* Paper A outlines the updating scheme. The sensitivity-based method is implemented to update numerical model parameters based on the in-situ identified modal parameters. The challenge of an ill-posed model updating setting is addressed by applying a regularization approach. In this regard, the thesis contributes by providing practical guidance on the uncertainty of the input parameters, used as a regularization term.

The study presented in paper A is limited to:

- Estimating responses from idling states of the turbine. This limitation is related to the chosen system identification method, which assumes the external excitation to be white-Gaussian. Consequently, the operational cases, that include rotor frequency and hence violate the excitation assumption, are excluded.

- Using global modes of the structure as responses. This limitation is a consequence of the particular sensor setup chosen independently of

this study. The decision has been taken to include only sensors located above the sea-water level; that is a popular decision due to practical constraints. Such sensor setup only allows for identification of global structural modes.

- Updating mean values of the physical parameters. In this study we focus on updating mean values of the physical parameters. The uncertainties associated with the mean value are not updated.

- Using simplified models of the transition piece and the turbine. No detailed information about the transition piece geometry nor blades was available due to confidential reasons, hence simplified models of these components were used.

Chapter 2. System identification and model updating
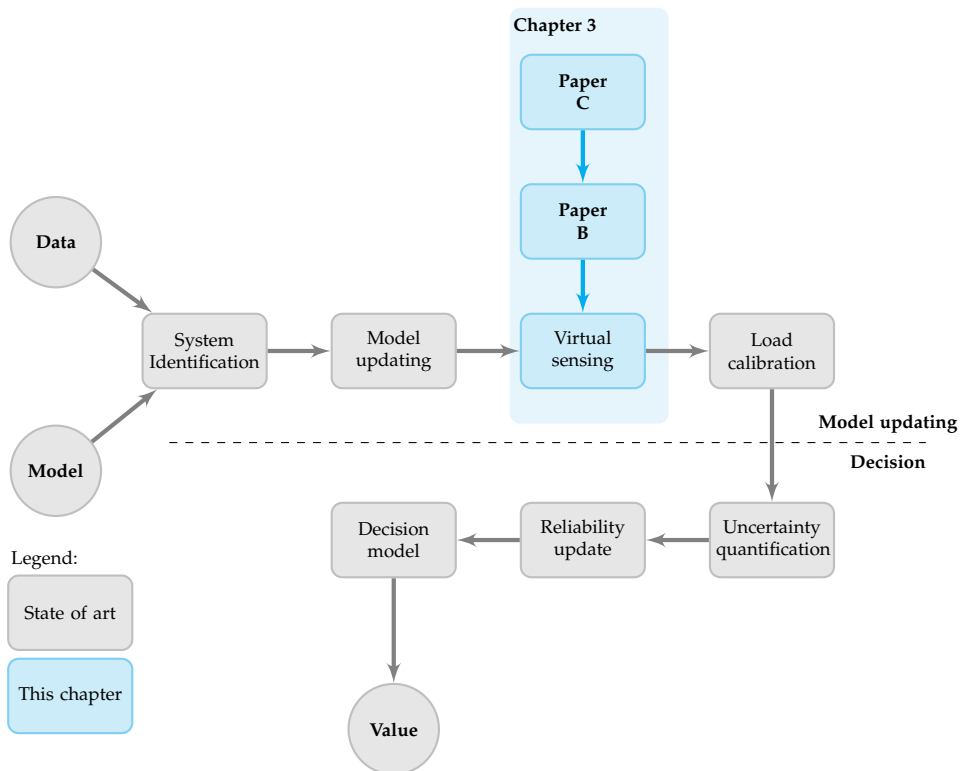
Chapter 3

Virtual sensing

Fig. 3.1: Digital twin framework for improved decision models in the offshore wind application. The blue boxes indicate the parts of the framework discussed in chapter 3.

This chapter describes the parts of the digital twin framework related

to virtual sensing as indicated in Fig. 3.1. Section 3.1 holds review of the state-of-the-art virtual sensing methods and presents the challenges associated with the existing methods in the context of offshore wind applications. In section 3.2 where two feasibility studies addressing some of the vital challenges are summarized based on the study described in papers B and C. The chapter closes with a summary provided in section 3.3.

3.1 State-of-the-art

Measurements and analysis of the response due to external loading are of great importance in many engineering applications. Such measurements can be used to monitor fatigue damage consumption, to assess the structural integrity assessment after an extreme event, and to derive optimal control strategies. In most practical applications, however, full-field measurements are either impractical or expensive to attain. For example, monitoring all hot spots in an offshore jacket substructure is expensive due to the large number of joints, and measurements of subsoil locations are impossible after installation of a structure. To circumvent this challenge, virtual sensing methods are typically used in practical applications.

Virtual sensing methods aim at estimating the full-field response based on a few (physical) sensors and a mathematical model representing the structural system in question. In the context of the presented digital twin framework, virtual sensing methods are used to obtain full-field stress measurements. The virtual measurements are used to calibrate numerical load models and subsequently to quantify the uncertainty in the fatigue damage prediction. This section provides a brief review of virtual sensing methods, with a special focus on applicability for offshore wind substructures. Virtual sensing methods can be categorized according to the graph presented in Fig. 3.2. The review is limited to the offshore wind application. For a comprehensive literature survey, the reader is referred to (Tarpø, 2020).

Filtering approach

Filtering techniques originate from control theory, where a state-space model is applied to represent the physical system. These techniques aim at estimating the full state (displacements and velocities) of the system in an optimal (probabilistic-wise) sense, including modeling error and process noise. The techniques act as a low pass filter, hence the name of the family. The most widely used are the Kalman filer (KF) methods. Among the multitude of variations of Kalman filters (KF), it is worth noticing a few methods, which are explored heavily in the literature: extended KF (Mariani and Corigliano, 2005), unscented KF (Chatzi and Smyth, 2009), particle filter (Ching et al.,
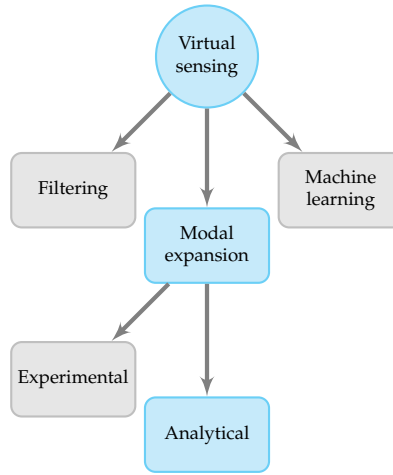
Fig. 3.2: Overview of virtual sensing methods for engineering structures. The blue boxes indicate methods considered in this thesis.

2006), augmented KF (Lourens et al., 2012b), and joint input-state estimation (Lourens et al., 2012a).

Kalman filters in the field of virtual sensing were first applied in 2011 (Papadimitriou et al., 2011) to estimate strains in a metallic body for fatigue estimation. Lourens et al. (2012a) proposed an extended version of KF to remove the assumption of white noise, zero-mean Gaussian excitation. The method, however, required displacement or strain measurements, additional to acceleration measurements, to remove low-frequency drift. Chatzi and Fuggini (2012) proposed adding an excitation to address the issue of low-pass drift, and (Naets et al., 2015) further developed this idea. Palanisamy et al. (2015) suggested multi-sensor fusion, including tilt sensor and accelerometers to cope with non-zero mean excitation. Maes et al. (2016) compared KF (the traditional and the joint input-state estimation algorithm) and modal expansion techniques for dynamic strain estimation of an offshore wind monopile substructure. They concluded that the two techniques for the considered application deliver comparable results. Dertimanis et al. (2016a) combined dual KF and unscented KF for fatigue prediction in an output-only setting. In the same year, the same authors investigated the feasibility of unscented KF for fatigue monitoring of a railway bridge (Dertimanis et al., 2016b).

The main advantages of filtering methods:

- The methods can be easily extended to a non-linear setting (to account for a non-linear soil and a non-linear controller).

- No assumptions on damping modelling is required (which is advantageous when multiple damping sources should be combined, for exam-

ple, soil, hydrodynamic, aerodynamic, material).

- They have been validated for many structural applications

The drawbacks of filtering methods:

- They require prior knowledge on the state covariance, which is typically not known.

- The filter results can be unstable if a recursive algorithm is implemented.

Machine learning

It should be acknowledged that during the last decade machine learning techniques have been widely applied in different engineering fields, including virtual sensing. A general principle of machine learning includes training a mathematical model based on a large amount of input (parameters) and output (results) data to establish an input-output relation. Once such relation is established, output data can be predicted solely based on measured input data. The machine learning approach in the context of data reconstruction in structural health monitoring is investigated by (Bao et al., 2020). Zaidan et al. (2020) explore virtual sensing of air quality measurement using low-cost sensors. The state-of-the-art in predictive modeling for offshore structures using a machine learning approach is investigated by (Tygesen et al., 2018). Although this avenue is promising, further research proving practical feasibility is required.

Modal decomposition and expansion

Modal decomposition and expansion (MDE) methods aim at reconstructing full-field measurements in a two-step process: 1) the structural response is decomposed into a number of modal responses and subsequently 2) the responses in unmeasured locations are reconstructed by using mode shapes and modal participation factors. The main assumption of these methods is that the physical system can be approximated with a linear and time-invariant model and that the response can be sufficiently represented by a few modes. A crucial part of the methods is determining the subspace of expansion vectors included in the expansion matrix. Typically, the first few mode shapes are included in the expansion matrix to reconstruct the measurements. In case the response includes a significant portion of quasi-static vibrations, the dynamic modes are not sufficient and quasi-static modes should be considered to account for quasi-static vibrations. The selected subspace vectors must be able to cover the frequency content and spatial distribution of the applied external loading. Moreover, the methods require solving an inverse

problems, which might be ill-posed depending on the size and the rank of the expansion matrix. To avoid such a situation, the number of sensor signals must be greater or equal to the number of included expansion vectors, and the linear independence of the vectors should be maximized to avoid an ill-conditioned matrix. Alternatively, response can be filtered into low-frequency and high-frequency part and each part can be expanded using different expansion matrix.

This paragraph provides a brief overview of the development and current practice in the field of virtual sensing using MDE methods. Early versions of MDE were developed by (Okubo and Yamaguchi, 1995) at the end of the 1990s. The authors applied a transformation matrix and pseudo-inverse to transform displacements to strain. The first full-field strain estimation was applied in a laboratory case study by (Hjelm et al., 2005) and (Graugaard-Jensen et al., 2005). The latter study investigated modal expansion of a lattice tower using a finite element model and operational modal analysis and documented satisfactory results. The same authors subsequently applied modal expansion to fatigue monitoring and documented that by improving stress predictions the number of inspections related to fatigue monitoring can be reduced when combined with a risk-based inspection planning strategy. Lee (2007) combined modal expansion and model updating and concluded that strain estimation is improved after model updating is performed. Avitabile and Pingle (2012) investigated the effect of the position and number of sensors for modal expansion and concluded that the best results are obtained if 1) the mode shapes are able to reconstruct vibrations for a particular loading pattern applied, 2) the inverse problem is overdetermined, and 3) the expansion vectors are linearly independent. (Baqersad et al., 2015) applied modal expansion to a wind turbine rotor in a laboratory setting and confirmed that mode shape selection is a crucial step in MDE. Iliopoulos et al. (2016, 2017) applied modal expansion to estimate the full-field strain response of an operating offshore wind turbine. They addressed two challenges by application of multi-band modal expansion: 1) issue of undetermined inverse problem and 2) expansion of low-frequency wind-induced response. In their method, the response signal is filtered into three frequency bands, and each band is expanded using an optimal set of modes representative of the source of external loading. Following a similar premise of targeting specific sources of loading with dedicated modes, (Skafte et al., 2017) applied Ritz vectors to expand wave-induced strains on a laboratory scale model of an offshore oil and gas platform. Henkel et al. (2019) applied modal expansion to an offshore wind application with successful results for selected elements and load case scenarios.

Experimental and analytical   Modal decomposition and expansion methods can be subdivided into experimental and analytical. The classification is based on how the vectors in the expansion basis are obtained.

The analytical methods derive vectors directly from a mathematical model. The vectors are obtained by solving the eigenvalue problem to derive mode shapes used to expand the dynamic part of the response. The static and wave-deponent modes are derived as static deflection shapes where a representative load vector is applied. For example, (Iliopoulos et al., 2017) apply a unit force at the top of the offshore wind turbine tower to represent the static wind thrust force. Skafte et al. (2017) apply Ritz vectors to represent wave loading on an offshore oil and gas platform. The quality of the expansion depends, among others, on how well the model-based vectors represent the temporal and spatial characteristics of loading applied to the given physical system.

The structural vibrations can be used to derive expansion vectors using the experimental methods. For example, system identification methods can be used to derive experimental mode shapes, and these can be used directly in the expansion matrix. For the expansion of experimental modes, one can use a system equivalent reduction expansion process (SEREP) (O'Callahan et al., 1989) or a local correspondence principle (Brincker et al., 2014).

The advantage of experimental-based methods is that, under the assumption of no measurement uncertainty, they provide more accurate estimates of operational modes. However, the methods come with a disadvantage as they are fitting-based and hence introduce additional errors. Tarpø et al. (2020a) compared analytical and experimental methods and concluded that analytical-based modes outperform experimental ones and recommended that the latter should be used with care. In a general case, the choice between the two approaches boils down to uncertainty a particular application. The experimental modes deliver the unbiased (if modes are derived based on, for example, the SSI method) estimates on modes with some covariance. On the other hand, the numerical model used to attain the analytical modes delivers a biased estimate, as the numerical model inherently contains errors due to simplifications and uncalibrated models. So the method that contains less uncertainty in a specific case should be chosen.

In the context of this thesis, model updating prior to virtual sensing is proposed. In such instance, the mode shapes derived based on the numerical model are guaranteed to reflect the physical structure in an optimal way according to the chosen objective function. Therefore, the MDE method based on analytical modes is proposed to be used in the digital twin framework in this thesis.

Discussion   The main advantages of the MDE methods:

- The methods are conceptually and numerically easy to implement.

- Given that the LTI assumption holds and that sensors are placed optimally (minimizing the condition number of the employed expansion matrix), the expansion quality is high (Pedersen et al., 2019).

- The methods are not iterative, hence no stability issue arises.

- The methods have been documented to provide high-quality results in many engineering applications, including offshore structures (Tarpø et al., 2020b; Tygesen et al., 2018) and offshore wind structures, both for monopiles (Iliopoulos et al., 2016, 2017; Maes et al., 2016) and jackets for legs elements (Henkel et al., 2020).

- The MDE methods are output-only methods, hence they do not require estimation of the input (external loading).

The drawbacks of the MDE methods:

- The methods cannot capture non-linear and time-variant responses.

- The sensor placement significantly affects expansion quality.

- The expansion basis must be selected carefully to deliver high-quality results.

Virtual sensing implementation

A number of virtual sensing methods have been reviewed in this chapter. The focus is put on their limitations and applicability towards offshore wind substructures. Based on this review, the modal expansion is chosen for further investigation. The basic theory of the modal expansion method is briefly described.

The modal expansion method requires the structural system to be linear and time-invariant (LTI). Wind turbine structures (both onshore and offshore) violate this assumption due to environmental and operational variability (EOV) (Hansen, 2007; Skjoldan and Hansen, 2012). Nevertheless, previous modal expansion studies investigating offshore wind turbines resulted in, to some extent, adequate results (Henkel et al., 2020; Iliopoulos et al., 2017; Maes et al., 2016). Consequently, in this thesis, the modal expansion method is used along with the LTI assumption, which implies that the structural system can be described by

$$\mathbf{M}\ddot{\mathbf{u}}(t) + \mathbf{C}\dot{\mathbf{u}}(t) + \mathbf{K}\mathbf{u}(t) = \mathbf{f}(t), \tag{3.1}$$

where $\mathbf{M}$, $\mathbf{C}$, $\mathbf{K} \in \mathbb{R}^{n_a \times n_a}$ are the mass, damping, and stiffness matrices, n_a is the number of degrees of freedom (dof), $\ddot{\mathbf{u}}(t)$, $\dot{\mathbf{u}}(t)$, $\mathbf{u}(t) \in \mathbb{R}^{n_a}$ are the acceleration, velocity, and displacement vectors, and $\mathbf{f}(t) \in \mathbb{R}^{n_a}$ is the load

vector. It is assumed that the system matrices are positive definite, $\mathbf{M}$, $\mathbf{C}$, $\mathbf{K} \succ 0$. Moreover, the damping in system (3.1) is assumed to be classically distributed, which implies, as specified by (Caughey, 1960), that $\mathbf{M}^{-1}\mathbf{K}$ and $\mathbf{M}^{-1}\mathbf{C}$ commute such the eigenvectors of system (3.1) equal the undamped ones.

The output (displacements in this case, but the procedure can be applied to velocities, and accelerations) can be partitioned into n_m (measured) outputs, $\mathbf{u}_m(t) \in \mathbb{R}^{n_m}$, and $n_e = n_a - n_m$ (virtual, expanded) outputs, $\mathbf{u}_e(t) \in \mathbb{R}^{n_e}$. Then,

$$\mathbf{u}(t) = \begin{bmatrix} \mathbf{u}_m(t) \\ \mathbf{u}_e(t) \end{bmatrix} \tag{3.2}$$

and $\mathbf{u}_e(t)$ can be estimated based on $\mathbf{u}_m(t)$. Assuming $\mathbf{u}(t)$ is governed by n_q modes, it can be expressed by a (truncated) modal formulation

$$\mathbf{u}(t) \approx \boldsymbol{\Phi}(t)\mathbf{q}(t) = \begin{bmatrix} \boldsymbol{\Phi}_m(t) \\ \boldsymbol{\Phi}_e(t) \end{bmatrix} \mathbf{q}(t), \tag{3.3}$$

where $\mathbf{q}(t) \in \mathbb{R}^{n_q}$ contains the modal displacements (velocities or accelerations depending on physical output) associated with the n_q governing modes and $\boldsymbol{\Phi}(t) \in \mathbb{R}^{n_a \times n_q}$ is the expansion matrix, which is partitioned into $\boldsymbol{\Phi}_m(t) \in \mathbb{R}^{n_m \times n_q}$ and $\boldsymbol{\Phi}_e(t) \in \mathbb{R}^{n_e \times n_q}$.

Assuming $n_m \geq n_q$ and rank$(\boldsymbol{\Phi}_m(t)) = n_q$, an estimate on $\mathbf{q}(t)$ that minimizes $\|\boldsymbol{\Phi}_m(t)\mathbf{q}(t) - \mathbf{u}_m(t)\|_2$ is given by

$$\hat{\mathbf{q}}(t) = \left(\boldsymbol{\Phi}_m(t)^T \boldsymbol{\Phi}_m(t) \right)^{-1} \boldsymbol{\Phi}_m(t)^T \mathbf{u}_m(t) = \boldsymbol{\Phi}_m(t)^\dagger \mathbf{u}_m(t), \tag{3.4}$$

with overhead ˆ denoting an estimate. Then, the virtual part of the output can be estimated as

$$\hat{\mathbf{u}}_e(t) = \boldsymbol{\Phi}_e(t)\hat{\mathbf{q}}(t). \tag{3.5}$$

Challenges related to virtual sensing In the context of offshore wind applications with jacket substructures, the main violations of an LTI system are associated with non-linear response to the external loading (wind and wave), non-linear soil stiffness, and non-linear and time-variant controller characteristics. In this subsection, the impact of such violations on virtual sensing is discussed.

The variability in controller parameters alters the modal parameters of the given wind turbine system (Hansen, 2007; Skjoldan and Hansen, 2012). Such variation cannot be captured with an LTI model and hence leads to reduced expansion quality. Paper B investigates the effect of controller variability on virtual sensing quality for a particular method, namely, the modal expansion method.

The wave loading imposed on an offshore structure is non-linear as it depends on the relative velocity between the incident wave and the structural response. However, for bottom-fixed structures, the response velocity is limited and hence the non-linear effect can be neglected (DNVGL-RP-C205, 2010). Effectively, the non-linear behavior stemming from wave loading does not introduce large errors when simplified with an LTI model. Similar conclusions can be applied to non-linearities stemming from the aerodynamic coupling between the blades and air particle, assuming no large deformations or plasticity is introduced IEC-61400-1:2019 (2019).

The soil stiffness depends on the applied load level. Typically, a reduction in soil stiffness is observed for increased load levels. Varying soil stiffness affects support conditions of an offshore wind structure and hence results in varying modal parameters, especially mode shapes and eigenfrequencies Bom et al. (2020). However, for the majority of power production cases, a modeling approach with an initial soil stiffness yields an accurate estimation of soil stiffness (API-RP-2A, 2014). For extreme cases, alternative soil stiffness should be assumed resulting in sea state-dependent soil stiffness and sea state-dependent modal parameters.

3.2 Virtual sensing of an offshore wind jacket substructure

This section presents two papers investigating virtual sensing of offshore wind jacket substructure. Paper B studies the feasibility of virtual sensing for offshore wind jacket substructures. The focus is on mitigating offshore wind-specific challenges associated with expanding wave-induced vibrations and accounting for the substructure and turbine interaction. Furthermore, paper C investigates the extent to which offshore wind turbines behave non-linearly and time-variant. An overview of when the LTI assumption is violated severely—and therefore when the MDE methods should be used with care—is provided.

3.2.1 Feasibility of the modal expansion method

Paper B investigates the feasibility of modal expansion-based virtual sensing in the context of offshore wind jacket substructures. Two different expansion setups, namely a basic and an extended one, are employed. The basic setup resembles a typical sensor configuration investigated in various studies (Henkel et al., 2020; Iliopoulos et al., 2017), where only easily accessible sensors above the water level are installed. The basic setup fails to provide high-quality expansion results for idling conditions when vibrations
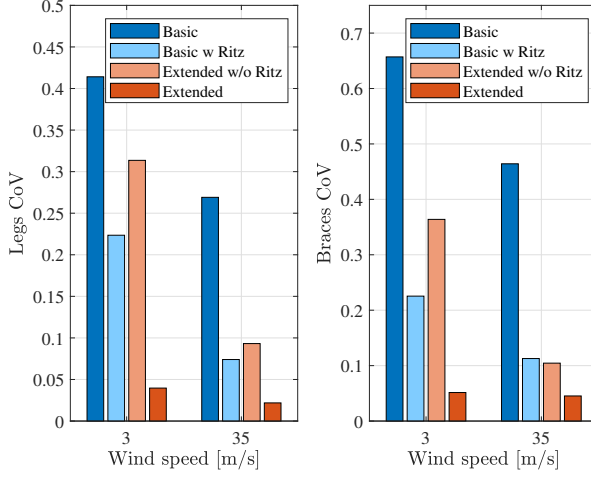
Fig. 3.3: CoV values obtained using modified (with/without Ritz modes) basic and extended setups for the idling load cases (Augustyn et al., 2021b).

are dominated by the wave loading. Moreover, low expansion quality is documented in brace elements for both the idling and operational conditions. This is due to the fact the basic setup is not able to capture local vibrations nor wave-induced vibrations.

In paper B, the noted shortcomings are suggested to be alleviated by applying the extended expansion setup. The setup includes sub-sea sensors and a wave radar sensor. The sub-sea sensors allow for extracting mode shapes beyond the first and second global bending modes, which are the only ones typically included in a basic setup. By including additional local modes and wave-related modes, local brace vibrations are captured. Including a wave radar sensor adds information about local wave conditions, which allows for precisely expanding wave-induced vibrations. Wave information, in terms of wave direction and wave surface elevation, serves as input to derive Ritz vectors for enhanced wave expansion. The inclusion of local brace and wave modes in the expansion improves the expansion quality significantly as indicated in Fig. 3.3. The quality of expansion is studied based on the coefficient of variation (CoV) for two wind speeds and a turbine in idling conditions. The basic setup yields the highest uncertainty. For idling cases, adding a wave radar sensor improves the expansion quality more than adding sub-sea sensors.

The expansion quality as a function of wind speed for two case studies, with the control system active and inactive, is depicted in Fig. 3.4. A reduction in expansion quality can be observed when the control system is active.
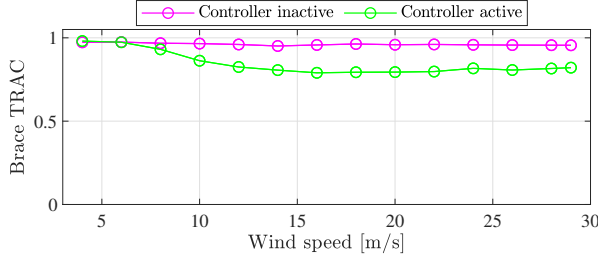
Fig. 3.4: Time response assurance criterion (TRAC) value as a function of wind speed obtained for an inactive and active control system (Augustyn et al., 2021b).

Such a decrease arises because the control system introduces non-linear and time-variant behavior, which is not accounted for in the employed expansion method. Indeed, when the same case study was considered with the controller inactive, the expansion quality was high and constant across the analyzed wind speeds. This is due to the fact that when the controller is inactive, the model adheres to the LTI assumption.

3.2.2 Environmental and operational variability

Paper C explores the effect of EOV on the modal parameters of offshore wind substructures. A non-linear numerical model of a representative offshore wind turbine supported by a jacket substructure is established and analyzed under the exposure of EOV. In particular, the study investigates time-periodic effects, non-classical aerodynamic damping, and operational variability imposed by the turbine controller. The same turbine and substructure model as in paper B are considered to further investigate if the controller variation can be a root-cause of the reduction in modal expansion quality. The study is not only confined to investigating mode shape variability (specifically relevant for modal expansion), but it also includes an investigation of damping and eigenfrequencies. These parameters are used in other fields of research where the LTI model is assumed, for example, in model updating (Mottershead et al., 2011; Ulriksen, 2018), structural health monitoring (Bernal and Ulriksen, 2019; Martinez-Luengo et al., 2016), and control (Staino et al., 2012).

The modal parameters from different operational states are computed using linearized, time-periodic system formulations, and the variability in the modal parameters is discussed. The results illustrate the variation of the extracted modal parameters, which is found to be governed by two main sources; namely, 1) the wind turbine control and 2) interaction of system modes. The former explains the variation in modes that are highly affected by modifications of the controller variables, while the latter explains the variation in the modes that become closely spaced and hence prone to mutual
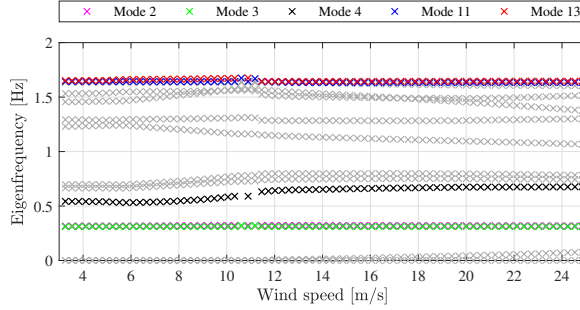
Fig. 3.5: Eigenfrequencies as functions of the wind speed (Augustyn et al., 2021a).

interaction. The former source is quantitatively correlated with the reduction in expansion quality.

The variations in eigenfrequencies as a function of wind speed is found to be limited as documented in Fig. 3.5. Worth noticing is the fact that the variations in the first and second eigenfrequencies are negligible. The small variations found in this numerical study is confirmed by the in-situ system identification results documented in paper A. In conclusion, an LTI system assumption for the identification of the first and second modes is fair. However, the torsional modal frequency and mode shape is observed to vary more than the first and second modes. It should be confirmed that a similar variation can be observed in system identification results, as it can significantly affect the modal expansion results when the torsional mode is of importance.

The variation in mode shapes due to wind speed quantified by the modal assurance criterion (MAC) is summarized in Fig. 3.6. A relatively larger variation in mode shapes, compared to eigenfrequencies, is documented. Especially the second mode shape and the first torsional mode shape vary noticeably. The reduction in MAC value for these modes follows qualitatively the pattern of the reduction in expansion quality. That is due to the fact that the expansion is based on mode shapes computed for a standing still turbine model. Hence, the deviation of these modes (quantified by the MAC value computed between the standing still and the wind-speed linearized modes) will directly be transferred into a reduction in expansion quality. Note the peculiar reduction of MAC value around rated wind speed ($U = 11$ ms^{-1} in the second mode shape (mode 11 in Fig. 3.6). The reduction is due to closely spaced modes, which for this EOV configuration lead to complex interaction (merging of two modes). This pattern is not visible in the reduction of the expansion quality. One potential explanation is that vibrations in this direction (perpendicular to the wind speed) do not contribute significantly to the total vibrations of the considered location.
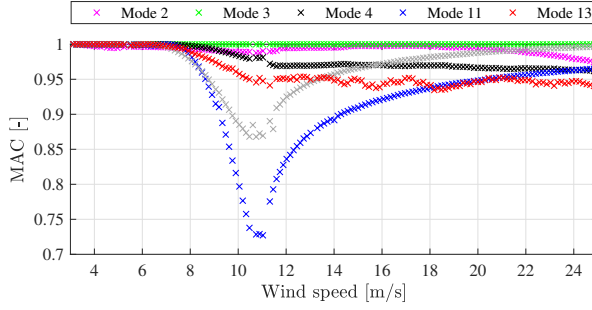
Fig. 3.6: MAC values as functions of the wind speed (Augustyn et al., 2021a).

3.3 Summary

This chapter investigates virtual sensing in the context of implementing it in a digital twin framework for offshore wind turbine jacket substructure.

Papers B and C discuss the following thesis research question:

- Papers B and C directly address the first research question defined in section 1.2, namely: *How to establish a digital twin of an offshore wind substructure?* Paper B provides a feasibility study of the third step in establishing a digital twin, namely, virtual sensing. The study considers a particular virtual sensing method, namely, modal expansion, where the offshore wind substructure is approximated with an LTI model. Paper C investigates the validity of the widely adopted LTI assumption.

Furthermore, the last two research sub-questions, addressing challenges in the current state-of-the-art, are investigated:

- *Can existing virtual sensing methods accurately and precisely predict vibrations of an offshore wind jacket substructure?* Paper B investigates the feasibility of modal expansion in the context of an offshore wind jacket substructure. Modal expansion method assuming a typically suggested sensor setup fails at delivering high quality results in the brace elements. After applying the recommendations from the paper B, namely, higher order modes and wave-dependent Ritz vectors, the expansion quality is improved. However, for high wind speed cases, the expansion quality is systematically reduced. Paper C further investigates this effect.

- *What is the impact of environmental and operational variability on modal parameters of an operating offshore wind turbine?* Paper C investigates the EOV of a representative offshore wind turbine supported by a jacket

substructure. It is documented that, among others, the mode shapes of the substructure vary with both the environmental and operational parameters. This variation is neglected in modal expansion, that employs an LTI model, which can potentially explain the observed reduction in expansion quality for higher wind speeds.

- *Can linear and time-invariant models approximate non-linear and time-variant systems?* One LTI model cannot accurately approximate modal parameters for all ranges of the analyzed environmental and operational variation. One potential mitigation to capture EOV is to include non-linear expansion methods, for example, modification of filtering methods. Alternatively, one can use modal expansion with mode shapes linearized for particular environmental and operational conditions.

The studies presented in papers B and C are limited to:

- Paper B focuses on the theoretical feasibility of virtual sensing for offshore wind jacket substructure by investigating results from a numerical study. Consequently, a number of practical challenges are neglected. The expansion is based on displacement signals, which, in practice, are obtained from accelerations after double integration. The problem with this approach is that the low-frequency content in the signals is lost and the signal drifts. To capture low-frequency signal content, other types of sensors can be considered such as strain gauges. The Ritz vectors require wave forces as input. In this study, the wave forces are obtained directly from the numerical model. However, in practice, the wave forces should be reconstructed, for example, from measured wave surface elevation time series. Obtaining such information in practice is not straight forward due to practical issues with wave force reconstruction and the high costs associated with the required instrumentation.

- Paper C investigates EOV of one particular type of a substructure and wind turbine model. It would be beneficial to investigate how susceptible other types of structures are to mode interaction. In the context of virtual sensing, it would be interesting to investigate if by applying multiple linearized wind turbine models (instead of one LTI), the expansion quality is improved for the cases which deliver poor quality for the LTI modal expansion.

Chapter 4

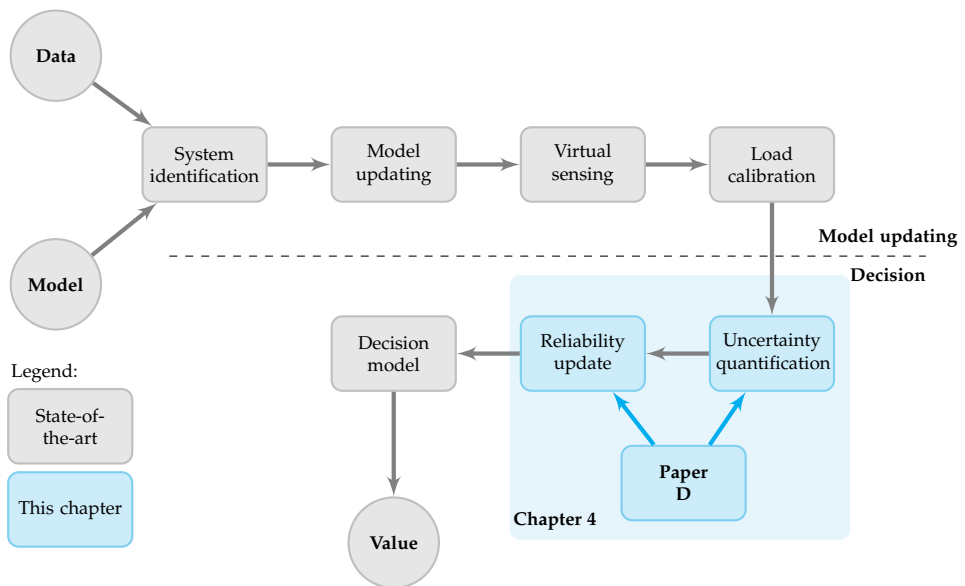# Uncertainty quantification and reliability assessment

Fig. 4.1: Digital twin framework for improved decision models in the offshore wind application. The blue boxes indicate the parts of the framework discussed in chapter 4.

4.1 State-of-the-art

This chapter describes the parts of the digital twin framework related to uncertainty quantification and reliability assessment as indicated in Fig. 4.1. In section 4.1, the state-of-the-art methods for uncertainty quantification and reliability assessment are briefly reviewed. A description of uncertainty modeling in fatigue damage prediction of offshore wind structures is provided. Subsequently, uncertainty quantification methods applied in the field of wind engineering are presented. Finally, methods aiming at assessing structural reliability are presented, including the described uncertainties. Section 4.2 presents the digital twin framework implementation case study based on the study described in paper D. The chapter closes with a summary in section 4.3.

4.1.1 Uncertainty modeling and quantification

Uncertainty modeling

The uncertainties in engineering applications can generally be categorized into aleatory and epistemic (ISO-2394:2015, 2015; Sørensen and Toft, 2010) uncertainties. The former represents inherent variability in the physical parameters. For example, in the context of offshore wind applications (Dong et al., 2012), aleatory uncertainty includes variation in met-ocean parameters (wind speed, wave height, wave period, wind direction, wave direction), structural strength, structural stiffness (soil, steel, etc.), and mass. These uncertainties can be estimated by measuring the variation either in-situ (met-ocean, soil) or in a laboratory (steel, mass). The uncertainties can be included in the design procedure of a wind turbine substructure; either directly via probabilistic methods (uncertainties included as stochastic variables) or via deterministic methods (uncertainties included as characteristic values and safety factors). The aleatory uncertainty, representing natural variability in physical quantity, for example stiffness or wind speed, can be estimated, however, it can not be controlled, nor reduced. The epistemic uncertainty represents a lack of knowledge, insufficient data, and/or noise in the measurements. Insufficient data represents too short measurements (for example, wind speed measured over few weeks not capturing a sufficient amount of storms and year-to-year variation) and is reflected in statistical uncertainty. In-situ measurements are inherently contaminated with equipment noise which is modeled as measurement uncertainty. The epistemic uncertainty is typically modeled as model, statistical, and measurement uncertainty and can be reduced if more advanced models are used and/or more data becomes available.

The uncertainty modeling related to fatigue damage accumulation is summarized in Fig. 4.2. Model uncertainties in fatigue damage prediction of
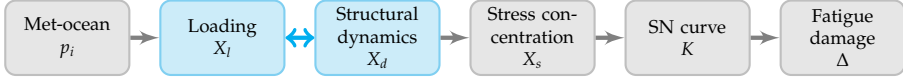
Fig. 4.2: Stochastic variables modeling uncertainty in fatigue damage accumulation (Augustyn et al., 2021c). The light blue boxes indicate stochastic variables estimated based on generic, design-based recommendations. The dark blue boxes indicate stochastic variables that can be quantified and updated based on new information from a digital twin.

offshore wind structures reflect uncertainties in structural dynamics, load modeling, stress concentrations, and fatigue damage calculation. In addition to these model uncertainties statistical and measurement uncertainties may be important to include. Often the statistical and measurement uncertainties are included indirectly in the model uncertainties. This is also assumed in the proposed model. The aleatory uncertainties are directly included by investigating a number of load cases with representative met-ocean parameters and probabilities based on met-ocean distributions. In this thesis, the aim is set to quantify and include the structural dynamics and loading uncertainties based on information from digital twins. These uncertainties are highlighted in blue in Fig. 4.2. For the remaining uncertainties, recommended (standard-based) values are assumed. However, a brief discussion on how they could be quantified is provided. A brief characteristic of each uncertainty source and its modeling strategy is presented in the following part of the section.

Met-ocean model The joint probability distribution of the wind-wave climate is discretized by a finite number of short-term sea state simulations, including random wind and wave seeds to model a stochastic process (IEC-61400-1:2019, 2019). Met-ocean uncertainty is included in (4.6) by the yearly probability of each sea state, denoted p_i. The met-ocean uncertainty can be quantified if long-term climate parameters are monitored (Hübler et al., 2018; Mai et al., 2019). When quantified, the uncertainty can be modeled by a stochastic variable of wind, wave, wind direction, wave direction, wave period, and turbulence. On top of these physical uncertainties epistemic uncertainties related to limited data available (statistical uncertainty) must be included.

Loading Depending on the location of the wind turbine, the loading may include the following exogenous sources and their inherent uncertainties:

- Hydrodynamic loading: uncertainty related to calculating wave loads that stems from different wave theories (linear vs. non-linear), Morison's equation, stretching, and mass and drag coefficients.

- Aerodynamic loading: uncertainty related to calculating wind loads that stems from wind turbulence, wake model, and shear coefficient.

- Ice loading: uncertainty related to calculating ice loads, for example, ice thickness, ice crushing strength, and ice failure regime.

- Earthquake loading: uncertainty related to calculating earthquake loads, for example, earthquake acceleration profile, structural response, soil-structure integration, and force transfer.

If the loading uncertainty is quantified based on information from digital twins, the main part of the uncertainty is related to obtaining the structural response due to external loading. This response is typically estimated based on virtual sensing methods, which are associated with uncertainties (Augustyn et al., 2021b; Iliopoulos et al., 2017). The loading uncertainty is included in (4.6) through the stochastic variable X_l.

Structural dynamics   Estimating dynamic system properties is associated with uncertainties (Reynders et al., 2008). The uncertainties stem from EOV, non-stationary sea states (fluctuating mean sea water level), time-variant structural conditions (corrosion, scour), output noise, and the formulation of the structural model, including modeling of highly uncertain parameters such as soil stiffness, joint stiffness, and damping. It should be noted that the output noise relates to the noise in the acceleration and/or strain signals, which is propagated through system identification procedures and results in uncertainty of the updated structural model parameters (Reynders et al., 2008). The structural dynamics uncertainty is included in (4.6) through the stochastic variable X_d.

Stress concentration   A fatigue design is typically performed based on SN curves, which define a number of cycles required to initiate rapid crack growth for specific hot spot stress ranges. Three different approaches are proposed to calculate stresses: nominal, hot spot, and notch (Fricke, 2003). Similar definition is adopted in design standards, for example (DNVGL-RP-C203, 2016; DNVGL-ST-0126, 2016). The hot spot stresses include the nominal stress (calculated in the member some distance from the weld) and additional stresses from geometric effects, for example, weld toes and fabrication tolerances. The ratio of hot spot stress to local nominal stress is called the stress concentration factor (DNVGL-RP-C203, 2016). The hot spot stress ranges can be estimated based on simplified parametric equations, for example, (Efthymiou and Durkin, 1985) or detailed finite element models. In the proposed framework, the hot spot stress method is included, and the stress concentration factor uncertainty is included in (4.6) through the stochastic variable X_s. The stress concentration uncertainty can be quantified if a detailed FE model is used to establish hot spot stresses (Lee et al., 2010) or if hot spot stresses are measured directly.
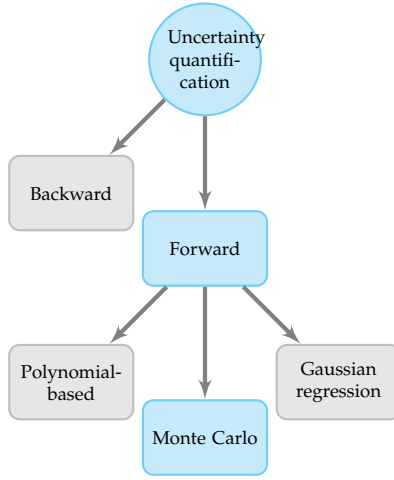
Fig. 4.3: Overview of uncertainty quantification methods for engineering structures. The blue boxes indicate the methods considered in this thesis.

SN curve The uncertainty in parameter estimation from the SN curve approach (DNVGL-RP-C203, 2016) is included in (4.6) through the stochastic variable K and the deterministic parameter m. The stochastic models for fatigue damage accumulation have originally been developed for reliability- and risk-based inspection planning of offshore (Faber, 2002; Onoufriou, 1999; Straub and Faber, 2005) and offshore wind (Rangel-Ramírez and Sørensen, 2012) structures. If a bi-linear SN curve is used, then stochastic variables are used to model the two branches of the SN curve. The SN curve uncertainty can be quantified if fatigue testing is performed, including parameter uncertainty if a limited number of tests is performed (DNVGL-RP-C203, 2016).

Fatigue damage The uncertainty related to the fatigue damage accumulation model (Miner's rule (Miner, 2021)) and the crack propagation method (Paris–Erdogan (Paris and Erdogan, 1963) or fracture mechanics) are included in (4.6) by modeling the resistance, Δ, as a stochastic variable (DNVGL-RP-C203, 2016). The fatigue damage accumulation model, including uncertainty modeling is described in (Wirsching, 1984; Wirsching and Chen, 1988).

Uncertainty quantification

The uncertainty quantification methods, for the purpose of this thesis discussion, are categorized as presented in Fig. 4.3. First the difference between the backward and forward uncertainty quantification methods is provided, followed by further review of the forward methods considered in this thesis.

Backward uncertainty quantification methods   Backward uncertainty propagation methods aim at inferring distributions of the input parameters based on output parameter distributions, see Fig. 4.4. The methods are typically applied when measurements or data from high-fidelity models become available. Based on this data and an established model, one aims at obtaining the most probable set of input parameters resulting in the measured outputs. In the literature (depending on the application goal), these methods appear as calibration methods, model updating, or inverse problems. Some of the established methods within the backward uncertainty quantification family include the least-squares approach (Smith, 2013) and Bayesian calibration (Kennedy and O'Hagan, 2001). The former methods are well-established and widely used, while the latter methods recently gained significant attention in various engineering applications, including offshore wind.

Chapter 2 describes the application and limitations of the backward uncertainty quantification methods, in the context of optimal parameter estimation (system identification and model updating). Note that paper A examines the uncertainty in updated model parameters in the context of the digital twin framework. Therein the distribution of the model parameters based on indirect, sensitivity-based model updating methods was established. The main prohibiting factor in backward uncertainty propagation application—in the context of estimating fatigue damage uncertainty, which we target in this thesis—is that we are not able to directly measure fatigue damage. However, we are able to directly obtain other parameters, for example, the distributions of the numerical model parameters. Given that the uncertainties in the input parameters are quantified (via model calibration methods), they can be propagated through the numerical model to obtain uncertainty in fatigue damage predictions, based on the forward uncertainty quantification methods.

Forward uncertainty quantification methods   Forward uncertainty quantification methods aim at estimating uncertainty in the output parameters, given the distribution of the input parameters is known and a model defining a relationship between the input and the output parameters is established. Figure 4.4 depicts the main principle of the forward uncertainty propagation methods. These methods, in the context of offshore wind energy, can be used to estimate uncertainty in output parameters that are otherwise difficult or impossible to measure directly (fatigue damage, probability of failure, energy production, and cost of energy). These methods are typically used as preprocessors to risk assessment, design optimization, and decision-making.

Among a multitude of forward propagation methods, sampling-based are widely used. The main principle is to sample from the distributions of the input parameters, to evaluate output parameters from the sampled input distributions, and repeat sampling a number of times. Consequently, one

obtains a distribution of the output parameters from statistical properties can be estimated, hence quantifying the uncertainty in the output parameters. The Monte Carlo method (Metropolis and Ulam, 1949) is a versatile and easy-to-implement method, which has been successfully applied in forward propagating in various applications in wind energy. One of the limitations of the Monte Carlo method is that a large number of samples is required for the solution to converge. To address this issue, various sampling techniques (differentiating from classical random sampling) have been applied. For example, the Latin hypercube sampling (Helton and Davis, 2003) is one of the widely applied methods. Instead of a (potentially) costly evaluation of a full model for every sampled input parameter vector, one can consider developing an approximation of the output via surrogate models. Some variations of surrogate modeling include polynomial chaos expansion (Blatman and Sudret, 2011; Knio and Maître, 2006), stochastic collocation (Eldred and Burkardt, 2009), and Gaussian regression (Kriging) (Lockwood and Anitescu, 2012). Surrogate modeling can also be used to evaluate sensitivity of the input parameters onto the variance of output parameters. For example, Sudret (2008) applies PCE to investigate global sensitivity of a mathematical model using a well-established Sobol' indices approach (Sobol, 2001). A comprehensive computational framework for uncertainty quantification can be found in, for example, UQLab software package (Marelli and Sudret, 2014).

Both surrogate and direct Monte Carlo sampling methods have been applied for forward uncertainty quantification in the context of wind energy. Multiple studies have investigated the uncertainty in levelized cost of energy (LCoE). Kwon (2010) quantified the uncertainty in the power curve due to wind speed variation and uncertainty in surface roughness by using Monte Carlo methods. (Witteveen and Iaccarino) applied stochastic collocation to investigate the uncertainty in turbine response and sound pressure levels due to blade geometry variation. Rinker (2016) applied surface response methods to investigate the variation in turbine response due to uncertainty in turbulent wind parameters. Polynomial chaos expansion (PCE) was applied in (Murcia et al., 2015) to quantify the uncertainty in annual energy production and LCoE. Liu et al. (2014) applied low-order PCE and compared the results to coarse Monte Carlo simulations and reported good agreement between the two methods. It should be expected that Monte Carlo simulations (for a converged number of simulations) deliver more accurate results than surrogate models. For the same computational effort, surrogate models should deliver higher accuracy than Monte Carlo simulations.

Given that the considerations of the previously discussed methods, Monte Carlo methods are proposed in this thesis for uncertainty propagation methods, as they are general, highly versatile methods. At the same time, their limitations due to potentially prohibitive computational costs are noted. But in this thesis we focus on investigating the feasibility of the proposed frame-
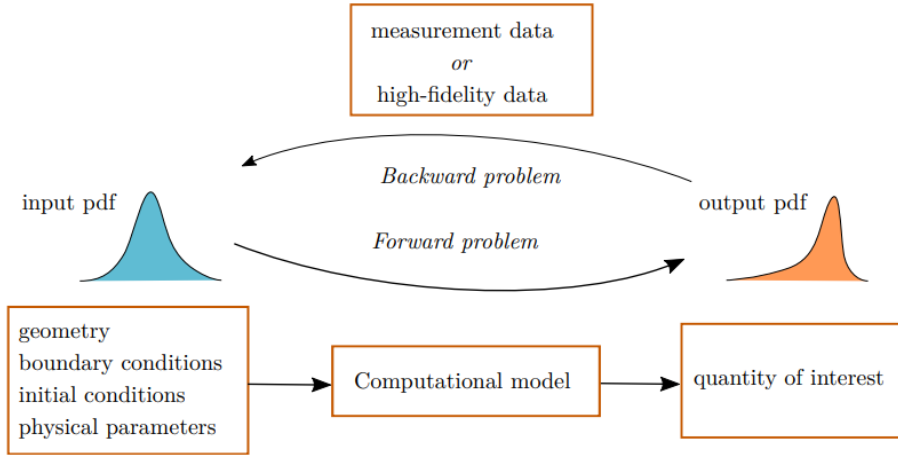
Fig. 4.4: Comparison of backward and forward uncertainty quantification methods (reproduced from (van deBos and Sanderse, 2017)).

work, and given it is applicable, the efficiency issue can subsequently be studied by means of, for example, the mentioned surrogate models.

Monte Carlo methods

In the proposed framework, the uncertainty related to structural dynamics and loading are quantified based on a two-step procedure applying Monte Carlo methods. First, a stochastic model is formulated related to the structural and loading parameters in the digital twin. Next, realizations from that model are simulated and a fatigue damage stochastic model is fitted by the maximum likelihood method. By applying this two-step procedure, the uncertainty of each numerical model parameter can be propagated into the uncertainty in fatigue damage. The implementation of the procedure is explained in details in section 4.2.

4.1.2 Reliability assessment

A key indicator when designing and operating engineering structures is structural reliability, which is defined as *the ability of a structure or structural member to fulfil the specified requirements, during the working life, for which it has been designed.* (ISO-2394:2015, 2015). The structural reliability of every structure must be confirmed to comply with a minimum reliability level, depending on consequence of failure and relative cost of safety measure. The minimum reliability level is incorporated in every standard accounting for economical and human risk considerations. In order to estimate reliability, we can apply structural reliability methods. In this subsection, a brief

overview of structural reliability assessment methods is provided for use in the proposed digital twin framework.

Structural reliability assessment is performed for every structure at the design stage. ISO-2394:2015 (2015) defines three levels of design approaches: semi-probabilistic, reliability based, and risk informed. The methods are categorized in Fig. 4.5.

Semi-probabilistic The semi-probabilistic method, called the partial factors format, is recommended for application in the majority of cases for new structures under typical design conditions and matured design concepts/technologies (ISO-2394:2015, 2015). The stochastic nature of the resistance, loading effects on structures, and uncertainty are accounted for by applying characteristic values and accompanying safety factors. The characteristic values and safety factors (under the assumption of particular probabilistic models) result in a particular reliability level for the designed structures. The main limitation of the semi-probabilistic method is that the representative uncertainty and target reliability level are assumed when calibrating the safety factors. The assumed models might not reflect in-situ conditions of a specific structure; consequently, the derived design might have higher or lower reliability compared to the target reliability.

Reliability based The reliability based methods estimate the reliability of a structure by probabilistic evaluation of appropriate limit states and relevant stochastic variables including uncertainties. These methods are relevant in case a new concept is considered in order to account for the lack of experience in such a design. These methods are also used in case an unexpected event occurs during the operation of a structure which put in question structural reliability requirements, for example, an accident or repair event. When new information (not present in the design stage) becomes available, the structural reliability can be updated to reflect the new knowledge. The updated reliability level is compared to the required safety level, and no mitigation actions are required given that the reliability is sufficient.

The new information can be understood very broadly as any piece of evidence, which brings improved knowledge of the structural performance, compared to the design predictions. Historically, in the oil and gas field, such information was delivered by, for example, physical inspections and measurements of wind and wave climate. However, as briefly indicated in section 1.1, inspections are considered to be prohibitively expensive for offshore wind applications. Hence, other sources of information are considered instead. This thesis implements information from digital twins is implemented using well-established reliability methods. The structural reliability is updated and subsequently serves as a basis for updating decision models.
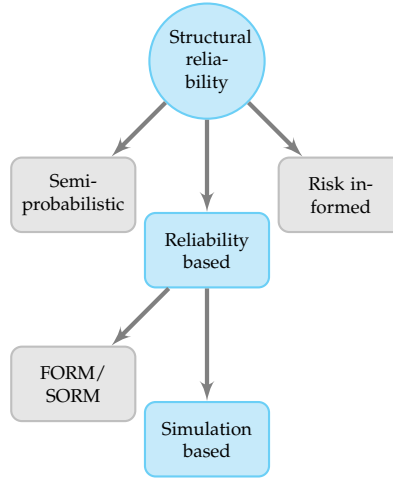
Fig. 4.5: Overview of structural reliability assessment methods for engineering structures. The blue boxes indicate methods considered in this thesis.

FORM/SORM In the context of offshore wind applications, the reliability based methods can be divided into first-order reliability method (FORM)/second-order reliability method (SORM) and simulation based, as indicated in Fig. 4.5.

The FORM/SORM methods aim at estimating reliability based on closed-form analytical expressions. The most widely-applied methods include the FORM (Ditlevsen and Madsen, 1996; Du, 2008; Low and Tang, 2007; Madsen et al., 2006) and the SORM (Der Kiureghian and Dakessian, 1998). The FORM/SORM methods provide an approximate solution to the closed-form procedures by transforming input stochastic distributions and limit state equations into normal distribution (u-)space. In the standard space, the design point is found as the point with the smallest distance between the failure zone (limit state equal to zero) and the origin of the space. The limit state is approximated with the linear function (FORM) or quadratic function (SORM). The probability of failure is estimated by integrating the area of the (linearized) failure zone. The advantage of FORM/SORM methods is the numerical efficiency and direct sensitivity analysis. The FORM/SORM methods are limited to the limit states which can be approximated with (close to) linear failure zones, and non-multiple design points (ISO-2394:2015, 2015). In the context of offshore wind, the FORM/SORM methods are widely applied (Jiang et al., 2017).

Simulation based In case that the limit state function cannot be approximated with FORM/SORM methods, simulation-based methods can be used.

The Monte Carlo methods are based on simulations that draw random samples from the original stochastic variable space (unlike the FORM/SORM methods, where additional transformation is required) and evaluate the limit state function for a given realization vector. The probability of failure is estimated by a number of realizations resulting in failure normalized to the total number of realizations. As the direct Monte Carlo methods sample randomly, a large number of simulations is required to obtain a converged solution. Similarly, as for the uncertainty quantification methods, other sampling methods can be applied to increase the numerical efficiency of Monte Carlo methods, for example, the importance sampling method (ISM) (Grooteman, 2008), subset simulations (Au et al., 2007), Latin hypercube (Sheikholeslami and Razavi, 2017), and asymptotic sampling (Bucher, 2009). The present thesis applies direct Monte Carlo methods to allow for a general limit state function and a large number of stochastic variables. Similarly as in the case of uncertainty quantification, focus on the general feasibility of this method is prioritized.

Risk informed Risk informed methods combine probability of failure (reliability) and consequences of failure (risk). The main objective of these methods is to minimize the total expected risk. In the context of offshore structures, the risk methods are widely applied in two main aspects; namely, 1) quantitative analyses and 2) qualitative analyses. The quantitative analyses aim at, for example calibrating the required reliability level based on sociotechnical analyses. In case of no risk of human loss, the optimal reliability level can be estimated based on cost optimization methods for new structures (Sørensen and Tarp-Johansen, 2005) and for existing structures (Nielsen and Sørensen, 2021). The qualitative analyses can be used to identify and mitigate various risks related to the design and operation of offshore structures. Such analyses are typically applied in an early stage of a design, where limited information is available, hence no quantitative analyses can be applied. Some risk informed methods include: failure mode and maintenance analysis (FMMA), failure mode and effect analysis (FMEA), threat matrix (Luengo and Kolios, 2015), tree and graphical analysis (fault tree (FT), bow-tie (BT)) (Ferdous et al., 2012), hazard analyses (hazard identification (HAZID) (Mokhtari et al., 2011), and hazard and operability studies (HAZOP)).

Challenges related to reliability assessment Although fully physics-based digital twins have not yet been applied to improve decision models for wind turbines, some publications already indicate how measurement data can be used to achieve such an improvement. Nielsen and Sørensen (2017) applied dynamic Bayesian networks to calibrate a Markov deterioration model based on past inspection data for wind turbine blades. Ziegler and Muskulus (2016)

investigated the feasibility of lifetime extension for offshore wind monopile substructures, with particular focus on identifying important parameters to monitor during the operational phase of the turbines. Leser et al. (2020) presented a general framework for fatigue damage estimation based on in-situ measurements. Mai et al. (2019) focused on prediction of the remaining useful lifetime of wind turbine support structure joints using met-ocean in-situ data. Augustyn et al. (2019) extended a conceptual framework for decision model updating based on information from a digital twin, initially proposed by (Tygesen et al., 2018), to be applied to offshore wind substructures. In the framework, a digital twin is established with an updated structural model and an updated load model, and then the digital twin is used to quantify uncertainty and update the structural reliability. In paper D, the framework by (Augustyn et al., 2019) is extended beyond its conceptual level where a probabilistic method is proposed for updating the structural reliability of offshore wind turbine substructures based on new information obtained from digital twins.

4.2 Reliability updating by use of digital twin information

A structural component must fulfill a number of structural checks, denoted as limit states. A limit state, according to (ISO-2394:2015, 2015), is defined as *a state beyond which a structure no longer satisfies the design criteria*. The limit states can be related to structural failure in extreme scenarios (the ultimate limit state), excessive vibrations or permanent deformations (the serviceability limit state), or damage accumulation due to dynamic loading (the fatigue limit state). In the proposed framework, the focus is placed on reliability update of structural components that are driven by the fatigue limit state. Once the structural reassessment for the fatigue limit state is confirmed, the other limit state must be confirmed. However, in practice, the fatigue limit state is typically driving for the majority of the critical structural components of jacket type substructures, for example joints. The remaining components, like piles, should typically be analyzed in terms of the ultimate limit state (given no special conditions like an aggressive corrosion environment is present).

The reliability assessment framework proposed in this thesis is summarized in Fig. 4.6. The framework consists of four steps. The first step is to establish distributions of the parameters, α_j, from numerical models that are updated. The numerical models include structural models and load models. The updated parameters can be, for example, soil stiffness, jacket stiffness, transition piece stiffness, water added mass, rotor mass, flange mass, scour, corrosion rate, inertia wave loading coefficient, drag wave loading coefficient.

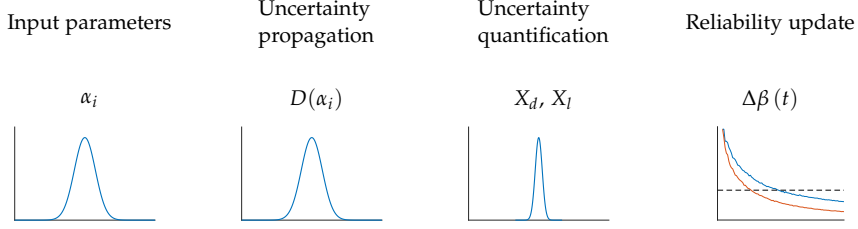| Input parameters	Uncertainty propagation	Uncertainty quantification	Reliability update
α_i	$D(\alpha_i)$	X_d, X_l	$\Delta\beta(t)$

Fig. 4.6: Structural reliability updating framework based on information from a digital twin. Updated parameters from digital twins are used to quantify uncertainty in fatigue damage accumulation. Subsequently, the structural reliability is updated that forms basis for decision model updating (Augustyn et al., 2021c).

The distributions are obtained from the model updating and load calibration steps, which are part of the process of establishing a digital twin, see Fig. 1.3. The second step is to propagate the uncertainty in the updated parameters and obtain the distributions of the corresponding fatigue damage, $D(\alpha_j)$ due to a particular updated parameter, α_j. The third step is to convert the uncertainty in fatigue damage (bias and variance of the distribution) into uncertainty in stress ranges, X_d, and X_l. The uncertainty in stress ranges, rather than in fatigue damage is required to comply with the probabilistic model for fatigue damage accumulation. The X_d uncertainty is calculated based on parameters that affect structural dynamics, while the X_l uncertainty is calculated from the parameters affecting loading. Finally, in step four, the updated reliability can be calculated using a probabilistic model where the updated X_d and X_l uncertainty are overwriting the generic, standard-based values. In the following part of this section more detailed description of proposed framework is provided.

Assume the fatigue damage is modeled as a stochastic variable depending on the uncertain parameters α_j. The fatigue damage is normally distributed, $D(\alpha_j) \sim \mathcal{N}\left(\mu_{D_j}, \sigma_{D_j}^2\right)$, with mean value μ_{D_j} and standard deviation σ_{D_j}). The mean value and standard deviation can be found through the maximum likelihood method, where the likelihood is defined as

$$L\left(\mu_{D_j}, \sigma_{D_j}\right) = \prod_{i=1}^{n} \frac{1}{\sqrt{2\pi}\sigma_{D_j}} \exp\left(-\frac{1}{2}\left(\frac{D_i - \mu_{D_j}}{\sigma_{D_j}}\right)^2\right), \qquad (4.1)$$

with D_i being the fatigue damage associated with the ith realization of α_j computed based on the updated structural model contained in the digital twin.

The log-likelihood function becomes

$$\ln L\left(\mu_{D_j}, \sigma_{D_j}\right) = -n \ln\left(\sqrt{2\pi}\sigma_{D_j}\right) - \sum_{i=1}^{n} \frac{1}{2}\left(\frac{D_i - \mu_{D_j}}{\sigma_{D_j}}\right)^2, \qquad (4.2)$$

and the optimal parameters are found as

$$\underset{\mu_{D_j}, \sigma_{D_j}}{\operatorname{argmax}} \ln L\left(\mu_{D_j}, \sigma_{D_j}\right). \qquad (4.3)$$

The fatigue damage accumulation, D, is proportional to the stress ranges, Δs, according to $D \propto \Delta s^m$ (assuming a linear SN curve), from which it follows $\Delta s \propto D^{1/m}$. The stress range distribution parameters can be computed from Monte Carlo simulations. Alternatively, assuming the damage distribution function is normal, the stress range distribution's mean, $\mu_{\Delta s}$, and coefficient of variation (CoV), $c_{\Delta s}$, can be approximated as

$$\mu_{\Delta s} = \mu_i^{1/m}, \qquad (4.4)$$

and

$$c_{\Delta s} = \frac{c_i}{m}, \qquad (4.5)$$

where μ_i and c_i are the mean and CoV of the fatigue damage distribution due to the uncertainty associated with α_j.

Fatigue damage accumulation can be modeled by a linear SN curve and Miner's rule. In such instance, the fatigue limit state, $g(t)$, at year $t \in \mathbb{N}$ for a structural component can be expressed as (IEC-61400-1:2019, 2019; Velarde et al., 2020)

$$g(t) = \Delta - \sum_{i=1}^{l} \sum_{j=1}^{z} \frac{N_{i,j} p_i t}{K \Delta s_{i,j}^{-m}} \left(X_d X_l X_s\right)^m, \qquad (4.6)$$

where Δ is the fatigue resistance and the double summation expresses the accumulated fatigue damage. In particular, Δ is a stochastic variable representing the limit value of the accumulated fatigue damage estimated using, for example, SN curves, including the uncertainty related to the application of Miner's rule for linear fatigue damage accumulation. In the expression for the fatigue damage, p_i is the yearly probability of occurrence for sea state i (including wind and wave parameters), $N_{i,j}$ is the number of cycles for the ith sea state and jth stress range $\Delta s_{i,j}$, and K and m are the parameters related to the SN curve, with m being the Wöhler exponent (Szala and Ligaj, 2014). The uncertainty related to the SN curve approach is included by modeling K as a stochastic variable. X_d, X_l, and X_s are stochastic variables that reflects the uncertainties associated with the structural dynamics, load modeling, and stress concentration according to models presented in (Sørensen

and Toft, 2014). Note that the presented linear SN curve formulation can be extended to a bi-linear one. Alternatively to the SN curve approach (linear or bi-linear), the fracture mechanics approach can be implemented.

In paper D, a probabilistic framework for updating the structural reliability of offshore wind turbine substructures based on digital twin information is presented. The updated reliability can be used as input to optimize decision models for the operation and maintenance of existing structures and the design of new structures. We present two case studies to exemplify the practical application of the framework by using information from previously established digital twins in papers A and B.

The first case study presents an application of the framework to the lifetime extension of existing structures. We use information from paper A, where a numerical model is updated, and use this updated model to investigate the impact of updating on fatigue lifetime estimation. Furthermore, we investigate the implication of load model updating, focusing on the impact of virtual sensing uncertainty. The uncertainties related to virtual sensing, quantified in paper B, are propagated to investigate their impact on fatigue lifetime estimation.

The second case study focuses on optimizing new structures. In this application, we assume that a digital twin will be established during the lifetime. In the design process this information is used to optimize the new structure. The application is based on Bayesian pre-posterior theory, which allows for including future (yet to be realized) information already in the design stage.

The paper applies well-known uncertainty quantification and reliability assessment methods. The uncertainty quantification is obtained by applying forward uncertainty propagation with subsequent maximum likelihood quantification. The reliability assessment, including updated uncertainty, is implemented by applying fatigue limit state. The uncertainty quantification and reliability assessment are applied in a simulation-based setting by using direct Monte Carlo methods. The main focus of the paper is on developing a theoretical framework with a direct link between established digital twins and decision models. Hence, together with the former steps described in this thesis, a complete framework linking data and value creation by using digital twin technology is delivered.

4.3 Summary

This chapter investigates uncertainty quantification and structural reliability are investigated. It is discussed how the state-of-the-art methods within uncertainty quantification and reliability assessment can be extended in the context of the offshore wind digital twin framework.

Paper D discusses the following thesis research question:

- Paper D directly addresses the second research question defined in section 1.2, namely: *How can an established digital twin be utilized to improve decision models of existing structures and optimize new structures?* The new information from the established digital twins is used to quantify the uncertainty in fatigue damage prediction. The quantified uncertainty is subsequently used to update the structural reliability. With the updated structural reliability, the decision models for existing and new structures can be optimized.

Furthermore, three specific research sub-questions, addressing challenges in the current state-of-the-art, are investigated:

- *How to quantify uncertainty in fatigue damage accumulation from a digital twin?* Paper D proposes a simulation-based Monte Carlo uncertainty propagation method. The distributions of the numerical parameters (updated from digital twins) are propagated and result in structural and loading uncertainty, which is quantified.

- *How to update reliability estimates based on quantified uncertainty?* A probabilistic model for fatigue damage reliability estimation is established, including uncertainty modeling. The structural and loading uncertainties are explicitly included and, given that they are quantified based on digital twin information, they substitute generic, standard-based values, hence allowing for updating the structural reliability. The structural reliability is updated based on the Monte Carlo method including updated uncertainty values.

- *How to use information from digital twins as decision basis for assessment of existing and design of new offshore wind structures?* Structural reliability estimation forms a basis for a decision-making process. By updating the structural reliability, for example, by using digital twins, the decision models driving the lifetime of existing structures, and material usage of new structures can be optimized. The updated reliability can be applied in well-established reliability- or risk-based inspection planning to optimize the lifetime of existing structures and the design of new structures.

The study presented in paper D is limited to:

- The reliability update procedure presented in paper D focuses on updating structural reliability of fatigue driven components. In principle, the reliability regarding the remaining limit states (ultimate, serviceability, accidental) should be fulfilled.

- In the proposed framework considering the fatigue limit state, only the structural dynamics and loading uncertainties are quantified. These

uncertainties are related to the loading side of the probabilistic model, while the uncertainty related to the resistance side, for example, fatigue damage accumulation and SN curve uncertainty, are not updated. If more data and experiments for the resistance side are obtained, the associated uncertainty can be updated and, together with the loading side uncertainty, be used to update the reliability by using the proposed method. Moreover, if other limit states are considered, uncertainty modeling should be revisited.

• Paper D focuses on the feasibility of the framework and not on its implementation efficiency. Consequently, application examples are presented where a limited number of parameters are considered at the same time. If more parameters are included, numerically efficient Monte Carlo methods suited for multidimensional space could be implemented, for example, surrogate models.

• The updating procedure focuses on updating structural reliability. The framework could be extended to include consequences of failure, hence applying risk-based methods. The benefit of including the risk-based framework is the possibility of including economical aspects directly in the formulation by deriving, instead of assuming, optimal reliability level.

Chapter 5

Conclusions and future perspective

This thesis investigates the practical feasibility of a digital twin concept in the context of offshore wind turbine jacket substructures. The state-of-the-art conceptual framework of digital twin developed for oil and gas application is extended in this thesis to account for offshore wind-specific aspects. The framework consists of a number of steps where each step is investigated in a separate chapter of this thesis as repeatedly indicated for the reader's convenience in Fig. 5.1. In this final chapter of the thesis, section 5.1 provides a summary and general conclusions based on the research described in the main body of the thesis. The general conclusion section is followed by future work suggestions in section 5.3, which could be considered to further mature the proposed digital twin framework.

5.1 Summary and general conclusions

Based on the research documented in the main body of this thesis and the appended papers, the following conclusions with regard to the investigated research questions are formulated:

- *How to establish a digital twin of an offshore wind substructure?*

    - A framework that allows establishing a digital twin of an offshore wind substructure is proposed. The system identification and model updating steps of the digital twin framework are exemplified with measurement data from operating offshore wind substructures. The virtual sensing, uncertainty quantification, and reliability update steps are exemplified by numerical studies.
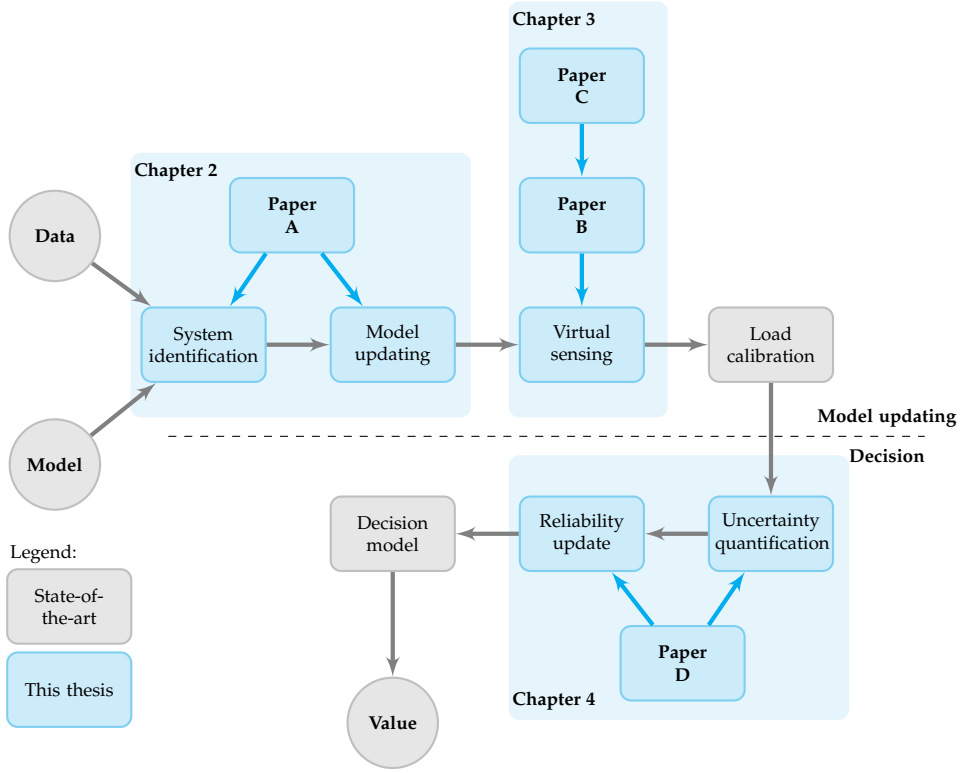
Fig. 5.1: Digital twin framework for improved decision models in the offshore wind application. The grey boxes indicate the state-of-the-art framework and the blue boxes indicate the contributions developed in the course of this thesis.

- This thesis contributes with novel full-scale validations and theoretical improvements of existing methods with a special focus on the offshore wind application. Particularly, the system identification and model updating steps are investigated based on measurements. The virtual sensing step is investigated based on numerical studies where improvements to the state-of-the-art methods are proposed by addressing wind turbine-foundation dynamics coupling and wave loading expansion.

- *How can an established digital twin be utilized to improve decision models of existing structures and optimize new structures?*

  - An established digital twin is used to update the structural reliability that forms the basis for optimization of reliability-based decision models. The proposed probabilistic framework is applicable to structural components in jacket substructures driven by

fatigue damage. The framework is executed in two steps: 1) quantification of uncertainty in fatigue damage estimation stemming from structural dynamics and loading effects (the two main components updated in the process of establishing a digital twin) and 2) reliability reassessment based on new, improved knowledge (in the form of updated models and quantified uncertainty).

– The novel contributions of this work consist of establishing an interface between digital twins and probabilistic procedures for reliability reassessment. Consequently, the information from digital twins can be used to optimize decision models, as digital twins bring superior information about structural conditions compared to the information available in the design stage. The framework is exemplified based on the digital twins established to address the first research question. Two application studies are presented; one that addresses lifetime extension of existing structures and one that addresses design optimization of new structures.

The first research question (establishing a digital twin) is investigated deeply. State-of-the-art methods for the digital twin steps have been applied or adjusted, and either experimental or numerical validation studies have been provided. The second question is investigated from a more fundamental research perspective. The use of the established digital twin is investigated in a theoretical framework (though with practical case study examples) and, as such, would benefit from further validation.

5.2 Industrial challenges

A successful industrial implementation of the digital twin concept requires addressing not only technical but also industrial challenges. A few of these industrial challenges—which have been identified but not fully addressed during the course of the thesis—are summarized below.

- Data sharing policy. Data is key in establishing a digital twin. In order to successfully develop and subsequently use a digital twin, various types and sources of data are required. A numerical model of both the foundation and the turbine is required. Typically, these models are prepared by specialized companies which do not necessarily share the detailed information required to establish the models. For example, a foundation designer establishes detailed models of a substructure, including modeling and calibration of soil stiffness, joint stiffness (in case of a jacket substructure), and a high-fidelity model of a transition piece. Even though information required to establish such models (geometry

and input soil parameters) are documented in design reports, modeling requires a significant amount of time and expertise to convert such information into high-quality numerical models. A wind turbine vendor is responsible for preparing a numerical model of the wind turbine, including detailed geometry of the blades, nacelle, and control system. Typically, such information is confidential and not explicitly shared externally. Consequently, high-quality numerical models of a turbine are difficult to obtain for any party but a turbine producer, as described in paper A. From a digital twin perspective, it would be beneficial to agree on some level of data sharing and transparency. In fact, a similar problem has already been solved in the design process where a wind turbine vendor and a foundation designer exchange information by means of simplified, yet representative models, for example, super elements. A similar approach can be explored for a digital twin application. Alternatively, a surrogate model of the turbine could be used in order to perform relative comparisons as basis for decision making; in the same way as site assessment for new turbines.

- Data continuity. In case the ownership of a wind turbine changes over the lifetime of a turbine, data should be exchanged to allow a new owner to benefit from information on past performance and incidents regarding the structure. Such aspect is especially important if continuous monitoring is applied. In case full and detailed documentation regarding monitoring can be transferred, it can save costs when (re)establishing a digital twin.

- Certification of new digital twin technology. A final goal of establishing a digital twin is to perform better decisions regarding operation and maintenance and design of structures. Considering the operational phase, one avenue to explore is to extend the lifetime of the structure. In order to confidently operate a structure beyond its lifetime, an operator must document sufficient reliability beyond an initial lifetime. Typically, a certification body is involved in this process to confirm that the used procedures are valid and sound. In case new procedures are used (as will be the case at least at the beginning of digital twin applications), extensive validation is required. This process can take some time and additional cost, which should be taken into account when considering the first digital twin applications.

- Business case. Current substructure design practices focus on providing a robust design that results in a structure that does not require any inspections of the main load-bearing components (legs, piles, joints) during the design lifetime. Consequently, a large portion of the costs is associated with CAPEX, while the OPEX portion is minimized. Such

design philosophy could be challenged, resulting in more optimized designs and increasing requirements for in-service inspection. Historically, this possibility has not been pursued as the notion was that the in-service inspections are expensive due to the offshore environment. However, this argument can be challenged when physical inspections can be substituted with digital twins based on remote measurements. In paper D, an application study is provided where a digital twin can be used to optimize new structures. Despite the theoretical readiness of such application, further discussion should follow and modifications to currently used business cases are required to fully benefit from this possibility.

5.3 Future perspective

In the course of this thesis, a number of challenges have been addressed as described in the previous section. Nevertheless, some points remain open and new ones have been discovered. Below, suggestions for future work related to particular steps in the proposed digital twin framework are outlined.

- System identification. In the proposed framework, system identification results were carefully selected in order to minimize uncertainties stemming from the violation of the system identification assumptions. Consequently, only a portion of the available data was used. It would be interesting to investigate system identification uncertainty for both idling and operational cases with the aim of including the operational cases as well.

- Model updating. The inverse problem solved in the proposed sensitivity-based updating scheme is typically ill-posed due to more parameters to be updated compared to the identified responses. One way to address this problem is the proposed regularization. Alternatively, one could increase the number of responses. It could be done either directly by identifying more responses/modes or indirectly by exploring a closed-loop updating scheme. The former can be explored by extending sensor setups and thereby allowing for identification of more physical modes.

- Virtual sensing. Within the modal expansion methods, one could further investigate practical challenges in sensor techniques, for example, signal drift due to acceleration integration, wave surface elevation reconstruction, and sensor fusion. To address the issue of non-linear systems (non-linear response stemming from the controller and soil stiffness), one could investigate (conditional for particular environmental

and operational parameters) linear approximations of non-linear systems for mildly non-linear conditions or techniques suited for non-linear system identification. Alternatively to modal expansion, other virtual sensing methods, for example, Kalman filters, could be investigated.

- Load calibration. Although load calibration is an important part of the framework, it is not addressed in this thesis due to data and time constraints encountered during the execution phase of the project. Hence, it would be beneficial to first conduct a literature survey exploring the feasibility of various load calibration methods in the context of offshore wind applications. The literature is present for wind calibration for onshore wind turbines and wave calibration for offshore structures. These studies form a good starting point for an extension to offshore wind structures. The main challenge in this context lays in updating wind, wave, and potentially other sources of loading at the same time.

- Uncertainty quantification. In the proposed framework, the uncertainties in the input parameters are estimated and subsequently propagated through the numerical model for fatigue damage estimation. Alternatively, the Bayesian approach could be explored. This approach has a strong merit in explicit and rigorous uncertainty quantification and (more importantly for practical applications) the ability to build in prior knowledge in terms of, for example, expert knowledge. The latter is especially valuable if poor or incomplete data is present, which still allows for updating uncertainty, unlike in the classical uncertainty quantification methods.

- Reliability update. The existing reliability-based methods aim at updating the structural reliability, which can be used to update decision models based on the probability of failure. The proposed framework can benefit from extending the decision models with consequences of failure, which potentially can change over time, especially if different cost models are considered for various stages of the lifetime (design vs. operation stages). This potential has been raised in recent studies proposing varying target reliability levels for design and operating turbines. By applying a risk based decision model, this effect could be accounted for. Moreover, optimal (risk-wise) inspection planning could be considered. For example, repair and control of the wind turbine could be preformed when predicted fatigue damage is high and price of electricity is low. The presented framework focuses on reliability assessment for a particular component. Interaction between components is not taken into account. The framework can be extended to account for correlation between components and hence explore the reliability of

a system as a whole instead of independent components. The system approach can be beneficial to consider for structurally redundant systems, for example, jacket substructures, where the possibility for force redistribution in case of failure is possible.

Chapter 5. Conclusions and future perspective

Bibliography

API-RP-2A (2014). "Recommended Practice for Planning, Designing and Constructing Fixed Offshore Platforms." *Report no.*, American Petroleum Institute.

Au, S., Ching, J., and Beck, J. (2007). "Application of subset simulation methods to reliability benchmark problems." *Structural Safety*, 29(3), 183–193 A Benchmark Study on Reliability in High Dimensions.

Augustyn, D., Cosack, N., and Ulriksen, M. D. (2021a). "On the influence of environmental and operational variability on modal parameters of offshore wind support structures." *Submitted to: Marine Structures*.

Augustyn, D., Pedersen, R. R., Tygesen, U. T., Ulriksen, M. D., and Sørensen, J. D. (2021b). "Feasibility of modal expansion for virtual sensing in offshore wind jacket substructures." *Marine Structures*, 79, 103019.

Augustyn, D., Smolka, U., Tygesen, U. T., Ulriksen, M. D., and Sørensen, J. D. (2020). "Data-driven model updating of an offshore wind jacket substructure." *Applied Ocean Research*, 104, 102366.

Augustyn, D., Tygesen, U. T., Ulriksen, M. D., and Sørensen, J. D. (2019). "Data-driven design and operation of offshore wind structures." *The Proceedings of The Twenty-ninth (2019) International Offshore and Polar Engineering Conference*, Vol. 1, 491–498.

Augustyn, D., Ulriksen, M. D., and Sørensen, J. D. (2021c). "Reliability updating of offshore wind substructures by use of digital twin information." *Energies*, 14(18).

Avitabile, P. and Pingle, P. (2012). "Prediction of full field dynamic strain from limited sets of measured data." *Shock and Vibration*, 19(5), 765 – 785.

Bao, Y., Tang, Z., and Li, H. (2020). "Compressive-sensing data reconstruction for structural health monitoring: a machine-learning approach." *Structural Health Monitoring*, 19(1), 293–304.

Baqersad, J., Niezrecki, C., and Avitabile, P. (2015). "Extracting full-field dynamic strain on a wind turbine rotor subjected to arbitrary excitations using 3d point tracking and a modal expansion technique." *Journal of Sound and Vibration*, 352, 16–29.

Beck, J. L. and Au, S.-K. (2002). "Bayesian updating of structural models and reliability using markov chain monte carlo simulation." *Journal of Engineering Mechanics*, 128(4), 380–391.

Beck, J. L. and Katafygiotis, L. S. (1998). "Updating models and their uncertainties. i: Bayesian statistical framework." *Journal of Engineering Mechanics*, 124(4), 455–461.

Bibliography

Bendat, J. S. and Piersol, A. G. (1980). *Engineering applications of correlation and spectral analysis.*

Berg, B. (2004). *Introduction to Markov Chain Monte Carlo simulations and their statistical analysis.* 1–52.

Bernal, D. and Ulriksen, M. D. (2019). "Subspace exclusion zones for damage localization." *Mechanical Systems and Signal Processing*, 114, 120–127.

Bernal, D., Ulriksen, M. D., and Memarzadeh, E. (2022). "Static constraints in direct model updating." *Mechanical Systems and Signal Processing*, 163, 108170.

Bertha, M. and Golinval, J.-C. (2017). "Identification of non-stationary dynamical systems using multivariate arma models." *Mechanical Systems and Signal Processing*, 88, 166–179.

Blatman, G. and Sudret, B. (2011). "Adaptive sparse polynomial chaos expansion based on least angle regression." *Journal of Computational Physics*, 230(6), 2345–2367.

Bodeux, J.-B. and Golinval, J.-C. (2003). "Modal identification and damage detection using the data-driven stochastic subspace and armav methods." *Mechanical Systems and Signal Processing*, 17(1), 83–89.

Bom, L., Siedler, S., and Tautz-Weinert, J. (2020). "Validation of cpt-based initial soil stiffness in sand for offshore wind jacket piles." *Proceedings of the Messen in der Geotechnik*, 1–21 (02).

Brincker, R., Skafte, A., López-Aenlle, M., Sestieri, A., D'Ambrogio, W., and Canteli, A. (2014). "A local correspondence principle for mode shapes in structural dynamics." *Mechanical Systems and Signal Processing*, 45(1), 91–104.

Bucher, C. (2009). "Asymptotic sampling for high-dimensional reliability analysis." *Probabilistic Engineering Mechanics*, 24(4), 504–510.

Cauberghe, B., Guillaume, P., Verboven, P., and Parloo, E. (2003). "Identification of modal parameters including unmeasured forces and transient effects." *Journal of Sound and Vibration*, 265(3), 609–625.

Caughey, T. K. (1960). "Classical normal modes in damped linear dynamic systems." *Journal of Applied Mechanics*, 27(2), 269–271.

Caughey, T. K. and O'Kelly, M. E. J. (1965). "Classical Normal Modes in Damped Linear Dynamic Systems." *Journal of Applied Mechanics*, 32(3), 583–588.

Ceravolo, R. and Abbiati, G. (2013). "Time domain identification of structures: Comparative analysis of output-only methods." *Journal of Engineering Mechanics*, 139(4), 537–544.

Chatzi, E. and Fuggini, C. (2012). "Structural identification of a super-tall tower by gps and accelerometer data fusion using a multi-rate kalman filter." *Life-cycle and Sustainability of Civil Infrastructure Systems*, Leiden, CRC Press, 144 – 151.

Chatzi, E. N. and Smyth, A. W. (2009). "The unscented kalman filter and particle filter methods for nonlinear structural system identification with non-collocated heterogeneous sensing." *Structural Control and Health Monitoring*, 16(1), 99–123.

Ching, J., Beck, J. L., and Porter, K. A. (2006). "Bayesian state and parameter estimation of uncertain dynamical systems." *Probabilistic Engineering Mechanics*, 21(1), 81–96.

Ching, J. and Chen, Y.-C. (2007). "Transitional markov chain monte carlo method for bayesian model updating, model class selection, and model averaging." *Journal of Engineering Mechanics*, 133(7), 816–832.

Bibliography

Collins, J. D., Hart, G. C., Hasselman, T. K., and Kennedy, B. (1974). "Statistical identification of structures." *AIAA Journal*, 12(2), 185–190.

Der Kiureghian, A. and Dakessian, T. (1998). "Multiple design points in first and second-order reliability." *Structural Safety*, 20(1), 37–49.

Dertimanis, V., Chatzi, E., Azam, S. E., and Papadimitriou, C. (2016a). "Output-only fatigue prediction of uncertain steel structures." *8th European Workshop on Structural Health Monitoring (EWSHM 2016)*, Vol. 2, 869 – 879.

Dertimanis, V. K., Chatzi, E., Eftekhar Azam, S., and Papadimitriou, C. (2016b). "Fatigue assessment in steel railway bridges using output only vibration measurements and partial structural information." *Proceedings of the Third International Conference on Railway Technology: Research, Development and Maintenance*, Vol. 110, 139.

Devriendt, C., Magalhaes, F., Weijtjens, W., De Sitter, G., Cunha, A., and Guillaume, P. (2013). "Automatic identification of the modal parameters of an offshore wind turbine using state-of-the-art operational modal analysis techniques." *Proceedings of the 5th International Operational Modal Analysis Conference, IOMAC 2013* (01).

Ditlevsen, O. and Madsen, H. (1996). *Structural Reliability Methods*. John Wiley & Sons Ltd.

DNVGL-RP-C203 (2016). "Fatigue design of offshore steel structures." *Report no.*

DNVGL-RP-C205 (2010). "Environmental conditions and environmental loads." *Report no.*, DNV GL.

DNVGL-ST-0126 (2016). "Support structures for wind turbines." *Report no.*

Dong, W., Moan, T., and Gao, Z. (2012). "Fatigue reliability analysis of the jacket support structure for offshore wind turbine considering the effect of corrosion and inspection." *Reliability Engineering & System Safety*, 106, 11–27.

Dong, X., Lian, J., Yang, M., and Wang, H. (2014). "Operational modal identification of offshore wind turbine structure based on modified stochastic subspace identification method considering harmonic interference." *Journal of Renewable and Sustainable Energy*, 6(3), 033128.

Du, X. (2008). "Unified Uncertainty Analysis by the First Order Reliability Method." *Journal of Mechanical Design*, 130(9) 091401.

Efthymiou, M. and Durkin, S. (1985). "Stress concentrations in t/y and gap/overlap k-joints." *Proceedings of the 4th International Conference on Behaviour of Offshore Structures*, 12.

Eldred, M. and Burkardt, J. (2009). *Comparison of Non-Intrusive Polynomial Chaos and Stochastic Collocation Methods for Uncertainty Quantification*.

Ewins, D. (2009). *Modal Testing: Theory, Practice and Application*. John Wiley & Sons.

Ewins, D. J. and Imregun, M. (1988). "On the reliability of computational dynamic response prediction capabilities (dynas)." *Journal of the Society of Environmental Engineers*, 27(116), 3–13.

Faber, M. H. (2002). "Risk-based inspection: The framework." *Structural Engineering International*, 12(3), 186–195.

Ferdous, R., Khan, F., Sadiq, R., Amyotte, P., and Veitch, B. (2012). "Handling and updating uncertain information in bow-tie analysis." *Journal of Loss Prevention in the Process Industries*, 25(1), 8–19.

Bibliography

Fox, R. L. and Kapoor, M. P. (1968). "Rates of change of eigenvalues and eigenvectors.." *AIAA Journal*, 6(12), 2426–2429.

Fricke, W. (2003). "Fatigue analysis of welded joints: state of development." *Marine Structures*, 16(3), 185–200.

Friswell, M. I., Mottershead, J. E., and Ahmadian, H. (1998). "Combining Subset Selection and Parameter Constraints in Model Updating." *Journal of Vibration and Acoustics*, 120(4), 854–859.

Gil, P., Santos, F., Palma, L., and Cardoso, A. (2015). "Recursive subspace system identification for parametric fault detection in nonlinear systems." *Applied Soft Computing*, 37, 444–455.

Global Wind Energy Council (2020). "Global offshore wind report 2020." *Report no.*, <https://gwec.net/wp-content/uploads/2020/12/GWEC-Global-Offshore-Wind-Report-2020.pdf>.

Goller, B., Broggi, M., Calvi, A., and Schuëller, G. I. (2011). "A stochastic model updating technique for complex aerospace structures." *Finite Elem. Anal. Des.*, 47(7), 739–752.

Govers, Y. and Link, M. (2010). "Stochastic model updating—covariance matrix adjustment from uncertain experimental modal data." *Mechanical Systems and Signal Processing*, 24(3), 696–706.

Graugaard-Jensen, J., Brincker, R., Hjelm, H., and Munch, K. (2005). "Modal based fatigue monitoring of steel structures." *Structural Dynamics EURODYN 2005*, C. Soize and G. Schuëller, eds., 305–310.

Grooteman, F. (2008). "Adaptive radial-based importance sampling method for structural reliability." *Structural Safety*, 30(6), 533–542.

Hansen, M. H. (2007). "Aeroelastic instability problems for wind turbines." *Wind Energy*, 10(6), 551–577.

Helton, J. and Davis, F. (2003). "Latin hypercube sampling and the propagation of uncertainty in analyses of complex systems." *Reliability Engineering & System Safety*, 81(1), 23–69.

Henkel, M., Häfele, J., Weijtjens, W., Devriendt, C., Gebhardt, C., and Rolfes, R. (2020). "Strain estimation for offshore wind turbines with jacket substructures using dual-band modal expansion." *Marine Structures*, 71, 102731.

Henkel, M., Weijtjens, W., and Devriendt, C. (2019). "Validation of virtual sensing on subsoil strain data of an offshore wind turbine." *8th IOMAC - International Operational Modal Analysis Conference, Proceedings 2019*, 8th IOMAC - International Operational Modal Analysis Conference, Proceedings, 765–774 (5).

Heylen, W. and Sas, P. (2005). "Modal analysis theory and testing.

Hjelm, H., Brincker, R., Graugaard-Jensen, J., and Munch, K. (2005). "Determination of stress histories in structures by natural input modal analysis." *Conference Proceedings*, United States, Society for Experimental Mechanics. null ; Conference date: 31-01-2005 Through 03-02-2005.

Huang, C. (2001). "Structural identification from ambient vibration measurement using the multivariate ar model." *Journal of Sound and Vibration*, 241(3), 337–359.

Häckell, M. W. and Rolfes, R. (2013). "Monitoring a 5mw offshore wind energy converter—condition parameters and triangulation based extraction of modal parameters." *Mechanical Systems and Signal Processing*, 40(1), 322 – 343.

Bibliography

Hübler, C., Gebhardt, C. G., and Rolfes, R. (2018). "Methodologies for fatigue assessment of offshore wind turbines considering scattering environmental conditions and the uncertainty due to finite sampling." *Wind Energy*, 21(11), 1092–1105.

IEC-61400-1:2019 (2019). "Wind energy generation systems - Part 1: Design requirements." *Report no.*, International Electrotechnical Commission.

Iliopoulos, A., Weijtjens, W., Van Hemelrijck, D., and Devriendt, C. (2016). *Full-field strain prediction applied to an offshore wind turbine*, Vol. 3 of *Conference Proceedings of the Society for Experimental Mechanics Series*. Springer International Publishing, 1 edition, 1–9, 1 edition.

Iliopoulos, A., Weijtjens, W., Van Hemelrijck, D., and Devriendt, C. (2017). "Fatigue assessment of offshore wind turbines on monopile foundations using multi-band modal expansion." *Wind Energy*, 20(8), 1463–1479.

ISO-2394:2015 (2015). "General principles on reliability for structures." *Report no.*

James, III, G. H., Carne, T. G., and Lauffer, J. P. (1993). "The natural excitation technique (next) for modal parameter extraction from operating wind turbines.

Jiang, Z., Hu, W., Dong, W., Gao, Z., and Ren, Z. (2017). "Structural reliability analysis of wind turbines: A review." *Energies*, 10(12).

Juang, J.-N. (1994). *Applied System Identification*. Prentice-Hall, Inc., USA.

Juang, J.-N. and Pappa, R. S. (1985). "An eigensystem realization algorithm for modal parameter identification and model reduction." *Journal of Guidance, Control, and Dynamics*, 8(5), 620–627.

Katafygiotis, L. S. and Beck, J. L. (1998). "Updating models and their uncertainties. ii:model identifiability." *Journal of Engineering Mechanics*, 124(4), 463–467.

Kennedy, C. C. and Pancu, C. D. P. (1947). "Use of vectors in vibration measurement and analysis." *Journal of the Aeronautical Sciences*, 14(11), 603–625.

Kennedy, M. C. and O'Hagan, A. (2001). "Bayesian calibration of computer models." *Journal of the Royal Statistical Society: Series B (Statistical Methodology)*, 63(3), 425–464.

Kerschen, G., Worden, K., Vakakis, A. F., and Golinval, J.-C. (2006). "Past, present and future of nonlinear system identification in structural dynamics." *Mechanical Systems and Signal Processing*, 20(3), 505–592.

Knio, O. M. and Maître, O. P. L. (2006). "Uncertainty propagation in CFD using polynomial chaos decomposition." *Fluid Dynamics Research*, 38(9), 616–640.

Kwon, S.-D. (2010). "Uncertainty analysis of wind energy potential assessment." *Applied Energy*, 87(3), 856–865.

Larimore, W. (1990). "Canonical variate analysis in identification, filtering, and adaptive control." *29th IEEE Conference on Decision and Control*, 596–604 vol.2.

Lee, G.-M. (2007). "Prediction of strain responses from the measurements of displacement responses." *Mechanical Systems and Signal Processing*, 21(2), 1143–1152.

Lee, J.-M., Seo, J.-K., Kim, M.-H., Shin, S.-B., Han, M.-S., Park, J.-S., and Mahendran, M. (2010). "Comparison of hot spot stress evaluation methods for welded structures." *International Journal of Naval Architecture and Ocean Engineering*, 2(4), 200–210.

Bibliography

Leser, P. E., Warner, J. E., Leser, W. P., Bomarito, G. F., Newman, J. A., and Hochhalter, J. D. (2020). "A digital twin feasibility study (part ii): Non-deterministic predictions of fatigue life using in-situ diagnostics and prognostics." *Engineering Fracture Mechanics*, 229, 106903.

Link, M. (1993). "Updating of analytical models – procedure and experience." *Proceedings of Conference on Modern Practice in Stress and Vibration Analysis* (April).

Liu, C. W., Wu, J. Z., and Zhang, Y. G. (2011). "Review and prospect on modal parameter identification of spatial lattice structure based on ambient excitation." *Advances in Structural Engineering*, Vol. 94 of *Applied Mechanics and Materials*, Trans Tech Publications Ltd, 1271–1277 (10).

Liu, Z., Wang, X., and Kang, S. (2014). "Stochastic performance evaluation of horizontal axis wind turbine blades using non-deterministic CFD simulations." *Energy*, 73(C), 126–136.

Lockwood, B. A. and Anitescu, M. (2012). "Gradient-enhanced universal kriging for uncertainty propagation." *Nuclear Science and Engineering*, 170(2), 168–195.

Lourens, E., Papadimitriou, C., Gillijns, S., Reynders, E., De Roeck, G., and Lombaert, G. (2012a). "Joint input-response estimation for structural systems based on reduced-order models and vibration data from a limited number of sensors." *Mechanical Systems and Signal Processing*, 29, 310–327.

Lourens, E., Reynders, E., De Roeck, G., Degrande, G., and Lombaert, G. (2012b). "An augmented kalman filter for force identification in structural dynamics." *Mechanical Systems and Signal Processing*, 27, 446–460.

Low, B. K. and Tang, W. H. (2007). "Efficient spreadsheet algorithm for first-order reliability method." *Journal of Engineering Mechanics*, 133(12), 1378–1387.

Luczak, M., Manzato, S., Peeters, B., Branner, K., Berring, P., and Kahsin, M. (2014). "Updating finite element model of a wind turbine blade section using experimental modal analysis results." *Shock and Vibration*, 2014.

Luengo, M. M. and Kolios, A. (2015). "Failure mode identification and end of life scenarios of offshore wind turbines: A review." *Energies*, 8(8), 8339–8354.

Madsen, H. O., Krenk, S., and Lind, N. C. (2006). *Methods of structural safety*. Courier Corporation.

Maes, K., Iliopoulos, A., Weijtjens, W., Devriendt, C., and Lombaert, G. (2016). "Dynamic strain estimation for fatigue assessment of an offshore monopile wind turbine using filtering and modal expansion algorithms." *Mechanical Systems and Signal Processing*, 76-77, 592–611.

Magalhães, F., Caetano, E., and Álvaro Cunha (2007). "Challenges in the application of stochastic modal identification methods to a cable-stayed bridge." *Journal of Bridge Engineering*, 12(6), 746–754.

Mai, Q. A., Weijtjens, W., Devriendt, C., Morato, P. G., Rigo, P., and Sørensen, J. D. (2019). "Prediction of remaining fatigue life of welded joints in wind turbine support structures considering strain measurement and a joint distribution of oceanographic data." *Marine Structures*, 66, 307–322.

Marelli, S. and Sudret, B. (2014). *UQLab: A Framework for Uncertainty Quantification in Matlab*. 2554–2563.

Mares, C., Mottershead, J., and Friswell, M. (2006). "Stochastic model updating: Part 1—theory and simulated example." *Mechanical Systems and Signal Processing*, 20(7), 1674–1695.

Bibliography

Mariani, S. and Corigliano, A. (2005). "Impact induced composite delamination: state and parameter identification via joint and dual extended kalman filters." *Computer Methods in Applied Mechanics and Engineering*, 194(50), 5242–5272.

Martinez-Luengo, M., Kolios, A., and Wang, L. (2016). "Structural health monitoring of offshore wind turbines: A review through the statistical pattern recognition paradigm." *Renewable and Sustainable Energy Reviews*, 64, 91–105.

McFarland, J., Mahadevan, S., Romero, V., and Swiler, L. (2008). "Calibration and uncertainty analysis for computer simulations with multivariate output." *AIAA Journal*, 46(5), 1253–1265.

Metropolis, N. and Ulam, S. (1949). "The monte carlo method." *Journal of the American Statistical Association*, 44(247), 335–341 PMID: 18139350.

Miner, M. A. (2021). "Cumulative Damage in Fatigue." *Journal of Applied Mechanics*, 12(3), A159–A164.

Moaveni, B., He, X., Conte, J. P., Restrepo, J. I., and Panagiotou, M. (2011). "System identification study of a 7-story full-scale building slice tested on the ucsd-nees shake table." *Journal of Structural Engineering*, 137(6), 705–717.

Mokhtari, K., Ren, J., Roberts, C., and Wang, J. (2011). "Application of a generic bow-tie based risk analysis framework on risk management of sea ports and offshore terminals." *Journal of Hazardous Materials*, 192(2), 465–475.

Mottershead, J., Link, M., and Friswell, M. (2011). "The sensitivity method in finite element model updating: A tutorial." *Mechanical Systems and Signal Processing*, 25(7), 2275–2296.

Mühle, F., Schottler, J., Bartl, J., Futrzynski, R., Evans, S., Bernini, L., Schito, P., Draper, M., Guggeri, A., Kleusberg, E., Henningson, D. S., Hölling, M., Peinke, J., Adaramola, M. S., and Sætran, L. (2018). "Blind test comparison on the wake behind a yawed wind turbine." *Wind Energy Science*, 3(2), 883–903.

Murcia, J. P., Réthoré, P. E., Natarajan, A., and Sørensen, J. D. (2015). "How many model evaluations are required to predict the AEP of a wind power plant?." *Journal of Physics: Conference Series*, 625, 012030.

Naets, F., Cuadrado, J., and Desmet, W. (2015). "Stable force identification in structural dynamics using kalman filtering and dummy-measurements." *Mechanical Systems and Signal Processing*, 50-51, 235–248.

Nielsen, J. S. and Sørensen, J. D. (2017). "Bayesian estimation of remaining useful life for wind turbine blades." *Energies*, 10(5).

Nielsen, J. S. and Sørensen, J. D. (2021). "Risk-based derivation of target reliability levels for life extension of wind turbine structural components." *Wind Energy*, 24(9), 939–956.

Noël, J. and Kerschen, G. (2017). "Nonlinear system identification in structural dynamics: 10 more years of progress." *Mechanical Systems and Signal Processing*, 83, 2–35.

O'Callahan, J., Avitabile, P., and Riemer, R. (1989). "System equivalent reduction expansion process (serep).." *The Proceedings of The 7th International Modal Analysis Conference (IMAC)*.

Okubo, N. and Yamaguchi, K. (1995). "Prediction of Dynamic Strain Distribution Under Operating Condition by Use of Modal Analysis." *Proceedings of the 13th International Modal Analysis Conference*, Vol. 2460 of *Society of Photo-Optical Instrumentation Engineers (SPIE) Conference Series*, 91 (January).

Bibliography

Onoufriou, T. (1999). "Reliability based inspection planning of offshore structures." *Marine Structures*, 12(7), 521–539.

Pakenham, B., Ermakova, A., and Mehmanparast, A. (2021). "A review of life extension strategies for offshore wind farms using techno-economic assessments." *Energies*, 14(7).

Palanisamy, R. P., Cho, S., Kim, H., and Sim, S. (2015). "Experimental validation of kalman filter-based strain estimation in structures subjected to non-zero mean input." *Smart Structures and Systems*, 15, 489–503.

Papadimitriou, C., Fritzen, C.-P., Kraemer, P., and Ntotsios, E. (2011). "Fatigue predictions in entire body of metallic structures from a limited number of vibration sensors using kalman filtering." *Structural Control and Health Monitoring*, 18(5), 554–573.

Paris, P. and Erdogan, F. (1963). "A Critical Analysis of Crack Propagation Laws." *Journal of Basic Engineering*, 85(4), 528–533.

Patelli, E., Govers, Y., Broggi, M., Gomes, H., Link, M., and Mottershead, J. (2017). "Sensitivity or bayesian model updating: a comparison of techniques using the dlr airmod test data." *Archive of Applied Mechanics*, 87(5), 905–925.

Pedersen, M. W., Andersen, K., E., Ulriksen, M. D., and Damkilde, L. (2019). "Examination of modal expansion and kalman filtering techniques for vibration estimation." *9th ECCOMAS Thematic Conference on Smart Structures and Materials*, 1515–1526.

Peeters, B., Auweraer, H., Guillaume, P., and Leuridan, J. (2004). "The polymax frequency-domain method: a new standard for modal parameter estimation?." *Shock and Vibration*, 11, 395–409.

Rainieri, C. and Fabbrocino, G. (2014). "Influence of model order and number of block rows on accuracy and precision of modal parameter estimates in stochastic subspace identification." *International Journal of Lifecycle Performance Engineering*, 1(4), 317–334 PMID: 64099.

Rangel-Ramírez, J. G. and Sørensen, J. D. (2012). "Risk-based inspection planning optimisation of offshore wind turbines." *Structure and Infrastructure Engineering*, 8(5), 473–481.

Reynders, E. (2012). "System identification methods for (operational) modal analysis: Review and comparison." *Archives of Computational Methods in Engineering*, 19, 51–124.

Reynders, E., Pintelon, R., and Roeck, G. (2008). "Uncertainty bounds on modal parameters obtained from stochastic subspace identification." *Mechanical Systems and Signal Processing*, 22(4), 948 – 969 Special Issue: Crack Effects in Rotordynamics.

Reynders, E. and Roeck, G. D. (2008). "Reference-based combined deterministic–stochastic subspace identification for experimental and operational modal analysis." *Mechanical Systems and Signal Processing*, 22(3), 617–637.

Reynders, E., Teughels, A., and De Roeck, G. (2010). "Finite element model updating and structural damage identification using omax data." *Mechanical Systems and Signal Processing*, 24(5), 1306–1323 Special Issue: Operational Modal Analysis.

Rinker, J. M. (2016). "Calculating the sensitivity of wind turbine loads to wind inputs using response surfaces." *Journal of Physics: Conference Series*, 753, 032057.

Sayer, F., Antoniou, A., Goutianos, S., Gebauer, I., Branner, K., and Balzani, C. (2020). "ReliaBlade project: A material's perspective towards the digitalization of wind turbine rotor blades." *IOP Conference Series: Materials Science and Engineering*, 942, 012006.

Bibliography

Schedlinski, C., Wagner, F., Bohnert, K., Frappier, J., Irrgang, A., Lehmann, R., and Muller, A. "Experimental modal analysis and computional model updating for a car body in white." *Proceedings of ISMA2004*.

Schwarz-Wolf, B. M., Ulriksen, M. D., Augustyn, D., Jensen, M. S., and Pedersen, R. R. (2021). "Closed-loop updating of wind turbine models using blade pitch excitation." *Proceedings of The Tenth (2021) International Conference on Structural Health Monitoring of Intelligent Infrastructure, SHMII10*.

Sheikholeslami, R. and Razavi, S. (2017). "Progressive latin hypercube sampling: An efficient approach for robust sampling-based analysis of environmental models." *Environmental Modelling & Software*, 93, 109–126.

Shih, C., Tsuei, Y., Allemang, R., and Brown, D. (1988). "Complex mode indication function and its applications to spatial domain parameter estimation." *Mechanical Systems and Signal Processing*, 2(4), 367–377.

Shokravi, H., Shokravi, H., Bakhary, N., Rahimian Koloor, S. S., and Petrů, M. (2020). "Health monitoring of civil infrastructures by subspace system identification method: An overview." *Applied Sciences*, 10(8).

Skafte, A., Kristoffersen, J., Vestermark, J., Tygesen, U. T., and Brincker, R. (2017). "Experimental study of strain prediction on wave induced structures using modal decomposition and quasi static ritz vectors." *Engineering Structures*, 136, 261 – 276.

Skjoldan, P. F. and Hansen, M. H. (2012). "Implicit floquet analysis of wind turbines using tangent matrices of a non-linear aeroelastic code." *Wind Energy*, 15(2), 275–287.

Smith, R. C. (2013). *Uncertainty Quantification: Theory, Implementation, and Applications*. Society for Industrial and Applied Mathematics, USA.

Sobol, I. (2001). "Global sensitivity indices for nonlinear mathematical models and their monte carlo estimates." *Mathematics and Computers in Simulation*, 55(1), 271–280 The Second IMACS Seminar on Monte Carlo Methods.

Soize, C. (2003). "Random matrix theory and non-parametric model of random uncertainties in vibration analysis." *Journal of Sound and Vibration*, 263(4), 893–916.

Staino, A., Basu, B., and Nielsen, S. R. K. (2012). "Actuator control of edgewise vibrations in wind turbine blades." *Journal of Sound and Vibration*, 331(6), 1233–1256.

Straub, D. and Faber, M. H. (2005). "Risk based inspection planning for structural systems." *Structural Safety*, 27(4), 335–355.

Sudret, B. (2008). "Global sensitivity analysis using polynomial chaos expansions." *Reliability Engineering & System Safety*, 93(7), 964–979 Bayesian Networks in Dependability.

Szala, G. and Ligaj, B. (2014). "Effect of the exponent in the description of wöhler fatigue diagram on the results of calculations of fatigue life." *14th Fracture and Fatigue of Materials and Structures*, Vol. 598 of *Key Engineering Materials*, Trans Tech Publications Ltd, 231–236 (3).

Sørensen, J. D. and Tarp-Johansen, N. J. (2005). "Reliability-based Optimization And Optimal Reliability Level of Offshore Wind Turbines." *International Journal of Offshore and Polar Engineering*, 15(02).

Sørensen, J. D. and Toft, H. (2010). "Probabilistic design of wind turbines." *Energies*, 3(2), 241–257.

Bibliography

Sørensen, J. D. and Toft, H. S. (2014). "Safety Factors—IEC 61400-1 ed. 4 — background document." *Report no.*, DTU Wind Energy-E-Report-0066(EN).

Tarpø, M. (2020). "Stress estimation of offshore strucutres." Doctoral dissertation, Aarhus University,

Tarpø, M., Nabuco, B., Georgakis, C., and Brincker, R. (2020a). "Expansion of experimental mode shape from operational modal analysis and virtual sensing for fatigue analysis using the modal expansion method." *International Journal of Fatigue*, 130, 105280.

Tarpø, M., Nabuco, B., Georgakis, C., and Brincker, R. (2020b). "Expansion of experimental mode shape from operational modal analysis and virtual sensing for fatigue analysis using the modal expansion method." *International Journal of Fatigue*, 130, 105280.

Tcherniak, D., Chauhan, S., and Hansen, M. H. (2011). "Applicability limits of operational modal analysis to operational wind turbines." *Structural Dynamics and Renewable Energy, Volume 1*, T. Proulx, ed., New York, NY, Springer New York, 317–327.

Tygesen, U. T., Jepsen, M., Vestermark, J., Dollerup, N., and Pedersen, A. (2018). "The true digital twin concept for fatigue re-assessment of marine structures." *Proceedings of the ASME 2018 37th International Conference on Ocean, Offshore and Arctic Engineering OMAE2018* (06).

Tygesen, U. T., Worden, K., Rogers, T., Manson, G., and Cross, E. (2019). "State-of-the-art and future directions for predictive modelling of offshore structure dynamics using machine learning." *Dynamics of Civil Structures, Volume 2*, Springer International Publishing, 223–233.

Ulriksen, M. D. (2018). "Damage localization for structural health monitoring: An exploration of three new vibration-based schemes." Doctoral dissertation, Aalborg University,

Ulriksen, M. D., Bram, M. V., Pedersen, H. H., Liniger, J., Pedersen, S., Augustyn, D., Binderup, O., and Pedersen, R. R. (2021). "A framework for updating structural wind turbine models by use of output feedback." *In preparation*.

U.S. Department of Energy (2018). "2018 Offshore Wind Technologies Market Report." *Report no.*, <https://www.energy.gov/sites/prod/files/2019/08/f65/2018

van deBos, L. and Sanderse, B. (2017). "Uncertainty quantification for wind energy applications." *Scientific Computing & Instrumentation*.

Van Overschee, P. and De Moor, B. (1994). "N4sid: Subspace algorithms for the identification of combined deterministic-stochastic systems." *Automatica*, 30(1), 75–93 Special issue on statistical signal processing and control.

van Overschee, P. and de Moor, L. (1996). *Subspace identification for linear systems: theory, implementation, applications*. Kluwer Academic Publishers.

Velarde, J., Kramhøft, C., Sørensen, J. D., and Zorzi, G. (2020). "Fatigue reliability of large monopiles for offshore wind turbines." *International Journal of Fatigue*, 134, 105487.

Velenturf, A. P. M. (2021). "A framework and baseline for the integration of a sustainable circular economy in offshore wind." *Energies*, 14(17).

Verhaegen, M. (1994). "Identification of the deterministic part of mimo state space models given in innovations form from input-output data." *Automatica*, 30(1), 61–74 Special issue on statistical signal processing and control.

Vicario, F., Phan, M. Q., Betti, R., and Longman, R. W. (2015). "Output-only observer/kalman filter identification (o3kid)." *Structural Control & Health Monitoring*, 22, 847–872.

Bibliography

Vold, H., Kundrat, J., Rocklin, G. T., and Russell, R. (1982). "A multi-input modal estimation algorithm for mini-computers." *SAE Transactions*, 91, 815–821.

Wagg, D. J., Worden, K., Barthorpe, R. J., and Gardner, P. (2020). "Digital twins: State-of-the-art and future directions for modeling and simulation in engineering dynamics applications." *ASCE-ASME Journal of Risk and Uncertainty in Engineering Systems, Part B: Mechanical Engineering*, 6(3), 030901.

Willoughby, R. (1979). "Solutions of ill-posed problems (a. n. tikhonov and v. y. arsenin)." *SIAM Review*, 21(2), 266–267.

Wind Europe (2020). "Offshore Wind in Europe. Key Statistics 2020." *Report no.*

Wirsching, P. H. (1984). "Fatigue reliability for offshore structures." *Journal of Structural Engineering*, 110(10), 2340–2356.

Wirsching, P. H. and Chen, Y.-N. (1988). "Considerations of probability-based fatigue design for marine structures." *Marine Structures*, 1(1), 23–45.

Witteveen, J. and Iaccarino, G. *Simplex Elements Stochastic Collocation for Uncertainty Propagation in Robust Design Optimization*.

Ye, Y., Yang, Q., Yang, F., Huo, Y., and Meng, S. (2020). "Digital twin for the structural health management of reusable spacecraft: A case study." *Engineering Fracture Mechanics*, 234, 107076.

Yuen, K. V. (2010). *Model Updating Using Eigenvalue–Eigenvector Measurements*. John Wiley & Sons, Ltd, Chapter 5, 193–211.

Zaidan, M. A., Hossein Motlagh, N., Fung, P. L., Lu, D., Timonen, H., Kuula, J., Niemi, J. V., Tarkoma, S., Petäjä, T., Kulmala, M., and Hussein, T. (2020). "Intelligent calibration and virtual sensing for integrated low-cost air quality sensors." *IEEE Sensors Journal*, 20(22), 13638–13652.

Zhang, E., Feissel, P., and Antoni, J. (2011). "A comprehensive bayesian approach for model updating and quantification of modeling errors." *Probabilistic Engineering Mechanics*, 26(4), 550–560.

Zhao, Y., Pan, J., Huang, Z., Miao, Y., Jiang, J., and Wang, Z. (2020). "Analysis of vibration monitoring data of an onshore wind turbine under different operational conditions." *Engineering Structures*, 205, 110071.

Ziegler, L. and Muskulus, M. (2016). "Fatigue reassessment for lifetime extension of offshore wind monopile substructures." *Journal of Physics: Conference Series*, 753, 092010.

Åström, K. (1980). "Maximum likelihood and prediction error methods." *Automatica*, 16(5), 551–574.

Åström, K. and Eykhoff, P. (1971). "System identification—a survey." *Automatica*, 7(2), 123–162.

Bibliography

Part II

Papers

Paper A

Paper A

Data-driven model updating of an offshore wind jacket substructure

Dawid Augustyn[*,a,b], Ursula Smolka[c], Ulf T. Tygesen[b], Martin D. Ulriksen[d], John D. Sørensen[a]

[a] *Department of the Built Environment, Aalborg University, Denmark*
[b] *Ramboll Energy, Esbjerg, Denmark*
[c] *Ramboll Energy, Hamburg, Germany*
[d] *Department of Energy Technology, Aalborg University, Denmark*

A B S T R A C T

The present paper provides a model updating application study concerning the jacket substructure of an offshore wind turbine. The updating is resolved in a sensitivity-based parameter estimation setting, where a cost function expressing the discrepancy between experimentally obtained modal parameters and model-predicted ones is minimized. The modal parameters of the physical system are estimated through stochastic subspace identification (SSI) applied to vibration data captured for idling and operational states of the turbine. From a theoretical outset, the identification approach relies on the system being linear and time-invariant (LTI) and the input white noise random processes; criteria which are violated in this application due to sources such as operational variability, the turbine controller, and non-linear damping. Consequently, particular attention is given to assess the feasibility of extracting modal parameters through SSI under the prevailing conditions and subsequently using these parameters for model updating. On this basis, it is deemed necessary to disregard the operational turbine states—which severely promote non-linear and time-variant structural behaviour and, as such, imprecise parameter estimation results—and conduct the model updating based on modal parameters extracted solely from the idling state. The uncertainties associated with the modal parameter estimates and the model parameters to be updated are outlined and included in the updating procedure using weighting matrices in the sensitivity-based formulation. By conducting the model updating based on in-situ data harvested from the jacket substructure during idling conditions, the maximum eigenfrequency deviation between the experimental estimates and the model-predicted ones is reduced from 30% to 1%.

1. Introduction

The offshore wind industry has experienced strong growth over the last decade (U.S. Department of Energy, 2018). As a result, the cumulative capacity of installed offshore wind turbines has reached 23 GW in 2018 with additional 40 GW planned to be operational within the next 5 years (Global Wind Energy Council, 2018). Building upon a commercial success of this technology, more structures are being installed and instrumented with measurement equipment, thus allowing to capture more operational information. In fact, some authorities, including the German certification body Federal Maritime and Hydrographic Agency, have already requested new structures to be equipped with monitoring systems (BSH-7005, 2015).

Access to information from monitoring systems can bring vital insight into a revised, more accurate estimate of the condition of the structures. Given proper processing, such insight can be used to optimize the operation of existing structures and to improve design procedures for structures to follow. A specific approach is to use the concept of a digital twin (Grieves, 2019), where operational data is used to calibrate numerical models to reflect, in the best possible way according to some performance measure, the behaviour of a physical asset. The digital twin concept is well established and widely used in many industries, i.a., aerospace engineering (Kritzinger et al., 2018) and the oil and gas industry (Tygesen et al., 2018). Recently, a digital twin has also been presented as a key element for establishing a data-driven conceptual framework for enhanced operation of offshore wind structures (Augustyn et al., 2019). Therein the model updating methods are implemented to establish a digital twin, which is subsequently used to perform lifetime extension, either 1) deterministically or 2) probabilistically, as illustrated in Fig. 1.

To establish a digital twin, one normally starts with developing an initial model based on a generic estimation of the physical parameters. Afterwards, operational data is collected and features extracted and compared to model predictions. Typically, one compares a subset of

*Corresponding author at: Department of the Built Environment, Aalborg University, Fredrik Bajers Vej 5, 9100 Aalborg, Denmark.
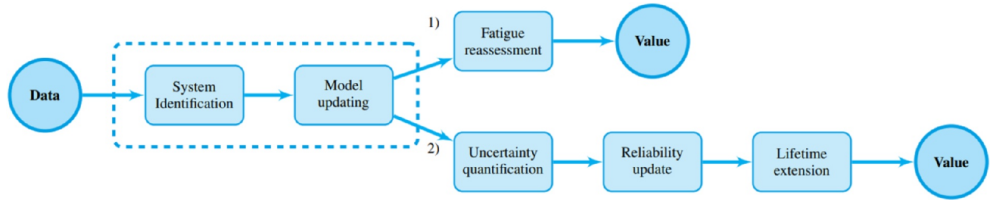*E-mail address:* dawa@ramboll.com (D. Augustyn).

Fig. 1. Application of a digital twin for lifetime extension (Augustyn et al., 2019). The dashed rectangle highlights the scope of this paper.

modal parameters as it can be conveniently estimated from operational data by means of system identification methods. Some full scale validations of system identification methods have been performed for onshore wind structures (Tcherniak et al., 2011), offshore platforms (Tygesen et al., 2019), offshore wind tripod substructures (Hackell and Rolfes, 2013), and offshore wind monopile substructures (Devriendt et al., 2014). However, limited publications exist that explore the applicability of the system identification methods for offshore wind jacket substructures. The challenge for this type of substructures lies in the dynamic blade-substructure coupling (Popko et al., 2013) and in the non-linear behaviour of the controller.

Once the discrepancy between a physical structure and its digital counterpart is quantified, model updating methods can be used to reduce the difference by updating selected physical parameters of the numerical model (Bernal and Ulriksen, 2018; Friswell and Mottershead, 1995). Again, various methods have been validated for aerospace and automotive applications (Patelli et al., 2017; Schedlinski et al., 2004) and for wind turbine blade structures (Luczak et al., 2014). However, to the authors' knowledge, no dedicated application study has been presented for updating offshore wind turbine substructures.

The present paper aims to address the above-mentioned research gap by applying a model updating framework in the context of an offshore wind jacket substructure. The contributions of this paper are; 1) applying the model updating framework based on in-situ data (including system identification results) and 2) providing recommendations on practical implementation of the framework.

2. Methodology

In this section, the theoretical background for the methods used in the model updating framework is presented. Well-established procedures for both system identification and model updating are summarized, followed by a discussion on the validity of the main assumptions in the context of offshore wind applications.

2.1. System identification

The covariance-based stochastic subspace identification (SSI-cov) method is used to estimate modal parameters of the wind turbine jacket substructure (van Overschee and de Moor, 1996). The merits of the SSI-cov method include its simplicity in implementation and numerical robustness (van Overschee and de Moor, 1996). The former merit is especially attractive from a user perspective as the method requires only a model order as input, while the remaining parameters can be estimated accordingly. The numerical robustness implies that no issues with convergence arise, hence making the method applicable for large structures and data sets. Consequently, this particular method is extensively applied in the offshore wind and oil and gas industries (Devriendt et al., 2013; Hackell and Rolfes, 2013; Tcherniak et al., 2011; Tygesen et al., 2018).

Consider the state-space formulation of a linear, time-invariant (LTI) system

$$\begin{bmatrix} \mathbf{x}_{i+1} \\ \mathbf{y}_i \end{bmatrix} = \begin{bmatrix} \mathbf{A} \\ \mathbf{C} \end{bmatrix} \mathbf{x}_i + \begin{bmatrix} \mathbf{w}_i \\ \mathbf{v}_i \end{bmatrix}, \tag{1}$$

where $\mathbf{x}_i \in \mathbb{R}^n$ and $\mathbf{y}_i \in \mathbb{R}^m$ are the state and output vectors for time instance t_i. $\mathbf{A} \in \mathbb{R}^{n\times n}$ and $\mathbf{C} \in \mathbb{R}^{m\times n}$ are the state and output matrices, respectively. The unknown input $\mathbf{w}_i \in \mathbb{R}^n$ and measurement noise $\mathbf{v}_i \in \mathbb{R}^m$ are modelled as discrete, white-Gaussian sequences with zero mean; thus, $\mathbf{w}_i \sim \mathcal{N}(\mathbf{0}, \Sigma_W)$ and $\mathbf{v}_i \sim \mathcal{N}(\mathbf{0}, \Sigma_v)$ with the following covariance matrices:

$$\mathbb{E}\left[\begin{pmatrix} \mathbf{w}_p \\ \mathbf{v}_p \end{pmatrix} (\mathbf{w}_q^T \quad \mathbf{v}_q^T) \right] = \begin{bmatrix} \Sigma_{\mathbf{w}} & \Sigma_{\mathbf{wv}} \\ \Sigma_{\mathbf{wv}}^T & \Sigma_{\mathbf{v}} \end{bmatrix} \delta_{pq} \geqslant 0, \tag{2}$$

where δ_{pq} is the Kronecker delta, $\Sigma_w \in \mathbb{R}^{n\times n}$, $\Sigma_v \in \mathbb{R}^{m\times m}$, and $\Sigma_{wv} \in \mathbb{R}^{n\times m}$. The input term and measurement noise are assumed to be spatially and temporally uncorrelated.

Let $\mathbf{Y}_{i|i} \in \mathbb{R}^{m\times j}$ be the output Hankel matrix and $\hat{\mathbf{X}}_i \in \mathbb{R}^{n\times j}$ a state sequence estimate, then the state-space matrices can be estimated as

$$\begin{bmatrix} \hat{\mathbf{A}} \\ \hat{\mathbf{C}} \end{bmatrix} = \begin{bmatrix} \hat{\mathbf{X}}_{i+1} \\ \mathbf{Y}_{i|i} \end{bmatrix} \hat{\mathbf{X}}_i^{\dagger}, \tag{3}$$

where superscript † denotes Moore-Penrose pseudo-inverse and n_s is the selected model order. From $\hat{\mathbf{A}} \in \mathbb{R}^{n_s \times n_s}$ and $\hat{\mathbf{C}} \in \mathbb{R}^{m\times n_s}$, the eigenfrequencies, f_i, damping ratios, ζ_i, and mode shapes, ϕ_i, can be estimated.

The SSI-cov method hinges on a number of assumptions, including 1) the system is LTI and 2) the input is ergodic, white, Gaussian, and spatially and temporally uncorrelated. The validity of the assumptions for offshore wind applications is briefly discussed below.

In practice, the LTI assumption is always violated, as each system changes its properties with respect to both loading conditions and time. For offshore wind applications, the non-linear behaviour is mostly introduced due to the turbine controller, and to a lesser degree by the soil behaviour. A turbine controller is constantly adjusting turbine properties (pitch, yaw) to harvest the maximum amount of energy. Such adjustments alter the dynamic properties of the system, which leads to varying modal parameters.

The SSI-cov method requires no prior knowledge on the input. Effectively it is assumed ergodic, white-noise Gaussian, and spatially and temporally uncorrelated. Assuming the input emulates the turbine's exposition to environmental conditions it is evident that wind and wave properties can change from one sea state to another, thus violating the ergodicity property. Moreover, the frequency spectrum originating from wind and wave excitation is far from being white-noise Gaussian due to rotating machinery, the peak period in the wave spectrum, and background turbulence in the wind spectrum.

Finally, some major assumptions are made with respect to damping. In Eq. (1), the damping is assumed to follow a linear viscous model, which is typically established on the premise of the distribution being classical. This is, by no means, a fully representative model of the damping sources present in offshore wind applications, e.g., radiation soil damping, hydrodynamic damping, and aerodynamic damping.

The above-mentioned assumptions are, in principle, violated for all practical applications. Nevertheless, useful results for estimating modal

parameters are reported for, e.g., offshore wind monopile turbines (Devriendt et al., 2013), onshore turbines (Tcherniak et al., 2011), and offshore oil and gas jacket platforms (Tygesen et al., 2018). On that basis the applicability of the SSI-cov system identification method in the context of an offshore wind jacket substructure is explored in this paper.

2.2. Sensitivity-based model updating

Model updating techniques can be used to update a set of selected physical parameters of the model to better reflect the in-situ conditions. The sensitivity-based method, widely used in adjacent industries (Patelli et al., 2017), is implemented here. Below, key elements of the theoretical framework are presented, followed by a discussion of the assumptions made. For a comprehensive derivation of the model updating method, the reader is referred to (Mottershead et al., 2011).

We define the discrepancies in modal responses, $\Delta\Lambda$, as a difference between estimated responses, Λ_s, and numerical predictions, $\Lambda_{M(\Theta)}$. In this study, eigenmodes and eigenfrequencies are used as modal responses. $\Delta\Lambda$ can be approximated by the linear Taylor expansion

$$\Delta\Lambda \approx \mathbf{S}\Delta\Theta, \qquad (4)$$

where $\Delta\Theta$ contains the parameter shifts to be estimated and $\mathbf{S}$ is the sensitivity/Jacobian matrix, thus

$$S_{jk} = \left[\frac{\partial\Lambda_j}{\partial\Theta_k}\right], \qquad (5)$$

where Λ_j is the j'th response and Θ_k is the k'th parameter. The sensitivity matrix is obtained via perturbations directly from the numerical model.

The measurements and response estimates are inherently corrupted with uncertainties. These uncertainties are included in the updating procedure, as elaborated in Section 2.3. In many applications, the number of parameters to be updated is larger than the number of responses identified from the physical structure. This poses a central problem for model updating in engineering applications, as the solution obtained is non-unique. To address this problem, a regularization scheme, originating from Tikonov (Willoughby, 1979), is applied in the paper to add a penalty on the objective function. A regularization coefficient, α, is included in the formulation of the objective function to minimize the weighted parameter change.

The objective function accounting for the above-mentioned extensions is defined as

$$J = \Delta\Lambda^T\mathbf{W}_\Lambda\Delta\Lambda + \alpha\Delta\Theta^T\mathbf{W}_\Theta\Delta\Theta, \qquad (6)$$

where $\mathbf{W}_\Lambda = \text{diag}\left(\sigma^2_{\Lambda_j}\right)^{-1}$ is a diagonal weighting matrix expressing uncertainties in the responses and $\mathbf{W}_\Theta = \text{diag}(\sigma^2_{\Theta_k})^{-1}$ is a diagonal weighting matrix expressing uncertainties in the model parameters. The weighting coefficients σ^2_Λ, σ^2_Θ include variance of responses and parameters, respectively. The optimal parameter set is obtained iteratively by minimizing the objective function in Eq. (6), $\arg\min_{\Delta\Theta}J$, hence

$$\Theta_{i+1} = \Theta_i + [\mathbf{S}_i^T\mathbf{W}_\Lambda\mathbf{S}_i + \alpha\mathbf{W}_\Theta]^\dagger\mathbf{S}_i^T\mathbf{W}_\Lambda\Delta\Lambda_i. \qquad (7)$$

The regularization ensures that the parameter changes are minimized. It is assumed that parameter uncertainties are uncorrelated. Nevertheless, fully populated covariance matrices could easily be included, if correlation between parameters is deemed critical, e.g., correlated mass or stiffness parameters.

2.3. Uncertainties included in the updating procedure

The main types of uncertainties related to the parameters, Θ, and modal response estimations, Λ_s, are summarized below along with their implementation in the updating procedure. Quantification of the

uncertainties, based on engineering judgement, is provided in Section 5.

Uncertainties in the context of modal updating can be divided into two categories: 1) aleatory, related to the natural variation in a physical system (stiffness, mass, and damping), and 2) epistemic, related to lack of knowledge describing a system (modelling quality, statistical uncertainties, and measurement quality). Once the system is realized and some measurands are captured, aleatory uncertainty can be reduced with the expense of the additionally introduced (epistemic) uncertainties, e.g., stiffness/geometry becomes deterministic within the precision of the measurement equipment. The premise of model updating for fatigue reassessment is that the gain in reducing aleatory uncertainty is larger than the additional epistemic uncertainties, thus improving the final model. Below, some examples of uncertainties introduced in the updating procedure are listed, following the uncertainty definition provided in Sørensen and Toft (2010). Aleatory uncertainty (for the context of this paper) stems from inherent variation in physical parameters describing stiffness, damping, and, to a lesser degree, mass of a system. These quantities are modelled by prior (generic) distribution functions of the physical parameters assumed at the design stage. During the updating procedure, these distribution functions are substituted with most likely mean values based on novel (in-situ) information from the operational stage. The aleatory uncertainties are included in the updating procedure in the weighting matrix $\mathbf{W}_\Theta$ as described in Sections 2.2 and 5.3.

Epistemic uncertainties stem from data processing and are, in the framework of model updating, realized as measurement, statistical, and model uncertainties. Measurement uncertainties are governed by the quality of the sensor setup (sensor type and sensor placement). These uncertainties affect the number of dynamic modes that can be quantified. Typically, a sensor setup is a balance between practical limitations and the targeted quality of the information extracted. Moreover, this uncertainty accounts for signal noise and various pre-processing steps. Statistical uncertainties are related to the amount of data captured. A data set should be sufficiently large to capture a statistically sound estimation of the variation (uncertainties) in the modal parameters extracted. Model uncertainties are related to the method and algorithm used in the updating procedure, including the system identification. For SSI, the associated uncertainties can be quantified as described in, e.g., (Reynders et al., 2008). The summarized epistemic uncertainties are included in the updating procedure in the weighting matrix $\mathbf{W}_\Lambda$ as described in Sections 2.2 and 5.2.

The updating procedure described in Section 2.2 aims at improving the accuracy of a numerical model by updating the mean values of selected physical parameters in the presence of uncertainties. Thus, the uncertainties are not updated but merely serve as input to $\mathbf{W}_\Lambda$ and $\mathbf{W}_\Theta$. Updating of the uncertainties can be performed by, e.g., Bayesian methods; however, this is outside of the scope of this paper.

3. Measurement campaign

The model updating framework is applied in the context of a measurement campaign within the 350 MW Wikinger wind farm. The farm consists of 70 Adwen 5 MW wind turbines located in the German exclusive economic zone of the Baltic Sea. Measurements from one turbine are used to perform model updating. The chosen wind turbine is placed on a 4-legged jacket substructure, see Fig 2. The hub height (A-A) of the wind turbine is approximately 90 m above the mean sea level (MSL). The interface level between the transition piece (TP) and the wind turbine tower is approximately 18 m above MSL (C-C), and the tower length is approximately 72 m. The water depth at the location of the instrumented wind turbine is approximately 38 m MSL, the jacket height (including TP) is approximately 54 m, and the pile penetration depth is approximately 30 m beneath the sea bed. The soil is mainly considered as clay.

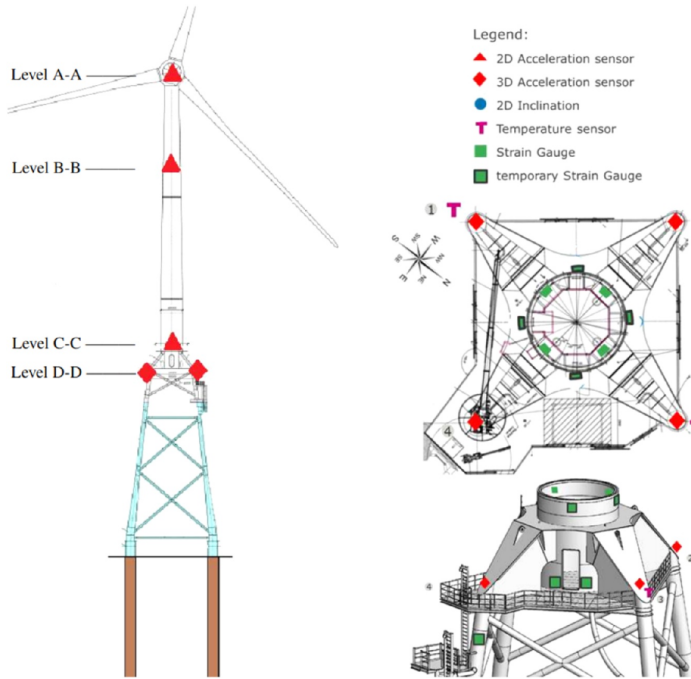The measurement data used for model updating is composed of

Fig. 2. Wind turbine geometry and measurement setup.
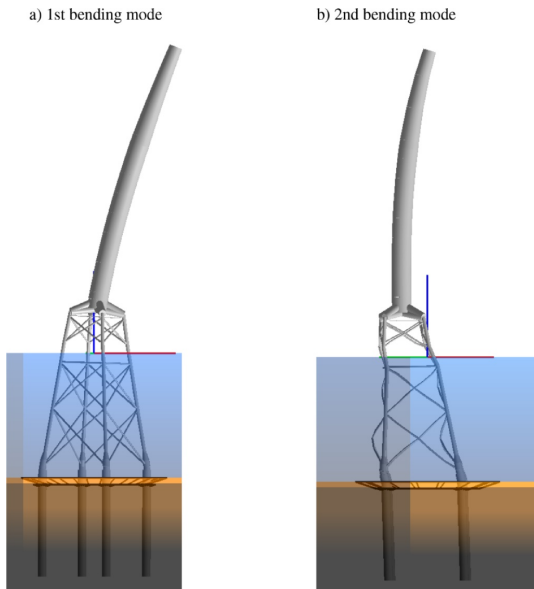
a) 1st bending mode

b) 2nd bending mode

Fig. 3. Global eigenmodes (fore-aft/side-side): a) 1st bending, b) 2nd bending.

acceleration signals captured over a period of 1 month. The sensor setup includes 4 triaxial accelerometers at the TP (section D-D, one accelerometer per leg), 1 biaxial accelerometer installed at the tower bottom (section C-C), 1 biaxial accelerometer in the tower,

approximately at 2/3 of the height (section B-B), and 1 biaxial accelerometer at the tower top (section A-A). The approximate locations of the sensors are depicted in Fig. 2. The chosen configuration is primarily aimed at identification of the first 5 global dynamic modes, including 2 global bending modes (both in fore-aft and side-side direction) and a torsional mode. A sketch of the 1st and 2nd global bending modes is presented in Fig. 3. Fig. 3a shows the 1st global bending mode in both fore-aft and side-side directions, where major deformation is observed in the tower of the structure. These modes correspond to eigenmodes 1 and 2 of the structure. Fig. 3b shows the 2nd global bending mode in fore-aft and side-side directions, where major lateral deformation is observed in the TP level. These modes correspond to eigenmodes 4 and 5 of the structure. Note that eigenmode 3, which is the first torsional mode, is not presented here.

In addition to the acceleration signals, a subset of SCADA (supervisory control and data acquisition) data is also recorded. The turbine data and ambient wind data are collected as 10-min statistics. In Fig. 4, some SCADA data are presented to visualize the wind speed and operational state of the turbine during the measurement campaign. The
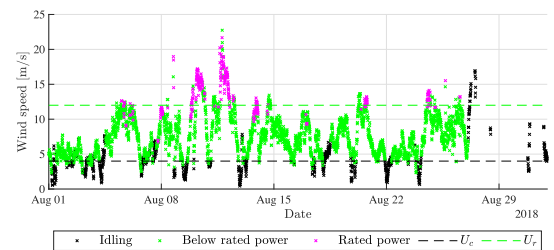
Fig. 4. Wind speed and operational states of the turbine during the measurement campaign.

recorded wind speeds span from 0 m/s to slightly above 20 m/s. Within this range, the turbine states are divided into 3 categories: 1) idling or parked state where aerodynamic and rotor forces are reduced, 2) operational state below the rated power with the blades pitching and the rotor altering its angular velocity, and 3) operational state with the blades pitching to keep the angular velocity of the rotor and the power output constant. The cut-in and rated wind speeds, i.e., $U_c = 4$ m/s and $U_r = 12$ m/s, respectively, are depicted in Fig. 4 with dashed lines. The turbine states are categorized based on the power output, which is more precise compared to relying solely on the wind speed. This can be noticed in Fig. 4, as in some cases the rated power is reached for wind speeds below 12 m/s. Moreover, in other cases, the wind turbine is idling despite the wind speed exceeding the cut-in value, which can be due to, e.g., maintenance.

4. System identification of the wind turbine substructure

The input for the system identification analysis is the time series measured by the 7 accelerometers, resulting in $m = 18$ channels (4×3 directions in the TP and 3×2 directions in the tower). For each day, successive 30 min. data blocks are processed, resulting in maximum 48 time-frames per day. A separate system identification analysis is performed for each data block. The initial sampling frequency of 25 Hz is reduced to 5 Hz to focus on the global bending modes. A model order of 20 is used in the SSI-cov algorithm. This model order is found appropriate to capture the modes of interest.

Fig. 5 presents frequencies estimated using the SSI-cov algorithm. One can observe that within the range of interest (up to approximately 2.5 Hz) a large number of frequencies is identified. In order to identify poles representing the structural modes of interest, a classifier algorithm based on the modal assurance criterion (MAC) (Allemang, 2003) and mode complexity estimate (Imregun and Ewins, 1995) has been applied. The algorithm calculates MAC values between the SSI-cov estimated modes and the numerical modes of interest. SSI-cov modes with MAC values above 0.80 are classified as structural, while the remaining are disregarded. Fig. 6 presents a subset of frequencies classified as structural eigenfrequencies after applying the classifier algorithm with only the MAC criterion. Stable clusters of eigenfrequencies around 0.3 HZ and 2.0 Hz can be observed. They contain the 1st and 2nd global bending modes. The 1st torsional mode is not identified, which presumably is due to the fact that the sensor setup was intended to capture global bending modes and not the torsional one (hence resulting in a high noise-to-signal ratio for the torsional mode). Consequently, only the global bending modes are considered in the remainder of the paper.

As the classifier does not distinguish between the fore-aft and the side-side modes, the clusters potentially contain both directions. Moreover, in Fig. 6, one can also observe a large number of additional frequencies in the range of 0.3–0.7 Hz. These modes are correlated with SCADA data and have been identified as P-frequencies originating from rotor revolution (1P), blades passing the tower (3P), and their
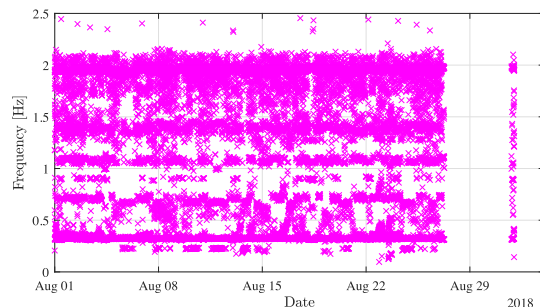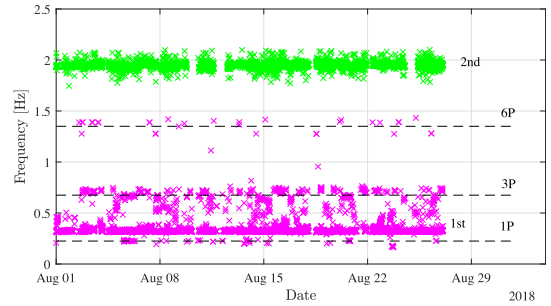

Fig. 6. Identified frequencies processed with MAC classifier.

harmonics (6P). The dashed lines in Fig. 6 represent the upper bound of the P-frequencies based on the rated rotor velocity. The P-frequencies are falsely classified as the 1st bending mode shape, as the mode shapes associated with the P-frequencies are geometrically indistinguishable (with the current sensor setup) from the 1st bending mode shape based on the MAC classifier only (variation in the wind pressure leads to varying wind force translated to the tower top).

To remove the P-frequencies from the results, the classifier algorithm is extended with the mode complexity criterion based on the Argand diagram (Imregun and Ewins, 1995). The assumption is that the P-frequencies introduce non-classical damping, which results in complex modes. The complexity of the modes is estimated based on the imaginary part of the mode shapes, as proposed in Olsen et al. (2013). Effectively, modes with high complexity around the expected P-frequency (estimated based on rotor revolution) are classified as P-frequencies and disregarded. Note that the P-frequencies are correlated with varying rotor revolution speed, hence the scatter between 1P and 3P. This scatter can be correlated with the rotor revolution from SCADA data and be used to further filter the P-frequencies. The complexity criterion can also be applied to further improve the classification of the remaining structural modes assuming that the mode complexity of these modes is low.

After applying the mode complexity criterion, a subset of identified eigenfrequencies including those of the 1st and 2nd global modes is obtained. Fig. 7 depicts the subset, and one can observe that the P-frequencies are successfully filtered and the scatter in the 2nd eigenfrequency is reduced due to the removal of highly complex and hence potentially erroneous realizations. The mean values of the identified frequencies are $f_1 = 0.32$ Hz and $f_2 = 1.95$ Hz, respectively. The results are derived based on both idling and operational states, covering all possible yaw directions and varying wind speeds. The coefficient of variation (CoV) for the eigenfrequencies of the 1st and 2nd global
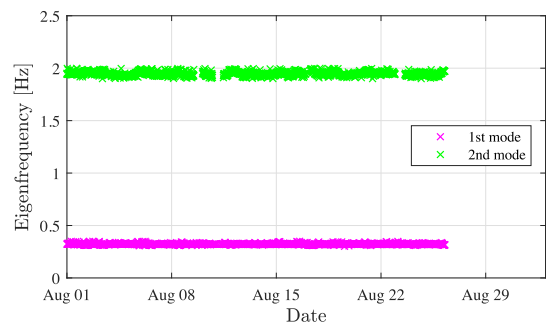

Fig. 5. Identified frequencies (no post-processing).

Fig. 7. Identified eigenfrequencies after MAC classifier extended with complexity criterion.

bending modes are $\mathrm{CoV}f_1 = 0.015$ and $\mathrm{CoV}f_2 = 0.017$, respectively.

5. Model updating of the wind turbine substructure

5.1. Numerical model

The wind turbine structure and the jacket substructure are modelled using Ramboll's software ROSAP (Ramboll Offshore Structural Analysis Package), version 53 (Ramboll, 2018). ROSAP is a general-purpose finite element package intended for both static and dynamic analysis of offshore structures. The jacket substructure is modelled with 3D Bernoulli-Euler beam elements (Cook et al., 2001), including the added mass of the surrounding water. The soil-structure interaction is modelled using a Winkler model (Cook et al., 2001) in which the steel pile elements are additionally supported by linearized springs representing the surrounding soil. The soil springs are linearized according to the API method (API-RP-2A, 2014). The stiffness of the joints are modified to account for additional flexibility of the tubular joints according to Buitrago et al. (1993). The TP is modelled in a simplistic manner by a representative 3D Bernoulli-Euler beam system. The tower is modelled using 3D Bernoulli-Euler beam elements, including added masses representing internal secondary steel elements and flanges. The rotor-nacelle-assembly (RNA) comprising the nacelle, hub, and blades is modelled as a two-point mass system, including a mass moment of inertia tensor to reflect the difference in properties in the fore-aft and the side-side direction of the RNA. The parameters used in the initial numerical model are based on the information available in the design stage of the structure.

5.2. Input for model updating

The numerical model is updated in a setting where the eigenfrequencies and mode shapes of the first two bending modes are utilized as responses. The responses are estimated in the system identification Section 4. To discard realizations that severely violate the system identification assumptions, the selection criteria presented in Table 1 are employed. The first criterion excludes results with excessive yawing and pitching to comply with the LTI system assumption. The second criterion only includes results where the turbine is in idling or parked conditions to minimize the presence of non-white excitation stemming from wind and rotating machinery. Physical modes related to the fore-aft and side-side directions are expected to be perpendicular due to a large stiffness disproportion in these directions. Therefore, similar properties are expected from the identified modes (criteria 3 and 4). After applying the 4 criteria, 9 sets containing modal parameters are selected as input for model updating.

The first criterion excludes results with excessive yawing and pitching to comply with the LTI system assumption. The second criterion only includes results where the turbine is in either the idling or the parked condition to minimize the presence of non-white excitation stemming from wind and rotating machinery. Due to a large stiffness disproportion in fore-aft and side-side directions, physical modes related to these directions are expected to be perpendicular. Therefore, similar properties are expected from the identified modes (criteria 3 and 4). After applying the above-mentioned criteria, 9 sets containing modal parameters are selected as input for model updating.

Table 1
Selection criteria for model updating input.

Assumptions	Criteria
LTI system	no yawing, pitching
white-noise excitation	idling/parked condition
1st and 2nd modes	4 eigenmodes identified
FA/SS symmetry planes	perpendicular modes

The uncertainties related to the selected modal parameter sets are quantified based on the eigenfrequencies' CoVs and are included in the weighting matrix, $\mathbf{W}_\Lambda$. $\mathrm{CoV}f_1 = 0.015$ and $\mathrm{CoV}f_2 = 0.017$ are assumed for the 1st and 2nd bending eigenfrequencies, respectively. The uncertainties of the mode shapes are assumed to be tenfold of the respective eigenfrequencies CoVs, thus $\mathrm{CoV}m_1 = 0.15$ and $\mathrm{CoV}m_2 = 0.17$. The additional uncertainty is primarily attributed to the fact the uncertainties on both the state matrix and the output matrix are propagated to the mode shape estimates when using the SSI-cov method (Reynders et al., 2008). The uncertainty estimations applied here only account for a portion of the measurement and statistical uncertainties related to these quantities. However, as mentioned in Section 2.3, the scope of the paper is to update the mean values of the parameters, thus such level of details is deemed sufficient.

5.3. Physical parameters to be updated

The number of physical parameters included in a numerical model can become large and updating all of them can, for many practical applications, result in an ill-posed optimization problem. Thus, some criteria for selecting a subset of parameters to be updated must be implemented. Below, such an attempt is presented based on the principle of Fisher information (sensitivity vs. uncertainty) supplemented with engineering judgment. The assumption is to update parameters that are highly uncertain and, in the same time, affect the chosen modal parameters (frequencies and modes).

To select which model parameters should be updated, their sensitivities to modal parameters are quantified. This study involves modifying each model parameter in the numerical model independently and extracting the shifted modal parameters. Model parameters whose alterations result in high shifts in the modal parameters are assigned a high sensitivity metric, while model parameters whose alterations do not yield a substantial modal parameter shift are assigned a low sensitivity metric. Subsequently, the uncertainties of the parameters are determined in a separate study. Highly uncertain parameters are assigned a high uncertainty metric (e.g., CoV, assuming no bias), while parameters believed to be estimated with high precision are assigned a low uncertainty metric. Such analysis has been performed and the results are presented in Table 2. A large set of parameters is initially screened to select potential candidates for model updating. The parameters with medium or high sensitivity towards global modes are soil stiffness, corrosion, marine growth, hub mass, turbine stiffness, and TP stiffness. The most uncertain parameters (metric 2 or 3) are expected to be turbine stiffness, TP stiffness, joint stiffness, scour, corrosion, marine growth, added mass, and, especially, soil stiffness. By selecting highly uncertain and/or highly sensitive parameters, 10 are considered for updating. These are indicated by the asterisk in Table 2.

The generic uncertainty metric from Table 2 is now supplemented with CoV of the selected parameters. The uncertainties are estimated based on a literature review, supplemented with engineering judgement where no reference could be found. The jacket stiffness is assumed to be varied via Young's modulus of the material used. The CoV is well-described and found to be 0.05 (Sadowski et al., 2015). Therefore, this value is used. The turbine stiffness represents the stiffness of the structure above the interface including tower, RNA, and blades. As a simplified model is used for this superstructure large uncertainty of 0.25 is assumed based on engineering judgement. The uncertainty associated with the pile and TP stiffness is a combination of a Young's modulus uncertainty and any modelling uncertainties due to simplifications in the modelling approach, e.g., beam vs. shell elements and PY soil curves vs. 3D soil model. Thus, the initial 0.05 value is increased to 0.10 and 0.25 for the pile and TP elements, respectively. The increase accounts for uncertainty in modelling of a pile element with contribution from the structural component (steel) and surrounding soil. The uncertainty for the TP element is increased to account for the simplified beam representation used.

Table 2
Sensitivity and uncertainty matrix for model parameters.

Parameter		Uncertainty			Sensitivity
Type	Symbol	Metric	CoV	Reference	
Jacket stiffness*	k_j	1	0.05	Sadowski et al. (2015)	1
Turbine stiffness*	k_t	2	0.25	**	2
TP stiffness*	k_{TP}	2	0.25	**	2
Piles stiffness*	k_p	1	0.10	**	2
Joint stiffness*	LJF	2	0.50	Nielsen et al. (2019)	1
Leg diameter	D_l	0	–	–	2
Leg thickness	t_l	1	–	–	1
Brace diameter	D_b	0	–	–	1
Brace thickness	t_b	1	–	–	0
Scour*	sc	2	–	–	1
Corrosion*	corr	2	–	–	2
Marine growth*	mg	2	–	–	2
added mass*	a_m	2	0.50	**	1
hub mass*	m_h	1	0.02	Confidential author (2016)	3
lateral soil stiffness*	py	3	1.00	Negro et al. (2014); Yeter et al. (2019)	1
axial soil stiffness*	tz	3	1.00	Yeter et al. (2019)	2
pile tip stiffness*	qw	3	1.00	Bertossa (2015)	0

Metric (uncert./sensit.): 0– negligible, 1– low, 2– medium, 3– high * Parameters to be updated; Uncertainty estimation: ** Engineering judgement.

The uncertainty on the hub mass is very low as the element is weighed prior to installation, thus a value of 0.02 is assumed based on the available as-built weight reports (Confidential author, 2016). The added mass parameter represents the added mass contribution on the submerged part of the jacket substructure due to the surrounding water. It is modelled as a multiplication factor of the initially estimated added mass. The added mass uncertainty depends on the shape of the structural element and its orientation, which changes as waves pass. To reflect these uncertainties, a value of 0.50 is chosen. The local joint flexibility representing the effective stiffness of a tubular joint is modelled via the simplified Buitrago equations (Buitrago et al., 1993). This approach is known to be imprecise (Nielsen et al., 2019), so to account for this uncertainty, a value of 0.50 is chosen. The soil stiffness is modified via correction parameters, py, tz, qw, which update the initial stiffness of the linearized API curves (API-RP-2A, 2014). The soil stiffnesses are considered to be the most uncertain parameters, thus a CoV of 1.00 is assumed for these. The value is chosen based on literature studies regarding soil uncertainty estimation (Bertossa, 2015; Negro et al., 2014; Yeter et al., 2019).

In this study, boundaries are imposed on the model parameters to be updated to reflect physical limitations of the mass and stiffness, i.e., only positive values are allowed. Other boundaries can also be adopted, e.g., the validity range of the parameters provided in guidelines/standards.

5.4. Results

In this subsection, model updating results are presented. The update is performed using the one modal parameter set which is the most consistent with the selection criteria defined in Section 5.2. The frequencies and MAC results for different stages of the update are presented in Tables 3 and 4. The discrepancies between the initial (design)

Table 3
Estimated and model-predicted eigenfrequencies.

Configuration	f_1 [Hz]		f_2 [Hz]	
	FA	SS	FA	SS
Estimated (measurements)	0.32	0.32	1.96	1.99
Design (model)	0.30	0.30	1.37	1.40
As-built (model)	0.31	0.31	1.57	1.63
Updated (model)	0.32	0.32	1.94	2.00

Table 4
Estimated and model-predicted MAC.

Configuration	Mode 1 [−]		Mode 2 [−]	
	FA	SS	FA	SS
Estimated (measurements)	1.00	1.00	1.00	1.00
Design (model)	0.96	0.98	0.85	0.93
As-build (model)	0.97	0.99	0.98	0.99
Updated (model)	0.96	0.98	0.99	0.99

model and the estimated eigenfrequencies are 6% and 30% for the 1st and 2nd global bending mode, respectively. The corresponding MAC values are 0.96 and 0.85.

The model updating is performed in two steps. The first step involves updating the parameters based on the as-built reports. These reports are normally available after the installation is completed. They include some information like the as-built weight of the structure and information from pile driving (e.g., pile stick-up). In this stage of the update, it is also assumed that no scour, corrosion, or marine growth have developed. This assumption is based on the fact that the measurement campaign was performed 1 year after the installation, thus it is assumed that these processes did not have enough time to initiate in the specific environment. After including this information, the frequency discrepancies are reduced to 3% and 20% for the 1st and 2nd global modes, with MAC values of 0.97 and 0.98. Finally, the model updating procedure based on measurement data is performed as described in Section 2.2. After the update, the discrepancy between the measured and modelled 1st global frequency is reduced from the initial 6% to 0.3%. The discrepancy in the 2nd global frequency is reduced from the initial 30% to 1.0%. The MAC value after the update is 0.96 and 0.99 for the 1st and 2nd global mode, respectively.

The parameter set obtained after the model updating is presented in Table 5. The jacket stiffness, k_j, the structural pile stiffness, k_p, the hub mass, m_h, and the local joint flexibility, LJF, remain almost unchanged after the update. Substantial updating is observed in the TP stiffness, k_{TP}, with a reduction of 64%. The TP stiffness change is not surprising, as the simplified beam modelling strongly depends on the estimation of the representative stiffness, which can be difficult to assess without a detailed 3D model. A substantial update is also observed in the turbine stiffness, k_t. The stiffness is increased by 83%. Large update of this parameter can be explained by the fact that a low-fidelity turbine model (RNA and blades) is used. Its representative parameters are inferred

Table 5

Updated mean values of the selected model parameters.

Parameter			Value		
Type	Symbol	Unit	Initial	Updated	Normalized
Jacket stiffness	k_j	–	1.00e+0	9.95e−1	0.99
Turbine stiffness	k_t	–	1.00e+0	1.83e+0	1.83
TP stiffness	k_{TP}	–	1.00e+0	3.41e−1	0.36
Pile stiffness	k_p	–	1.00e+0	1.02e+0	1.02
Added mass	a_m	–	1.00e+0	0.84e+0	0.84
Hub mass	m_h	kg	1.44e+5	1.47e+5	1.01
lateral soil stiffness	py	–	1.00e+0	1.33e−1	0.13
axial soil stiffness	tz	–	1.00e+0	6.96e−2	0.07
pile tip stiffness	qw	–	1.00e+0	6.62e−1	0.66
Joint stiffness	LJF	–	1.00e+0	1.02e+0	1.02

Table 6

Pile head stiffness update.

Configuration	k_{xy} [kN/m]		k_z [kN/m]	
	Value	Ratio	Value	Ratio
Design	2.8e+5	1.0	1.0e+6	1.0
As-built	4.4e+5	1.6	1.3e+6	1.3
Updated	1.3e+6	4.7	6.0e+6	6.0

from implicit, confidential data (blade moments of inertia) and thus prone to imprecise estimation. Worth noting is the significant update of the soil parameters. While the py, tz, qw parameters are convenient from a modelling perspective, they are difficult to interpret on a physical level. Thus, additional results have been extracted, namely, the pile head stiffness in the lateral and the axial direction, k_{xy} and k_z, respectively. The results are presented in Table 6. The soil stiffness is increased by a factor of 4.7 and 6.0 for the lateral and axial directions, respectively. An elaborate discussion on the profound update of the TP, turbine, and soil stiffnesses is provided in Section 6.

5.5. Sensitivity of the updating procedure

As the estimated modal parameters exhibit some scatter (CoV$_{f1}$ = 0.015 and CoV$_{f2}$ = 0.017), it is investigated how sensitive the updated parameters are towards variation in the modal parameters. To investigate this effect, the estimated modal parameters from 9 different idling time-frames, see Section 5.2, are used to perform model updating. The model updating setup uses the same starting values for the parameters and the same weighting matrices, $\mathbf{W}_\Lambda$ and $\mathbf{W}_\Theta$; effectively altering only the input modal parameters. The scatter in the updated mean values of the model parameters is presented in Table 7. The scatter is reported as CoV on the updated mean values of the parameters. The updated values for jacket stiffness and hub mass present negligible scatter (CoV < 0.01). The turbine stiffness, k_t, TP stiffness, k_{TP}, and added mass, a_m, exhibit low scatter, namely, CoV of 0.04, 0.06, and 0.05. Finally, the soil stiffness CoV are 0.12 and 0.11 for k_{xy} and k_z,

Table 7

Scatter in the updated mean values of the model parameters for varying sets of modal parameters.

Parameter	Unit	Mean	CoV of mean value
k_j	–	9.95e−1	< 0.01
k_t	–	1.92e+0	0.04
k_{TP}	–	3.30e−1	0.06
a_m	–	8.59e+0	0.05
m_h	kg	1.47e+5	< 0.01
k_{xy}	kN/m	1.18e+6	0.12
k_z	kN/m	5.50e+6	0.11
LJF	–	1.02e+0	0.02

respectively. The mean value of the updated parameters based on 9 modal parameter sets, see Table 7, are close to, yet not identical with, the updated parameters provided in Table 5.

6. Discussion

This section offers a discussion of the model updating procedure and appertaining results presented in Sections 4 and 5.4. Particular focus is assigned to the initial deviation in the 2nd bending eigenfrequency and the profound update of selected model parameters.

6.1. On the initial eigenfrequency discrepancy

Based on the system identification results provided in Section 4 and the corresponding model predictions presented in Section 5.1, a discrepancy of 30% was reported for the 2nd bending eigenfrequency. Part of that discrepancy can be explained by merely stating that the two estimations aim to describe different stages of the same ageing structure. The numerical model is based on the design parameters, which, according to the design recommendations (DNVGL-ST-0126, 2016), are representative for the averaged conditions during the lifetime of the structure, typically 25 years. However, the in-situ estimation is derived based on the structural condition 1 year after installation. This is especially relevant in the context of phenomena accumulating over time, e.g., corrosion and marine growth, as these affect the discussed eigenfrequency. After adjusting the numerical model to a representative 1 year condition, the eigenfrequency discrepancy is reduced to 20%. The bulk of the remaining discrepancy can be attributed to the misprediction of the soil stiffness. It is commonly accepted in the industry that the soil stiffness estimation is highly uncertain (Bertossa, 2015; Negro et al., 2014; Yeter et al., 2019) and different measures are currently being explored to improve the accuracy of soil stiffness models (Byrne et al., 2019). As an example, a recent publication (Bom et al., 2020) investigated the effect of soil stiffness modelling uncertainty on the eigenfrequencies of an offshore wind jacket substructure. The results estimated based on a number of state-of-the-art procedures were subsequently compared to the in-situ estimations, and discrepancies of up to 40% were reported. In order to reduce the discrepancies, a substantial soil stiffness update was proposed, which is in line with the updating results documented in the present study.

6.2. On the update of the turbine, TP, and soil stiffnesses

In Section 5.4, the updated model parameters are stated, and it is found that substantial updating of the turbine stiffness, TP stiffness, and soil stiffness is required. Since the soil stiffness has been addressed in Section 6.1, the present subsection discusses the updated turbine and TP stiffnesses. As elaborated in Section 5.1, the numerical models of the turbine and the TP are simplified. The turbine's two-point mass system neglects the stiffness of the blades and their potential coupling to the substructure, especially to the brace elements. The simplified beam model of the TP is calibrated to represent global bending stiffness properties of the structure, while neglecting local effects. Despite the mentioned shortcomings, the simplified modelling approaches have been taken in this paper due to the following reasons; 1) state-of-the-art modelling approaches are used and 2) high-fidelity models are often not available due to practical and confidentiality reasons. Below, a few remarks on the high-fidelity models and the updated parameters are provided.

Worth noting is the fact that the turbine stiffness and the TP stiffness are updated in opposite directions, i.e., a reduction of the TP stiffness and an increase of the turbine stiffness. Since both of these parameters affect the bending stiffness in the same direction, a positive correlation of the updated parameters could be expected. However, the initial value of the parameters is derived independently. Consequently, depending on the precision of the initial estimates, one can imagine a situation

where the two parameters after the update can be positively correlated (given both initial stiffnesses are simultaneously either under- or over-estimated) or, as presented in this paper, where the parameters are updated in the opposite directions (given the initial stiffnesses are over- and under-estimated).

High-fidelity modelling of the TP using shell and/or solid finite elements would result in a TP model of a size of at least an order of magnitude larger than the entire remaining model. Assuming each element would introduce two parameters to be updated (mass and stiffness), such a TP model would result in an infeasible number of parameters to be updated. Modelling of the turbine, including an explicit beam formulation of the blades, is possible in a number of commercial aeroelastic software, e.g., FAST (Jonkman and Buhl, 2005), Bladed (DNVGL, 2020), and FLEX (Øye, 2001). By using such software (in combination with access to turbine data) a high-fidelity turbine model can be obtained, where the coupling between the braces and the blades is included. However, access to such data is typically restricted to wind turbine vendors. As a result, these models are not widely available. Moreover, the brace-blade coupling is not expected to be of crucial importance for model updating when low-order, global bending modes are used as responses (note that the 1st bending mode is dominated by the tower top displacement, while the 2nd bending mode is dominated by lateral TP displacement). On the contrary, brace-blade coupling can become critical if higher-order mode shapes dominated by the local brace displacements are included. Consequently, it is deemed impractical, at least in the presented framework and design procedures, to include high-fidelity TP and turbine models. Nevertheless, a resulting substantial update of the TP and turbine parameters might indicate insufficient precision of the modelling approach implemented in this study or imprecise initial estimation of the parameters related to the simplified models.

Alternatively, one can perform model updating of the substructure alone. The merit of this approach lays in removing the uncertainties related to the turbine modelling, consequently increasing sensitivity to the remaining highly uncertain parameters, namely, those associated with the soil stiffness. However, this approach has two main limitations; 1) it is only applicable to new structures instrumented prior to commissioning and 2) it introduces an additional complication in the installation schedule to obtain comprehensive measurement data.

7. Conclusions

This paper demonstrates the application of model updating in the context of an offshore wind jacket substructure exposed to both environmental and operational variability. It is shown how the sensitivity-based model updating, employing a subset of experimentally estimated modal parameters as responses, enables updating of physical parameters within the model to more accurately reflect in-situ conditions. For the considered example, the initial maximum eigenfrequency discrepancy of 30%, between the experimental findings and the model-predicted ones, is reduced to 1% after the update. The bulk of the initial discrepancy is attributed to a highly uncertain soil stiffness estimation.

The present study is limited to 1) estimating responses from idling states of the turbine, 2) using global modes of the structure as responses, 3) updating mean values of the physical parameters, and 4) using simplified models of the TP and the turbine. The first limitation is related to the chosen system identification method, the second is the consequence of the given sensor setup, the third one is characteristic for the sensitivity-based updating scheme, while the last one is due to practical/confidential reasons. Regardless of the mentioned limitations, the presented framework is general and its applicability for in-situ data is demonstrated in the paper.

CRediT authorship contribution statement

Dawid Augustyn: Conceptualization, Methodology, Formal

analysis, Writing - original draft. **Ursula Smolka:** Data curation, Funding acquisition. **Ulf T. Tygesen:** Methodology, Validation, Writing - review & editing. **Martin D. Ulriksen:** Conceptualization, Writing - original draft, Supervision. **John D. Sørensen:** Conceptualization, Writing - review & editing, Supervision.

Declaration of Competing Interest

The authors declare that they have no known competing financial interests or personal relationships that could have appeared to influence the work reported in this paper.

Acknowledgements

Supplementary material

Supplementary material associated with this article can be found, in the online version, at 10.1016/j.apor.2020.102366

References

Allemang, A.J., 2003. The modal assurance criterion (MAC): twenty years of use and abuse. J. Sound Vib. 37, 14–21.

API-RP-2A, 2014. Recommended Practice for Planning, Designing and Constructing Fixed Offshore Platforms. Technical Report.

Augustyn, D., Tygesen, U.T., Ulriksen, M.D., Sørensen, J.D., 2019. Data-driven design and operation of offshore wind structures. Proceedings of the 29th International Offshore and Polar Engineering Conference, ISOPE2019. pp. 491–498.

Bernal, D., Ulriksen, M.D., 2018. Output feedback in the design of eigenstructures for enhanced sensitivity. Mech. Syst. Signal Process. 112, 22–30. https://doi.org/10.1016/j.ymssp.2018.04.032.

Bertossa, A.. Evaluating geotechnical uncertainty for Offshore Wind Turbine foundation design at St. Brieuc Wind Farm. 10.1680/ecsmge.60678.vol3.178.

Bom, L., Siedler, S., Tautz-Weinert, J., 2020. Validation of CPT-based initial soil stiffness in sand for offshore wind jacket piles. Proceedings of the Messen in der Geotechnik.

BSH-7005, 2015. Standard design. minimum requirements concerning the constructive design of offshore structures within the Exclusive Economic Zone (EEZ). Technical Report.

Buitrago, J., Healy, B., Chang, T., 1993. Local joint flexibility of tubular joints. Proceedings of the 12th International Conference on Offshore Mechanics and Arctic Engineering, OMAE.

Byrne, B.W., Burd, H.J., Zdravkovic, L., McAdam, R.A., Taborda, D.M.G., Houlsby, G.T., Jardine, R.J., Martin, C.M., Potts, D.M., Gavin, K.G., 2019. Pisa: new design methods for offshore wind turbine monopiles. Rev. Francaise Geotech. 158. https://doi.org/10.1051/geotech/2019009.

Confidential author, 2016. As-Built Report. Technical Report.

Cook, R.D., Malkus, D.S., Plesha, M.E., Witt, R.J., 2001. Concepts and Applications of Finite Element Analysis, fourth ed. John Wiley & Sons.

Devriendt, C., Magalhaes, F., Weijtjens, W., De Sitter, G., Cunha, A., Guillaume, P., 2013. Automatic identification of the modal parameters of an offshore wind turbine using state-of-the-art operational modal analysis techniques. Proceedings of the 5th International Operational Modal Analysis Conference, IOMAC 2013.

Devriendt, C., Magalhes, F., Weijtjens, W., Sitter, G., Cunha, Guillaume, P., 2014. Structural health monitoring of offshore wind turbines using automated operational modal analysis. Struct. Health Monit. 13 (6), 644–659. https://doi.org/10.1177/1475921714556568.

DNVGL, 2020. Wind turbine design software - bladed.

DNVGL-ST-0126, 2016. Support structures for wind turbines. Technical Report.

Friswell, M.I., Mottershead, J.E., 1995. Finite Element Model Updating in Structural Dynamics. Kluwer Academic Publishers, Dordrecht.

Global Wind Energy Council, 2018. Global Wind Report 2018. Technical Report.

Grieves, M.V., 2019. Virtually Intelligent Product Systems: Digital and Physical Twins. https://doi.org/10.2514/5.9781624105654.0175.0200.

Hackell, M.W., Rolfes, R., 2013. Monitoring a 5 MW offshore wind energy converter" condition parameters and triangulation based extraction of modal parameters. Mech. Syst. Signal Process. 40, 322–343. https://doi.org/10.1016/j.ymssp.2013.04.004.

Imregun, M., Ewins, D., 1995. Complex modes - origins and limits. Proceedings of the 13th International Modal Analysis Conference, IMAC 1995.

Jonkman, J.M., Buhl, M.L., 2005. FAST User's Guide-Updated August 2005. Technical Report.

Kritzinger, W., Karner, M., Traar, G., Henjes, J., Sihn, W., 2018. Digital twin in manufacturing: a categorical literature review and classification. Proceedings of the 16th Symposium on Information Control Problems in Manufacturing, INCOM 2018. pp. 1016–1022. https://doi.org/10.1016/j.ifacol.2018.08.474.

Luczak, M., Manzato, S., Peeters, B., Branner, K., Berring, P., Kahsin, M., 2014. Updating finite element model of a wind turbine blade section using experimental modal analysis results. Shock Vib. 2014. https://doi.org/10.1155/2014/684786.

Mottershead, J.E., Link, M., Friswell, M.I., 2011. The sensitivity method in finite element model updating: a tutorial. Mech. Syst. Signal Process. 25 (7), 2275–2296. https://doi.org/10.1016/j.ymssp.2010.10.012.

Negro, V., Lpez-Gutirrez, J., Esteban, M., Matutano, C., 2014. Uncertainties in the design of support structures and foundations for offshore wind turbines. Renew. Energy 63, 125–132. https://doi.org/10.1016/j.renene.2013.08.041.

Nielsen, M.B., Jensen, J.F., Harper, C., Knudsen, L., Pedersen, R.R., 2019. State-of-the-art framework for structural design of offshore wind jacket foundations. Proceedings of the 1st Nordic Steel Construction Conference, Nordic Steel 2018. pp. 817–822. https://doi.org/10.1002/cepa.1139.

Olsen, P., Skafte, A., Hansen, J., Hovgaard, M., Brincker, R., Ventura, C., 2013. Identification of systems with complex modes using OMA. Proceedings of the 5th IOMAC International Operational Modal Analysis Conference.

van Overschee, P., de Moor, L., 1996. Subspace Identification for Linear Systems: Theory, Implementation, Applications. Kluwer Academic Publishers https://doi.org/10.1007/978-1-4613-0465-4.

Patelli, E., Govers, Y., Broggi, M., Gomes, H., Link, M., Mottershead, J.E., 2017. Sensitivity or Bayesian model updating: a comparison of techniques using the dlr airmod test data. Arch. Appl. Mech. 87 (5), 905–925. https://doi.org/10.1007/s00419-017-1233-1.

Popko, W., Vorpahl, F., Antonakas, P., 2013. Investigation of local vibration phenomena of a jacket sub-structure caused by coupling with other components of an offshore wind turbine. Proceedings of the 23rd International Offshore and Polar Engineering Conference, ISOPE2013. pp. 491–498.

Ramboll, 2018. ROSAP - Ramboll Offshore Structural Analysis Package, version 53. Technical Report.

Reynders, E., Pintelon, R., Roeck, G., 2008. Uncertainty bounds on modal parameters obtained from stochastic subspace identification. Mech. Syst. Signal Process. 22 (4), 948–969. https://doi.org/10.1016/j.ymssp.2007.10.009. Special Issue: Crack Effects in Rotordynamics

Øye, S., 2001. Various FLEX 5 documentation. Technical Report.

Sadowski, A., Rotter, J., Reinke, T., Ummenhofer, T., 2015. Statistical analysis of the material properties of selected structural carbon steels. Struct. Saf. 53, 26–35. https://doi.org/10.1016/j.strusafe.2014.12.002.

Schedlinski, C., Wagner, F., Bohnert, K., Frappier, J., Irrgang, A., Lehmann, R., Muller, A., 2004. Experimental modal analysis and computational model updating for a car body in white. Proceedings of the 1st International Conference on Noise and Vibration Engineering, ISMA2004.

Sørensen, J.D., Toft, H.S., 2010. Probabilistic design of wind turbines. Energies 3, 241–257. https://doi.org/10.3390/en3020241.

Tcherniak, D., Chauhan, S., Hansen, M., 2011. Applicability Limits of Operational Modal Analysis to Operational Wind Turbines. Springer New York https://doi.org/10.1007/978-1-4419-9716-6_29.

Tygesen, U.T., Jepsen, M., Vestermark, J., Dollerup, N., Pedersen, A., 2018. The true digital twin concept for fatigue re-assessment of marine structures. Proceedings of the 37th International Conference on Ocean, Offshore and Arctic Engineering, OMAE2018. https://doi.org/10.1115/OMAE2018-77915.

Tygesen, U.T., Worden, K., Rogers, T., Manson, G., Cross, E., 2019. State-of-the-Art and Future Directions for Predictive Modelling of Offshore Structure Dynamics Using Machine Learning. Springer International Publishing.

Willoughby, R., 1979. Solutions of ill-posed problems (A. N. Tikhonov and V. Y. Arsenin). SIAM Rev. 21, 266–267. https://doi.org/10.1137/1021044.

Yeter, B., Garbatov, Y., Soares, C., 2019. Uncertainty analysis of soil-pile interactions of monopile offshore wind turbine support structures. Appl. Ocean Res. 82, 74–88. https://doi.org/10.1016/j.apor.2018.10.014.

U.S. Department of Energy, 2018. Offshore Wind Technologies Market Report. Technical Report.

Paper A. Paper A

Paper B

Paper B
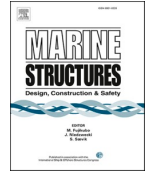
Feasibility of modal expansion for virtual sensing in offshore wind jacket substructures

Dawid Augustyn [a,b,*], Ronnie R. Pedersen [b], Ulf T. Tygesen [b], Martin D. Ulriksen [c], John D. Sørensen [a]

[a] *Department of the Built Environment, Aalborg University, Denmark*
[b] *Ramboll Energy, Esbjerg, Denmark*
[c] *Department of Energy Technology, Aalborg University, Denmark*

A B S T R A C T

The present paper investigates the feasibility of modal expansion-based virtual sensing in the context of offshore wind jacket substructures. For this specific application, issues have been reported when expanding wind-driven brace vibrations and wave-driven vibrations in the splash-zone based on a sensor network placed solely above the sea level. These limitations are addressed in this paper by extending the sensor network with sub-sea vibration sensors and a wave radar sensor, which allow for capturing local brace vibration modes and the wave-driven vibration response. The brace expansion is thus improved by including the local brace vibration modes in the expansion basis, while the representation of wave-driven vibrations is improved by including load-dependent Ritz vectors computed based on input from the wave radar sensor. The merit of the proposed extension is explored using a numerical model of an offshore wind turbine supported by a jacket substructure in a simulation setting with different operational and environmental conditions. It is documented that the extended setup provides an improvement in the expansion-based estimation of both wind- and wave-driven vibrations. The former improvement is particularly relevant for operational cases, while the latter is relevant for idling cases. Despite the documented improvements, a systematic reduction in the expansion quality is observed for higher wind speeds in operational cases for both the basic and the extended setup. It is contended that this phenomenon is due to the operational variability of the controller, which violates the fundamental assumption of the structural system being linear and time-invariant.

1. Introduction

Structural vibration response composes a pivotal part in many civil and mechanical engineering applications; i.a., structural monitoring (including fatigue estimation) [1,2] and control [3,4]. In practice, direct vibration measurements can be obtained from an installed sensor network, which covers a limited number of locations. The response at the remaining locations can subsequently be estimated using, e.g., virtual sensing methods [5–9], where the response at the unmeasured (virtual) locations is predicted based on the available measurements.

Virtual sensing has been widely adopted for vibration estimation in offshore structures. Successful applications have been

demonstrated for offshore (oil and gas) jacket structures [10,11] and monopile substructures of offshore wind turbines [12,13]. A recent publication by Henkel et al. [14] investigates the feasibility of a particular virtual sensing method, namely, modal expansion, for application to offshore wind jacket substructures. These structures are different from the previous applications due to their lattice topology and the coupled wind-wave loading. Henkel et al. [14] report high accuracy of the expansion in the leg elements, while low expansion quality is obtained for the brace elements due to the inherent limitations of the employed setup. In particular, the findings suggest that the implemented sensor network, which only includes vibration sensors above the sea level, does not allow for an adequate representation of the local brace modes or the quasi-static contribution from the wave loading. In the literature, the latter issue has been addressed in the context of system reduction [15–17] and earthquake engineering [18–20] by applying load-dependent Ritz vectors. A similar approach is implemented in this paper and its feasibility in the context of virtual sensing of offshore wind jacket substructures is investigated.

The present paper addresses the limitations that Henkel et al. [14] report on modal expansion for virtual sensing of wind turbine jacket substructures. More specifically, we examine an extended setup in which sub-sea vibration sensors and a wave radar sensor are added to capture both local brace modes and wave-governed modes, which are then included in the modal expansion basis. Two expansion scenarios—the basic one employed in Ref. [14] and the proposed extension incorporating sub-sea and wave sensors—are tested. The study is conducted using a numerical model of a 5 MW wind turbine with a jacket substructure in a simulation setting with different operational and environmental conditions.

The remainder of the paper is organized as follows. In Sec. 2, we outline the modal expansion theory used for virtual sensing, Sec. 3 establishes the setup of the numerical wind turbine case study, and Sec. 4 presents the appertaining virtual sensing results. The results are summarized in Sec. 4.3 and further discussed in Sec. 5, while the paper closes with some concluding remarks in Sec. 6.

2. Modal expansion theory

Modal expansion requires the structural system in question to be linear and time-invariant (LTI). Obviously, wind turbines violate this due to environmental and operational variability [21,22]. Yet, previous modal expansion studies concerning offshore wind turbines have operated on the premise of LTI conditions and resulted in, to some extent, adequate results [12–14]. The premise of the present study is to apply the well-established modal expansion method and focus on improving the expansion quality in cases where low quality has been reported. Consequently, this study also adapts the LTI assumption, which implies that the structural system can be described by

$$\mathbf{M}\ddot{\mathbf{u}}(t) + \mathbf{C}\dot{\mathbf{u}}(t) + \mathbf{K}\mathbf{u}(t) = \mathbf{f}(t), \tag{1}$$

where $\mathbf{M}, \mathbf{C}, \mathbf{K} \in \mathbb{R}^{n_a \times n_a}$ are the mass, damping, and stiffness matrices, n_a is the number of degrees of freedom (dof), $\ddot{\mathbf{u}}(t), \dot{\mathbf{u}}(t), \mathbf{u}(t) \in \mathbb{R}^{n_a}$ are the acceleration, velocity, and displacement vectors, and $\mathbf{f}(t) \in \mathbb{R}^{n_a}$ is the load vector. It is assumed that the system matrices are positive definite, $\mathbf{M}, \mathbf{C}, \mathbf{K} \succ 0$, and that the damping in system (1) is classically distributed. The latter implies, as specified by Caughey [23], that $\mathbf{M}^{-1}\mathbf{K}$ and $\mathbf{M}^{-1}\mathbf{C}$ commute such the eigenvectors of system (1) equal the undamped ones.

2.1. Modal expansion

Let the output—here taken as displacements, but the same relations hold for velocities and accelerations—be partitioned into n_m measured outputs, $\mathbf{u}_m(t) \in \mathbb{R}^{n_m}$, and $n_e = n_a - n_m$ virtual, expanded outputs, $\mathbf{u}_e(t) \in \mathbb{R}^{n_e}$. Then,

$$\mathbf{u}(t) = \begin{bmatrix} \mathbf{u}_m(t) \\ \mathbf{u}_e(t) \end{bmatrix}, \tag{2}$$

and the aim of modal expansion is to estimate $\mathbf{u}_e(t)$ based on $\mathbf{u}_m(t)$. If $\mathbf{u}(t)$ is governed by n_q modes, a modally truncated approximation writes

$$\mathbf{u}(t) \approx \boldsymbol{\Phi}(t)\mathbf{q}(t) = \begin{bmatrix} \boldsymbol{\Phi}_m(t) \\ \boldsymbol{\Phi}_e(t) \end{bmatrix} \mathbf{q}(t), \tag{3}$$

where $\mathbf{q}(t) \in \mathbb{R}^{n_q}$ contains the modal displacements associated with the n_q governing modes and $\boldsymbol{\Phi}(t) \in \mathbb{R}^{n_a \times n_q}$ is the expansion matrix, which is partitioned into $\boldsymbol{\Phi}_m(t) \in \mathbb{R}^{n_m \times n_q}$ and $\boldsymbol{\Phi}_e(t) \in \mathbb{R}^{n_e \times n_q}$. $\boldsymbol{\Phi}$ will be specified in Subsec. 2.2.

Assuming $n_m \geq n_q$ and $\text{rank}(\boldsymbol{\Phi}_m(t)) = n_q$, an estimate on $\mathbf{q}(t)$ that minimizes $||\boldsymbol{\Phi}_m(t)\mathbf{q}(t) - \mathbf{u}_m(t)||_2$ is given by

$$\widetilde{\mathbf{q}}(t) = \left(\boldsymbol{\Phi}_m(t)^T \boldsymbol{\Phi}_m(t)\right)^{-1} \boldsymbol{\Phi}_m(t)^T \mathbf{u}_m(t) = \boldsymbol{\Phi}_m(t)^\dagger \mathbf{u}_m(t), \tag{4}$$

with superscript $\dagger$ and overhead $\sim$ denoting, respectively, pseudo-inversion and an estimate. Thus, an estimate of the virtual part of the displacement output can be computed as

$$\widetilde{\mathbf{u}}_e(t) = \boldsymbol{\Phi}_e(t)\widetilde{\mathbf{q}}(t). \tag{5}$$

2.2. The expansion matrix

The expansion matrix, which includes a mixture of dynamic and static modes, is given by

$$\mathbf{\Phi}(t) = \begin{bmatrix} \mathbf{\Phi}^{(d)} & \mathbf{\Phi}^{(s)} & \mathbf{\Phi}^{(R)}(t) \end{bmatrix}, \tag{6}$$

where $\mathbf{\Phi}^{(d)}$ contains eigenvectors of system (1), while $\mathbf{\Phi}^{(s)}$ and $\mathbf{\Phi}^{(R)}(t)$ capture the static response due to, respectively, wind and wave loading. The modes are extracted for the dof corresponding to the measured, $\mathbf{\Phi}_m(t)$, and virtual, $\mathbf{\Phi}_e(t)$, locations. It is assumed that the static modes are calculated individually for specific sea states. The static wave modes, $\mathbf{\Phi}^{(R)}(t)$, are constructed based on input from a wave radar sensor.

2.2.1. Dynamic modes

The dynamic modes, $\mathbf{\Phi}^{(d)}$, contain a subset of the eigenvectors of system (1). The particular eigenvectors are selected such that the governing dynamics of the wind turbine system are adequately described. Compared to previous studies [12–14], where only the first few dynamic modes of the jacket/monopile substructure were considered, we include higher modes with significant local brace participation.

In this study, both the measured and the virtual partition of $\mathbf{\Phi}^{(d)}$ are obtained from the numerical model of system (1). Alternatively, the measured partition can be taken directly as the experimental mode shapes or as a combination of these and the model predictions using, e.g, the SEREP method [24] or the local correspondence principle [10,25].

2.2.2. Static wind modes

The static displacement response to wind loading can be computed as

$$\mathbf{\Phi}^{(s)} = \mathbf{K}^{-1} \mathbf{F}_s, \tag{7}$$

in which $\mathbf{F}_s \in \mathbb{R}^{n_a \times 6}$ collects 6 linearly independent unit loads (3 translational and 3 rotational) that are applied to the top of the wind turbine tower. This procedure follows the approach suggested by Iliopoulos et al. [12] who, however, restrict it to lateral translation.

2.2.3. Static wave modes

The static displacement response to wave loading is—as done by Skafte et al. [11] for oil and gas structures—estimated as Ritz vectors [26], thus

$$\mathbf{\Phi}^{(R)}(t) = \mathbf{K}^{-1} \mathbf{f}_R(t), \tag{8}$$

where $\mathbf{f}_R(t) \in \mathbb{R}^{n_a}$ is the wave load estimated for a given sea state. The wave loading can be reconstructed by using information from, e. g., a wave radar. The wave radar captures a time history of the wave surface elevation, which is subsequently used to estimate wave kinematics, using appropriate wave theory, e.g., Stokes fifth-order wave theory [27]. The wave kinematics are used to estimate the wave forces acting on individual structural members using the Morison equation [28]. A further discussion on estimating wave loading, with special focus on practical issues, is provided in Subsec. 5.4.

2.3. Validity of LTI model for modal expansion

In practice, the LTI assumption is always violated, as each system changes its properties with respect to both loading conditions (non-linear system) and time (time-variant system). In the context of an offshore wind jacket substructure, the system is non-linear and time-variant due to, i.a., non-linear wind loads, controller variability, non-linear wave forces, and soil. The impact of each violation on modal expansion is briefly discussed in this subsection.

The non-linearities introduced due to wind forces stem from aero-dynamic coupling between the blades and air particles. Assuming no large deformation and/or plasticity are present in the substructure, and this assumption is valid for normal production cases [29], the non-linearities introduced from wind forces do not affect modal expansion in the substructure.

The controller variability is known to alter the modal parameters (including mode shapes) of wind turbine structures [21,22]. Since each wind turbine structure is coupled to a substructure, any alternation of the mode shapes of the turbine affects the substructure dynamics as well. The effect of neglecting the controller variability, which has been reported as one of the sources of reduced expansion quality for higher wind speeds in Ref. [14], is further investigated in Subsec. 5.1 in the present paper.

The wave forces are non-linear as they include the effect of the relative velocity between the wave and the structure, as typically modelled by use of the relative-velocity Morison equation [28]. For bottom-fixed offshore structures, the effect of relative velocity is small [28], and therefore the error introduced by neglecting it in this study with a bottom-fixed jacket substructure (to comply with the LTI assumption) is not critical.

The soil stiffness is non-linear with respect to the applied load. Variable soil stiffness affects the mode shapes used to expand both the static and the dynamic part of the response. In the LTI model, the soil stiffness has to be linearized for representative conditions. Consequently, any variation in soil stiffness is neglected. For a typical offshore wind application, the soil stiffness is linearized according to the initial stiffness [30], which is representative for power production cases where the majority of fatigue damage is generated. For extreme cases, a different linearization point could be selected to account for the modified soil stiffness. Consequently,

by deriving a number of modal expansion sets, representative for each loading condition and hence soil stiffness configuration, the soil stiffness variation can, indirectly, be accounted for.

3. Case study setup

The case study is based on synthetic displacement data obtained from a numerical model of a 5 MW wind turbine exposed to different load cases. The model is described in Subsec. 3.1. The displacement data are extracted from both physical output locations and virtual output locations. The former is used as input to the modal expansion, while the latter is used to validate the expanded, virtual results. The particular locations are specified in Subsec. 3.2 for the basic and extended sensor configurations. The load cases considered in this study are described in Subsec. 3.3.

3.1. Modelling

The jacket substructure and its appertaining wave loading are modelled using ROSAP (Ramboll Offshore Structural Analysis Package), version 53 [31]. The jacket substructure considered in this study, which is depicted in Fig. 1a, has a total height of approximately 50 m. The substructure comprises four legs, each with a diameter of approximately 2 m, and three brace bays, each with a diameter of approximately 0.5 m. The substructure model includes, i.a., soil-pile interaction, local joint flexibility, scour, marine growth, and appurtenance masses. The water depth is 40 m and the soil conditions are characterized as clay. The substructure includes 30 m grouted piles. The soil-structure interaction is modelled by use of soil curves linearized according to the API method [30]. The substructure carries a representative 5 MW turbine modelled in LACflex aero-elastic code [32]. The turbine includes a 70 m tubular tower with a diameter ranging between 4 m and 6 m. Along the tower, three concentrated masses are assumed to emulate the effect of secondary-structures. The aero-elastic code employs a modal-based representation of the turbine (including the tower, rotor, and blades), while the substructure is represented as a Craig-Bampton superelement [33]. The structural damping is modelled according to the Rayleigh model [34] assuming 0.5% and 1% modal damping in the first and second bending modes, respectively.

The aero-hydro-servo-elastic simulation is performed in a sequentially coupled manner as described by Nielsen et al. [35]. The key steps of the procedure are as follows. 1) the substructure model and corresponding wave loading are reduced to a superelement with 30 internal modes accounting for internal substructure dynamics. A convergence study has been performed to ascertain that the reduced model (including 30 modes) adequately captures the relevant modal parameters of the non-reduced system. Subsequently, 2) the wind loading is computed through aero-elastic analyses, in which the synchronized wave loading and the substructure superelement are included. Finally, 3) the force-controlled recovery run outlined by Nielsen et al. [17] is performed, where the response of the substructure is recovered and relevant measurements are extracted.

3.2. Sensor layout

The two employed sensor configurations are depicted in Fig. 1c and d. Each configuration consists of physical sensors, which are assumed installed on the structure to deliver the displacement measurements constituting $\mathbf{u}_m(t)$ in (2), and virtual sensors, which are placed at locations where the displacement response is estimated through modal expansion. In this study, the displacement
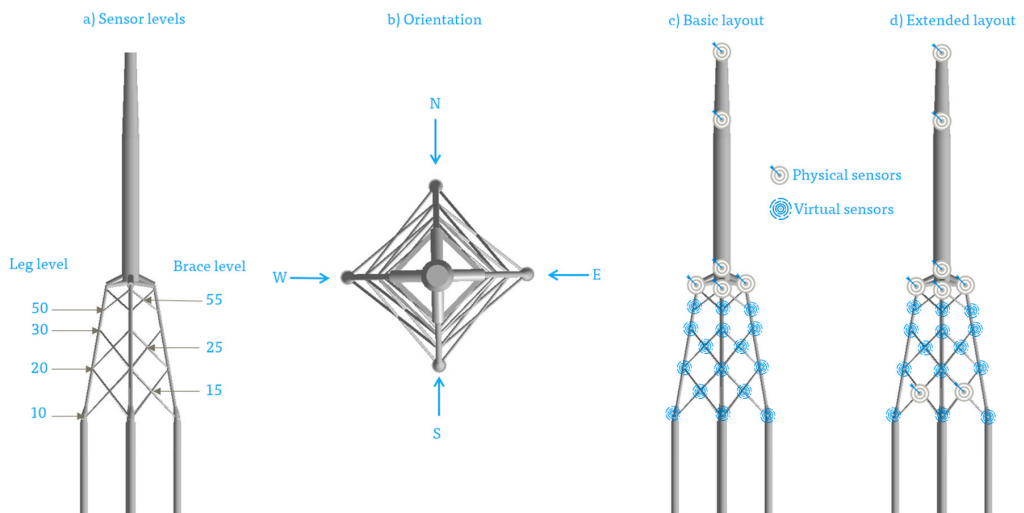
Fig. 1. Instrumentation of the jacket substructure. a) sensor levels, b) substructure direction, c) basic sensor layout, and d) extended sensor layout.

measurements are obtained directly from the numerical model. In practice, the vibration sensors would be composed of accelerometers, so the displacements would be obtained through double integration of the temporal acceleration signals and/or a linear transformation of the temporal strain signals. The basic configuration described in Subsec. 3.2.1 corresponds to the setup utilized by Henkel et al. [14], while the extended setup described in Subsec. 3.2.2 contains sub-sea vibration sensors and a wave radar sensor.

3.2.1. Basic sensor configuration

The basic sensor setup, which is depicted in Fig. 1c, contains 7 bi-axial vibration sensors (measuring displacements). The sensors are located in the nacelle, on the tower (at the bottom and at approximately 2/3 of the tower height), and at the top of each jacket leg. The measurements are expanded to the virtual locations indicated in Fig. 1c. These virtual locations include nodes in the K-joints and X-joints. The joints are named after the level at which they are positioned. The level numbering is indicated in Fig. 1a.

3.2.2. Extended sensor configuration

The extended sensor setup includes bi-axial sub-sea vibration sensors in the lower X-joints at level 15. The approximate locations of the sensors are indicated in Fig. 1d. In addition to the displacement sensors, a wave radar sensor is included to capture the wave surface elevation. Subsequently, the wave surface elevation is used to compute the static wave modes, as elaborated in Subsec. 2.2.3.

3.3. Load cases

Two turbine states are considered in the simulations; 1) operational where the control system is active and 2) idling where the control system is inactive and the blades are pitched 90° to minimize the wind loading. The load cases are defined in accordance with the IEC standard [36] from which load cases 1.2 and 6.4 are considered. These two load cases—which are further described in Subsecs. 3.3.1 and 3.3.2 and summarized in Table 1—are assumed to be representative for the operational and idling turbine states.

3.3.1. Operational

The vibration response of the turbine and its jacket substructure is simulated for a wind speed range of $U \in [4, 29]$ m/s, which is where the turbine is assumed to generate power. The lower and upper limits of $U = 4$ m/s and $U = 29$ m/s are denoted the cut-in and cut-out wind speeds. While operating within these limits, the control system is activated to maximize the energy yield by altering the rotor's angular velocity and the blades' pitch angle up to the rated wind speed, which is approximately 12 m/s for this particular turbine. Above the rated wind speed and up to the cut-out wind speed, the control system stabilizes the rotor's angular velocity and alters the blades' pitch angle to produce the rated power and minimize the wind loads. A varying turbulence intensity is applied according to the IEC normal turbulence model [36]. Consequently, stochastic wind speed time-series (turbulent wind) are generated for each load case. Each time series has a duration of 800 s of which the first 200 s is neglected to avoid an initiation disturbance.

In addition to the wind loads, wave loading is incorporated by applying irregular sea states characterized by the wave height, H_s, and the wave period, T_p. For these, we assume $H_s \in [0.5, 5.5]$ m and $T_p \in [0.4, 6.4]$ s, which is a representative set for the substructure considered in this study. The irregular waves are generated based on the JONSWAP spectrum [37] with the peak-enhanced factor $\gamma = 3.3$, while the drag and mass coefficients are set to 0.65 and 2, respectively. The wind and wave loading is assumed to be fully aligned and approaching the structure from direction N, see Fig. 1b. Stationary conditions are assumed within each sea state.

3.3.2. Idling

The vibration response of the turbine and jacket substructure is simulated below the cut-in wind speed and above the cut-out wind speed. Under these conditions, the blades are pitched 90° to minimize the wind-induced loading, and the angular velocity of the rotor is negligible. As a result, the structural response is predominantly governed by the wave loading.

The response of the structure is simulated for two wind speeds; $U = 3$ m/s, which is below the cut-in wind speed, and $U = 35$ m/s, which corresponds to the representative extreme wind speed [36]. The wave loading is, in analogy to the procedure for the operational cases, generated by applying irregular waves characterized by wave height and period. The wave parameters used in the two simulations are $H_s \in \{0.4, 6.4\}$ m and $T_p \in \{3.7, 6.7\}$ s, corresponding to a representative set for the substructure considered in this study. The same loading direction and alignment as selected in the operational cases are used in the idling cases.

3.4. Modal expansion performance indicators

The quality of the conducted modal expansion is assessed based on four performance indicators. Let $\mathbf{u}_i, \tilde{\mathbf{u}}_i \in \mathbb{R}^N$ denote the measured and estimated displacement signals at sensor i, then the first performance indicator is the time response assurance criterion (TRAC) [38] defined by

Table 1
Load case definitions according to IEC [36] and representative site-specific parameters.

Turbine state	Wind speed, U [m/s]	Turbulence, TI [−]	Wave height, H_s [m]	Wave period, T_p [s]	Direction
Operational	4–29	0.21–0.09	0.5–5.5	3.8–6.6	N
Idling	3 and 35	0.23 and 0.08	0.4 and 6.4	3.7 and 6.7	N

$$\mathscr{T} = \frac{\left(\mathbf{u}_i^T \tilde{\mathbf{u}}_i\right)^2}{\left(\mathbf{u}_i^T \mathbf{u}_i\right)\left(\tilde{\mathbf{u}}_i^T \tilde{\mathbf{u}}_i\right)} \in [0, 1], \tag{9}$$

hence yielding a measure of the temporal correlation between the measured and estimated signals. $\mathscr{T} = 0$ indicates no correlation, while $\mathscr{T} = 1$ indicates full temporal correlation.

Since the TRAC does not account for the amplitudes of the signals, the coefficient of determination (CoD),

$$R^2 = 1 - \frac{\mathrm{E}\left[\left(\mathbf{u}_i - \tilde{\mathbf{u}}_i\right)^2\right]}{\mathrm{Var}[\mathbf{u}_i]} \in (-\infty, 1), \tag{10}$$

is introduced to capture potential amplitude errors. Here, E[.] and Var[.] denote the expectation and variance operators.

Two metrics related to estimation of the amplitude range uncertainty are employed, namely, bias and coefficient of variation (CoV). The bias is defined as the expected value of the cumulative amplitude range ratios of the displacement signal, thus

$$b = \mathrm{E}\left[\frac{\Delta \mathbf{u}_i}{\Delta \tilde{\mathbf{u}}_i}\right], \tag{11}$$

where $\Delta \mathbf{u}_i \in \mathbb{N}^m$ is a cumulative rainflow count of the measured displacements over one time-series, $\Delta \tilde{\mathbf{u}}_i \in \mathbb{N}^m$ is a cumulative rainflow count of the predicted displacements, and m is the number of rainflow count bins. The CoV is defined as

$$c_v = \frac{\sqrt{\mathrm{Var}\left[\frac{\Delta \mathbf{u}_i}{\Delta \tilde{\mathbf{u}}_i}\right]}}{b}, \tag{12}$$

which is the standard deviation of the cumulative amplitude range ratios for all amplitude bins normalized to the bias.

4. Case study results

Modal expansion results are presented for the two sensor configurations described in Subsec. 3.2 and the load cases described in Subsec. 3.3. The expansion setups are summarized in Table 2, and a subset of the modes constituting the expansion matrix, $\mathbf{\Phi}$, is illustrated in Fig. 2.

4.1. Basic expansion setup

The basic setup includes sensors located above the seawater level with simple access. As a result, the captured dynamic response is dominated by the first 2 global bending modes and the first torsion mode, so 5 dynamic modes in total are included in $\mathbf{\Phi}^{(d)}$. Even though 14 signals are obtained in this setup (allowing to include up to 14 modes in the expansion basis), the frequency content of the signals is dominated by the first 5 modes. Consequently, there is no benefit of including more modes. With this basic setup, the local brace modes cannot be captured, hence local brace vibrations are neglected in this setup. The static wind modes included in $\mathbf{\Phi}^{(s)}$ are established in accordance with (7). The 6 static wind modes represent wind load applied at the top of the tower, i.e., 3 translations and 3 rotations. Since no sub-sea sensors are available in the basic setup, the static wave modes are not included in $\mathbf{\Phi}$. The expansion matrix, $\mathbf{\Phi}$, contains 11 modes in total in the basic setup.

4.1.1. Operational results

Displacement time-series obtained at leg level 50 and brace level 15 for wind speed $U = 6$ m/s are presented in Fig. 3. Here, both the measured signals and the expansion-based estimates are shown, and it can be seen that the displacements in the leg element are expanded well, while the expansion for the brace element yields an underestimation of the amplitudes.

Table 2
Overview of sensors and modes included in the expansion setups.

Setup	Sensor location		Expansion basis			
	Above water	Below water	Dynamic		Static	
			Global	Local	Wind	Wave
Basic	Yes	No	Yes	No	Yes	No
Extended	Yes	Yes	Yes	Yes	Yes	Yes
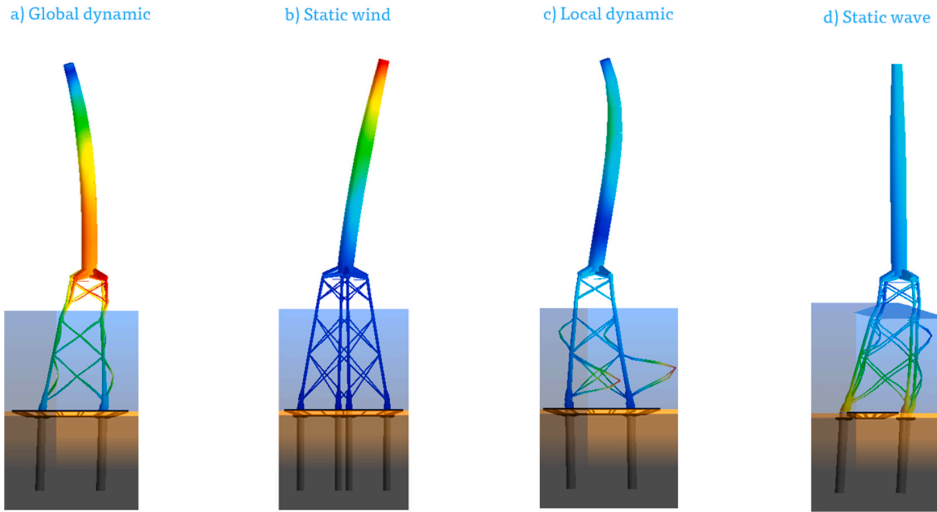
Fig. 2. A subset of modes included in the expansion matrix, **Φ**. a) 2nd global bending mode included in $\mathbf{\Phi}^{(d)}$, b) static wind mode due to unit translation included in $\mathbf{\Phi}^{(s)}$, c) local brace mode included in $\mathbf{\Phi}^{(d)}$, and d) static wave (Ritz) mode included in $\mathbf{\Phi}^{(R)}(t)$.
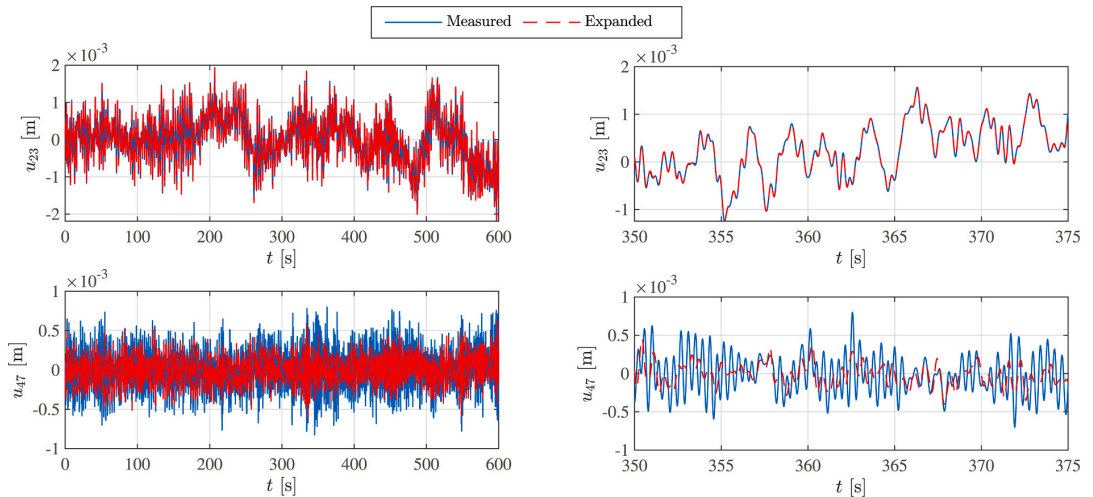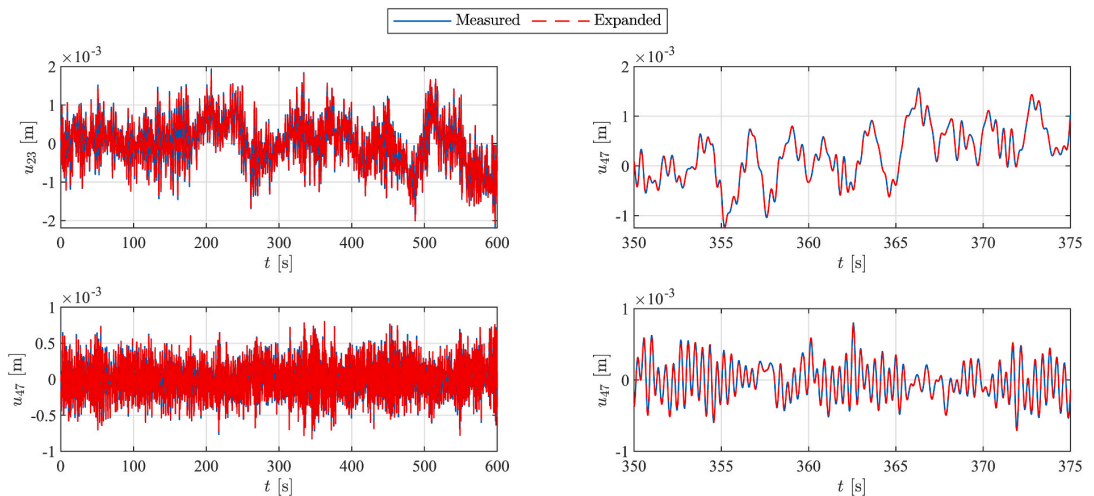

Fig. 3. Measured (blue) and expanded (red) displacements using the basic setup. u_{23}, leg level 50 (top) and u_{47}, brace level 15 (bottom). (For interpretation of the references to colour in this figure legend, the reader is referred to the Web version of this article.)

The TRAC and CoV results averaged for all operational load cases are presented in Fig. 4. Evidently, high TRAC values are obtained for the leg elements; with the highest value being 1 (observed at level 50) and the lowest being 0.90 (observed at level 10, which is close to the mudline). A general trend of reduced TRAC is observed for the leg elements in the lower part of the substructure.

A large variation in TRAC values is observed for the brace elements. The brace element at level 55—which is the one closest to the transition piece—obtains a TRAC value of 1, the brace element at the intermediate level 25 a TRAC value of 0.75, and the brace element at the lowest level (i.e., number 15) a TRAC value of 0.50. In accordance with the leg element observations, the brace element expansion decreases in quality for the lower part of the substructure. The CoV ranges between 0.05 and 0.15 for the leg elements and 0.05 and 0.50 for the brace elements. Generally, the lowest uncertainty is observed in the top part of the jacket, while the largest uncertainty is observed in the lowest brace level 15.

To investigate the effect of the operational variability on the expansion quality, the TRAC value as a function of wind speed is presented in Fig. 5 for the different leg and brace elements. The highest TRAC values are generally obtained for the lowest wind speed,
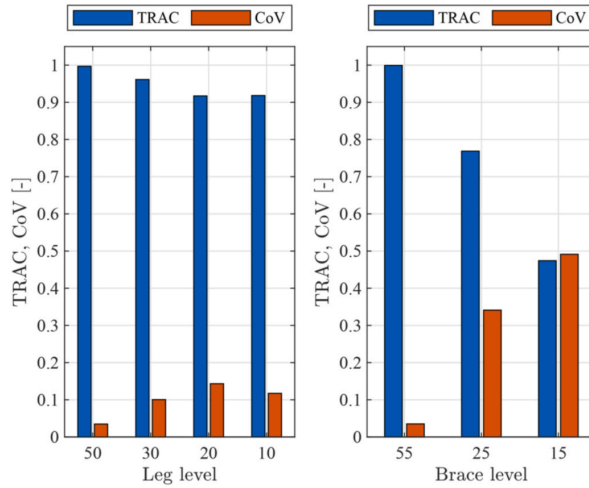
Fig. 4. Averaged expansion results for the operational load cases using the basic setup.

while a gradual quality reduction is observed between $U = 4$ m/s and $U = 12$ m/s. The expansion quality stabilizes for $U > 12$ m/s, which is the rated wind speed. The impact of the operational variability is further discussed in Sec. 4.3.

4.1.2. Idling results

The average TRAC and CoV values for the idling cases are presented in Fig. 6. Evidently, we obtain TRAC values between 0.4 and 0.8 and CoV values between 0.2 and 0.7, which are lower than the corresponding results for the operational cases. The reduced expansion quality is governed by the increased wave contribution, which is captured poorly in the basic expansion setup.

4.2. Extended expansion setup

The extended setup includes additional displacement sensors located sub-sea and a wave radar sensor. As a result, $\boldsymbol{\Phi}$ can, compared to the configuration used for the basic setup, be extended with 7 local brace modes included in $\boldsymbol{\Phi}^{(d)}$ and 1 static wave Ritz mode included in $\boldsymbol{\Phi}^{(R)}(t)$. Thus, the expansion matrix, $\boldsymbol{\Phi}$, contains 19 modes in the extended setup.
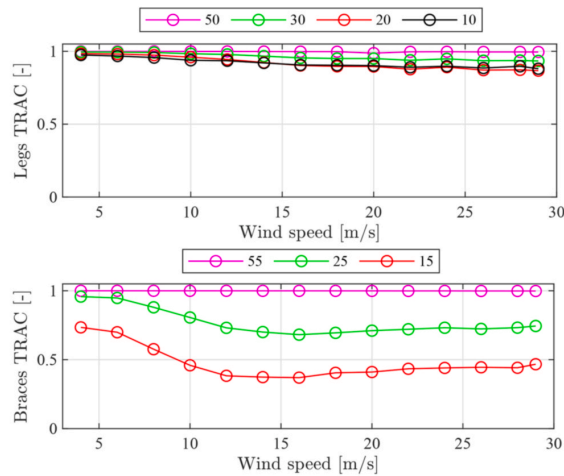
Fig. 5. TRAC values as functions of the wind speed obtained using the basic setup; a) leg levels and b) braces levels.
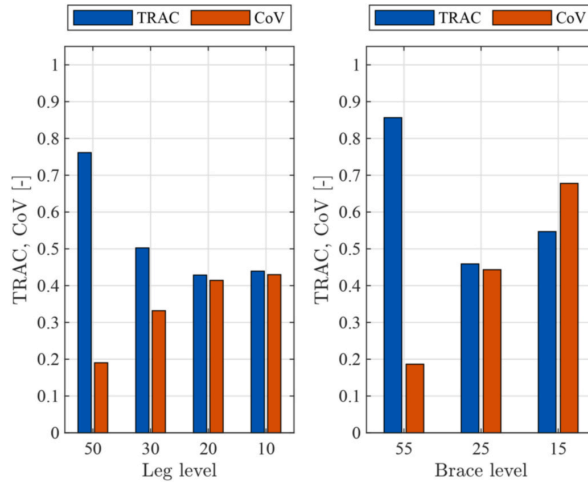
Fig. 6. Averaged expansion results for the idling load cases using the basic setup.

4.2.1. Operational load case

The measured and expanded displacements at leg level 50 and brace level 15 for $U = 6$ m/s are presented in Fig. 7. The average TRAC and CoV values for all the leg and brace levels are presented in Fig. 8. TRAC values close to 1 are observed across all the leg levels and at brace levels 55 and 15. The lowest TRAC value of 0.85 is observed at brace level 25. The CoV values for all the leg elements and the brace elements at levels 55 and 15 are below 0.05, while the CoV value is 0.15 for the brace element at level 25.

The TRAC value as a function of wind speed is presented in Fig. 9 for the different leg and brace elements. Evidently, TRAC values of 1 are obtained for all wind speeds at every level except brace level 25. Here, we observe an average TRAC value of 0.95 below rated wind speed and an average TRAC value of 0.80 above rated wind speed. This variation is further discussed in Subsec. 5.1.

4.2.2. Idling load cases

The average TRAC and CoV values for the idling cases are presented in Fig. 10. TRAC values close to 1 are observed across all the leg and brace levels, and the CoV values are below 0.05 for the leg elements and 0.10 for the brace elements.

Fig. 7. Measured (blue) and expanded (red) displacements using the extended setup. u_{23}, leg level 50 (top) and u_{47}, brace level 15 (bottom). (For interpretation of the references to colour in this figure legend, the reader is referred to the Web version of this article.)
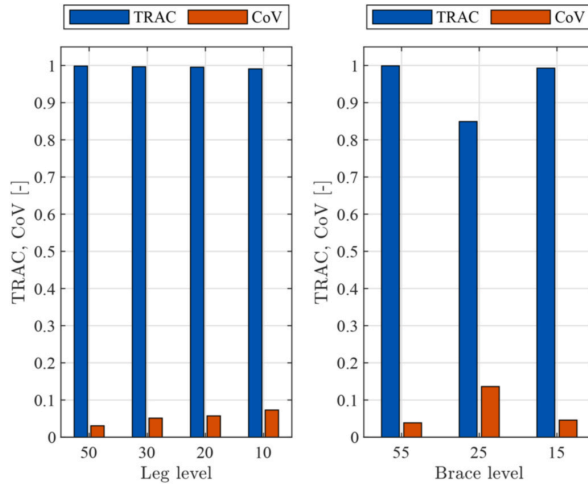
**Fig. 8.** Averaged expansion results for the operational load cases using the extended setup.
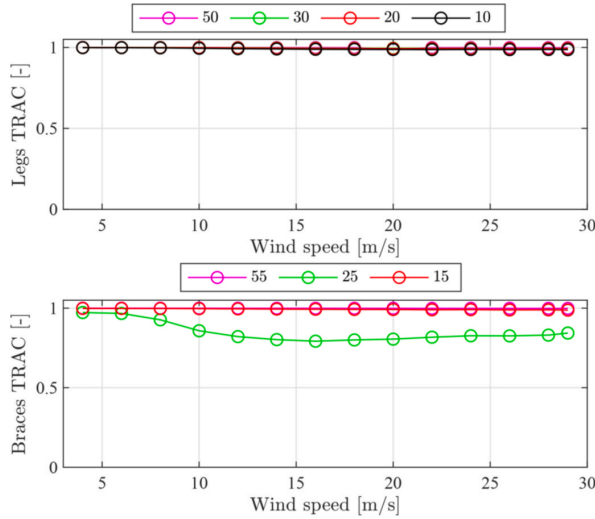
Fig. 9. TRAC values as functions of the wind speed obtained using the extended setup; a) leg levels and b) braces levels.

4.3. Summary of the results

The expansion quality gained by including vibration sensors below the water level and a wave radar sensor is summarized in this subsection. The operational and idling results are discussed in Subsec. 4.3.1 and Subsec. 4.3.2, respectively.

The averaged expansion quality indicators for the basic and extended setups are presented in Table 3. The expansion quality across the considered load cases and virtual sensor locations is increased after implementing the extended setup. In particular, the average TRAC value is increased from 0.69 to 0.99, while the average CoV value is reduced from 0.26 to 0.05. The CoD is increased from −3.70 to 0.99, while the bias is reduced from 1.15 to 1.03.

4.3.1. Operational results

The expansion results, in terms of TRAC and CoV values, for the operational cases are presented in Figs. 11 and 12 for comparison purposes. Implementation of the extended expansion setup yields an increase in average TRAC value for all leg elements from 0.95 to 1, while the corresponding CoV value is reduced from 0.10 to 0.05. For the brace elements, the average TRAC value is increased from 0.70
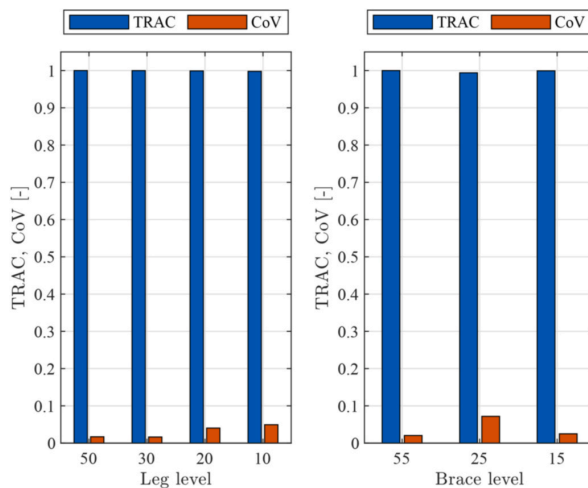
Fig. 10. Averaged expansion results for the idling load cases using the extended setup.

Table 3
Averaged quality indicators for the basic and extended expansion setups.

| Setup	Load case	TRAC ($\mathcal{T}$)		CoD (R^2)		Bias (b)		CoV (c_v)	
		Legs	Braces	Legs	Braces	Legs	Braces	Legs	Braces
Basic	Operational	0.95	0.70	0.90	0.75	1.05	2.00	0.10	0.25
	Idling	0.50	0.60	−9.50	−7.00	0.80	0.75	0.30	0.40
Extended	Operational	1.00	0.95	1.00	0.95	1.05	1.05	0.05	0 05
	Idling	1.00	1.00	1.00	1.00	1.00	1.00	0.05	0.05
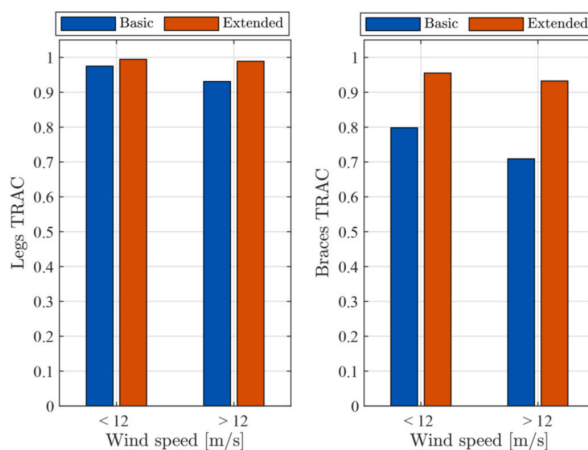
Fig. 11. TRAC values obtained using the basic (blue) and extended (orange) setup for the operational load cases. Legs (left) and braces (right). (For interpretation of the references to colour in this figure legend, the reader is referred to the Web version of this article.)

to 0.95, and the CoV value is reduced from 0.25 to 0.05.

4.3.2. Idling results

The expansion improvement obtained by implementing the extended setup in the idling cases is indicated in Figs. 13 and 14. We observe an increase in average TRAC value for all leg elements from 0.50 to 1, while the corresponding CoV value is reduced from 0.30
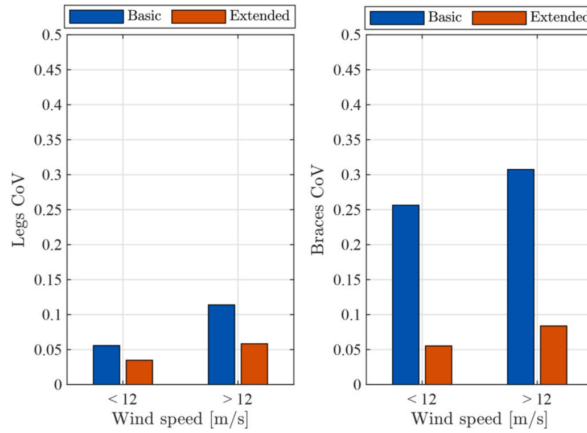
Fig. 12. CoV values obtained using the basic (blue) and extended (orange) setup for the operational load cases. Legs (left) and braces (right). (For interpretation of the references to colour in this figure legend, the reader is referred to the Web version of this article.)
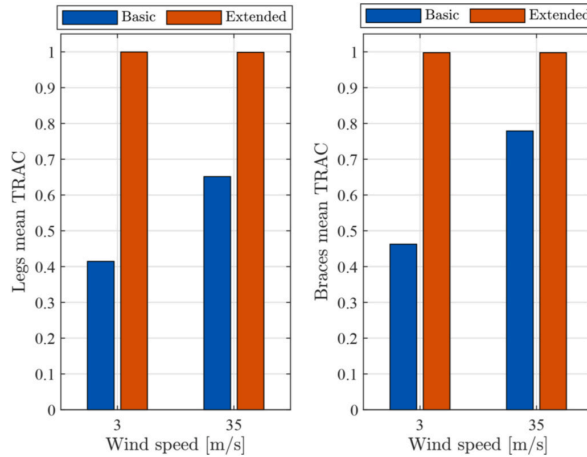
Fig. 13. TRAC values obtained using basic (blue) and extended (orange) setup for the idling load cases. Legs (left) and braces (right). (For interpretation of the references to colour in this figure legend, the reader is referred to the Web version of this article.)

to 0.05. For the brace elements, the average TRAC value is increased from 0.60 to 1, and the CoV value is reduced from 0.40 to 0.05.

5. Discussion

This section offers a discussion on the presented results and some practical aspects of the implemented modal expansion method. The effect of operational variability on the expansion quality is discussed in Subsec. 5.1, followed by a discussion in Subsec. 5.2 on the importance of including higher-order dynamics and wave loading information in the expansion. An optimal sensor placement strategy is discussed in Subsec. 5.3, and the section closes by addressing the limitations and practical feasibility of modal expansion for offshore wind application in Subsec. 5.4.

5.1. Effect of operational variability on the expansion quality

The time-variant and non-linear effects in the substructure are negligible when the full system (wind turbine and substructure) operates under operational conditions. However, the wind turbine system exhibits time-variant and non-linear behaviour, which affects its dynamic properties. The non-linearities are promoted by, among other factors, large deflections of the blades and potential contact problems in the rotor, while the time-variant effects stem from the controller and environmental (temperature, humidity, etc.)
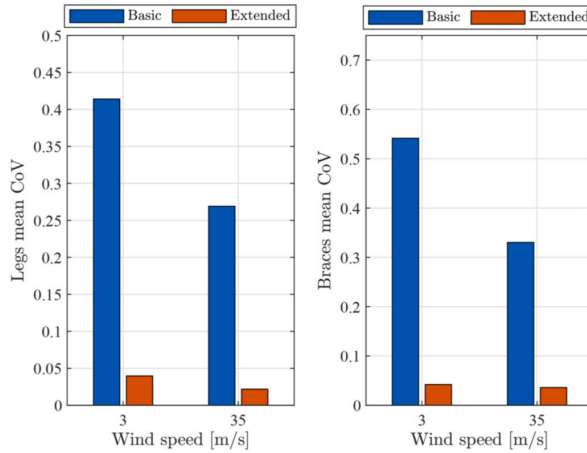
Fig. 14. Uncertainties obtained using the basic (blue) and extended (orange) setup for the idling load cases. Legs (left) and braces (right). levels. (For interpretation of the references to colour in this figure legend, the reader is referred to the Web version of this article.)

variation. As a result, the modal properties of the combined system (including the substructure mode shapes used in the expansion, $\Phi^{(d)}$), are time-variant, thus a reduced expansion quality is expected when, as done in the present study, operating with an LTI basis. The observations reported below support this proposition.

A systematic reduction in the expansion quality is observed in Figs. 5 and 9 for higher wind speeds in operational cases. To investigate this effect, expansion results in the brace element at level 25 for two wind-only cases are presented in Fig. 15. The first case considers the turbine during operation with the control system activated and the second case an idling setting with the control system being inactive. Evidently, when the control system is active, the TRAC value decreases monotonically as the wind speed increases up to the rated wind speed, while the TRAC value remains more or less constant when the control system is inactive. As the controller parameters alter to optimize the power output, the modal parameters become time-variant. This time-variance cannot be captured in the LTI model, hence resulting in the noted expansion quality reduction for the case with an active controller.

5.2. On the higher-order dynamics and wave loading

The extended setup adds two additional sensor types (sub-sea vibration sensors and a wave sensor). The added value of each sensor type varies for different structures and operational conditions. In this subsection, the value of including the two sensor types separately is discussed in the context of typical offshore wind substructures and operational conditions.

A wave sensor improves the expansion quality for structures whose response is driven by wave loading. In the context of offshore wind applications, such structures are 1) the ones carrying old turbines generating low wind loading compared to wave loading, 2) all turbines in idling cases, where wind forces are significantly reduced compared to operational cases, and 3) monopile structures, which attract more wave loading compared to, e.g., jacket substructures. To quantify the improvement in the expansion quality due to wave radars only, two additional sensor setups are defined. The first one corresponds to the basic setup with a wave radar, while the second one is the extended setup with the wave radar removed. For the sake of brevity, we present the results for the idling cases as these are wave-driven, and hence the effect of the wave radar is the most profound, although the same (qualitative-wise) conclusion holds for the operational cases. Results attained using the four setups (including the basic and the extended one) are presented in Figs. 16 and 17 for the TRAC and CoV values, respectively. The TRAC values are improved for both the leg and brace elements when the wave radar is
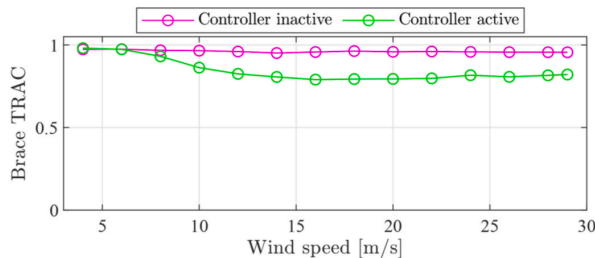

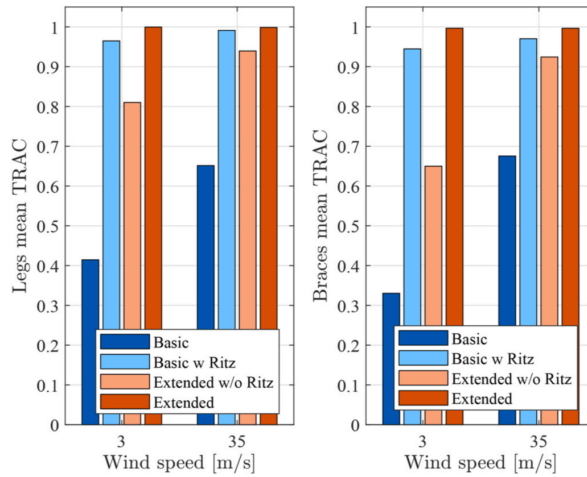**Fig. 15.** TRAC value as a function of wind speed obtained for an inactive and active control system.

Fig. 16. TRAC values obtained using modified (with/without Ritz modes) basic and extended setups for the idling load cases.
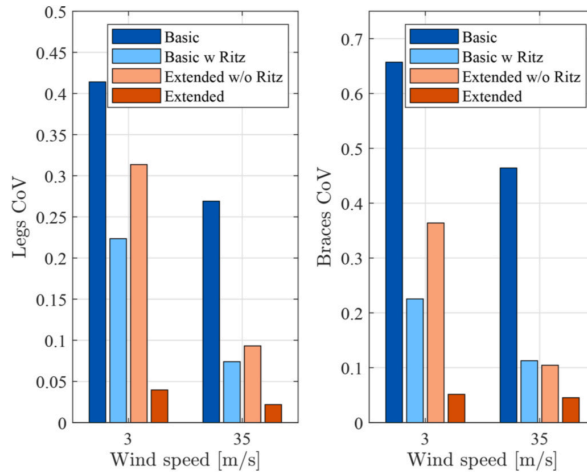

Fig. 17. CoV values obtained using modified (with/without Ritz modes) basic and extended setups for the idling load cases.

included, as indicated in Fig. 16. The largest improvement is observed for the basic setup for wind speed $U = 3$ m/s, where the TRAC value is increased from 0.3 to 0.95 for the brace elements by including only the wave radar. The improvement in the extended setup is less profound; with the TRAC value increasing from 0.65 to 1. A similar trend—namely, improvement of the expansion quality when the wave radar is included—is displayed by the CoV values presented in Fig. 17.

The sub-sea vibration sensors improve the expansion quality for structures whose response is driven by high-frequency dynamic response. For a typical offshore wind turbine under power production conditions, the turbulent wind loading results in dynamic response of the blades, which is further transferred to the substructure due to blade-brace coupling [39]. Consequently, local brace modes are activated and therefore the expansion requires sub-sea sensors to accurately capture these vibrations.

5.3. Optimal sensor placement

The location and number of physical sensors affect the expansion quality. In general, increasing the number of installed sensors improves the expansion quality, as exemplified for the basic and extended sensor setup in Subsec. 4.3. Due to practical and economic constraints, a limited number of sensors can be installed in real-life applications, which necessitates a careful selection of the sensor locations. The modal expansion method delivers optimal (in an ℓ_2-norm sense) modal displacements, which are subsequently used to expand for virtual sensing. The precision of the virtual sensing estimate depends on the linear dependence of the mode shapes in the

expansion basis matrix [40]. The linear dependence can be reduced to increase the expansion quality by placing sensors according to, e.g., the effective independence (EI) method [41]. In this method, the optimal sensor placement is derived by maximizing some suitable norm of the Fisher information matrix, effectively minimizing linear dependence of the available mode shapes. The merit of placing sensors using the EI method in the context of modal expansion-based virtual sensing has been verified by Andersen et al. [40].

In this study, the sensor distribution is selected based on the EI method under the assumptions that; 1) all locations are accessible, 2) the cost of installation is immaterial, and 3) one level of bracing can be monitored as a sub-sea location. These engineering judgement criteria are chosen to increase the robustness of the sensor setup with respect to potential sensor failure during operation. Consequently, brace level 15 is chosen, as the braces at this level are the longest and hence the most prone to excessive vibrations. Given other brace levels should be monitored instead, the expansion quality would be reduced. Recall that the chosen sensor setup and mode shapes in the expansion basis yield a high linear correlation between the dynamic modes (first bending) and the static wind modes (lateral deflection). Despite the large linear correlation between the two mode shapes, their strain energy differs [12]. Moreover, a large correlation is not problematic, as a full linear correlation resulting in a singular expansion matrix, and hence poor expansion, is not possible.

5.4. Limitations and practical feasibility

This paper investigates the theoretical feasibility of modal expansion based on data generated from a numerical model, without taking into account any of the associated practical challenges and issues. In this subsection, a brief discussion on the limitations and a few practical challenges related to modal expansion is provided.

In this study, virtual sensing is applied based on displacements, according to Eqs. (4) and (5). In practice, displacements are rarely measured directly. For a typical offshore wind application, accelerations are preferred due to a better signal-to-noise ratio [12]. The accelerations are then double-integrated with respect to time to obtain a high-frequency part of the displacement response. The issue with this approach is that the low-frequency (quasi-static) content of the response is lost. Hence, it has to be augmented with information from an additional sensor type, which is able to capture the quasi-static response, e.g., a strain gauge, inclinometer, or GPS sensor. Consequently, sensor fusion techniques [42] have to be applied to combine different types of sensors to reconstruct the displacement signals. Alternatively, the displacements can be obtained directly from acceleration signals by applying the Walsh Transform as proven in the context of a seismic application [43]. In the present study, the displacements captured in the physical sensors are directly obtained from the numerical model, hence circumventing the above-mentioned issues.

The wave-induced displacements are expanded based on the Ritz vectors, as described in Subsec. 2.2.3. The Ritz vectors are derived based on the stiffness matrix and wave forces, see Eq. (8). In practice, the wave forces have to be estimated based on information from in-situ sensors, e.g., wave radars [44] or pressure transducers [45]. These sensors can be quite expensive and instrumenting each wind turbine in a park would require a substantial investment. Some researchers suggest instrumenting only a small number of structures, the so-called fleet leaders, and expanding/correlating this information to the remaining, lightly instrumented structures [46]. Moreover, even when a wave radar is directly installed on a structure, reconstructing wave forces is challenging because of the waves' irregular nature, their high frequency content [47], and the wave-structure interaction [48]. In the present study, the wave forces are obtained directly from the numerical model using a generic theoretical framework as described in Subsec. 2.2.3, hence neglecting a number of potential practical issues. Consequently, further research is required to investigate the practical application of wave reconstruction in the context of modal expansion.

6. Conclusions

This paper investigates the feasibility of modal expansion-based virtual sensing in the context of offshore wind jacket substructures. Two different expansion setups, namely, a basic and an extended one, are employed. It is evidenced how the basic setup, which only includes sensors above the seawater level, fails to deliver high-quality expansion results during idling conditions, where the vibrations are governed solely by the wave loading. Additionally, low expansion quality is observed for the brace elements during both idling and operational conditions. The expansion quality in these cases is low because the modes included in the basic setup do not adequately represent the wave-induced vibrations or the local brace modes.

To alleviate the noted shortcomings, the extended expansion setup is suggested in this paper. The setup includes sub-sea sensors and a wave radar sensor, which allow for extraction of, respectively, local sub-sea brace vibration modes and static wave modes. Inclusion of these modes in the expansion improves the expansion quality significantly.

For both setups, a systematic reduction in expansion quality is observed for the brace elements when the wind speed increases. It is contended that this decrease arises because the control system renders the structural behaviour non-linear and time-variant, which is not accounted for in the employed expansion method. This will be addressed explicitly in a separate publication by the authors.

Declaration of competing interest

The authors declare that they have no known competing financial interests or personal relationships that could have appeared to influence the work reported in this paper.

Acknowledgements

References

[1] Fritzen C-P. Vibration-based techniques for structural health monitoring. John Wiley & Sons, Ltd; 2010. p. 45–224. https://doi.org/10.1002/9780470612071. ch2. Ch. 2.

[2] Ulriksen MD. Damage localization for structural health monitoring: an exploration of three new vibration-based schemes, Doctoral dissertation. Aalborg University; 2018.

[3] Meirovitch L. Dynamics and control of structures. first ed. John Wiley & Sons, Inc.; 1990.

[4] Preumont A, Seto K. Active control of structures. John Wiley & Sons, Ltd; 2008. https://doi.org/10.1002/9780470715703.

[5] Ching J, Beck J, Porter K. Bayesian state and parameter estimation of uncertain dynamical systems. Probabilist Eng Mech 2006;21(1):81–96. https://doi.org/10.1016/j.probengmech.2005.08.003.

[6] Liu L, Kuo SM, Zhou M. Virtual sensing techniques and their applications. In: 2009 international conference on networking. Sensing and Control; 2009. p. 31–6. https://doi.org/10.1109/ICNSC.2009.4919241.

[7] Lourens E, Papadimitriou C, Gillijns S, Reynders E, De Roeck G, Lombaert G. Joint input-response estimation for structural systems based on reduced-order models and vibration data from a limited number of sensors. Mech Syst Signal Process 2012;29:310–27. https://doi.org/10.1016/j.ymssp.2012.01.011.

[8] Kullaa J. Virtual sensing of structural vibrations using dynamic substructuring, Mechanical Systems and Signal Processing 79 (2016). 2015. p. 203–24. https://doi.org/10.1016/j.ymssp.2016.02.045. http://www.sciencedirect.com/science/article/pii/S0888327016000960. special Issue from ICEDyn.

[9] Pedersen MW, Andersen EK, Ulriksen MD, Damkilde L. Examination of modal expansion and kalman filtering techniques for vibration estimation. In: 9th ECCOMAS thematic conference on smart structures and materials; 2019. p. 1515–26.

[10] Tarpø M, Nabuco B, Georgakis C, Brincker R. Expansion of experimental mode shape from operational modal analysis and virtual sensing for fatigue analysis using the modal expansion method. Int J Fatig 2020;130:105280. https://doi.org/10.1016/j.ijfatigue.2019.105280. http://www.sciencedirect.com/science/article/pii/S0142112319303846.

[11] Skafte A, Kristoffersen J, Vestermark J, Tygesen UT, Brincker R. Experimental study of strain prediction on wave induced structures using modal decomposition and quasi static ritz vectors. Eng Struct 2017;136:261–76. https://doi.org/10.1016/j.engstruct.2017.01.014. http://www.sciencedirect.com/science/article/pii/S0141029617300378.

[12] Iliopoulos A, Weijtjens W, Van Hemelrijck D, Devriendt C. Fatigue assessment of offshore wind turbines on monopile foundations using multi-band modal expansion. Wind Energy 2017;20(8):1463–79. https://doi.org/10.1002/we.2104. https://onlinelibrary.wiley.com/doi/abs/10.1002/we.2104.

[13] Maes K, Iliopoulos A, Weijtjens W, Devriendt C, Lombaert G. Dynamic strain estimation for fatigue assessment of an offshore monopile wind turbine using filtering and modal expansion algorithms. Mech Syst Signal Process 2016;76–77:592–611. https://doi.org/10.1016/j.ymssp.2016.01.004. http://www.sciencedirect.com/science/article/pii/S0888327016000066.

[14] Henkel M, Häfele J, Weijtjens W, Devriendt C, Gebhardt C, Rolfes R. Strain estimation for offshore wind turbines with jacket substructures using dual-band modal expansion. Mar Struct 2020;71:102731. https://doi.org/10.1016/j.marstruc.2020.102731. http://www.sciencedirect.com/science/article/pii/S0951833920300253.

[15] Voormeeren SN, van der Valk PLC, Nortier BP, Molenaar D-P, Rixen DJ. Accurate and efficient modeling of complex offshore wind turbine support structures using augmented superelements. Wind Energy 2014;17(7):1035–54. https://doi.org/10.1002/we.1617.

[16] D. Rixen, Generalized mode acceleration methods and modal truncation augmentation. doi:10.2514/6.2001-1300.

[17] Nielsen MB, Jensen JF, Augustyn D, Pedersen RR. Efficient response recovery procedures for detailed design of jacket foundations. In: Insights and innovations in structural engineering, mechanics and computation. first ed., vol. 1. United Kingdom: Taylor & Francis; 2016. p. 2060–5. https://doi.org/10.1201/9781315641645-341.

[18] Chang P, Heins C, Guohao L, Ding S. Seismic study of curved bridges using the Rayleigh-ritz method. Comput Struct 1985;21(6):1095–104. https://doi.org/10.1016/0045-7949(85)90164-6.

[19] Xia H, Humar JL. Frequency dependent ritz vectors. Earthq Eng Struct Dynam 1992;21(3):215–31. https://doi.org/10.1002/eqe.4290210303.

[20] Warburton GB. Response using the Rayleigh-ritz method. Earthq Eng Struct Dynam 1979;7(4):327–34. https://doi.org/10.1002/eqe.4290070404.

[21] Skjoldan PF, Hansen MH. Implicit floquet analysis of wind turbines using tangent matrices of a non-linear aeroelastic code. Wind Energy 2012;15(2):275–87. https://doi.org/10.1002/we.467.

[22] Hansen MH. Aeroelastic instability problems for wind turbines. Wind Energy 2007;10(6):551–77. https://doi.org/10.1002/we.242.

[23] Caughey TK. Classical normal modes in damped linear dynamic systems. J Appl Mech 1960;27(2):269–71. https://doi.org/10.1115/1.3643949.

[24] O'Callahan J, Avitabile P, Riemer R. System equivalent reduction expansion process (serep). In: The proceedings of the 7th international modal Analysis conference (IMAC); 1989.

[25] Brincker R, Skafte A, López-Aenlle M, Sestieri A, D'Ambrogio W, Canteli A. A local correspondence principle for mode shapes in structural dynamics. Mech Syst Signal Process 2014;45(1):91–104. https://doi.org/10.1016/j.ymssp.2013.10.025. http://www.sciencedirect.com/science/article/pii/S0888327013005669.

[26] Arnold R, Citerley R, Chargin M, Galant D. Application of ritz vectors for dynamic analysis of large structures. Comput Struct 1985;21(3):461–7. https://doi.org/10.1016/0045-7949(85)90123-3. http://www.sciencedirect.com/science/article/pii/0045794985901233.

[27] Fenton JD. A fifth order Stokes theory for steady waves. J Waterw Port, Coast Ocean Eng 1985;111(2):216–34. https://doi.org/10.1061/(ASCE)0733-950X(1985)111:2(216).

[28] DNVGL-RP-C205. Environmental conditions and environmental loads. DNV GL; 2010. Tech. rep.

[29] DNVGL-ST-0126. Support structures for wind turbines. DNV GL; 2016. Tech. rep.

[30] API-RP-2A. Recommended practice for planning, designing and constructing fixed offshore platforms. American Petroleum Institute; 2014. Tech. rep.

[31] Ramboll. ROSAP - Ramboll offshore structural Analysis package. Ramboll; 2018. Tech. rep., version 53.

[32] Ramboll. LACflex- aeroelastic simulation tool. Ramboll; 2018. Tech. rep.

[33] Craig RR, Bampton MCC. Coupling of substructures for dynamic analyses. AIAA J 1968;6(7):1313–9. https://doi.org/10.2514/3.4741. https://doi.org/10.2514/3.4741.

[34] Liu M, Gorman D. Formulation of Rayleigh damping and its extensions. Comput Struct 1995;57(2):277–85. https://doi.org/10.1016/0045-7949(94)00611-6. http://www.sciencedirect.com/science/article/pii/0045794994006116.

[35] Nielsen MB, Jensen JF, Harper C, Knudsen LS, Pedersen RR. State-of-the-art framework for design of offshore wind jacket foundations. Steel Construct. 2019;12(3):209–14. https://doi.org/10.1002/stco.201900016. https://onlinelibrary.wiley.com/doi/abs/10.1002/stco.201900016.

[36] IEC-61400-1:2019. Wind energy generation systems - Part 1: design requirements. International Electrotechnical Commission; 2019. Tech. rep.

[37] Isherwood R. Technical note: a revised parameterisation of the jonswap spectrum. Appl Ocean Res 1987;9(1):47–50. https://doi.org/10.1016/0141-1187(87)90030-7. http://www.sciencedirect.com/science/article/pii/0141118787900307.

[38] Avitabile P, Pingle P. Prediction of full field dynamic strain from limited sets of measured data. Shock Vib 2012;19(5):765–85. https://doi.org/10.3233/SAV-2012-0686.

[39] Popko W, Vorpahl F, Antonakas P. Investigation of local vibration phenomena of a jacket sub-structure caused by coupling with other components of an offshore wind turbine. In: The proceedings of the twenty-third (2013) international offshore and polar engineering conference, vol. 1; 2013. p. 491–8. https://www.onepetro.org/conference-paper/ISOPE-I-13-012.

[40] Andersen EK, Pedersen MW, Ulriksen MD, Damkilde L. Examination of sensor distribution schemes for vibration estimation. In: 9th ECCOMAS thematic conference on smart structures and materials; 2019. p. 1527–37.

[41] Kammer DC. Sensor placement for on-orbit modal identification and correlation of large space structures. J Guid Contr Dynam 1991;14(2):251–9. https://doi.org/10.2514/3.20635.

[42] Ren Z, Skjetne R, Jiang Z, Gao Z, Verma AS. Integrated gnss/imu hub motion estimator for offshore wind turbine blade installation. Mech Syst Signal Process 2019;123:222–43. https://doi.org/10.1016/j.ymssp.2019.01.008.

[43] Zhang Q, Zheng XY. Walsh transform and empirical mode decomposition applied to reconstruction of velocity and displacement from seismic acceleration measurement. Appl Sci 2020;10(10). https://doi.org/10.3390/app10103509.

[44] Plant WJ, Schuler DL. Remote sensing of the sea surface using one- and two-frequency microwave techniques. Radio Sci 1980;15(3):605–15. https://doi.org/10.1029/RS015i003p00605.

[45] Bishop CT, Donelan MA. Measuring waves with pressure transducers. Coast Eng 1987;11(4):309–28. https://doi.org/10.1016/0378-3839(87)90031-7.

[46] Weijtens W, Noppe N, Verbelen T, Iliopoulos A, Devriendt C. Offshore wind turbine foundation monitoring, extrapolating fatigue measurements from fleet leaders to the entire wind farm. J Phys Conf 2016;753:092018. https://doi.org/10.1088/1742-6596/753/9/092018.

[47] Aggarwal A, Pákozdi C, Bihs H, Myrhaug D, Alagan Chella M. Free surface reconstruction for phase accurate irregular wave generation. J Mar Sci Eng 2018;6(3). https://doi.org/10.3390/jmse6030105. URL https://www.mdpi.com/2077-1312/6/3/105.

[48] Liu J, Guo A. Nonlinear method for real-time wave force reconstruction on a cylinder by using measured wave elevation. Coast. Eng. Proc. 2020 structures.6doi: 10.9753/icce.v36v.structures.6.

Paper C

Paper C

On the influence of environmental and operational variability on modal parameters of offshore wind support structures

Dawid Augustyn[a,b,*], Nicolai Cosack[c], Martin D. Ulriksen[d]

[a]*Department of the Built Environment, Aalborg University, Denmark*
[b]*Ramboll Energy, Esbjerg, Denmark*
[c]*Ramboll Energy, Hamburg, Germany*
[d]*Department of Energy Technology, Aalborg University, Denmark*

Abstract

The present paper explores the effect of environmental and operational variability (EOV) on the modal parameters of offshore wind structures. A non-linear numerical model of a representative offshore wind turbine supported by a jacket substructure is established and analyzed under the exposure of EOV. In particular, the study investigates time-periodic effects, non-classical aerodynamic damping, and operational variability imposed by the turbine controller. The modal parameters of different operational states are computed using linearized, time-periodic system formulations, and the variability in the modal parameters is discussed. The results illustrate the variation of the extracted modal parameters, which is found to be governed by two main sources; namely, 1) controller variability and 2) interaction of system modes. The former explains the variation in modes that are highly affected by modifications of the controller parameters. The latter explains the variation in the modes that become closely spaced and hence prone to mutual interaction.

Keywords: wind turbines, jacket substructures, environmental and operational variability, modal parameters, mode interaction, time-periodic systems, Coleman transformation

1. Introduction

Modal parameters, i.e., eigenfrequencies, damping ratios, and mode shapes, compose vital input to a multitude of offshore wind applications. The modal parameters are used extensively in, i.a., structural health monitoring [1, 2, 3], model updating [4, 5, 6], fatigue monitoring [7, 8, 9], and control [10, 11, 12], which, obviously, calls for sufficiently accurate and precise estimates of these parameters. However, obtaining such estimates is not a trivial task, as offshore wind turbines are subjected to environmental and operational variability (EOV) [13, 14, 15] due to varying wind speed. EOV results in, i.a., variation of the control system's parameters, e.g., the pitch angle and angular velocity of the rotor. Consequently, the stiffness and damping of offshore wind turbine systems are time-variant, yielding time-variant modal parameters as observed in numerous studies [16, 14, 17, 18].

In many practical applications, such as those presented in [19, 20, 21, 22, 6], the modal parameters are inferred through stochastic system identification with a linear, time-invariant model (LTI) due to the conceptual simplicity and ease of numerical implementation. Consequently, the time-variant nature of the modal parameters is neglected, which inherently introduces errors that may or may not be of significance in the subsequent applications. In the research community, this has, at least to some degree, been addressed by quantifying the variation in modal parameters for onshore wind turbines [23, 24, 25]; considering eigenfrequency and damping variability [26, 27, 28] and mode shape

---

*Corresponding author. Ramboll Energy, Esbjerg, Denmark
Email address:* dawa@ramboll.com (Dawid Augustyn)

variability related to subparts of onshore wind turbines, e.g., blades [29], drive-trains [30], and tripod substructures [14]. However, to the authors' knowledge, there exist no studies that investigate the effect of EOV on the modal parameters of offshore-based substructures. This particular application differs from the onshore-based configuration due to the inherent coupling between the wind turbines and their support structures [31].

In the present paper, we investigate the effect of different sources of EOV on the modal parameters of offshore wind turbine substructures. Specifically, the study is conducted on the basis of a non-linear numerical model of a representative offshore wind turbine with a jacket foundation. The model is exposed to EOV representative for the power production and idling states of the wind turbine, and we confine the study such that the environmental variability is assumed governed by the wind speed, while the operational variability is assumed governed by the controller. The novel contributions of this paper include the investigation of 1) rotor-induced time-periodic effects, 2) complex mode shapes stemming from non-classical aerodynamic damping, and 3) environmental variability due to varying wind speed and operational variability due to varying pitch angle.

The remainder of the paper is organized as follows. In Sec. 2, we present some governing wind turbine dynamics and outline the theory related to the numerical modelling of an integrated wind turbine, including linearization of the system. Sec. 3 establishes the numerical model, and Sec. 4 presents the appertaining EOV results. The results are discussed in Sec. 5, and the paper closes with some concluding remarks in Sec. 6.

2. Theory

The dynamics of wind turbine systems are non-linear and time-variant. The non-linear effects stem from the controller, multi-physics interaction, geometric non-linearity, and soil non-linearity, while the time-variant effects are related to the controller, structural degradation (corrosion, scour), and environmental variability.

Consider a non-linear and time-variant system with input $\mathbf{f}_s(t) \in \mathbb{R}^r$ and output $\mathbf{y}_s(t) \in \mathbb{R}^m$ at time $t \in \mathbb{R}_{\geq 0}$. Then, the system's dynamics can be described by the first-order state-space formulation

$$\dot{\mathbf{x}}_s(t) = \mathcal{G}\left(\mathbf{x}_s(t), \mathbf{f}_s(t), t\right), \tag{1a}$$

$$\mathbf{y}_s(t) = \mathcal{H}\left(\mathbf{x}_s(t), \mathbf{f}_s(t), t\right), \tag{1b}$$

where $\mathbf{x}_s(t) \in \mathbb{R}^n$ is the state vector with $n \in 2\mathbb{N}$, while $\mathcal{G} : \mathbb{R}^n \times \mathbb{R}^r \times \mathbb{R}_{\geq 0} \to \mathbb{R}^n$ and $\mathcal{H} : \mathbb{R}^n \times \mathbb{R}^r \times \mathbb{R}_{\geq 0} \to \mathbb{R}^m$ are non-linear and time-variant functions. Generally, different types of stable and non-stable solutions exist for system (1), but in the present study we confine the solution set to the nominal, periodic steady-state trajectory defined by $(\mathbf{x}_0(t), \mathbf{f}_0(t), \mathbf{y}_0(t))$. It is assumed in the subsequent developments that $\mathcal{G}$ and $\mathcal{H}$ are well-behaved in a neighborhood of $(\mathbf{x}_0(t), \mathbf{f}_0(t), \mathbf{y}_0(t))$.

2.1. Linear, time-periodic system

The non-linear system (1) can be linearized from the outset of a small perturbation from the trajectory $(\mathbf{x}_0(t), \mathbf{f}_0(t), \mathbf{y}_0(t))$. Define the perturbations $\mathbf{x}(t) \triangleq \mathbf{x}_s(t) - \mathbf{x}_0(t)$, $\mathbf{f}(t) \triangleq \mathbf{f}_s(t) - \mathbf{f}_0(t)$, and $\mathbf{y}(t) \triangleq \mathbf{y}_s(t) - \mathbf{y}_0(t)$, then system (1) can be written as

$$\dot{\mathbf{x}}_0(t) + \dot{\mathbf{x}}(t) = \mathcal{G}\left(\mathbf{x}_0(t) + \mathbf{x}(t), \mathbf{f}_0(t) + \mathbf{f}(t), t\right), \tag{2a}$$

$$\mathbf{y}_0(t) + \mathbf{y}(t) = \mathcal{H}\left(\mathbf{x}_0(t) + \mathbf{x}(t), \mathbf{f}_0(t) + \mathbf{f}(t), t\right). \tag{2b}$$

Taylor series expansions of (2) about the nominal trajectory yield

$$\dot{\mathbf{x}}(t) = \left[\frac{\partial \mathcal{G}}{\partial \mathbf{x}}\right]_0 \mathbf{x}(t) + \left[\frac{\partial \mathcal{G}}{\partial \mathbf{f}}\right]_0 \mathbf{f}(t) + \text{H.O.T.}, \tag{3a}$$

$$\mathbf{y}(t) = \left[\frac{\partial \mathcal{H}}{\partial \mathbf{x}}\right]_0 \mathbf{x}(t) + \left[\frac{\partial \mathcal{H}}{\partial \mathbf{f}}\right]_0 \mathbf{f}(t) + \text{H.O.T.}, \tag{3b}$$

where $[\partial \mathcal{G}/\partial \mathbf{x}]_0 \in \mathbb{R}^{n \times n}$, $[\partial \mathcal{G}/\partial \mathbf{f}]_0 \in \mathbb{R}^{n \times r}$, $[\partial \mathcal{H}/\partial \mathbf{x}]_0 \in \mathbb{R}^{m \times n}$, and $[\partial \mathcal{H}/\partial \mathbf{f}]_0 \in \mathbb{R}^{m \times r}$ are the Jacobians evaluated at the nominal trajectory.

With $\mathbf{A}(t) \triangleq [\partial\mathcal{G}/\partial\mathbf{x}]_0$, $\mathbf{B}(t) \triangleq [\partial\mathcal{G}/\partial\mathbf{f}]_0$, $\mathbf{P}(t) \triangleq [\partial\mathcal{H}/\partial\mathbf{x}]_0$, and $\mathbf{Q}(t) \triangleq [\partial\mathcal{H}/\partial\mathbf{f}]_0$, the Jacobian linearization of (3) is

$$\dot{\mathbf{x}}(t) = \mathbf{A}(t)\mathbf{x}(t) + \mathbf{B}(t)\mathbf{f}(t), \tag{4a}$$

$$\mathbf{y}(t) = \mathbf{P}(t)\mathbf{x}(t) + \mathbf{Q}(t)\mathbf{f}(t), \tag{4b}$$

which constitutes a linear, time-periodic approximation of the non-linear, time-variant system (1). In system (4), $\mathbf{A}(t)$ is the state matrix, $\mathbf{B}(t)$ the input matrix, $\mathbf{P}(t)$ the output matrix, and $\mathbf{Q}(t)$ the transmission matrix.

2.2. Linear, time-invariant system

Formulation (4) contains time-variant quantities, which render both the eigenvectors and eigenvalues time-variant. Assuming the wind turbine rotor is isotropic, the Coleman transformation [32] can be applied to approximate system (4) by a linear, time-invariant system with state and output matrices [29, 33]

$$\mathbf{A}_C = \mathbf{T}^{-1}(t)\mathbf{A}(t)\mathbf{T}(t) - \mathbf{T}^{-1}(t)\dot{\mathbf{T}}(t), \tag{5a}$$

$$\mathbf{P}_C = \mathbf{T}^{-1}(t)\mathbf{P}(t)\mathbf{T}(t), \tag{5b}$$

where $\mathbf{T}(t)$ and $\dot{\mathbf{T}}(t)$ are the Coleman transformation matrix and its time-derivative, respectively. For a three-bladed isotropic rotor and with $c_i \triangleq \cos\psi_i$ and $s_i \triangleq \sin\psi_i$, where $\psi_i = \Omega t + 2\pi(j-1)/3$ is the mean azimuth angle of blade number $j = 1, 2, 3$, Ω is rotation speed, $\mathbf{T}(t)$ is given by [29]

$$\mathbf{T}(t) = \begin{bmatrix} \mathbf{I}_{N_b} & \mathbf{I}_{N_b}c_1 & \mathbf{I}_{N_b}s_1 & \mathbf{0} \\ \mathbf{I}_{N_b} & \mathbf{I}_{N_b}c_2 & \mathbf{I}_{N_b}s_2 & \mathbf{0} \\ \mathbf{I}_{N_b} & \mathbf{I}_{N_b}c_3 & \mathbf{I}_{N_b}s_3 & \mathbf{0} \\ \mathbf{0} & \mathbf{0} & \mathbf{0} & \mathbf{I}_{N_s} \end{bmatrix}, \tag{6}$$

where $\mathbf{I}_{N_b}$ and $\mathbf{I}_{N_s}$ are identity matrices of sizes N_b and N_s, with N_b and N_s being the number of blade and inertial degrees-of-freedom (dof). The dof are defined in Sec. 3. The framework can easily be extended to include anisotropic rotors by replacing the Coleman transformation with the Lyapunov-Floquet transformation [34].

2.2.1. Structural properties

The state matrix, $\mathbf{A}_C$, of the LTI system (5) is given by

$$\mathbf{A}_C = \begin{bmatrix} \mathbf{0} & \mathbf{I} \\ -\mathbf{M}^{-1}\mathbf{K} & -\mathbf{M}^{-1}\mathbf{C} \end{bmatrix}, \tag{7}$$

where $\mathbf{M}, \mathbf{C}, \mathbf{K} \in \mathbb{R}^{\frac{n}{2} \times \frac{n}{2}}$ are the mass, damping, and stiffness matrices. The stiffness matrix includes the centrifugal and aerodynamic terms in addition to the elastic structural stiffness terms. The damping matrix includes gyroscopic and aerodynamic terms in addition to the structural damping terms. The structural damping is assumed classically distributed, i.e., $\mathbf{M}^{-1}\mathbf{K}$ and $\mathbf{M}^{-1}\mathbf{C}$ commute, as specified by Caughey [35]. The centrifugal and gyroscopic terms originate from the revolving part of the turbine and the aeroelastic interaction.

2.2.2. Modal properties

The modal parameters of the LTI system with the state and output matrices given in (5) are computed by solving the eigenvalue problem

$$(\mathbf{A}_C - \lambda_i \mathbf{I})\boldsymbol{\phi}_i = 0, \tag{8}$$

where $\lambda_i \in \mathbb{C}$ and $\boldsymbol{\phi}_i \in \mathbb{C}^n$ are the eigenvalue and eigenvector of the ith mode. The mode shape, $\boldsymbol{\mu}_i$ can be derived as $\boldsymbol{\mu}_i = \mathbf{P}_C\boldsymbol{\phi}_i$. Assuming classical damping, the undamped eigenfrequency, ω_i, and the associated modal damping ratio, ζ_i, are computed as $\omega_i = |\lambda_i|$ and $\zeta_i = -\Re(\lambda_i)/|\lambda_i|$, where $\Re$ denotes the real part.

2.2.3. Closely spaced modes

The EOV may render a subset of modes closely spaced. In this instance, the assumption of classical damping is invalid and the notion of damping ratios does no longer strictly apply. Furthermore, closely spaced modes have *wobbly* eigenvectors and mode shapes, which can be appreciated from the developments by Nelson [36], who has shown that the mode shape sensitivities of two closely spaced modes with respect to a structural parameter is inversely proportional to the difference between the corresponding eigenvalues. From this outset, it is evident that when two eigenvalues approach each other, the sensitivities of the two mode shapes approach infinity. In the limit, the associated mode shapes do, as noted by Brincker [37], no longer exist as individual vectors. Instead, they span a subspace from which linear combinations can be extracted.

3. Numerical model

The numerical analysis in Sec. 4 is based on the wind turbine and jacket substructure seen in Fig. 1a. The turbine has three blades and the rated power of the turbine is 5 MW. The tower, which has a height of 75 m, comprises cylindrical thin-walled elements and connecting flanges. The jacket has four legs and three brace bays, totalling a height of 50 m, and the jacket substructure is connected with the soil through 30 m grouted piles. The soil is characterised as clay, and the water depth is approximately 40 m.

a) Integrated turbine and substructure model   b) Substructure dof $\mathbf{u}_F$ c) Blades rotating dof $\mathbf{u}_B$

Blade 1

Flap-wise u_1^j

Edge-wise u_1^j
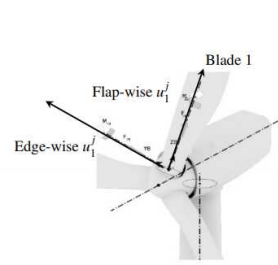
d) Turbine fixed coordinate dof $\mathbf{u}_N$

Yaw angle θ_y

Rotor azimuth angle θ_r Tilt angle θ_t
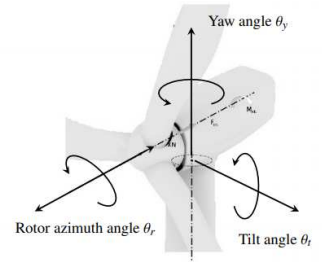
Figure 1: Wind turbine and substructure model.

The numerical model consists of $\frac{n}{2} = 51$ dof, which are gathered in

$$\mathbf{u} = \begin{bmatrix} \mathbf{u}_N^T & \mathbf{u}_B^T & \mathbf{u}_F^T \end{bmatrix}^T \in \mathbb{R}^{\frac{n}{2}}, \tag{9}$$

4

a) Mode 2 at 0.31 Hz   b) Mode 3 at 0.31 Hz   c) Mode 4 at 0.54 Hz   d) Mode 11 at 1.64 Hz   e) Mode 13 at 1.68 Hz
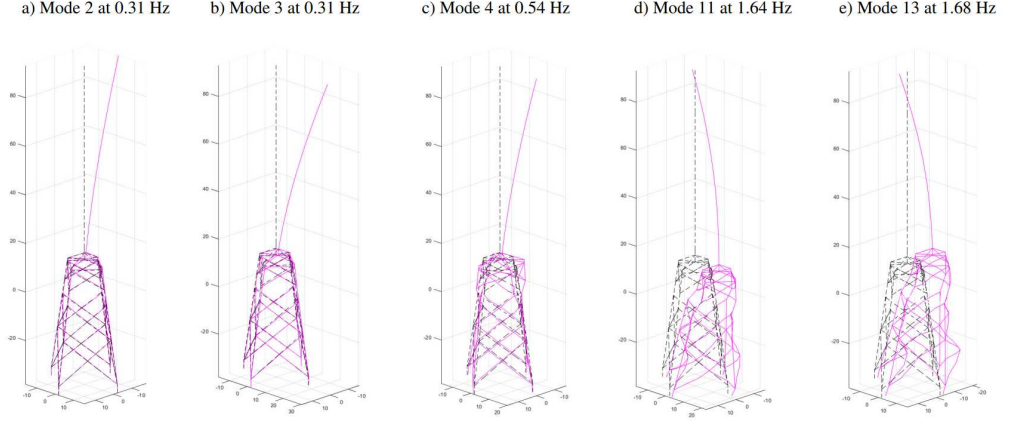
Figure 2: Integrated wind turbine mode shapes of the reference model (blades and piles not shown). The first global bending modes (2,3), the first torsional mode (4), and the second bending modes (11,13) are plotted. Black dashed line - undeformed structure, magenta full line - deformed structure.

where $\mathbf{u}_N$ contains the nacelle dof, $\mathbf{u}_B$ the blade dof, and $\mathbf{u}_F$ the foundation substructure (including the tower) dof, see Fig. 1 for dof overview. The nacelle model is discretized with the $n_R = 3$ dof

$$\mathbf{u}_N = \begin{bmatrix} \theta_y & \theta_t & \theta_r \end{bmatrix}^T \in \mathbb{R}^{n_R}, \tag{10}$$

which are defined in the inertial (time-invariant) frame of reference with θ_y being the yaw angle, θ_t the tilt angle, and θ_r the rotor azimuth angle. Each blade is modally truncated to $n_b = 4$ modes, hence totalling $n_B = 3n_b = 12$ blade dof for the three-bladed rotor. Each blade is represented by two flap-wise and two edge-wise modes. The blade dof, as indicated in Fig. 1c, are defined in the rotating (time-variant) frame of reference,

$$\mathbf{u}_B = \begin{bmatrix} u_1^1 & u_2^1 & u_3^1 & \cdots & u_1^j & u_2^j & u_3^j \end{bmatrix}^T \in \mathbb{R}^{n_B}, \tag{11}$$

where u_i^j indicates the jth dof of ith blade. The substructure, which is condensed into a superelement, is discretized with $n_F = 36$ dof,

$$\mathbf{u}_F = \begin{bmatrix} \mathbf{u}_G^T & \mathbf{u}_{CB}^T \end{bmatrix}^T \in \mathbb{R}^{n_F}, \tag{12}$$

which are split between $n_G = 6$ dof related to the static, Guyan partition of the superelement [38] and $n_{CB} = 30$ dof related to the dynamic, Craig-Bampton partition of the superelement [39]. The superelement reduction of the substructure is described in Subsec. 3.3.

3.1. Substructure model

The jacket substructure is modelled using Ramboll's software ROSAP (Ramboll Offshore Structural Analysis Package), version 53 [40]. ROSAP is a general-purpose finite element package intended for both static and dynamic analysis of offshore structures. The jacket substructure is modelled with 3D Bernoulli-Euler beam elements [41], including the added mass of the surrounding water. The soil-structure interaction is modelled using a Winkler model [41] in which the steel pile elements are additionally supported by linearized springs representing the surrounding soil. The soil springs are linearized according to the API method [42]. The stiffness of the joints are modified to account for additional flexibility of the tubular joints according to Buitrago et al. [43]. The transition piece (TP) is modelled in a simplistic manner by a representative 3D Bernoulli-Euler beam system. The tower is modelled using 3D Bernoulli-Euler beam elements, including added masses representing internal secondary steel elements and flanges.
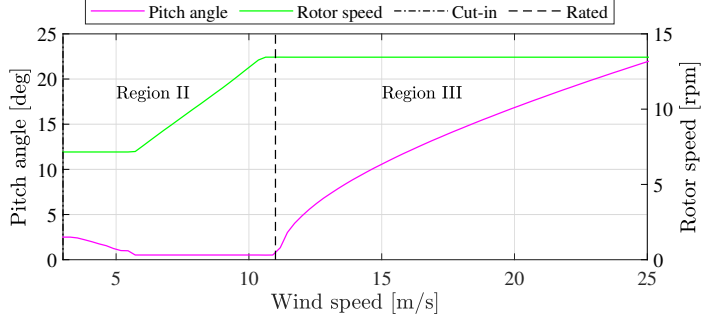
Figure 3: Controller properties: the pitch angle and rotor speed as functions of the wind speed.

3.2. Turbine model

The wind turbine model (rotor and nacelle) is implemented in LACflex aeroelastic code [44]. The blades are represented by few modal-based dof, while the nacelle is represented by physical (rotational) dof. The foundation is represented by a Craig-Bampton superelement [39]. The cone angle (out of rotor plane deflection of the blades) and tilt angle (angle between a shaft axis and the horizontal plane) are set to zero, and pitch and mass imbalances are omitted to comply with the isotropic rotor assumption in the Coleman transformation, as elaborated in Sec. 2.2.

A collective pitch control system (all blades controlled in the same way) is implemented. The control system is designed to balance the power output and wind forces acting on the structure. The target pitch angle and rotor speed as functions of the wind speed are presented in Fig. 3. As the power production state is considered in this study, region I (below the cut-in speed) is neglected. In region II, between the cut-in wind speed, U_{ci} = 3 m/s, and the rated wind speed, U_r = 11 m/s, the rotor speed increases up to the rated rotor speed while the pitch angle is constant. In region III, above the rated wind speed and below the cut-out wind speed, U_{co} = 25 m/s, the rotor speed is stabilized to keep the power output constant and minimize the wind force action. This is achieved by increasing the pitch angle from 0 deg to 28 deg. Above the cut-out wind speed, the turbine is assumed to switch into the parked state where production of power is stopped and the wind forces are significantly reduced compared to the production state.

3.3. Substructure and turbine coupling

The substructure is reduced into a Craig-Bampton superelement with 36 dof of which 6 are attachment dof and 30 internal dynamic dof. The substructure superelement is coupled to the turbine model in the LACflex aeroelastic code in accordance with the coupling procedures documented by Seidel [45] and Hald et al. [46]. The superelement representation of the substructure is linear, thereby neglecting any non-linear effects in the foundation, e.g., soil-structure interaction, wave-structure interaction, and plasticity.

4. Analysis and results

In this section, the analysis and key results illustrating the effect of EOV on modal parameters of offshore wind support structures are presented. In the analysis, the eigenvalue problem for different model configurations is solved. The corresponding modal parameters, in the form of eigenfrequencies, mode shapes, and damping ratios[1], are extracted and analyzed. The mode shapes are compared by use of the modal assurance criterion (MAC) [47] computed on the basis of the subset of dof related to the jacket substructure.

In the analysis, we consider the following three model configurations:

---

[1]Recall that a damping ratio is a notion for classically damped modes. In the present analysis, both classically and non-classically damped modes are explored. In the non-classical setting, we merely use the "damping ratios" as qualitative measures to indicate the relative influence of damping in each mode and to investigate the environmental variability of damping.
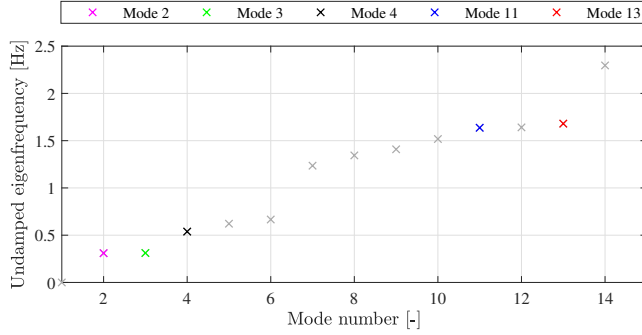
Figure 4: Undamped eigenfrequencies of the reference model.

- Reference (R) – the undamped eigenvalue problem is solved for a standing-still turbine, i.e., without taking into account any rotating part of the turbine nor damping. The pitch angle of the blades is 0 deg.

- Undamped operational (UO) – linearized state-space matrices of the system are extracted for constant wind speed and steady-state conditions; the Coleman transformation is performed to include the effect of varying azimuth; the undamped eigenvalue problem is solved—by setting $\mathbf{C} = 0$ in (8)—and the corresponding modal parameters are extracted.

- Damped operational (DO) – the same procedure as for the UO configuration is followed, with the only exception being that the damping contribution is included, i.e., the damped eigenvalue problem (8) is solved.

The section is organized as follows. The reference (R) results are established in Subsec. 4.1. Subsequently, the effect of EOV is investigated, with Subsec. 4.2 addressing the operational variability and 4.3 the environmental variability. To confine the study, we focus on four sources of EOV, namely, the azimuth angle, pitch angle, damping, and wind speed.

4.1. Reference results

The modal parameters of the turbine in the reference configuration (R) are considered in this subsection. An azimuth angle of 0 deg is used, corresponding to the first blade pointing upward. The effect of the aeroelastic coupling, rotating machinery, and damping is neglected.

The selected reference modal parameters (mode shapes and undamped frequencies) are presented in Fig. 2 and 4. The first fifteen undamped eigenfrequencies of the reference system are presented in Fig. 4. The modes of interest are indicated with color, while the remaining modes are indicated in grey. The first bending modes, Fig. 2a (mode 2) and Fig. 2b (mode 3), are dominated by the bending stiffness of the tower with a maximum deflection at the tower top. The eigenfrequency of these modes is approximately 0.31 Hz for both directions. The torsional mode (mode 4), which has an eigenfrequency of 0.54 Hz, is driven by rotation around the vertical axis of the tower. The rotation can clearly be noticed in the top part of the jacket substructure in Fig. 2c. Note, also, the lateral displacements of the tower, which stem from the rotor-nacelle-assembly eccentricity with respect to the tower axis. The second bending modes, Fig. 2d (mode 11) and Fig. 2e (mode 13), are dominated by lateral displacement around the TP level. The eigenfrequencies in the fore-aft and side-side directions are 1.68 Hz and 1.64 Hz, respectively. Note that the order of the fore-aft and side-side is shifted compared to the first bending mode set.

The correlation between mode shapes 2-15 of the turbine is presented in the auto-MAC matrix in Fig. 5. The matrix presents MAC values of different modes from the reference model, MAC(i, j), where i and j are modes of the reference model, with mode 1 (rigid body rotor revolution) being neglected. The diagonal values of the matrix are equal to one, as they indicate the correlation of each mode with itself, while the off-diagonal values measure the linear correlation between mode shapes of different modes. The first bending modes (mode 2 and 3) are close to orthogonal
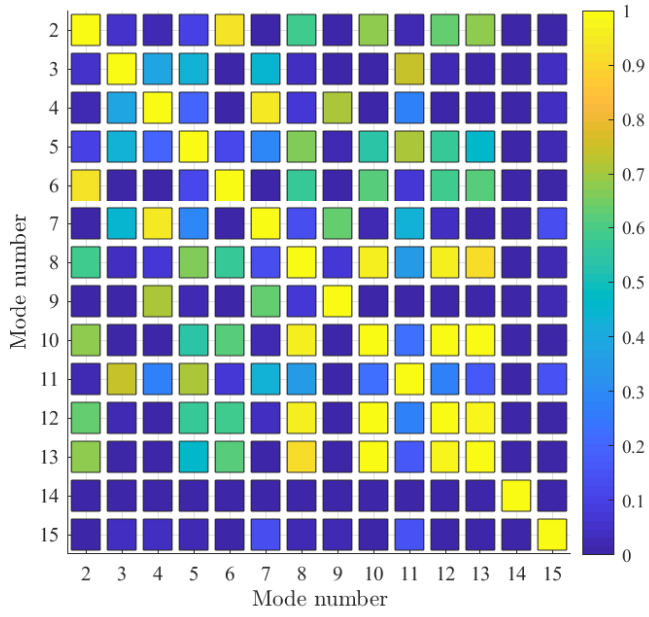
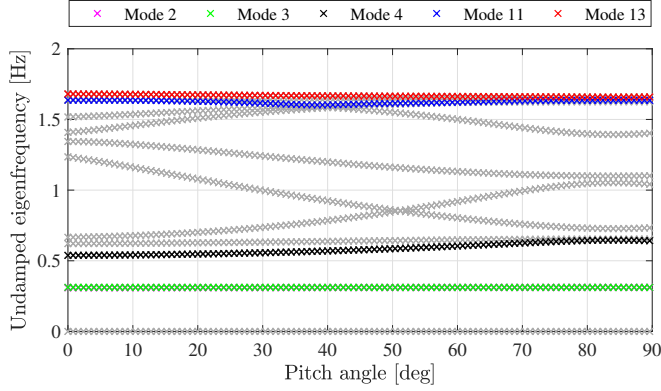Figure 5: Auto-MAC of the reference model.

Figure 6: Eigenfrequencies as functions of the pitch angle for the reference model.

to each other, hence, as expected, the MAC value is low, MAC(2, 3) = 0.05. Some linear correlation between the first bending modes and intermediate modes can be observed, e.g., MAC(2, 6) = 0.93, and between the first and second bending modes, e.g, MAC(2, 13)=0.69. The first torsional mode shape (mode 4) exhibits some correlation with the blade-dominated mode shapes (modes 7 and 9) with, e.g., MAC(4, 7)=0.95. The mode shapes dominated by the lateral deflection around the TP elevation, namely, the second bending modes (mode 11 and 13), are highly correlated with a number of other modes. In particular, the fore-aft second bending mode (mode 13) exhibits high correlation with modes 12 and 10, MAC(13, 12) = 0.98 and MAC(13, 10) = 0.98. The high correlation between different mode shapes indicates interaction between the turbine and the substructure.

4.2. Operational variability

The operational variability is investigated by extracting modal parameters for the system with varying azimuth angle and pitch angle. Subsec. 4.2.1 addresses the influence of the azimuth angle variation, while Subsec. 4.2.1 focuses on the pitch angle.

4.2.1. Pitch angle

Undamped modal parameters of the parked turbine are computed for varying pitch angle. The pitch angle, α, varies in the range $\alpha \in [0, 90]$ deg, where $\alpha = 90$ deg indicates that the blades are in a parked position. The results are compared to the reference solution, where $\alpha = 0$ deg is considered. Effectively, the only modification between the reference model and the model considered here is the pitch angle of the blades.

The undamped eigenfrequencies as functions of the pitch angle are presented in Fig. 6, where the selected modes of interest are indicated with a color, while the remainder of the first fifteen modes are indicated in grey. The first and second bending modes (modes 2, 3, 11, and 13) exhibit low variation in frequency (<2%). The torsional mode (mode 4) is affected more severely by the pitch angle variation, with a 20% increase in eigenfrequency for $\alpha > 30$ deg. This is caused by the increased in-plane rotor bending stiffness of the blades for higher pitch angle. Specifically, the difference between the in-plane rotor blade stiffness changes from flap-wise ($\alpha = 0$ deg) to edge-wise ($\alpha = 90$ deg). The latter stiffness is always higher, hence the increase in the torsional frequency.

The MAC values between the reference model with $\alpha = 0$ and $\alpha \in [0, 90]$ deg are shown in Fig. 7. The MAC values for the first bending modes (mode 2 and 3) vary significantly, with a monotonic decrease as the pitch angle increases. This indicates that the orthogonality of the mode shapes is significantly reduced for large pitch angles. The MAC value for the torsional mode shape (mode 4) is generally high within the analyzed pitch angle range; except for values close to $\alpha = 84$ deg. For this specific pitch angle, the MAC is close to zero, which is due to the increased interaction with mode 5.
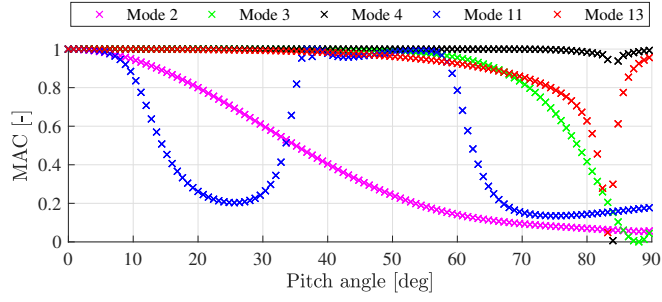
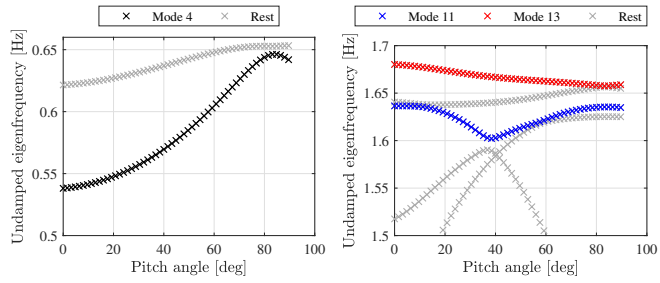Figure 7: MAC values as functions of the pitch angle.

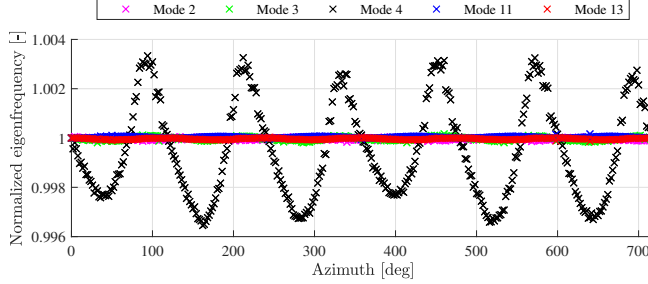Figure 8: Eigenfrequencies as functions of the pitch angle.

Figure 9: Normalized eigenfrequencies as functions of the azimuth angle.

To further investigate the noted interaction phenomenon, the eigenfrequencies of modes 4 and closely spaced mode (mode 5) are presented in the left subfigure of Fig. 8. Initially, for $\alpha = 0$ deg, the two modes are clearly separated with an eigenfrequency difference of 15% ($f_4 = 0.54$ Hz and $f_5 = 0.62$ Hz). The modes are, however, becoming closely spaced for $\alpha = 84$ deg, where the eigenfrequency difference is reduced to 1%. When two modes become closely spaced in terms of their eigenvalues, the mode shapes start to interact with each other and the physical notion of the individual mode shapes diminishes as elaborated in Subsec. 2.2.3. Instead, it is the subspace spanned by the mode shapes of the closely spaced modes that bears physical significance, and in the case with our two closely spaced modes, we can always make them comply with the orthogonality conditions that prevail for classically damped modes. In order to convey the effect of the mode interaction phenomenon, we have, however, chosen not to do this, and therefore the extensive MAC value drop is observed at $\alpha = 0.84$. For $\alpha > 0.84$, the frequencies become further separated and, as a result, the MAC value for mode 4 returns to a value close to 1. The same phenomenon can be observed for the second bending mode in the fore-aft direction (mode 13), which becomes closely spaced with mode 12 at $\alpha = 84$ deg, as indicated in Fig. 8. Consequently, the MAC value for mode 13 is reduced substantially around that pitch angle. Qualitatively, the same phenomenon elucidates the large variation in the MAC value for mode 11. As indicated in Fig. 8, mode 11 interacts with mode 12 for $\alpha < 20$ deg and modes 9 and 10 for $\alpha > 35$ deg.

4.2.2. Azimuth angle

To investigate the variation in modal parameters due to changes in the azimuth angle, modal parameters of the damped operational (DO) model are extracted for two full rotor revolutions; with 180 realizations per rotor revolution such that a total of 360 sets of modal parameters are attained. The model is operating in steady state at the rated wind speed, $U_r = 11$ m/s and the modal parameters are linearized for this wind speed.

The variations in damped eigenfrequencies due to a varying azimuth angle are presented in Fig. 9. The eigenfrequencies are normalized to those obtained for an azimuth angle of $\theta_r = 0$ deg, which corresponds to the first blade pointing upwards. The variations in eigenfrequencies are due to the varying mass distribution of the rotor (the position of the blades). The varying mass results in 0.7% eigenfrequency variation in the torsional mode (mode 4) and negligible eigenfrequency variation ($< 0.03\%$) in the remaining modes. The eigenfrequency variation of the torsional mode exhibits 120 deg periodicity, which is caused by the fact that the analyzed turbine has an isotropic rotor with three blades. Moreover, the minimum eigenfrequency within each 120 deg period is observed for the azimuth angle $(a - 1)120 + 45$ deg, where $a \in \mathbb{N}$, while the maximum eigenfrequency is observed for $(a - 1)120 + 90$ deg. These distinct peaks are located in positions where the mass distribution of the rotor leads to extreme moments of inertia.

The MAC values between the damped mode shapes attained for $\theta_r \in [0, 720]$ and those for $\theta_r = 0$ deg are computed. The MAC variations due to a varying azimuth angle are presented in Fig. 10. Evidently, the MAC variations are negligible for the considered modes, albeit the 120 deg periodicity observed for the eigenfrequencies is also present here.

The results presented in 9 and Fig. 10 imply that the variation of the modal parameters due to varying azimuth angle is negligible when the turbine operates in steady state at the rated wind speed. Similar steady-state analyses at other wind speeds show the same qualitative tendency.
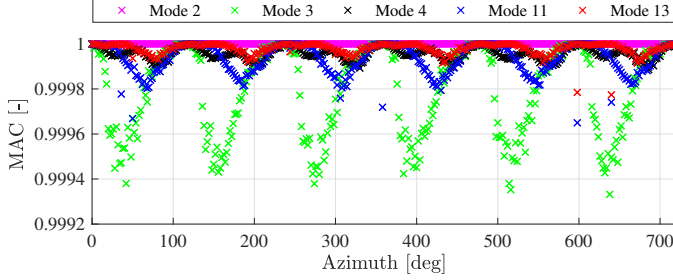
11

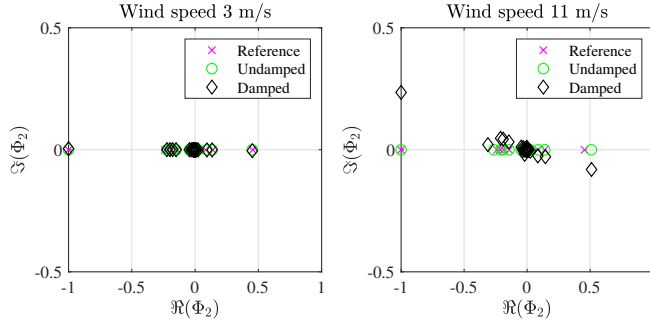Figure 10: MAC values as functions of the azimuth angle.

Figure 11: Mode shape (mode 2) extracted for 3 models (reference - magenta, undamped operational - green, and damped operational - black); linearized for a) 3 m/s and b) 11 m/s.

4.3. Environmental variability

The study of the impact of environmental variability on the modal parameters is confined to address the effect of two specific parameters, namely, damping and wind speed.

4.3.1. Damping

Given the damping is classical [35], the damped mode shapes are real-valued and identical to those associated with the undamped system. The damping in any wind turbine system is non-classically distributed due to, e.g., the aerodynamic contribution. Thus, the mode shapes are complex-valued. However, in many applications, the effect of damping is neglected and undamped mode shapes are used. In this subsection, damped and undamped mode shapes are compared to illustrate the influence of damping on the mode shapes. In addition, the variability of the damping ratios due to varying wind speeds is presented and discussed.

The mode shape of mode 2 derived based on the three model configurations (R, UO, and DO) is presented in Fig. 11. Among the three models, only the last one, DO, contains contributions from the non-classically distributed damping. Consequently, the first two mode shapes are real-valued, while the last one is complex-valued, with the imaginary part representing the non-classical damping contribution. The effect of damping is illustrated for two wind speeds, $U_i = 3$ and $U_i = 11$ m/s. The real part of the mode shape is comparable for the three models for both wind speeds. For low wind speeds, the imaginary part of the DO model is negligible. Hence, the three mode shapes are comparable. However, when the wind speed increases, the aerodynamic damping increases as well, and therefore a profound difference between the mode shapes is observed.

The damping ratios of the selected modes as functions of the wind speed are presented in Fig. 12. As can be seen, the ratios are positive, hence implying that the considered modes are stable. The largest damping ratio variation
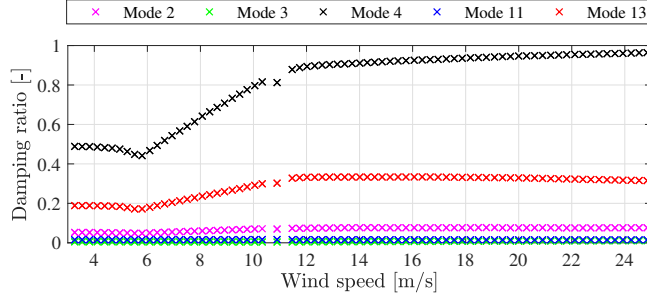
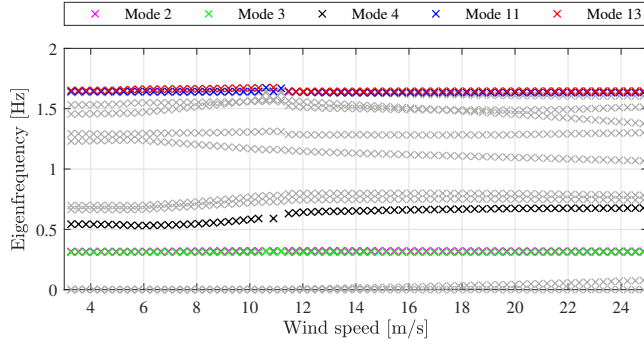Figure 12: Damping ratios as functions of the wind speed.

Figure 13: Eigenfrequencies as functions of the wind speed.

is observed for modes 4, 13, and, to some degree, mode 2. The damping ratio of mode 4 is almost doubled in the wind speed range $U_i \in [6, 11]$ m/s. This can be attributed to the controller variability, which in this range doubles the rotor speed, see Fig. 3. The damping ratios of the remaining modes (modes 3 and 11) are almost insensitive to the wind speed variation. Based on the presented results, which are, qualitatively, in line with those obtained in similar numerical studies [33], it can be concluded that modes 4 and 13 have the largest potential to be influenced by damping variation.

4.3.2. Wind speed

As the variability of the damping ratios has been explored in the previous subsection, we focus on eigenfrequencies and mode shapes. The modal parameters of the DO model are extracted for a range of wind speeds, $U_i \in [3, 25]$ m/s, where the turbine operates in the power production state.

The damped eigenfrequencies as functions of the wind speed are presented in Fig. 13. The largest eigenfrequency variation is observed for mode 4, where the eigenfrequency is increased by 30%. Qualitatively, the variation pattern for this mode is highly correlated with the variation of the controller parameters; specifically the rotor speed. The remaining modes (modes 2, 3, 11, and 13) exhibit low variability, with eigenfrequency variations of less than 5%.

The MAC values are computed between the mode shapes derived for the cut-in wind speed, $U_{ci} = 3$ m/s, and the mode shapes extracted at varying wind speeds, U_i. The MAC values as functions of the wind speed are presented in Fig. 14. The results are discriminated into three groups of modes with regards to the extent and pattern of the MAC value variation; 1) negligible variation, 2) variation correlated with damping variability, and 3) remaining. 1) the MAC
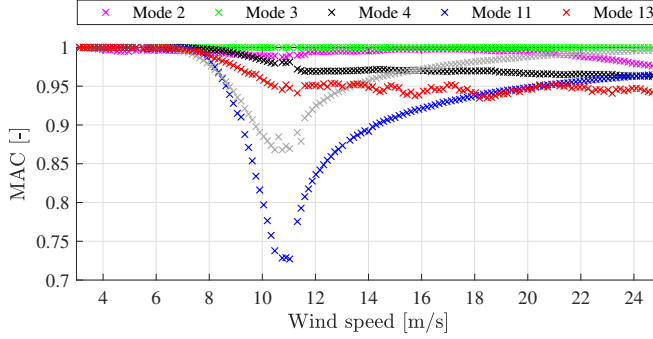
Figure 14: MAC values as functions of the wind speed.

value variations for modes 2 and 3 are deemed negligible (minimum MAC = 0.98) and are therefore not discussed further. 2) the MAC value variations for modes 4 and 13 are, qualitatively, highly correlated with the damping variation for these modes, see Fig. 12. For $U_i < 8$ m/s, the MAC values are close to 1, followed by a reduction of the MAC values in the range $U_i \in [8, 11]$ m/s. For $U_i > 11$ m/s, the MAC values are stabilized around 0.95. 3) the MAC values for mode 11 exhibit the largest variation with a non-monotonic pattern. Overall, high MAC values are observed with a global minimum of 0.72 reached for $U_i = 11$ m/s. For $U > 11$ m/s, a monotonic increase is observed up to the MAC=0.95 for $U = 25$ m/s. The result groups 2 and 3 are further discussed in Sec. 5.

5. Discussion

This section offers a discussion of the results presented in Subsecs. 4.3.1 and 4.3.2. Particular attention is assigned to potential sources of the observed MAC variations; 1) damping variation as discussed in Subsec. 5.1 and 2) mode interaction as discussed in Subsec. 5.2.

5.1. On damping-driven variation

As discussed in Sec. 4.3.1, the damping ratios vary with respect to the wind speed. The source of this variation is attributed to the controller variability; specifically the rotor speed. The mode shape variability results presented in Subsec. 4.3.2 indicate a high correlation with the damping variation. Specifically, the result group 2 (modes 4 and 13) are, qualitatively, highly correlated with the damping variation (Fig. 12). Moreover, these specific modes are highly damped, with damping ratios of an order of magnitude larger than the remaining considered modes. Based on these two characteristics, the variations of modes 4 and 13 are denoted damping-driven. On a general note, the modes whose damping ratios exhibit the above-mentioned characteristics—namely, 1) a significant damping contribution (measured by the damping ratio relative to the other modes) and 2) a large damping ratio variation as a function of the wind speed—are expected to be driven by variation in the damping.

5.2. On interaction-driven variation

The variation in mode shapes for the result group 3 (mode 11), presented in Subsec. 4.3.2, cannot be explained by the damping variation. To further investigate the mode shape variation, the eigenfrequency variations for mode 11 and the neighboring modes are presented in Fig. 15. Two modes in close (frequency-wise) proximity of mode 11 are identified, namely, mode 12 and 13. For an undamped case, it is enough to inspect frequency proximity, as confirmed for the pitch angle variation analysis in Subsec. 4.2.1. However, in the damped case, where the eigenvalues are complex, both frequency proximity and damping proximity are required to trigger interaction. Therefore, in Fig. 16, the damping ratios of modes 11 and 12 are presented. The damping ratios of modes 11 and 12 are, just like the eigenfrequencies, in close proximity. Consequently, these modes are prone to interaction. Note that the damping ratio
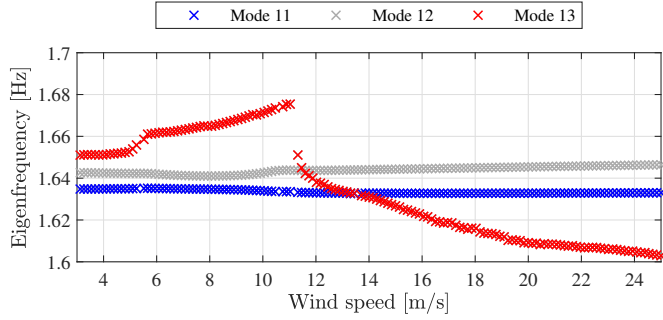
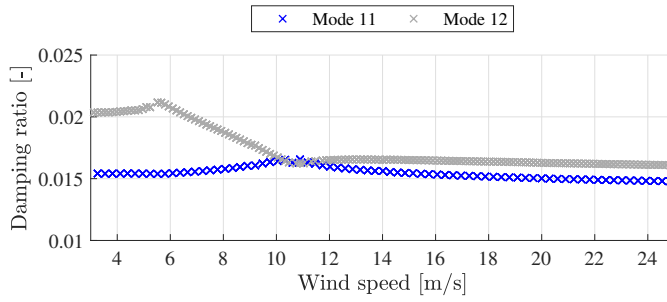Figure 15: Eigenfrequencies of modes 11-13 as functions of the wind speed.

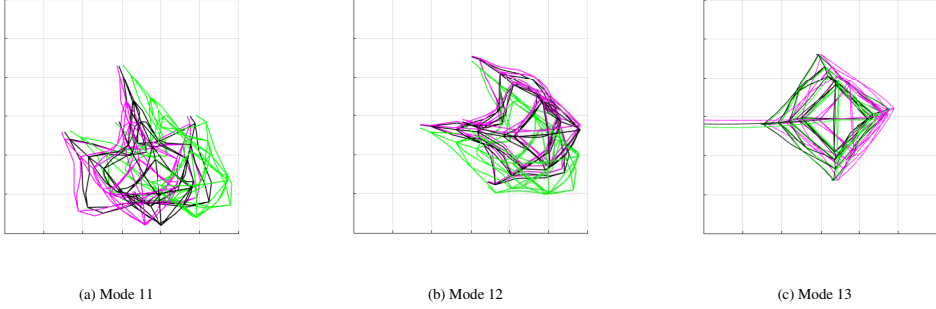Figure 16: Damping ratios of modes 11 and 12 as functions of the wind speed.

(a) Mode 11   (b) Mode 12   (c) Mode 13

Figure 17: Mode shapes plotted for varying wind speeds; magenta - U = 3 m/s, green - U = 11 m/s, and black - U = 25 m/s.

of mode 13 (Fig. 12) is an order of magnitude larger than that of modes 11 and 12, hence interaction with mode 13 is unlikely.

The MAC variations for modes 11 and 12 are, as presented in Fig. 14 (mode 12 indicated with grey color), positively correlated, with a global minimum at U_i = 11 m/s where the damping ratios commute. To confirm that modes 11 and 12 indeed do interact with each other, the mode shapes for three wind speeds, $U_i \in \{3, 11, 25\}$ m/s, are plotted in Fig. 17. Modes 11 and 12 geometrically represent the second bending mode in the side-side and fore-aft directions, see Figs. 17a and 17b. For U_i = 3 and U_i = 25 m/s (high MAC values), the mode shapes are close to orthogonal, as expected due to the turbine's symmetry. However, for U_i = 11 m/s (minimum MAC), the modes geometrically synchronize (the linear correlation of the modes increases), which confirms the mode interaction. Consequently, the variation in mode 11 is denoted interaction-driven. In the general case, the modes which are prone to the interaction-driven variation are the ones that belong to a subset of closely spaced modes.

6. Conclusions

This paper investigates the influence of EOV on the modal parameters of offshore wind support structures. A non-linear and time-variant numerical model of a representative wind turbine supported by a jacket substructure is exposed to different sources of EOV. The operational variability is studied by varying the turbine's azimuth and pitch angles, while the environmental variability is investigated by studying the effect of damping and varying wind speeds. The analysis results demonstrate that the modal parameters vary due to both the environmental and operational variability. The modal parameters related to the first torsional and the second bending modes appear as the most sensitive to the emulated EOV. In general, two main sources of modal parameter variation have been identified; 1) the controller variability and 2) the mode interaction. The former explains the variation in modes that are highly affected by modifications of the controller parameters, while the latter explains the variation in the modes that become closely spaced and hence prone to mutual interaction.

7. Acknowledgements

References

[1] C. R. Farrar, K. Worden, Structural health monitoring: A machine learning perspective, 1st Edition, John Wiley & Sons, 2013.

[2] J. F. Skov, M. D. Ulriksen, K. A. Dickow, P. H. Kirkegaard, L. Damkilde, On structural health monitoring of wind turbine blades, in: Damage Assessment of Structures X, Vol. 569 of Key Engineering Materials, Trans Tech Publications Ltd, 2013, pp. 628–635. `doi:10.4028/www.scientific.net/KEM.569-570.628`.

[3] M. Martinez-Luengo, A. Kolios, L. Wang, Structural health monitoring of offshore wind turbines: A review through the statistical pattern recognition paradigm, Renewable and Sustainable Energy Reviews 64 (2016) 91–105. `doi:https://doi.org/10.1016/j.rser.2016.05.085`.

[4] J. Mottershead, M. Link, M. Friswell, The sensitivity method in finite element model updating: A tutorial, Mechanical Systems and Signal Processing 25 (7) (2011) 2275–2296. `doi:https://doi.org/10.1016/j.ymssp.2010.10.012`.

[5] M. Bruns, B. Hofmeister, D. Pache, R. Rolfes, Finite element model updating of a wind turbine blade—a comparative study, in: H. Rodrigues, J. Herskovits, C. Mota Soares, A. Araújo, J. Guedes, J. Folgado, F. Moleiro, J. F. A. Madeira (Eds.), EngOpt 2018 Proceedings of the 6th International Conference on Engineering Optimization, Springer International Publishing, 2019, pp. 569–580.

[6] D. Augustyn, U. Smolka, U. T. Tygesen, M. D. Ulriksen, J. D. Sørensen, Data-driven model updating of an offshore wind jacket substructure, Applied Ocean Research 104 (2020) 102366. `doi:https://doi.org/10.1016/j.apor.2020.102366`.

[7] X.-S. Si, W. Wang, C.-H. Hu, D.-H. Zhou, Remaining useful life estimation – a review on the statistical data driven approaches, European Journal of Operational Research 213 (1) (2011) 1–14. `doi:http://dx.doi.org/10.1016/j.ejor.2010.11.018`.

[8] C. Devriendt, F. Magalhaes, W. Weijtjens, G. De Sitter, A. Cunha, P. Guillaume, Automatic identification of the modal parameters of an offshore wind turbine using state-of-the-art operational modal analysis techniques, in: Proceedings of the 5th International Operational Modal Analysis Conference, IOMAC 2013, 2013.

[9] A. Iliopoulos, W. Weijtjens, D. Van Hemelrijck, C. Devriendt, Fatigue assessment of offshore wind turbines on monopile foundations using multi-band modal expansion, Wind Energy 20 (8) (2017) 1463–1479. `doi:10.1002/we.2104`.

[10] A. Preumont, K. Seto, Active Control of Structures, John Wiley & Sons, Ltd, 2008. `doi:10.1002/9780470715703`.

[11] A. Staino, B. Basu, S. R. K. Nielsen, Actuator control of edgewise vibrations in wind turbine blades, Journal of Sound and Vibration 331 (6) (2012) 1233–1256. `doi:10.1016/j.jsv.2011.11.003`.

[12] C. Han, R. Nagamune, Position control of an offshore wind turbine with a semi-submersible floating platform using the aerodynamic force, in: 2016 IEEE Canadian Conference on Electrical and Computer Engineering (CCECE), IEEE, 2016, pp. 1–4.

[13] H. Sohn, Effects of environmental and operational variability on structural health monitoring, Philosophical Transactions of the Royal Society A: Mathematical, Physical and Engineering Sciences 365 (1851) (2007) 539–560. `doi:10.1098/rsta.2006.1935`.

[14] W.-H. Hu, S. Thöns, R. G. Rohrmann, S. Said, W. Rücker, Vibration-based structural health monitoring of a wind turbine system part ii: Environmental/operational effects on dynamic properties, Engineering Structures 89 (2015) 273–290. `doi:https://doi.org/10.1016/j.engstruct.2014.12.035`.

[15] T. Bull, M. D. Ulriksen, D. Tcherniak, The effect of environmental and operational variabilities on damage detection in wind turbine blades, in: Proceedings of the 9th European Workshop on Structural Health Monitoring (EWSHM), Manchester, UK, 2018.

[16] I. Antoniadou, N. Dervilis, E. Papatheou, A. E. Maguire, K. Worden, Aspects of structural health and condition monitoring of offshore wind turbines, Philosophical Transactions of the Royal Society A: Mathematical, Physical and Engineering Sciences 373 (2035) (2015) 20140075. `doi:10.1098/rsta.2014.0075`.

[17] M. W. Häckell, R. Rolfes, Monitoring a 5mw offshore wind energy converter—condition parameters and triangulation based extraction of modal parameters, Mechanical Systems and Signal Processing 40 (1) (2013) 322 – 343. `doi:https://doi.org/10.1016/j.ymssp.2013.04.004`.

[18] C. Devriendt, F. Magalhaes, W. Weijtjens, G. Sitter, A. Cunha, P. Guillaume, Structural health monitoring of offshore wind turbines using automated operational modal analysis, Structural Health Monitoring 13 (6) (2014) 644–659. `doi:10.1177/1475921714556568`.

[19] O. S. Salawu, Detection of structural damage through changes in frequency: a review, Engineering Structures 19 (9) (1997) 718–723. `doi:https://doi.org/10.1016/S0141-0296(96)00149-6`.

[20] K. Worden, G. Manson, D. Allman, An experimental appraisal of the strain energy damage location method, in: Damage Assessment of Structures IV, Vol. 204 of Key Engineering Materials, Trans Tech Publications Ltd, 2001, pp. 35–46. `doi:10.4028/www.scientific.net/KEM.204-205.35`.

[21] M. D. Ulriksen, Damage localization for structural health monitoring: An exploration of three new vibration-based schemes, Doctoral dissertation, Aalborg University (2018).

[22] M. Henkel, J. Häfele, W. Weijtjens, C. Devriendt, C. Gebhardt, R. Rolfes, Strain estimation for offshore wind turbines with jacket substructures using dual-band modal expansion, Marine Structures 71 (2020) 102731. `doi:https://doi.org/10.1016/j.marstruc.2020.102731`.

[23] D. Tcherniak, S. Chauhan, M. H. Hansen, Applicability limits of operational modal analysis to operational wind turbines, in: T. Proulx (Ed.), Structural Dynamics and Renewable Energy, Volume 1, Springer New York, New York, NY, 2011, pp. 317–327.

[24] M. S. Allen, M. W. Sracic, S. Chauhan, M. H. Hansen, Output-only modal analysis of linear time-periodic systems with application to wind turbine simulation data, Mechanical Systems and Signal Processing 25 (4) (2011) 1174–1191. `doi:10.1016/j.ymssp.2010.12.018`.

[25] L. Mevel, I. Gueguen, D. Tcherniak, Lptv subspace analysis of wind turbines data, in: Proceedings of the 7th European Workshop on Structural Health Monitoring, 2014.

[26] M. H. Hansen, Aeroelastic instability problems for wind turbines, Wind Energy 10 (6) (2007) 551–577. `doi:10.1002/we.242`.

[27] P. F. Skjoldan, M. H. Hansen, Implicit floquet analysis of wind turbines using tangent matrices of a non-linear aeroelastic code, Wind Energy 15 (2) (2012) 275–287. `doi:10.1002/we.467`.

[28] R. Riva, M. Spinelli, L. Sartori, S. Cacciola, A. Croce, Stability analysis of wind turbines with bend-twist coupled blades, Journal of Physics: Conference Series 1037 (2018) 062014. `doi:10.1088/1742-6596/1037/6/062014`.

[29] M. H. Hansen, Improved modal dynamics of wind turbines to avoid stall-induced vibrations, Wind Energy 6 (2) (2003) 179–195. `doi:10.1002/we.79`.

[30] M. El-Kafafy, C. Devriendt, P. Guillaume, J. Helsen, Automatic Tracking of the Modal Parameters of an Offshore Wind Turbine Drivetrain System, Energies 10 (4) (2017) 1–15.

[31] W. Popko, F. Vorpahl, P. Antonakas, Investigation of local vibration phenomena of a jacket sub-structure caused by coupling with other components of an offshore wind turbine, in: The Proceedings of The Twenty-third (2013) International Offshore and Polar Engineering Conference, Vol. 1, 2013, pp. 491–498.

[32] R.P. Coleman, Theory of Self-Excited Mechanical Oscillations of Hinged Rotor Blades, NACA Technical Report No. WR-L-308, Tech. rep. (1943).

[33] G. Bir, Multi-Blade Coordinate Transformation and its Application to Wind Turbine Analysis, 2008. `doi:10.2514/6.2008-1300`.

[34] G. Floquet, Sur les équations différentielles linéaires à coefficients périodiques, Annales scientifiques de l'École Normale Supérieure 2e série, 12 (1883) 47–88. `doi:10.24033/asens.220`.

[35] T. K. Caughey, Classical normal modes in damped linear dynamic systems, Journal of Applied Mechanics 27 (2) (1960) 269–271. `doi:10.1115/1.3643949`.

[36] R. B. Nelson, Simplified calculation of eigenvector derivatives, AIAA Journal 14 (9) (1976) 1201–1205. `doi:10.2514/3.7211`.

[37] R. Brincker, M. Lopez-Aenlle, Mode shape sensitivity of two closely spaced eigenvalues, Journal of Sound and Vibration 334 (2015) 377 – 387. `doi:https://doi.org/10.1016/j.jsv.2014.08.015`.

[38] R. J. Guyan, Reduction of stiffness and mass matrices, AIAA Journal 3 (2) (1965) 380–380. `doi:10.2514/3.2874`.

[39] R. R. Craig, M. C. C. Bampton, Coupling of substructures for dynamic analyses., AIAA Journal 6 (7) (1968) 1313–1319. `doi:10.2514/3.4741`.

[40] Ramboll, ROSAP - Ramboll Offshore Structural Analysis Package, version 53, Tech. rep., Ramboll (2018).

[41] R. D. Cook, D. S. Malkus, M. E. Plesha, R. J. Witt, Concepts and Applications of Finite Element Analysis, 4th Edition, John Wiley & Sons, 2001.

[42] API-RP-2A, Recommended Practice for Planning, Designing and Constructing Fixed Offshore Platforms, Tech. rep., American Petroleum Institute (2014).

[43] J. Buitrago, B. Healy, T. Chang, Local joint flexibility of tubular joints, in: Proceedings of OMAE 1993, 1993.

[44] Ramboll, LACflex- aeroelastic simulation tool, Tech. rep., Ramboll (2018).

[45] M. Seidel, M. von Mutius, P. Rix, D. Stuedel, Integrated analysis of wind and wave loading for complex support structures of offshore wind turbines, in: Proceedings of the Offshore Wind Conference, 2005.

[46] T. Hald, M. Høgedal, Implementation of a finite element foundation module in flex5 using craig-bampton substructuring, in: Proceedings of the Offshore Wind Conference, 2005.

[47] A. J. Allemang, The modal assurance criterion (mac): Twenty years of use and abuse, Sound Vib (2003) 14–21.

Paper C. Paper C

Paper D

Paper D

Article

Reliability Updating of Offshore Wind Substructures by Use of Digital Twin Information

Dawid Augustyn [1,2,*] **, Martin D. Ulriksen** [3] **and John D. Sørensen** [1]

1   Department of the Built Environment, Aalborg University, 9220 Aalborg, Denmark; jdas@build.aau.dk
2   Ramboll Energy, 6700 Esbjerg, Denmark
3   Department of Energy Technology, Aalborg University, 6700 Esbjerg, Denmark; mdu@et.aau.dk
*   Correspondence: dja@build.aau.dk

Abstract: This paper presents a probabilistic framework for updating the structural reliability of offshore wind turbine substructures based on digital twin information. In particular, the information obtained from digital twins is used to quantify and update the uncertainties associated with the structural dynamics and load modeling parameters in fatigue damage accumulation. The updated uncertainties are included in a probabilistic model for fatigue damage accumulation used to update the structural reliability. The updated reliability can be used as input to optimize decision models for operation and maintenance of existing structures and design of new structures. The framework is exemplified based on two numerical case studies with a representative offshore wind turbine and information acquired from previously established digital twins. In this context, the effect of updating soil stiffness and wave loading, which constitute two highly uncertain and sensitive parameters, is investigated. It is found that updating the soil stiffness significantly affects the reliability of the joints close to the mudline, while updating the wave loading significantly affects the reliability of the joints localized in the splash zone. The increased uncertainty related to virtual sensing, which is employed to update wave loading, reduces structural reliability.

Keywords: offshore wind substructures; reliability updating; probabilistic fatigue assessment; digital twins; uncertainty quantification

1. Introduction

The offshore wind industry has experienced significant growth over the last decade [1]. As a result, the number of offshore wind turbines operating in Europe has reached 5402 in 2020 [2], with much more planned to be installed worldwide in the close future [3]. The typical lifetime of an offshore wind turbine ranges between 20 and 25 years, which means that over the coming years a large number of these structures reach their intended lifetime, and operators will have to take actions regarding their assets. Potential actions, denoted as decision models, can be to decommission, re-power, perform inspections, or extend lifetime. An optimal decision depends on what specific business model the operator pursues, but, regardless of the business aspect, an accurate and precise estimation of the structural reliability is key in making such a decision [4].

A digital twin-defined as a digital replica of a physical asset [5,6]-can help us to assess the structural integrity of existing structures more accurately and precisely compared to predictions from generic design practices because consistent and updated information of the structure is available. This has been successfully demonstrated in the oil and gas industry [7,8], in aerospace engineering [9], and in the offshore wind industry as well [10]. In fact, a number of wind standardization committees, including Det Norske Veritas (DNV) [11,12], International Electrotechnical Commission (IEC) [13], and Federal Maritime and Hydrographic Agency (BSH) [14], are working on design recommendations on how to use measurement data and inspection information to optimize decision models for existing

wind turbines. Currently, a key missing aspect is how to use the improved structural models contained in digital twins to subsequently improve the decision models.

Although fully physics-based digital twins have not yet been applied to improve decision models for wind turbines, some publications already indicate how measurement data can be used to achieve such an improvement. Nielsen and Sørensen [15] applied dynamic Bayesian networks to calibrate a Markov deterioration model based on past inspection data of wind turbine blades. Ziegler and Muskulus [16] investigated the feasibility of lifetime extension for offshore wind monopile substructures, with particular focus on identifying important parameters to monitor during the operational phase of the turbines. Leser et al. [17] presented a general framework for fatigue damage estimation based on in situ measurements. Mai et al. [18] focused on prediction of the remaining useful lifetime of wind turbine support structure joints using met-ocean in situ data. Augustyn et al. [19] extended a conceptual framework for updating decision models based on information from a digital twin, initially proposed by Tygesen et al. [7], to be applied to offshore wind substructures. In the framework, a digital twin is established with an updated structural and load model, and subsequently the digital twin is used to quantify uncertainty and update the structural reliability.

In the present paper, we outline the framework by Augustyn et al. [19] beyond its conceptual level and propose a probabilistic method for updating the structural reliability of offshore wind turbine substructures based on new information obtained from digital twins. Depending on the information type available, various methods for updating reliability can be used [20]. If information on the structural integrity becomes available, for example, by an inspection of joints to identify potential cracks, risk-based inspection methods can be applied [21–24]. Even though the inspection planning methodology is matured and well-proven in industrial applications [25], its feasibility for the majority of offshore wind applications is questionable due to the profound inspection costs [26]. A more economically feasible alternative, in the form of condition-based monitoring, is typically investigated for offshore wind applications [27,28]. In this context, condition monitoring data can be applied to identify structural damage, and then the resulting integrity information can be employed for updating reliability [29]. Application studies have been presented for mechanical components in turbine [30] and wind turbine blades [4]. However, in these studies, the condition monitoring data merely provide structural integrity information at a global level-that is, if damage is present or not. In the present study, we aim at enhancing the spatial resolution of the integrity assessment and hereby provide information at a local (joint) level. Consequently, this paper proposes a framework where condition monitoring data are used to update structural models; these updated models are subsequently used to update structural reliability, including uncertainty stemming from the updating procedure.

The contribution of this paper consists of: (1) proposing a method on how the uncertainties related to the structural dynamics and load modeling in fatigue damage accumulation can be quantified and updated based on updated distribution functions of model parameters, which can be acquired with the aid of a digital twin. Subsequently, (2) we present a framework where the updated uncertainty is used to update the structural reliability based on a well-established probabilistic model [31,32]. Generally, the framework can be used for optimization of operation and maintenance of existing turbines and design of new structures. The framework is exemplified based on two numerical case studies, in which digital twins established in previous studies by the authors [33,34] are included.

The remainder of this paper is organized as follows. In Section 2, we outline the concept of structural reliability estimation and convey the motivation for the proposed structural reliability updating framework, which is presented in Section 3. The two following sections address the numerical case studies used to exemplify the framework for existing and new substructures; Section 4 describes the setup of the case studies and Section 5 presents the appertaining results. Finally, this paper closes with concluding remarks in Section 6.

2. Background and Problem Statement

A wind turbine consists of structural components, for which reliability analysis is performed using structural reliability theory [35], and electrical/mechanical components, for which classical reliability models can be used, with the main descriptor being the failure rate or the mean time between failure (MTBF). Regardless of the component type being addressed in the reliability analysis, a probabilistic model describing the component's integrity is required. The reliability of electrical/mechanical components is typically modeled by a Weibull model for the time to failure and the components are assumed to be statistically independent. Using, for example, failure tree analysis (FTA) and failure mode and effect analysis (FMEA), system reliability models can be established and the reliability update can be performed when new information becomes available [36–38]. In the present paper, jacket-type steel wind turbine substructures are considered, so structural reliability techniques are required to model loads, resistances, and model uncertainties and to account for the correlation between the components. The fatigue damage is often design driving for the structural components of offshore wind substructures, such as joints. In this instance, fatigue damage accumulation can be expressed in terms of probability of failure or, equivalently, by the reliability index [39].

Let $g(t)$ be the fatigue limit state at year $t \in \mathbb{N}$ for an offshore wind substructure; then [32,40],

$$g(t) = \Delta - \sum_{i=1}^{l} \sum_{j=1}^{z} \frac{N_{i,j} p_i t}{K \Delta s_{i,j}^{-m}} (X_d X_l X_s)^m, \tag{1}$$

where Δ is the fatigue resistance and the double summation expresses the accumulated fatigue damage. In particular, Δ is a stochastic variable representing the limit value of the accumulated fatigue damage estimated using, for example, SN curves, including the uncertainty related to application of Miner's rule for linear fatigue damage accumulation. In the expression for the fatigue damage, p_i is the yearly probability of occurrence for sea state i (including wind and wave parameters), $N_{i,j}$ is the number of cycles for the ith sea state and jth stress range $\Delta s_{i,j}$, and K and m are the parameters related to the SN curve, with m being the Wöhler exponent [41]. The uncertainties related to the SN curve approach are included by modeling K as a stochastic variable. X_d, X_l, and X_s are stochastic variables that model the uncertainties associated with the structural dynamics, load modeling and stress concentration.

If $g(t) \leq 0$, the limit state is exceeded and the structure fails, while $g(t) > 0$ implies that the structure is safe. The probability of fatigue failure in the time interval $t \in [0, T]$, $P_f(t) = P(g(t) \leq 0)$ can be estimated by first-order and second-order reliability methods [39] or, as is the case in this paper, by Monte Carlo methods [42]. The corresponding reliability index, β, can be computed as $\beta(t) = -\Phi^{-1}\left(P_f(t)\right)$, where Φ is the standard normal distribution function. The annual reliability index, $\Delta\beta$, can be calculated analogically assuming a reference period of one year.

We note that (1) X_d and X_l may be correlated, and, in this instance, they should be modeled by a joint probability density function with correlation coefficient ρ and (2) a linear formulation of the limit state equation can be readily generalized for a bi-linear formulation of the SN curve. The parameters in model (1) are elaborated in Section 2.1.

2.1. Uncertain Parameters and Their Modeling

The uncertainty modeling related to structural reliability due to fatigue damage is summarized in Figure 1. In the framework proposed in Section 3, we focus on updating stochastic variables related to structural dynamics and loading uncertainty, as schematically indicated by the dark blue boxes in Figure 1. The remaining part of the uncertainty (the light blue boxes in Figure 1) can be quantified based on experiments and data. This is not considered in the proposed framework, but a brief discussion is provided in the present subsection for the sake of completeness.
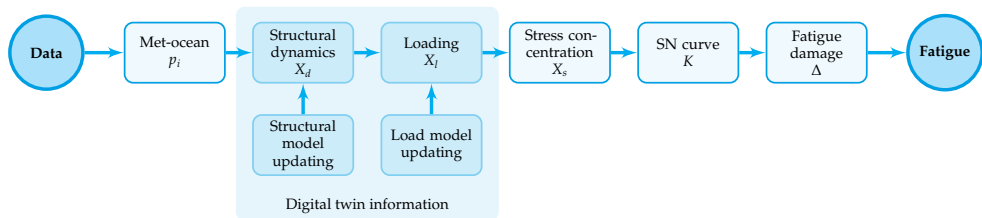
Figure 1. Stochastic variables modeling uncertainty in fatigue damage accumulation. The stochastic variables from the probabilistic model (1) are represented by separate boxes. The light blue boxes indicate stochastic variables estimated based on generic, design-based recommendations. The dark blue boxes indicate stochastic variables that can be quantified and updated based on new information from a digital twin.

2.1.1. Met-Ocean Model

The joint probability distributions of the wind-wave climate is discretized by a finite number of short-term sea state simulations including random wind and wave seeds to model a stochastic process [40]. Met-ocean uncertainty is included in (1) by the yearly probability of each sea state, denoted p_i. The met-ocean uncertainty can be quantified if long-term climate parameters are monitored [18,43].

2.1.2. Structural Dynamics

Estimating dynamic system properties is associated with uncertainties [44]. The uncertainties stem from environmental and operational variability, non-stationary sea states (fluctuating mean sea water level), time-variant structural conditions (corrosion, scour), output noise, and the formulation of the structural model, including modeling of highly uncertain parameters such as soil stiffness, joint stiffness and damping. We note that the output noise relates to the noise in the acceleration and/or strain signals, which is propagated through system identification procedures and results in uncertainty of the updated structural model parameters [44]. The structural dynamics uncertainty is included in (1) through the stochastic variable X_d.

2.1.3. Loading

Depending on the location of the wind turbine, the loading may include the following exogenous sources and their inherent uncertainties:

- Hydrodynamic loading-uncertainty related to calculating wave loads that stems from different wave theories (linear vs. non-linear), Morison's equation, stretching and mass and drag coefficients.
- Aerodynamic loading-uncertainty related to calculating wind loads that stems from wind turbulence, wake model, and shear coefficient.
- Ice loading-uncertainty related to calculating ice loads, for example, ice thickness, ice crushing strength and ice failure regime.
- Earthquake loading-uncertainty related to calculating earthquake loads, for example, earthquake acceleration profile, structural response, soil-structure integration, and force transfer.

If loading uncertainty is quantified based on information from digital twins, the main part of the uncertainty is related to obtaining the structural response due to external loading. This response is typically estimated based on virtual sensing methods, which are associated with uncertainties [34,45]. The loading uncertainty is included in (1) through the stochastic variable X_l.

2.1.4. Stress Concentration

Stress ranges in specific locations can be estimated based on simplified parametric equations, for example, Efthymiou [46] or detailed finite element (FE) models. The stress concentration uncertainty is included in (1) through the stochastic variable X_s. The stress

concentration uncertainty can be quantified if a detailed FE model is used to establish hot spot stresses [47] or if hot spot stresses are measured directly.

2.1.5. SN Curve

The uncertainty in parameter estimation from the SN curve approach [48] is included in (1) through the stochastic variable K and the deterministic parameter m. If a bi-linear SN curve is used, then stochastic variables are used to model the two branches of the SN curve. The SN curve uncertainty can be quantified if fatigue testing is performed [48].

2.1.6. Fatigue Damage

Uncertainties related to the accumulated fatigue damage model (Miner's rule [49]) and the crack propagation method (Paris–Erdogan [50] or fracture mechanics) is included in (1) by modeling the resistance, Δ, as a stochastic variable.

2.2. Current State-of-Practice for Reliability Updating

Design standards define a specific level of reliability that offshore wind substructures must fulfill, for example, a target annual reliability index of $\Delta\beta = 3.3$ in IEC 61400-1 [31,40]. Reliability levels indicated in standards assume a generic level of uncertainty representative for all types of substructures and locations. Because the uncertainty is assumed to cover a wide range of structures and locations, the resulting design is, in many cases, conservative. The level of conservatism can be quantified when new information specific to a particular structure becomes available. One way of obtaining such information is by means of digital twins, which can be used to quantify the uncertainty and subsequently update the structural reliability.

3. Structural Reliability Updating Framework

In this paper, we propose a probabilistic framework in which digital twin information is used to update the uncertainties associated with the fatigue damage accumulation, which are then used to update the structural reliability. In particular, we use the updated parameters from the established digital twins to quantify the model uncertainties of the structural dynamics, X_d, and load modeling, X_l. The updated uncertainties are quantified based on a forward propagation method, which allows quantifying separate uncertainty sources stemming from specific model parameters. Having updated the relevant uncertainty contributions from the updated model parameters, the reliability is updated based on the linear probabilistic limit state Equation (1). Finally, the updated reliability serves as a decision basis for a decision model update. A schematic illustration of the framework is seen in Figure 2, and steps one to six are described in Sections 3.1–3.6.
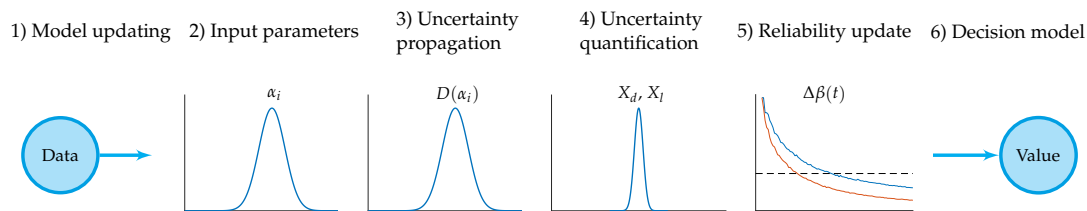

1) Model updating   2) Input parameters   3) Uncertainty propagation   4) Uncertainty quantification   5) Reliability update   6) Decision model

α_i $D(\alpha_i)$ X_d, X_l $\Delta\beta(t)$

Data   Value

Figure 2. Structural reliability updating framework based on information from a digital twin. Updated parameters from the digital twin are used to quantify uncertainty in fatigue damage accumulation. Subsequently, the structural reliability is updated.

3.1. Model Updating

It is assumed that an updated structural model (step one) is available, which can be obtained based on well-established model formulation and updating procedures [51].

3.2. Input Parameters

The distribution functions of the updated model parameters (available from step one) are used in step two as input for the uncertainty quantification procedure. The stochastic variables reflect both the aleatory and epistemic uncertainties, which constitute the updated X_d and X_l uncertainties.

3.3. Uncertainty Propagation

The effect of the updated model parameters on the fatigue damage accumulation is established by a Monte Carlo uncertainty propagation method [52], as indicated in step three in Figure 2. Based on the uncertainty in the input parameters (i.e., the distribution functions of the updated numerical model parameters), we obtain the distribution of fatigue damage, hence quantifying the uncertainties in fatigue damage due to the updated model parameters. The uncertainty quantification procedure is described next. The aim is to express the uncertainty as a stochastic variable multiplied to the fatigue stress ranges.

The uncertainty in fatigue damage accumulation due to an uncertain parameter, $\alpha_j \in \boldsymbol{\alpha}$, can be quantified by simulating n realizations from this parameter's distribution function and calculating the corresponding fatigue damage. When calculating fatigue damage, the remaining parameters are assumed to be deterministic. Moreover, the fatigue damage is calculated assuming one sea state parameter. In this way, the introduced uncertainty is solely governed by the variability of α_j, hence quantifying this parameter's contribution to the fatigue damage accumulation uncertainty. For example, a distribution function of updated soil stiffness implies structural dynamics uncertainty, while a distribution function of an updated inertia coefficient in Morison's equation implies loading uncertainty.

Among a number of uncertainty quantification methods [53], a Bayesian framework [54] is recommended by a number of standard committees, for example, IEC and Joint Committee on Structural Safety (JCSS), due to its sound theoretical basis and wide range of applicability. However, a main challenge in the Bayesian framework is the requirement of a prior distribution on the parameters to be quantified. In the context of offshore wind uncertainties, information on prior distributions is not available in the background documents for the above mentioned standards and committees. Consequently, in the proposed framework, we implemented a simplified method where we start with the uncertainty modeling consistent with the design standard of wind turbines [40], and subsequently we quantify the uncertain parameters already included in (1) using the maximum likelihood method.

Assuming the fatigue damage, modeled as a stochastic variable depending on the uncertain parameter α_j, is normally distributed, $D(\alpha_j) \sim \mathcal{N}\left(\mu_{D_j}, \sigma_{D_j}^2\right)$, the fatigue damage distribution (mean value μ_{D_j} and standard deviation σ_{D_j}) can be found through the maximum likelihood method, where the likelihood is defined as

$$L\left(\mu_{D_j}, \sigma_{D_j}\right) = \prod_{i=1}^{n} \frac{1}{\sqrt{2\pi}\sigma_{D_j}} \exp\left(-\frac{1}{2}\left(\frac{D_i - \mu_{D_j}}{\sigma_{D_j}}\right)^2\right), \tag{2}$$

with D_i being the fatigue damage associated with the ith realization of α_j computed based on the updated structural model contained in the digital twin.

The log-likelihood function becomes

$$\ln L\left(\mu_{D_j}, \sigma_{D_j}\right) = -n \ln\left(\sqrt{2\pi}\sigma_{D_j}\right) - \sum_{i=1}^{n} \frac{1}{2}\left(\frac{D_i - \mu_{D_j}}{\sigma_{D_j}}\right)^2, \tag{3}$$

and the optimal parameters are found to be

$$\underset{\mu_{D_j}, \sigma_{D_j}}{\text{argmax}} \ln L\left(\mu_{D_j}, \sigma_{D_j}\right). \tag{4}$$

3.4. Uncertainty Quantification

The procedure outlined in the previous subsection quantifies uncertainty in fatigue damage accumulation. However, the probabilistic model (1) requires uncertainty in stress ranges rather than in the fatigue damage. Therefore, it is now described how uncertainty in fatigue damage can be transformed into uncertainty in stress ranges, as indicated in step four in Figure 2.

The fatigue damage accumulation, D, is proportional to the stress ranges, Δs, according to $D \propto \Delta s^m$ (assuming a linear SN curve), from which it follows $\Delta s \propto D^{1/m}$. The stress range distribution parameters can be computed from Monte Carlo simulations. Alternatively, assuming the damage distribution function is normal, the stress range distribution's mean, $\mu_{\Delta s}$, and coefficient of variation (CoV), $c_{\Delta s}$, can be approximated as

$$\mu_{\Delta s} = \mu_i^{1/m} \tag{5}$$

and

$$c_{\Delta s} = \frac{c_i}{m}, \tag{6}$$

where μ_i and c_i are the mean and CoV of the fatigue damage distribution due to the uncertainty associated with α_j.

3.5. Reliability Update

The quantified and updated uncertainties can be consistently included in the probabilistic framework to update the reliability level. The probabilistic model (1) is used to derive an annual reliability level, $\Delta \beta(t)$, given the updated uncertainties. This procedure is indicated in the fifth step in Figure 2, where two reliability curves (with and without using information from a digital twin) are schematically presented. The outcome of the reliability update (increase or decrease) depends on the outcome of uncertainty quantification (increased or decreased).

3.6. Decision Models

Given new information from digital twins becomes available (either during operation or already in the design stage), the decision models can be updated as indicated by the last step in Figure 2. The digital twin information can be included based on Bayesian decision theory [24,55]. For existing structures, an operation and maintenance decision plan can be optimized based on an updated reliability level, for example, an updated inspection plan or lifetime reassessment. More specifically, a reliability-based inspection planning technique can be implemented [56] and some of the inspections can be removed (if any were planned during the lifetime of the structure in question) or new inspections can be included if the structural integrity is compromised. For new structures, the expected outcome of a future digital twin can be used to optimize structures already at the design stage (before the digital twin information becomes available) by the use of Bayesian pre-posterior theory [54].

4. Case Study Setup

To demonstrate an application of the proposed framework, we consider an example where information from a digital twin of an offshore wind jacket substructure is used to update the structural reliability of the substructure. The numerical models of the substructure and the turbine are described in Sections 4.1.1 and 4.1.2, followed by a description of the analyzed load case scenarios in Section 4.1.3. Based on the simulation results (in the form of stress range distributions), the structural reliability of selected joints is calculated in Section 4.2.1 by assuming a generic level of uncertainty. The results are nominal and are, in Section 5, compared with the results obtained by using digital twin information.

4.1. Modeling

We simulate a numerical model of a 7 MW jacket-supported turbine using the procedure outlined by Nielsen et al. [57] and applied by, e.g., Augustyn et al. [34]. The simulation procedure consists of the following steps: (1) the substructure model and corresponding wave loading are reduced to a Craig–Bampton superelement [58] with 30 internal modes accounting for internal substructure dynamics. A convergence study has been performed to ascertain that the reduced model (including 30 modes) adequately captures the relevant modal parameters of the non-reduced system. Subsequently, (2) the wind loading is computed through aero-elastic analyses, in which the substructure superelement is included. Finally, (3) the force-controlled recovery run outlined by Nielsen et al. [59] is performed, where the response of the substructure is recovered and relevant measurements are extracted. The applied model is formulated using state-of-the-art modeling approaches included in a typical design procedure for jacket substructures, and the model has been validated to accurately and precisely represent the structural dynamics of a combined substructure and wind turbine system [60,61].

4.1.1. Substructure

The jacket substructure and its appertaining wave loading were modeled using ROSAP (Ramboll Offshore Structural Analysis Programs), version 53 [62]. The jacket substructure considered in this study, which is depicted in Figure 3, has a total height of approximately 75 m. The substructure comprises three legs, each with a diameter ranging between 1.2 and 1.7 m, and four brace bays, each with a diameter ranging between 0.8 and 1.1 m. The substructure model includes, i.a., soil-pile interaction, local joint flexibility, scour, marine growth and appurtenance masses. The water depth is 55 m and the soil conditions are characterized as clay. The substructure includes 50 m grouted piles. The soil-structure interaction is modeled by the use of soil curves linearized according to the API method [63]. The structural damping was modeled according to a Rayleigh model [64] with 0.5% and 1% modal damping in the first and second bending modes, respectively.
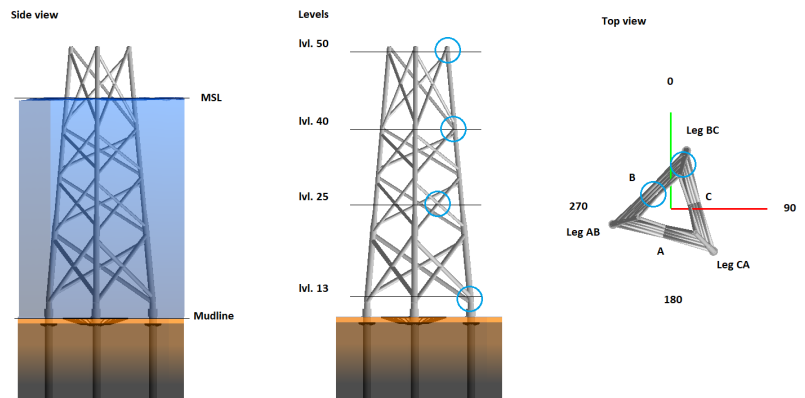

Figure 3. Substructure model used in the case studies. (**A**) Side view, (**B**) side view with indication of levels (blue circles indicate joints analyzed in the case studies) and (**C**) top view with indication of directions, side and leg names. NB: a wind turbine model is not shown in the figure.

The locations of the selected joints considered in the case studies are indicated in Figure 3B. The joint levels range between 13 (mudline) to 50 (top of the jacket). Results for sides B and C of the jacket, see Figure 3C, are provided. The joints are named in the following way: 50CL, where 50 indicates the level, C is the jacket side, and L indicates the lower element in the joint.

4.1.2. Wind Turbine

The substructure carries a representative 7 MW turbine, which is modeled in LACflex aero-elastic code [65]. The turbine includes a 90 m tubular tower with a diameter ranging between 4 and 6 m. Along the tower, three concentrated masses are assumed to emulate the effect of secondary-structures. The aero-elastic code employs a modal-based representation of the turbine (including the tower, rotor and blades). An aerodynamic damping contribution is included through the fluid-structure interaction when calculating aero-elastic forces. The wind turbine model was originally developed for industrial purposes, where it was applied in commercial projects. A rather similar model (albeit a 5 MW turbine instead of 7 MW), which adheres to the same modeling principles, has been applied in other studies on structural dynamics of wind turbines [34,66].

4.1.3. Load Cases

In this study, we consider the fatigue failure mode in the normal operating condition (design load case (DLC) 1.2 [40]). For a typical offshore wind jacket substructure, this DLC accounts for most of the fatigue damage [67].

The met-ocean parameters applied in this study are derived based on measurements from a representative North Sea site [68] and are summarized in Table 1. The wind speed ranges between 4 and 31 ms^{-1}, resulting in $n_b = 15$ wind speed bins. For each wind speed bin, representative wave parameters, i.e., the significant wave height and peak period, are assigned. The significant wave height ranges from 0.1 to 7.9 m while the peak period ranges from 3.0 to 9.6 s. The met-ocean parameters along with their yearly probability of occurrence are derived from a site-specific joint probability distribution function, which is a common design practice [40]. A total of $n_d = 12$ wind directions are analyzed (wind and waves are assumed fully aligned). For each wind speed, a total of $n_{TI} = 5$ turbulence intensity quantiles, namely, $q \in [q_{10}, q_{30}, q_{50}, q_{70}, q_{90}]$, are considered. The quantiles for each wind speed are calculated based on the Weibull distribution according to the IEC standard [40] for turbulence class B. The turbulence intensities for the given site ranges from 0.09 to 0.31. The fatigue damage is scaled with the corresponding turbulence intensity quantile probability, hence representing the target Weibull distribution. Every load case (wind speed, wave height, peak period and turbulence intensity) is simulated with $n_s = 6$ seeds. The total number of load cases analyzed is $n_t = n_b n_d n_{TI} n_s = 5400$.

Table 1. Load case definitions according to IEC [40] and representative site-specific parameters.

Turbine State	DLC	Wind Speed, U (ms^{-1})	Turbulence, TI (-)	Wave Height, H_s (m)	Wave Period, T_p (s)	Direction (deg)
Operational	1.2	4–31	0.31–0.09	0.1–7.9	3.0–9.6	0–330

4.2. Nominal Results

The structural reliability of selected joints of the jacket substructure is evaluated based on model (1) and the variables are summarized in Table 2. The stress ranges, $\Delta\sigma$, and number of cycles, N, were obtained from simulations. The SN curves for tubular joints in air and in seawater with cathodic protection are used according to [48]. The SN curve for the air environment are applied to the joint at level 50. For the remaining joints, the SN curve for seawater with cathodic protection is applied. For tubular joints exposed to seawater with cathodic protection, negative inverse slopes of $m_1 = 3$ and $m_2 = 5$ and intercepts of $\log K_{c_1} = 12.18$ and $\log K_{c_2} = 16.13$ are assumed to calculate the characteristic SN curve. For tubular joints in air environment, the following values can be used: $\log K_{a1} = 12.48$ and $\log K_{a2} = 16.13$, while assuming the same m values as for seawater environment. The mean SN curve for the probabilistic analysis was calculated from the characteristic SN curve's intercepts assuming a standard deviation of 0.20 [48].

Table 2. Variables used in the probabilistic model to estimate fatigue damage accumulation in the nominal case [32].

Variable	Distribution	Mean	CoV	Std. Dev.	Ref.
Δ	N	1.00	0.30	N/A	[69]
$\log K_{c1}$	N	12.58	N/A	0.20	[48]
$\log K_{c2}$	N	16.53	N/A	0.20	[48]
$\log K_{a1}$	N	12.88	N/A	0.20	[48]
$\log K_{a2}$	N	16.53	N/A	0.20	[48]
m_1	D	3	N/A	N/A	[48]
m_2	D	5	N/A	N/A	[48]
X_d	LN	1.00	0.10	N/A	[31]
X_l	LN	1.00	0.10	N/A	[70,71]
X_S	LN	1.00	0.05	N/A	[70]

Distribution: N-normal, LN-logNormal, D-deterministic.

4.2.1. Annual Reliability

The annual reliability index as a function of time, $\Delta\beta(t)$, is calculated based on the state-of-the-art probabilistic methods described in Section 2. The limit state Equation (1) was applied using the standard-based variables provided in Table 2. The reliability indices are presented in Figure 4 and Table 3 and are denoted as the nominal results. The results represent the situation where no additional knowledge from a digital twin is available. The results are provided for 10 selected joints, which are typically critical for a jacket design.

The structure is designed to have a fatigue lifetime of 25 years. The fatigue lifetime ends when the annual reliability index reaches the target value $\Delta\beta = 3.3$, which serves as the basis for reliability-based calibration of safety factors in recognized design codes [31,40]. For the considered case study, the design driving joints are 13BU and 40CU with a lifetime of 25 and 27 years. Joint 13BU is located close to the mudline, while joint 40CU is located slightly below the splash zone. Joints 40CL, 40BL, 25BU and 25BL have a lifetime between 50 and 100 years, while the remaining joints have a lifetime above 100 years.

Table 3. Fatigue lifetime derived based on probabilistic model (1) and stochastic variables presented in Table 2.

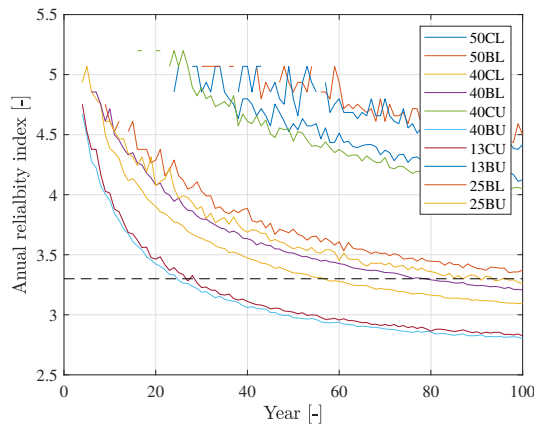| Joint	Fatigue Lifetime (Years)
50CL	>100
50BL	>100
40CL	54
40BL	77
40CU	>100
40BU	25
13CU	27
13BU	>100
25BL	98
25BU	86

Figure 4. Structural reliability as function of time for the nominal model.

5. Case Study Results

In this section, we exemplify how new information from digital twins can be included in the proposed framework to quantify uncertainty and subsequently update structural reliability for the particular case study. We use information from previously established digital twins [33,34]. The effect of structural dynamics uncertainty, X_d, is investigated based on a model updating study presented in [33], where the soil stiffness, k_s, was calibrated based on in situ measurements. The effect of loading uncertainty, X_l, is investigated based on a virtual sensing study [34], where modal expansion was used to estimate unmeasured field quantities. The results are presented and discussed based on two design driving joints, namely, 13CU and 40BU.

5.1. Updating Structural Dynamics Uncertainty

In this subsection, we present the updated structural reliability based on an updated structural dynamics uncertainty. First, we present a sensitivity study on updating soil stiffness, followed by a case study based on in situ soil stiffness calibration [33].

5.1.1. Soil Stiffness Sensitivity

The effect of updating the soil stiffness mean value, μ_{k_s}, for joint 13CU is presented in Figure 5 and in Table 4. It is assumed that new information from a digital twin is obtained; in this particular case, the mean value of uncertainty related to structural dynamics, μ_{X_d}, is updated. The results are derived by using the limit state Equation (1) with the standard-based variables provided in Table 2 and updated values for μ_{X_d}.

As seen in Figure 5, the soil stiffness has a significant impact on the fatigue lifetime. Updating the soil stiffness by a factor of 0.5 (resulting in reducing the mudline pile stiffness by half) results in a reduction in lifetime by a factor of 0.3. In contrast, increasing the soil stiffness by a factor of 2.0 results in a lifetime increase by more than fourfold (>100 years). The effect of updating soil stiffness on joint 40BU is negligible, as indicated in Figure 6.

Note that in Figures 5 and 6 (and the other figures describing structural reliability as a function of time), the reliability generally decreases with time, albeit non-monotonically in some cases. For example, consider the green curve in Figure 5, where a local increase in reliability around year 20 is observed. This is due to a limited number of Monte Carlo simulations, but we note that this limitation does not qualitatively affect the conclusions drawn from the analyses.

Table 4. Fatigue lifetime derived for different distributions of X_d.

k_s	13CU			40BU		
	μ_{X_d}	CoV X_d	Lifetime	μ_{X_d}	CoV X_d	Lifetime
0.50	1.20	0.10	7	0.98	0.10	26
0.75	1.10	0.10	15	0.99	0.10	25
1.00	1.00	0.10	25	1.00	0.10	25
1.25	0.90	0.10	85	1.01	0.10	25
1.50	0.80	0.10	>100	1.02	0.10	24
2.00	0.70	0.10	>100	1.04	0.10	22
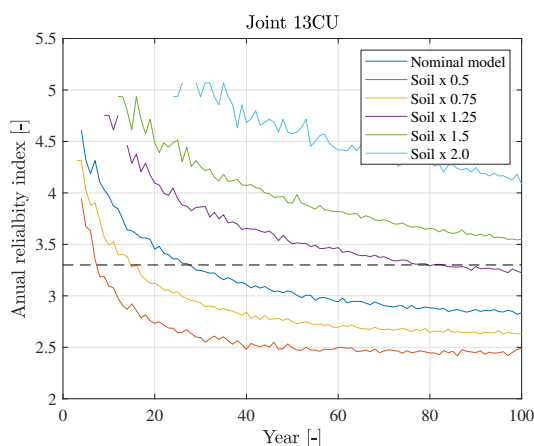
Figure 5. Impact of updating soil stiffness on structural reliability-joint 13CU.
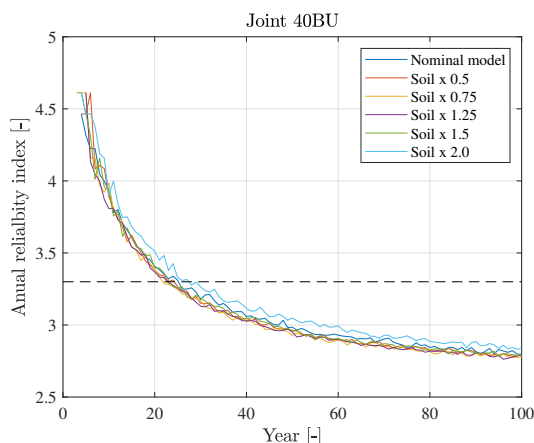
Figure 6. Impact of updating soil stiffness on structural reliability-joint 40BU.

5.1.2. Reliability Update-Soil Stiffness

Based on the results presented in [33], we assume the soil stiffness distribution function after the update can be approximated by a normal distribution with mean value of 4.7 and CoV = 0.12, i.e., $k_s \sim \mathcal{N}\left(4.7, (4.7 \times 0.12)^2\right)$. The soil stiffness uncertainty is propagated through the numerical model, and the uncertainty on stress ranges was estimated according to the method presented in Section 3.3. It was assumed, for illustrative purposes, that

the soil stiffness is the only uncertain parameter affecting the X_d uncertainty, i.e., $\alpha = k_s$. The X_d uncertainty is quantified and its updated value was applied together with the nominal uncertainty values for the remaining stochastic variables in (1). The updated X_d distribution (mean value and CoV) as a result of the soil updating is presented in Table 5.

The soil stiffness update results in a reduction in the mean value of X_d for all joints except three joints in the splash zone (joints 40CL, 40BL and 40CU). The CoV of X_d is reduced for all joints because the CoV of X_d is reduced from the initial value of 0.10 for all joints. The structural reliability after the soil update is presented in Figure 7 alongside the lifetime compared to the nominal model presented in Table 5. After the soil update, we can observe an increase in fatigue life in four joints close to the mudline (13CU and 13BU) and in the lowest X-joint (25BL and 25BU). Compared to the nominal model, we can conclude that for both critical joints (40BU and 13CU), the fatigue lifetime is increased after the update. Note that the fatigue lifetime in joint 40BL is reduced despite a reduced CoV. That is due to the fact that for this joint, two opposite effects of the soil update are merged; namely, the positive effect of the reduced CoV (0.006 vs. 0.10) and the negative effect of the increased mean value (1.07 vs. 1.00).

The general conclusion holds that if both the mean value and CoV are reduced, then the fatigue lifetime is increased, while if both of the values are increased, then the opposite result holds. If either mean or CoV is reduced while the other is increased, the fatigue lifetime can either increase or decrease depending on the extent of the increase/decrease in mean value and CoV.

Table 5. Effect of updating soil stiffness on fatigue lifetime.

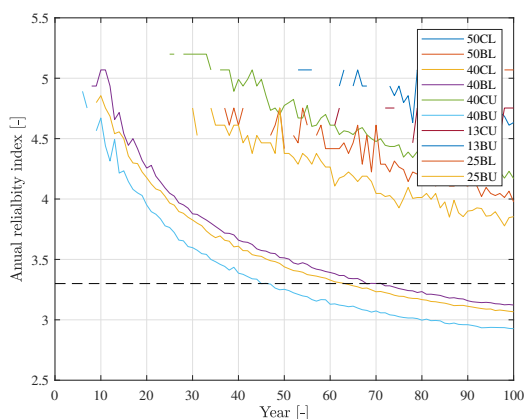| Joint	μ_{X_d}	CoV X_d	Lifetime (Years)	Compared to Table 3
50CL	0.98	0.004	>100	N/A
50BL	0.98	0.005	>100	N/A
40CL	1.04	0.004	62	+8
40BL	1.07	0.006	69	−8
40CU	1.05	0.003	>100	N/A
40BU	0.98	0.005	44	+19
13CU	0.65	0.058	>100	+
13BU	0.56	0.057	>100	N/A
25BL	0.90	0.013	>100	+
25BU	0.92	0.012	>100	+

Figure 7. Structural reliability after the soil stiffness update. (k_s update based on the study in [33]).

5.2. Loading Uncertainty Update

In this subsection, we investigate the effect of updating loading uncertainty on the structural reliability. First, we present a sensitivity study on wave loading calibration, followed by updating the reliability based on load calibration using two virtual sensing configurations. The virtual sensing study is presented based on uncertainty quantified in [34]. In this subsection, the X_l uncertainty is updated based on an updated C_m parameter. It is assumed, similarly as in Section 5.1, that only one uncertain parameter affects the uncertainty modeling, i.e., $\alpha = C_m$.

5.2.1. Wave Loading Sensitivity

The effect of updating the wave loading coefficient, C_m, on the structural reliability of joint 13CU is presented in Figure 8 and in Table 6. The mean value of the wave loading coefficient is modified by a factor of 0.8–1.2, which results in modifications of the loading uncertainty. It is assumed that new information from the digital twin is obtained; in this particular case, the mean value of uncertainty related to loading uncertainty, μ_{X_l}, is updated. The results are derived by using the limit state Equation (1) with the standard-based variables provided in Table 2 and updated values for μ_{X_l}.

The wave loading modification has a medium impact on the fatigue lifetime. Updating the wave loading by a factor of 0.8 (reducing the inertia-induced wave loading by 20%) results in an increased lifetime by a factor of 1.6. Increasing the wave loading by a factor of 1.2 results in reducing the lifetime by a factor of 0.7. The effect of updating wave loading on joint 40BU is more pronounced, as indicated in Figure 9. For this joint, reducing the wave loading by 20% results in a lifetime increase by more than fourfold (>100 years), while a wave loading increase by 20% results in a lifetime reduction by a factor of 0.3.
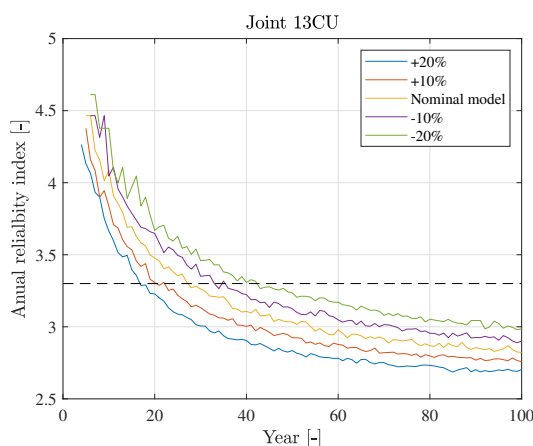

Figure 8. Impact of updating wave loading on structural reliability-joint 13CU.

Table 6. Fatigue lifetime derived for different distributions of X_l.

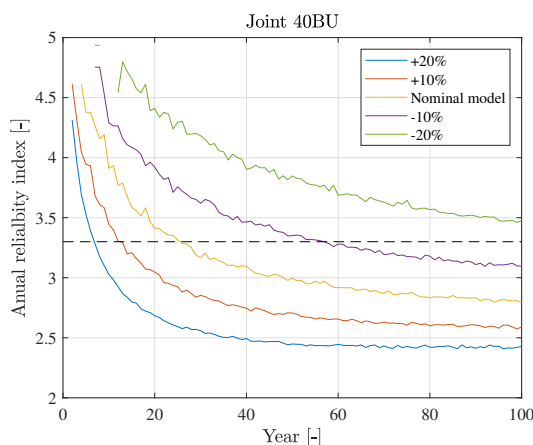| C_m	13CU			40BU		
	μ_{X_l}	CoV X_l	Lifetime	μ_{X_l}	CoV X_l	Lifetime
1.2	1.06	0.10	17	1.20	0.10	7
1.1	1.03	0.10	21	1.10	0.10	12
1.0	1.00	0.10	25	1.00	0.10	25
0.9	0.97	0.10	33	0.90	0.10	55
0.8	0.94	0.10	42	0.80	0.10	>100

Figure 9. Fatigue lifetime derived for different distributions of X_l-joint 40BU.

5.2.2. Reliability Update-Virtual Sensing Uncertainty

The virtual sensing uncertainty quantified for two virtual sensing configurations are considered based on results presented in [34]. The following virtual sensing uncertainty configurations are used: (1) basic setup: CoV = 0.10 and (2) extended setup: CoV = 0.05, while the mean value for both setups is assumed to be 1.00. The basic setup includes only acceleration sensors above the water level, while the extended one, in addition, includes sub-sea acceleration sensors and a wave radar sensor. It is assumed that the virtual sensing uncertainty are combined with the nominal X_l uncertainty. Furthermore, it is assumed, for illustrative purposes, that the mean value of X_l equals 0.9. The X_l distribution parameters used in this study are summarized in Table 7 for joints 40CU and 13BU.

The results for joint 40BU are presented in Figure 10. As each model update configuration results in the same mean value update so the only difference in the stochastic model is the CoV, the higher the CoV, the shorter lifetime we should derive. This is confirmed in the results as the direct sensing method (measuring directly), with CoV = 0.00 resulting in a lifetime of 60 years, followed by the extended virtual sensing method (lifetime of 50 years and CoV = 0.05), while the most uncertain method (basic virtual sensing with CoV = 0.10) results in a fatigue lifetime of 40 years. In this case, each configuration derives a fatigue lifetime larger than the nominal one, i.e., 25 years. However, this is not the case for joint 13CU, where the fatigue lifetime using the basic virtual sensing configuration is 22 years, as depicted in Figure 11. Even though the mean value of the update results in reduced fatigue damage ($\mu_{X_l} = 0.97$ for this case), the negative effect of increased uncertainty (CoV $X_l = 0.14$) results in a fatigue lifetime reduction of 3 years.

Table 7. Fatigue lifetime updated based on various uncertain wave loading calibration methods. X_l distribution is updated (mean and CoV).

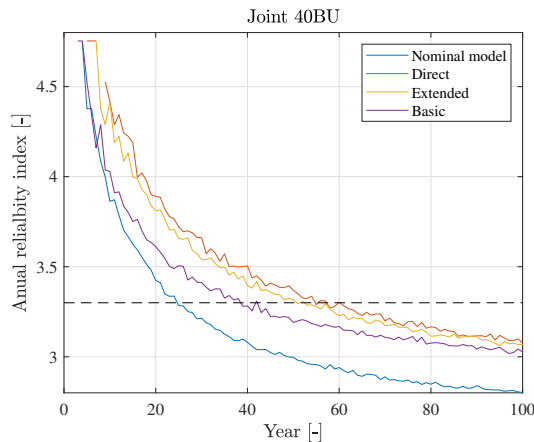| Configuration	13CU			40BU		
	μ_{X_l}	CoV X_l	Lifetime	μ_{X_l}	CoV X_l	Lifetime
Nominal	1.00	0.10	25	1.00	0.10	25
Basic	0.97	0.14	22	0.90	0.14	40
Extended	0.97	0.11	30	0.90	0.11	50
Direct sensing	0.97	0.10	35	0.90	0.10	60

Figure 10. Impact of updating wave loading based on uncertain virtual sensing methods-40BU.
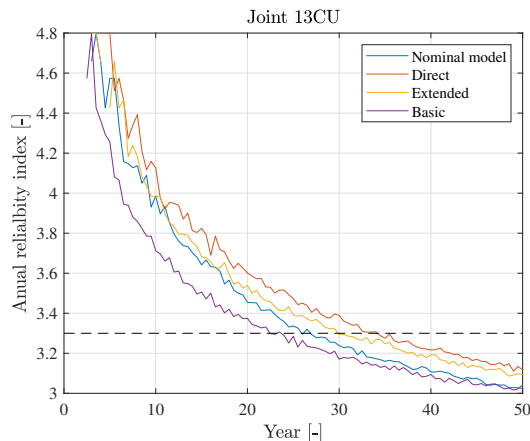

Figure 11. Impact of updating wave loading based on uncertain virtual. sensing methods-13CU.

5.3. Uncertainty Correlation

In the previous subsections, the X_d and X_l uncertainties were investigated separately, hence neglecting a potential correlation. In this subsection, we consider updating both X_d and X_l with varying correlation coefficients. The correlation can stem from interaction between the structural dynamics and loading parameters. For example, the loading parameters can be calibrated based on responses from a previously updated structural model.

We assume the structural and loading uncertainties are quantified based on new information from a digital twin, resulting in updated mean values of structural and load uncertainties: $\mu_{X_d} = 0.80$ and $\mu_{X_l} = 0.97$ and using the reference uncertainty level CoV = 0.10. The updated uncertainty value corresponds to increasing the soil stiffness by 50%, $k_s = 1.5$, and reducing the wave loading coefficient by 10%, $C_m = 0.9$. The results are presented for joint 13CU.

Three scenarios of correlation between X_d and X_l are investigated: (1) $\rho = 0$ (no correlation), which can be the case if the load calibration was performed without using information from the updated structural model, (2) $\rho = 1$ (full correlation), when, for example, load calibration using mode shapes from an updated structural model and (3) an intermediate case with $\rho = 0.5$, where both analytical and measured mode shapes were used for load calibration.

The structural reliability calculated for various scenarios is presented in Figure 12. The nominal setup yields a fatigue lifetime of 25 years, while the updated uncertainty results in a fatigue lifetime ranging between 23 and 48 years, where the difference stems solely from varying correlations. The largest fatigue lifetime is obtained when assuming no correlation, while the lowest lifetime is derived for full correlation. Note that despite reducing the mean values of X_d and X_l, the fatigue lifetime is reduced compared to the nominal result for the full correlation case. The results are in line with expectations, because positive correlation increases the combined $X_d X_l$ uncertainty.
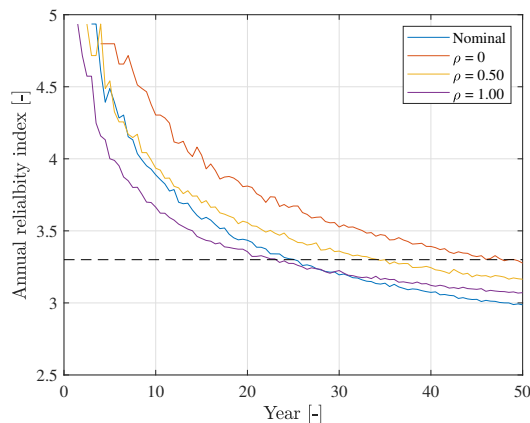
Figure 12. Impact of X_d and X_l correlation on structural reliability.

5.4. Application for New Structures

Assuming a number of digital twins for similar structures have been established in the past, we can, by applying the proposed framework, obtain a distribution function of $X_d X_l$, which indicates what is the expected outcome of updating the structural and load model. This knowledge can be used at the design stage, resulting in an optimized design given the expected model update is realized. However, the updated information may be at a preliminary stage of validation and therefore subject to some degree of uncertainty, i.e., the expected model update outcome only represents our (best) knowledge. Hence, we must confirm our expectation by performing model updates during the structural lifetime and consider all potential outcomes of the experiment (model update) in the design stage. This is accounted for by preparing a decision rule, which for any outcome introduces an action that guarantees that the wind turbine has a sufficient reliability level until the intended lifetime is reached. The proposed application is based on Bayesian pre-posterior decision theory [54] and has, in the offshore wind industry, been applied in, for example, optimization of operation and maintenance of wind turbines [55].

In the following, an illustrative example is presented for this application to new structures. Assume that, based on previous digital twins, we obtain a prior distribution function of quantified uncertainties, $X_f = X_d X_l$. This prior distribution can be regarded as the future (yet to be realized) distribution of the updated uncertainties and can be used already at the design stage.

For the sake of illustration, we assume that the future outcome of model updates can be modeled as $X_f \sim \mathcal{N}(0.9, (0.9 \times 0.05)^2)$, as depicted in Figure 13. The prior distribution is used together with model (1) to design the optimized structure. This is obtained by assuming that the generic structural dynamics and loading uncertainty are substituted with the expected uncertainty quantified based on the future experiment, $X_d X_l = X_f$. The decision models are derived based on (1), where, depending on the outcome of the model update, different values of X_f are assumed. The X_f values are summarized in Table 8. As a result, we derive an optimized structure, which has sufficient reliability until the intended

lifetime is reached. This is indicated in Figure 14 by the blue curve. In the design, we have used the prior distribution of the updated uncertainty and assumed that updating the model is performed during the operation of the structure to confirm our expectation (obtain the posterior distribution). The point in time when updating the model must be performed can be derived by applying model (1) with the nominal uncertainty from Table 2, as shown in Figure 13 with the orange curve. Finally, we derive a point when the structure reaches the target reliability level and some action is needed to confirm its structural reliability. This is indicated by the orange curve in Figure 14.

When the model update time is reached, updating of the model is performed. As a result of model update, we can obtain one of the three outcomes for X_f, which will have an impact on the decision models, as depicted in Figure 15. In particular, we have the following potential outcomes:

- Most likely: the mean value of the derived model update is close to the mean value of the prior distribution assumed in the design stage, $\mu_{X_d X_l} = \mu_{X_f}$. In such a case, the structure is fit for operation for the intended lifetime and no further action is required. This scenario is indicated by the green line in Figure 15.
- Unlikely positive: the mean value is less than the value assumed in the design stage, $\mu_{X_d X_l} < \mu_{X_f}$. This results in a longer lifetime than expected and no further action is required. This scenario is indicated by the yellow line in Figure 15.
- Unlikely negative: the mean value is greater than the value assumed in the design stage, $\mu_{X_d X_l} > \mu_{X_f}$. This results in a shorter lifetime than expected and action is required to ensure a sufficient reliability during the intended lifetime of the structure. This scenario is indicated by the dashed red line in Figure 15.

Given the expected or positive outcome of updating the model is realized, no further action is required. However, if the outcome of updating the model is unexpectedly negative, the following mitigation actions can be considered to ensure the required level of reliability during the intended lifetime: (1) strengthening or (2) curtailing of the wind turbine (thereby reducing fatigue damage) and operating until the end of the intended lifetime. If it is economically infeasible to continue the operation of a particular turbine given the model updating outcome, one can consider premature decommissioning. The reliability level after the mitigation action is performed as indicated by the solid red line in Figure 15.

Table 8. Pre-posterior stochastic model.

| Case	μ_{X_f}	CoV X_f	Comment	Information
Pre-posterior design	0.9	0.05	Prior knowledge on X_f	Generic design
Determine model update time	1.0	0.14	Using no extra information from digital twin	Generic design
Model updating (expected outcome)	0.9	0.05	The same as prior knowledge, lifetime as expected, no action	Digital twin
Model updating (positive outcome)	0.85	0.05	Positive outcome, longer lifetime than expected, potential for lifetime extension	Digital twin
Model updating (negative outcome)	0.95	0.05	Negative outcome, shorter lifetime than expected	Digital twin
Model updating (negative outcome + mitigation)	0.9	0.05	Mitigation (extra cost) required, after mitigation expected (or longer) lifetime achieved	Digital twin + mitigation
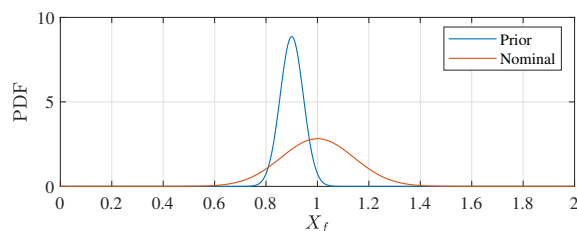
Figure 13. Stochastic model for pre-posterior design.
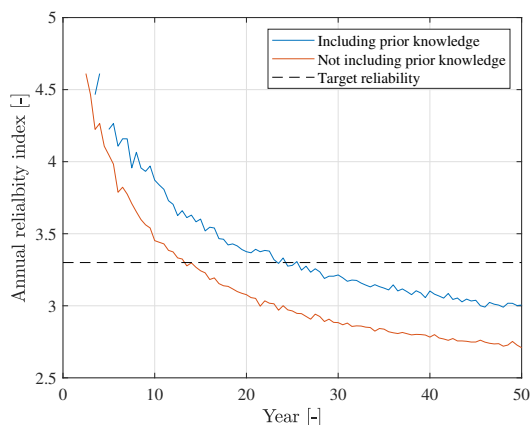
Figure 14. Benefit of including pre-posterior design (including prior knowledge on X_f).
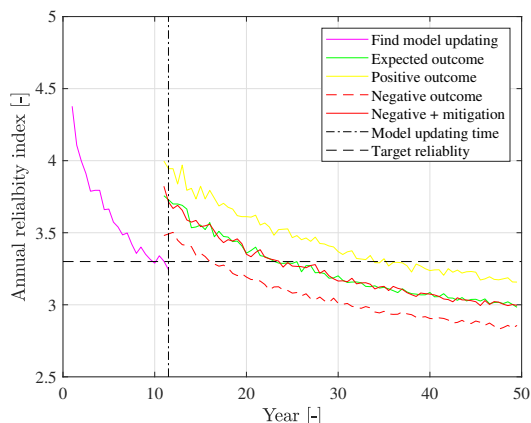

Figure 15. Pre-posterior design at inspection time.

6. Conclusions

In this paper, we propose a probabilistic framework for updating structural reliability of offshore wind substructures based on new information from digital twins. The digital twin information is consistently included in the framework by updating the uncertainty related to structural dynamics and load modeling and propagating this uncertainty to the fatigue damage accumulation. The resulting uncertainty is then converted into uncertainty of the stress ranges, which is included in a probabilistic model on structural reliability. The proposed framework is applicable to offshore wind substructures whose lifetimes are governed by fatigue damage accumulation.

The framework is applied to two case studies, where the potential for improved decision models for existing and new structures is demonstrated. In the former case, updating soil stiffness and wave loading is considered to investigate the potential for lifetime extension of fatigue critical joints. In the latter case, the framework is applied to optimize new structures by using Bayesian pre-posterior theory for future wave load calibration.

References

1. U.S. Department of Energy. *2018 Offshore Wind Technologies Market Report*; Technical Report; U.S. Department of Energy: Washington, DC, USA, 2018.
2. Wind Europe. *Offshore Wind in Europe. Key Statistics 2020*; Technical Report; Wind Europe: Brussels, Belgium, 2020.
3. Global Wind Energy Council. *Global Offshore Wind Report 2020*; Technical Report; Global Wind Energy Council: Brussels, Belgium, 2020.
4. Nielsen, J.S.; Tcherniak, D.; Ulriksen, M.D. A case study on risk-based maintenance of wind turbine blades with structural health monitoring. *Struct. Infrastruct. Eng.* **2021**, *17*, 302–318. [CrossRef]
5. Grieves, M. *Digital Twin: Manufacturing Excellence through Virtual Factory Replication*; White Paper; Michael W. Grieves, LLC: Winooski, VT, USA, 2015.
6. Grieves, M.; Vickers, J. Digital Twin: Mitigating Unpredictable, Undesirable Emergent Behavior in Complex Systems. In *Transdisciplinary Perspectives on Complex Systems: New Findings and Approaches*; Springer International Publishing: Cham, Switzerland, 2017; pp. 85–113. [CrossRef]
7. Tygesen, U.; Jepsen, M.; Vestermark, J.; Dollerup, N.; Pedersen, A. The True Digital Twin Concept for Fatigue Re-Assessment of Marine Structures. In Proceedings of the ASME 2018 37th International Conference on Ocean, Offshore and Arctic Engineering OMAE2018, Madrid, Spain, 17–22 June 2018. [CrossRef]
8. Pedersen, E.B.; Jørgensen, D.; Riber, H.J.; Ballani, J.; Vallaghé, S.; Paccaud, B. True Fatigue Life Calculation Using Digital Twin Concept and Operational Modal Analysis. In Proceedings of the Twenty-Ninth (2019) International Offshore and Polar Engineering Conference, Honolulu, HI, USA, 16–21 June 2019; Volume 1.
9. Kritzinger, W.; Karner, M.; Traar, G.; Henjes, J.; Sihn, W. Digital Twin in manufacturing: A categorical literature review and classification. *IFAC-PapersOnLine* **2018**, *51*, 1016–1022.
10. Sivalingam, K.; Sepulveda, M.; Spring, M.; Davies, P. A Review and Methodology Development for Remaining Useful Life Prediction of Offshore Fixed and Floating Wind turbine Power Converter with Digital Twin Technology Perspective. In Proceedings of the 2018 2nd International Conference on Green Energy and Applications (ICGEA), Singapore, 24–26 March 2018; pp. 197–204. [CrossRef]
11. DNVGL-ST-0262. *Lifetime Extension of Wind Turbines*; Technical Report; Det Norske Veritas Germanischer Lloyd: Høvik, Greater Oslo, Norway, 2016.
12. DNVGL-ST-0263. *Certification of Lifetime Extension of Wind Turbines*; Technical Report; Det Norske Veritas Germanischer Lloyd: Høvik, Greater Oslo, Norway, 2016.
13. IEC 61400-28 ED1. *Wind Energy Generation Systems-Part 28: Through Life Management and Life Extension of Wind Power Assets (Committee Draft)*; Technical Report; International Electrotechnical Commission: Geneva, Switzerland, 2021.
14. BSH-7005. *Standard Design. Minimum Requirements Concerning the Constructive Design of Offshore Structures within the Exclusive Economic Zone (EEZ)*; Technical Report; Bundesamt für Seeschifffahrt und Hydrographie: Hamburg, Germany, 2015.
15. Nielsen, J.S.; Sørensen, J.D. Bayesian Estimation of Remaining Useful Life for Wind Turbine Blades. *Energies* **2017**, *10*, 664. [CrossRef]
16. Ziegler, L.; Muskulus, M. Fatigue reassessment for lifetime extension of offshore wind monopile substructures. *J. Phys. Conf. Ser.* **2016**, *753*, 092010. [CrossRef]
17. Leser, P.E.; Warner, J.E.; Leser, W.P.; Bomarito, G.F.; Newman, J.A.; Hochhalter, J.D. A digital twin feasibility study (Part II): Non-deterministic predictions of fatigue life using in-situ diagnostics and prognostics. *Eng. Fract. Mech.* **2020**, *229*, 106903. [CrossRef]
18. Mai, Q.A.; Weijtjens, W.; Devriendt, C.; Morato, P.G.; Rigo, P.; Sørensen, J.D. Prediction of remaining fatigue life of welded joints in wind turbine support structures considering strain measurement and a joint distribution of oceanographic data. *Mar. Struct.* **2019**, *66*, 307–322. [CrossRef]

19. Augustyn, D.; Tygesen, U.T.; Ulriksen, M.D.; Sørensen, J.D. Data-Driven Design and Operation of Offshore Wind Structures. In Proceedings of the Twenty-Ninth (2019) International Offshore and Polar Engineering Conference, Honolulu, HI, USA, 16–21 June 2019; Volume 1, pp. 491–498.
20. Straub, D. Reliability updating with equality information. *Probabilistic Eng. Mech.* **2011**, *26*, 254–258. [CrossRef]
21. Zhang, R.; Mahadevan, S. Model uncertainty and Bayesian updating in reliability-based inspection. *Struct. Saf.* **2000**, *22*, 145–160. [CrossRef]
22. Schneider, R.; Thöns, S.; Straub, D. Reliability analysis and updating of deteriorating systems with subset simulation. *Struct. Saf.* **2017**, *64*, 20–36. [CrossRef]
23. Straub, D.; Faber, M.H. Risk based inspection planning for structural systems. *Struct. Saf.* **2005**, *27*, 335–355. [CrossRef]
24. Sørensen, J.D. Framework for risk-based planning of operation and maintenance for offshore wind turbines. *Wind Energy* **2009**, *12*, 493–506. [CrossRef]
25. Singh, M.; Markeset, T. A methodology for risk-based inspection planning of oil and gas pipes based on fuzzy logic framework. *Eng. Fail. Anal.* **2009**, *16*, 2098–2113. [CrossRef]
26. Hevia-Koch, P.; Klinge Jacobsen, H. Comparing offshore and onshore wind development considering acceptance costs. *Energy Policy* **2019**, *125*, 9–19. [CrossRef]
27. Netland, Ø.; Sperstad, I.B.; Hofmann, M.; Skavhaug, A. Cost-benefit Evaluation of Remote Inspection of Offshore Wind Farms by Simulating the Operation and Maintenance Phase. *Energy Procedia* **2014**, *53*, 239–247. EERA DeepWind' 2014, 11th Deep Sea Offshore Wind R&D Conference. [CrossRef]
28. Ulriksen, M.D. Damage Localization for Structural Health Monitoring: An Exploration of Three New Vibration-Based Schemes. Ph.D. Dissertation, Aalborg University, Aalborg, Denmark, 2018.
29. Simoen, E.; De Roeck, G.; Lombaert, G. Dealing with uncertainty in model updating for damage assessment: A review. *Mech. Syst. Signal Process.* **2015**, *56–57*, 123–149. [CrossRef]
30. Nielsen, J.S.; Sørensen, J.D. Computational framework for risk-based planning of inspections, maintenance and condition monitoring using discrete Bayesian networks. *Struct. Infrastruct. Eng.* **2018**, *14*, 1082–1094. [CrossRef]
31. Sørensen, J.D.; Toft, H.S. *Safety Factors-IEC 61400-1 ed. 4-Background Document*; Technical Report, DTU Wind Energy-E-Report-0066(EN); Technical University of Denmark (DTU): Lyngby, Denmark, 2014.
32. Velarde, J.; Kramhøft, C.; Sørensen, J.D.; Zorzi, G. Fatigue reliability of large monopiles for offshore wind turbines. *Int. J. Fatigue* **2020**, *134*, 105487. [CrossRef]
33. Augustyn, D.; Smolka, U.; Tygesen, U.T.; Ulriksen, M.D.; Sørensen, J.D. Data-Driven Model Updating of an Offshore Wind Jacket Substructure. *Appl. Ocean. Res.* **2020**, *104*, 102366. [CrossRef]
34. Augustyn, D.; Pedersen, R.R.; Tygesen, U.T.; Ulriksen, M.D.; Sørensen, J.D. Feasibility of modal expansion for virtual sensing in offshore wind jacket substructures. *Mar. Struct.* **2021**, *79*, 103019. [CrossRef]
35. Madsen, H.; Krenk, S.; Lind, N. *Methods of Structural Safety*, 2nd ed.; Dover Publications: New York, NY, USA, 2006.
36. Tavner, P. *Offshore Wind Turbines: Reliability, Availability and Maintenance*; Institution of Engineering and Technology: Stevenage, UK, 2012.
37. Arabian-Hoseynabadi, H.; Oraee, H.; Tavner, P. Failure Modes and Effects Analysis (FMEA) for wind turbines. *Int. J. Electr. Power Energy Syst.* **2010**, *32*, 817–824. [CrossRef]
38. Nguyen, T.A.; Min, D.; Choi, E.; Lee, J.W. Dependability and Security Quantification of an Internet of Medical Things Infrastructure based on Cloud-Fog-Edge Continuum for Healthcare Monitoring using Hierarchical Models. *IEEE Internet Things J.* **2021**. [CrossRef]
39. Madsen, H.O.; Krenk, S.; Lind, N.C. *Methods of Structural Safety*; Courier Corporation: Washington, DC, USA, 2006.
40. IEC-61400-1:2019. *Wind Energy Generation Systems-Part 1: Design Requirements*; Technical Report; International Electrotechnical Commission: Geneva, Switzerland, 2019.
41. Szala, G.; Ligaj, B. Effect of the Exponent in the Description of Wöhler Fatigue Diagram on the Results of Calculations of Fatigue Life. *Key Eng. Mat.* **2014**, *598*, 231–236. [CrossRef]
42. Naess, A.; Leira, B.; Batsevych, O. System reliability analysis by enhanced Monte Carlo simulation. *Struct. Saf.* **2009**, *31*, 349–355. [CrossRef]
43. Hübler, C.; Gebhardt, C.G.; Rolfes, R. Methodologies for fatigue assessment of offshore wind turbines considering scattering environmental conditions and the uncertainty due to finite sampling. *Wind Energy* **2018**, *21*, 1092–1105. [CrossRef]
44. Reynders, E.; Pintelon, R.; Roeck, G. Uncertainty bounds on modal parameters obtained from stochastic subspace identification. *Mech. Syst. Signal Process.* **2008**, *22*, 948–969. [CrossRef]
45. Iliopoulos, A.; Weijtjens, W.; Van Hemelrijck, D.; Devriendt, C. Fatigue assessment of offshore wind turbines on monopile foundations using multi-band modal expansion. *Wind Energy* **2017**, *20*, 1463–1479. [CrossRef]
46. Efthymiou, M.; Durkin, S. Stress concentrations in T/Y and gap/overlap K-joints. In Proceedings of the 4th International Conference on Behaviour of Offshore Structures, Delft, The Netherlands, 1–5 July 1985; p. 12.
47. Lee, J.M.; Seo, J.K.; Kim, M.H.; Shin, S.B.; Han, M.S.; Park, J.S.; Mahendran, M. Comparison of hot spot stress evaluation methods for welded structures. *Int. J. Nav. Archit. Ocean Eng.* **2010**, *2*, 200–210. [CrossRef]
48. DNVGL-RP-C203. *Fatigue Design of Offshore Steel Structures*; Technical Report; Det Norske Veritas Germanischer Lloyd: Høvik, Greater Oslo, Norway, 2016.

49. Miner, M.A. Cumulative Damage in Fatigue. *J. Appl. Mech.* **2021**, *12*, A159–A164. [CrossRef]
50. Paris, P.; Erdogan, F. A Critical Analysis of Crack Propagation Laws. *J. Basic Eng.* **1963**, *85*, 528–533. [CrossRef]
51. Friswell, M.I.; Mottershead, J.E. *Finite Element Model Updating in Structural Dynamics*; Kluwer Ademic Publishers: Amsterdam, The Netherlands, 1995.
52. Anderson, G. Error propagation by the Monte Carlo method in geochemical calculations. *Geochim. Cosmochim. Acta* **1976**, *40*, 1533–1538. [CrossRef]
53. ISO 13587:2012. *Three Statistical Approaches for the Assessment and Interpretation of Measurement Uncertainty*; Technical Report; International Electrotechnical Commission: Geneva, Switzerland, 2012.
54. Raiffa, H.; Schlaifer, R. *Applied Statistical Decision Theory*; Wiley & Sons: Hoboken, NJ, USA, 2000. [CrossRef]
55. Nielsen, J.J.; Sørensen, J.D. On risk-based operation and maintenance of offshore wind turbine components. *Reliab. Eng. Syst. Saf.* **2011**, *96*, 218–229. [CrossRef]
56. Onoufriou, T. Reliability based inspection planning of offshore structures. *Mar. Struct.* **1999**, *12*, 521–539. [CrossRef]
57. Nielsen, M.B.; Jensen, J.F.; Harper, C.; Knudsen, L.S.; Pedersen, R.R. State-of-the-art framework for design of offshore wind jacket foundations. *Steel Constr.* **2019**, *12*, 209–214. [CrossRef]
58. Craig, R.R.; Bampton, M.C.C. Coupling of substructures for dynamic analyses. *AIAA J.* **1968**, *6*, 1313–1319. [CrossRef]
59. Nielsen, M.B.; Jensen, J.F.; Augustyn, D.; Pedersen, R.R. Efficient response recovery procedures for detailed design of jacket foundations. In *Insights and Innovations in Structural Engineering, Mechanics and Computation*, 1st ed.; Taylor & Francis: London, UK, 2016; Volume 1, pp. 2060–2065. [CrossRef]
60. van der Valk, P.; Voormeeren, S. An overview of modeling approaches for complex offshore wind turbine support structures. In Proceedings of the ISMA2012-USD2012, Leuven, Belgium, 17–19 September 2012; pp. 1–4.
61. Passon, P. Offshore Wind Turbine Foundation Design. Ph.D. Thesis, DTU Wind Energy: Roskilde, Denmark, 2015.
62. Ramboll. *ROSAP-Ramboll Offshore Structural Analysis Package, Version 53*; Technical Report; Ramboll: Esbjerg, Denmark, 2018.
63. API-RP-2A. *Recommended Practice for Planning, Designing and Constructing Fixed Offshore Platforms*; Technical Report; American Petroleum Institute: Washington, DC, USA, 2014.
64. Liu, M.; Gorman, D. Formulation of Rayleigh damping and its extensions. *Comput. Struct.* **1995**, *57*, 277–285. [CrossRef]
65. Ramboll. *LACflex-Aeroelastic Simulation Tool*; Technical Report; Ramboll: Aarhus, Denmark, 2018.
66. Augustyn, D.; Cosack, N.; Ulriksen, M. On the influence of environmental and operational variability on modal parameters of offshore wind support structures. *Mar. Struct.* **2021**. submitted.
67. Kelma, S.; Schaumann, P. Probabilistic Fatigue Analysis of Jacket Support Structures for Offshore Wind Turbines Exemplified on Tubular Joints. *Energy Procedia* **2015**, *80*, 151–158. [CrossRef]
68. Anonymous. *Met-Ocean Report*; Technical Report; Confidential Publisher: New York, NY, USA, 2016.
69. Rasmus Folsø, S.O.; Parmentier, G. Reliability-based calibration of fatigue design guidelines for ship structures. *Mar. Struct.* **2002**, *15*, 627–651. [CrossRef]
70. Sørensen, J. Reliability-based calibration of fatigue safety factors for offshore wind turbines. *Int. J. Offshore Pol. Eng.* **2012**, *22*, 234–241.
71. JCSS. *Probabilistic Model Code*; Technical Report; Joint Committee on Structural Safety: Copenhagen, Denmark, 2001.